

Performance improvement of night ventilation for passive cooling of office buildings

Guo, Rui

DOI (link to publication from Publisher):
[10.54337/aau424058857](https://doi.org/10.54337/aau424058857)

Publication date:
2021

Document Version
Publisher's PDF, also known as Version of record

[Link to publication from Aalborg University](#)

Citation for published version (APA):
Guo, R. (2021). *Performance improvement of night ventilation for passive cooling of office buildings*. Aalborg Universitetsforlag. <https://doi.org/10.54337/aau424058857>

General rights

Copyright and moral rights for the publications made accessible in the public portal are retained by the authors and/or other copyright owners and it is a condition of accessing publications that users recognise and abide by the legal requirements associated with these rights.

- Users may download and print one copy of any publication from the public portal for the purpose of private study or research.
- You may not further distribute the material or use it for any profit-making activity or commercial gain
- You may freely distribute the URL identifying the publication in the public portal -

Take down policy

If you believe that this document breaches copyright please contact us at vbn@aub.aau.dk providing details, and we will remove access to the work immediately and investigate your claim.

PERFORMANCE IMPROVEMENT OF NIGHT VENTILATION FOR PASSIVE COOLING OF OFFICE BUILDINGS

**BY
RUI GUO**

DISSERTATION SUBMITTED 2021



AALBORG UNIVERSITY
DENMARK

PERFORMANCE IMPROVEMENT OF NIGHT VENTILATION FOR PASSIVE COOLING OF OFFICE BUILDINGS

by

Rui Guo



AALBORG UNIVERSITY
DENMARK

Dissertation submitted

Dissertation submitted: March 2020

PhD supervisor: Prof. Per K. Heiselberg,
Aalborg University

PhD committee: Associate Professor Mads Pagh Nielsen (chair)
Aalborg University

Professor Maria Kolokotroni
Brunel University London

Professor Guilherme Carrilho da Graca
University of Lisbon

PhD Series: Faculty of Engineering and Science, Aalborg University

Department: Department of the Build Environment

ISSN (online): 2446-1636
ISBN (online): 978-87-7210-915-2

Published by:
Aalborg University Press
Kroghstræde 3
DK – 9220 Aalborg Ø
Phone: +45 99407140
aauf@forlag.aau.dk
forlag.aau.dk

© Copyright: Rui Guo

Printed in Denmark by Rosendahls, 2021

CV

Personal details

Name: Rui Guo
Date of birth: 15-07-1991
Nationality: Chinese
Tel: +45 91806096
Email: rgu@build.aau.dk



Education

10.2017 – 02.2021 PhD, Civil Engineering, Aalborg University, Denmark,
09.2014 – 06.2017 Master of Engineering, Heating, Gas Supply, Ventilation and Air Conditioning Engineering, Chongqing University, China
09.2010 – 06.2014 Bachelor of Engineering, Building Environment and Facility Engineering, Chongqing University, China

Project experiences

- IEA EBC Annex 80: Resilient cooling (10.2018 – Present)
- EU Horizon 2020 ReCO2ST project- PCM enhanced ventilated window (01.2018 – Present)
- US-China Clean Energy Research Center Building Energy Efficiency Consortium for adaptivity of cool roofs in China (01.2015 – 03.2016)
- Postgraduate Scientific Research and Innovation Foundation of Chongqing for an air purification device of non-thermal plasma coupled with photocatalyst (05.2016 – 05.2017)
- National Undergraduate Innovation Foundation of China for a selective control system for temperature-humidity independent control air conditioner (05.2012 - 05.2013)

ENGLISH SUMMARY

Night ventilation (NV) is a promising and efficient passive technology to lessen the problems of increasing cooling demand and deteriorating indoor environments. However, the application of this technology might be hesitated by architects or designers due to the high uncertainty of NV performance that depends on many factors. Thus, this study proposes a holistic method integrating global sensitivity analysis, dynamic full-scale experiments, building energy simulation, and optimization to improve NV performance.

The thesis firstly revolves around the influential parameters for NV performance. The NV performance indicators are first reviewed and categorized. The influences of nine design parameters on nine selected performance indicators for different NV principles and climate conditions are then quantified by integrating Monte Carlo simulations with the regression method. The results indicate that the convective heat transfer coefficient (CHTC), thermal mass level, and night airflow rate are three crucial parameters. The usefulness and limitations of indicators are also analyzed based on the simulation results.

Based on the three influential parameters, the thesis focuses on the experiment on convective heat transfer for NV. A novel air distribution principle, diffuse ceiling ventilation (DCV), and a commonly used principle, mixing ventilation (MV), are integrated with NV. Various thermal mass distribution schemes, airflow rates, and supply temperatures are designed in the experimental cases. The CHTC with supply reference temperature is deduced to develop the CHTC correlations tailored for NV and compare with the previous empirical CHTC correlations. The comparison discloses that the empirical correlations produce large errors in predicting CHTC in most cases. The CHTC at a surface can be greatly augmented by increasing the thermal mass level and be somewhat affected by other surfaces' thermal mass distribution.

Finally, the thesis conducts the simulation and optimization of NV performance after validating the proposed CHTC correlations in a building energy simulation tool. Moreover, for DCV, the CHTC correlations for the surfaces in the plenum and diffuse ceiling are identified by comparing the simulated and measured data. The simulation results indicate that a general NV scheme saves the cooling energy and could lead to an overcooling penalty in a cold climate. DCV offers a greater energy-saving potential and better indoor thermal comfort than MV. Compared with the developed correlations, the empirical CHTC correlations overestimates the NV energy-saving potential and offer a discrepancy in thermal comfort prediction. Optimizing the night cooling with MV and DCV can both significantly save energy use and reduce the risk of draught. The performance of night cooling with DCV also improves more after the optimization.

DANSK RESUME

Natkøling med udeluft (NV) er en lovende og effektiv passiv teknologi til at reducere problemer med stigende kølebehov og forhøjede temperaturer i indeklimaet. Imidlertid tøver arkitekter eller designere med anvendelse af denne teknologi på grund af den høje usikkerhed om dets ydeevne, der afhænger af mange faktorer. Således foreslår denne undersøgelse en holistisk metode, der integrerer global følsomhedsanalyse, dynamiske fuldskalaeksperimenter, opbygning af energisimulering og optimering for at simulere og forbedre NV-ydeevne.

Afhandlingen analyserer først de indflydelsesrige parametre for NV-ydeevne. NV-ydeevne indikatorer gennemgås og kategoriseres først. Indflydelsen af ni designparametre på ni udvalgte ydeevneindikatorer for forskellige NV-koncepter og klimaforhold kvantificeres derefter ved at integrere Monte Carlo-simuleringer med følsomhedsanalyser. Resultaterne indikerer, at den konvektive varmeoverførselskoefficient (CHTC), niveau af termisk masse og udeluftmængden om natten er tre vigtige parametre. Indikatorernes anvendelighed og begrænsninger analyseres også på baggrund af simuleringresultaterne.

Baseret på de tre mest indflydelsesrige parametre fokuserer afhandlingen på en eksperimentel undersøgelse af konvektiv varmeoverførsel for NV. Et nyt koncept for luftfordeling, diffus loftsventilation (DCV) og et almindeligt anvendt koncept, opblandingsventilation (MV), anvendes med NV. I de eksperimentelle forsøg anvendes forskellige fordelinger af termisk masse, ventilationsluftmængder og indblæsningstemperaturer. CHTC baseret for indblæsningstemperatur som referencetemperatur er udledt, og udviklede CHTC-korrelationer skræddersyet til NV er sammenlignet med empiriske CHTC-korrelationer fra litteraturen. Sammenligningen afslører, at de empiriske sammenhænge frembringer store fejl i forudsigelse af CHTC i de fleste tilfælde. CHTC på en overflade kan i høj grad forøges ved at øge den termiske masse og påvirkes desuden lidt af de andre overfladers fordeling af termiske masse.

Endelig udføres i afhandlingen simulering og optimering af NV-ydeevne i et bygningsenergisimuleringsværktøj med de validerede korrelationer. Desuden identificeres CHTC-korrelationer for overfladerne i plenum og diffust loft ved DCV ved at sammenligne de simulerede og målte data. Simuleringresultaterne indikerer, at anvendelse af NV generelt sparer køleenergie og kan føre til overkøling i et koldt klima. DCV tilbyder et større energibesparelsespotential og bedre termisk komfort end MV. Sammenlignet med de udviklede korrelationer overvurderer de empiriske CHTC-korrelationer NV-energiebesparelsespotential og giver en uoverensstemmelse i forudsigelse af termisk komfort. Optimering af natkøling med MV og DCV kan både reducere energiforbruget betydeligt og reducere risikoen for træk. Ydeevnen af DCV forbedres også mere efter optimeringen.

ACKNOWLEDGEMENTS

The present thesis is a PhD project financed by the IEA EBC Annex 80 Resilient cooling and China Scholar Council (CSC No. 201706050001). This PhD project is under the supervision of Professor Per K. Heiselberg.

First, I appreciate a lot for my supervisor Per K. Heiselberg for his kindness, warmth, selflessness, and impressive and constructive supervision. He is the one who leads me into the world of research, broadens my horizon to the research, and gets me hooked on the challenges and sense of achievement in the field. This thesis is not just the end of a PhD study, also more like a node in my future academic career.

I would like to thank all my nice and dedicated colleagues at Aalborg University. I sincerely appreciate the nice, open, and supportive working environment. Special thanks to Chen Zhang, Mingzhe Liu, Yue Hu for the great help in sharing their knowledge of ventilation and building simulation experience and Rasmus L. Jensen, Hicham Johra, Kim T. Jønsson, Lars Isbach Poulsen, Vivi Søndergaard for all the experimental support and paper writing help.

Finally, I want to thank my family and friends for supporting and believing me to study in Denmark, a kingdom of the fairy tale. Without your so many years' support, I would not have gone so far.

Rui Guo

March 2021

TABLE OF CONTENTS

Chapter 1. Introduction	17
1.1. Principle of night ventilation.....	17
1.2. Air distribtuion principles	18
1.3. Objective of the thesis	20
1.4. Outline of the thesis.....	20
Chapter 2. Influential parameters on night ventilation performance through sensitivity analysis.....	23
2.1. Review of performance indicators.....	23
2.2. Global sensitivity analysis	24
2.2.1. Model and sensitivity analysis description	24
2.2.2. Sensitivity analysis results.....	27
2.3. Evaluation of performance indicators.....	29
2.4. Conclusion	29
Chapter 3. Experiments on convective heat transfer for night ventilation	31
3.1. Experimental descriptions.....	31
3.2. Data processing method.....	33
3.2.1. Calculation of CHTC and unCertainty analysis	33
3.2.2. General form of developed CHTC correlation	34
3.3. Experimental results of mixing ventilation	34
3.3.1. CHTC at the ceiling	35
3.3.2. CHTC at the floor	37
3.3.3. CHTC at walls	39
3.3.4. CHTC at tables	40
3.4. Experimental results of diffuse ceiling ventilation	42
3.4.1. CHTC at the floor	43
3.4.2. CHTC at walls	44
3.4.3. CHTC at tables	46
3.5. Development of simplified CHTC correlations.....	48
3.6. Conclusion	49

Chapter 4. Simulation and optimization of night ventilation performance	51
4.1. Validation of proposed correlations.....	51
4.1.1. Validation setup.....	51
4.1.2. Validation results	52
4.2. Simulation of night ventilation performance.....	53
4.2.1. Simulation setup	53
4.2.2. Simulation results	55
4.3. Optimization of night ventilation performance	57
4.3.1. Optimization setup.....	57
4.3.2. Optimization results	57
4.4. Conclusion	59
Chapter 5. Conclusions of the thesis.....	61
Chapter 6. Recommendation for future work.....	63
Literature list	65
Publication for the thesis	71
Appendices.....	73

TABLE OF FIGURES

Figure 1-1 Basic Concept of NV by (a) natural means and (b) mechanical means [6].	17
Figure 1-2 Principle of diffuse ceiling ventilation [29].	19
Figure 2-1(a) Case room model (b) plan of the three-story office building [44].	25
Figure 2-2 Outdoor air temperature and direct solar radiation of (a) Copenhagen, (b) Geneva, and (c) Rome from July 1 to September 1.	26
Figure 2-3 SRC of design parameters for the temperature efficiency [44].	28
Figure 2-4. Composition of the top three influential parameters [44].	28
Figure 3-1 Cutaway view of guarded hot box for the MV experiment [48].	32
Figure 3-2 Cutaway view of guarded hot box for the DCV experiment [49].	32
Figure 3-3 Tables (a) in the middle of the room, (b) close to walls, and (c) close to corners or walls [48].	33
Figure 3-4. Experimental values at the ceiling in the MV experiment [48].	37
Figure 3-5. Experimental values at the floor in the MV experiment [48].	39
Figure 3-6 Local air velocity contour of the (a) ceiling and (b) floor after two hours for design case 4 in the MV experiment [48].	39
Figure 3-7. Experimental values at (a) front, (b) right, (c) back, (d) left walls in the MV experiment [48].	40
Figure 3-8. Experimental values at table surfaces in the MV experiment [48].	42
Figure 3-9. Experimental values at the floor in the DCV experiment [49].	43
Figure 3-10. Experimental values at (a) front, (b) right, (c) back, (d) left walls in the DCV experiment [49].	45
Figure 3-11 Local air velocity over the front wall after two hours for design case 1 in the DCV experiment [49].	45
Figure 3-12. Experimental values at table surfaces in the DCV experiment [49].	48
Figure 4-1. (a) Vertical perspective drawing of the hot box model, (b) MV principle, and (c) DCV principle [59].	51
Figure 4-2 Measured and simulated (a) plenum air temperature and (b) diffuse ceiling temperature for design case 1 to 6 in DCV experiment [59].	53
Figure 4-3 MBE between simulated and measured surface temperatures under NV with (a) MV and (b) DCV [59].	53
Figure 4-4. Layout of case room 1NC.	54
Figure 4-5. HVAC electricity use and POR of MV cases with (a) ceiling diffuser algorithm and (b) validated correlations at night [59].	55
Figure 4-6 HVAC electricity use and POR of DCV cases with (a) ceiling diffuser algorithm and (b) validated correlations at night [59].	56
Figure 4-7 Parameters of the optimal cases and base cases [59].	58
Figure 4-8 Simulated HVAC electricity use and POR of relevant simulation cases [59].	59

Nomenclature

Latin symbols

c	Heat capacity
C	Constant
c_p	Specific heat capacity
EI	Embodied impact
h	Surface heat transfer coefficient
N	Number of data points
P	Power
q	Heat flux
OI	Operational impacts
Q	Cooling demands
t	Time
T	Temperature
\dot{m}	Airflow rate
wf	Weighing factor

Greek symbols

Δ	Change in a variable
----------	----------------------

Subscript

$conv$	Convective
$cond$	Conductive
e	end
rad	Radiative
ref	Reference
o	Outdoor
out	Outlet
s	Start
$scen$	Scenario
$surf$	Surface
i	Surface index or indoor
in	Inlet
j	Model instance j
m	Mean occupied zone temperature

Acronyms

ACH	Air change rate per hour
ADV	Ventilative cooling advantage
AHU	Air handling unit

BES	Building energy simulation
CCP	Climatic cooling potential
CFD	Computational fluid dynamics
CHTC	Convective heat transfer coefficient
COP	Coefficient of performance
CRR	Cooling requirements reduction
DCV	Diffuse ceiling ventilation
DF	Decrement factor
DhC	Degree-hours criterion
DI	Weighted discomfort temperature index
FDM	Finite difference model
LHS	Latin Hypercube Sampling
TDR	Temperature difference ratio
TE	Temperature efficiency
MBE	Mean bias error
MCA	Monte Carlo analysis
MV	Mixing ventilation
NV	Night ventilation
POR	Percentage outside the range
RMSE	Root mean squared error
SRC	Standard regression coefficient
VAV	Variable air volume

CHAPTER 1. INTRODUCTION

1.1. PRINCIPLE OF NIGHT VENTILATION

Buildings account for about 40% energy use of society, and its proportion tends to increase due to global warming [1]. The cooling energy demand of commercial buildings is predicted to increase by 275% in the mid-21st century, compared to 2016 [2]. More and more office buildings are equipped with space cooling systems in medium or cold regions of Europe [3]. Concerning the challenges of overheating and increasing cooling demand in buildings, particularly in office buildings [4], night ventilation (NV) is a hopeful and effective method to address or lessen those problems. The basic principle of NV is to cool down the building thermal mass and indoor air at night by inducing the relatively cold outdoor with mechanical or natural means (see Figure 1-1). The cooled buildings can then offer a heat sink during the next daytime to cut the cooling demands and improve thermal comfort [5].

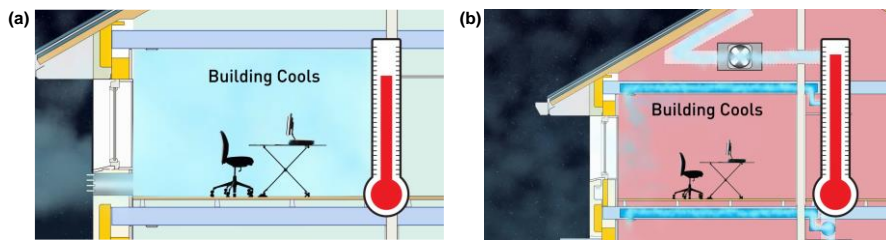


Figure 1-1 Basic Concept of NV by (a) natural means and (b) mechanical means [6].

For past decades, NV has been successfully and widely adopted [7]. However, architects or engineering still hesitates to leverage this technology despite its simple principle. The main reason is the high uncertainty of predicting the NV performance affected by many factors.

Numerous indicators have been proposed or used in prior studies to evaluate the NV performance in different aspects such as heat removal, energy-saving potential, thermal comfort [8–12]. Some indicators are independent of each other, while others have varying degrees of dependence on each other. More importantly, it is essential to have an overview of available performance indicators since the NV performance usually requires multiple types of indicators to be evaluated. Based on some performance indicators, the local or global sensitivity analysis method was leveraged to quantify the influence of relevant parameters [13–17]. Most previous studies were only for one NV mode with one daytime cooling method in one climate region or based on one or two performance indicators. To guide the NV design or optimize the NV performance, various cooling systems, performance indicators, and climatic

conditions should be considered comprehensively to identify the influential parameters.

Building energy simulation (BES) tools are usually leveraged to simulate or predict the NV performance. Unlike the main purpose of daytime mechanical cooling to ensure indoor thermal comfort, an air change rate per hour (ACH) up to 10 h^{-1} can be employed when the office buildings are not occupied at night [15]. The internal convective heat transfer coefficient (CHTC) is then more significant in accurately predicting the NV performance in BES since the convection between building elements and cold air mainly drives the heat removal at night. BES tools often use empirical values or CHTC correlations to calculate the surface's CHTC. However, those empirical values or correlations were deduced either by the steady-state or flat plate experiments [18], which may contribute to a great error in predicting NV performance. Prior research [9][19][20] experimentally investigated the convective heat transfer for NV with various air distribution principles. Those studies mainly concentrated on comparing the experimental CHTC with predicted CHTC by selected empirical correlations or analyzing the convective heat flows rather than developing the CHTC correlations tailored for NV. More importantly, those experiments were only based on one thermal mass level that was another important factor for the NV performance. BES tools can allow the users to set detailed envelope construction for the interior surface (e.g., ceiling, floor, walls), which can accurately consider the surface' thermal mass level. However, the furniture in the real environment is treated as the virtual equivalent planar elements in BES [21], which might not accurately consider the thermal mass of indoor furniture. Therefore, it is essential to experimentally develop the CHTC correlations tailored for NV under different thermal mass distribution (indoor furniture included) schemes.

A few studies optimized parameters that include the ACH and thermal mass level for NV design [22–25] to improve energy efficiency or thermal comfort. However, those optimization studies were based on a single performance indicator and used the one-time-factor method (i.e., altering one parameter while fixing the remaining parameters) with a few and wide parameter distribution intervals. Thus, the interaction between different parameters was rarely considered. Those studies might only find the local rather than the global optimal NV design solution. Simulation-based optimization has become a popular approach for improving building performance while fulfilling several constraints [26], which can be leveraged to optimize the NV performance comprehensively.

1.2. AIR DISTRIBUTION PRINCIPLES

Air distribution principles of ventilation are crucial for the indoor built environment. The efficient distribution of airflow in rooms and the energy-efficient elimination of heat and ventilation loads have been the focus of research over the last few decades. The air distribution principles can be divided into different types, such as mixing

ventilation (MV), diffuse ceiling ventilation (DCV), wall attached ventilation, and displacement ventilation [27]. Numerous studies have experimentally or numerically investigated the contaminant/heat removal effectiveness, indoor thermal comfort, protection efficiency, air exchange efficiency during the occupied hours [28]. However, few studies have been devoted to comparing NV performance with various air distribution principles in BES. As mentioned before, only a few studies [9][19][20] experimentally analyzed the effect of NV with wall attached ventilation, mixing ventilation, and displacement ventilation, which were not applicable in BES.

In those air distribution principles, DCV is relatively new, with the basic principle of supplying the air into the occupied room by penetrating the diffuse ceiling panel [27]. The DCV system consists of three components: plenum, diffuse ceiling, and occupied room, as shown in Figure 1-2.

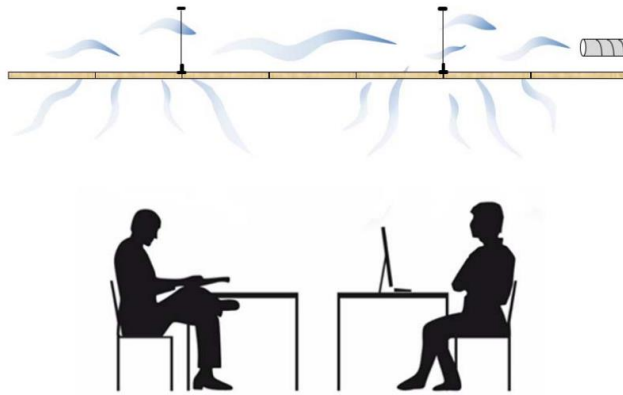


Figure 1-2 Principle of diffuse ceiling ventilation [29].

The plenum serves as a “duct” to supply air and can reduce or replace the normal duct. The suspended ceiling then acts as an “air diffuser” for air distribution [30]. For the sake of the large area of the suspended ceiling, the supply air velocity is quite low, which allows the DCV to deliver extremely cold air without elevating the draught’s risk [31]. Besides, the pressure drop across the suspended ceiling (<1.5 Pa) is quite low, which saves energy from fans and offers the potential for natural ventilation [32]. A design chart was put forward to compare the cooling capacity of different air distribution principles, which disclosed that the DCV had the highest cooling capacity (72 W/m^2) to remove the internal heat load [33]. DCV was expected to offer a great NV potential due to the advantages mentioned above [29]. Nevertheless, only two studies investigated the surface cooling effect and heat transfer of night cooling with DCV [34][35]. Those studies focused on the plenum rather than the occupied room that directly impacted the energy consumption and occupants’ thermal comfort. More significantly, no previous studies simulated the energy performance of DCV in BES tools [31]. The main reason is the lack of CHTC correlations tailored for DCV. Only

a room with thermally activated building systems in the ceiling slab under the DCV scenario was simulated in a BES tool [36]. The CHTC correlations selected in this study were unknown.

Therefore, the study of night cooling performance with DCV in BES tools is an area of research that needs to be filled. Additionally, other air distribution principles can also be selected for comparison. MV is a representative and the most widely used ventilation principle, where high momentum air is supplied from the sidewall or ceiling diffuser to mix with the room air directly, thereby diluting the concentration of pollutants and cooling or heating the room [28].

1.3. OBJECTIVE OF THE THESIS

The thesis aims to define, investigate and evaluate the NV performance in office buildings for improving building design, to be more energy-efficient, and to provide a better indoor thermal comfort for occupants. The investigations will be realized using different research tools such as building energy simulation (BES) and full-scale laboratory experiments. The specific objectives include:

- (1) To obtain a deep understanding of the influencing parameters on the NV performance through a systematic analysis and sensitivity study of the impact of different design parameters.
- (2) To develop CHTC correlations tailored for NV under various air distribution principles, thermal mass distributions, supply temperatures, and airflow rates.
- (3) To provide new solutions for optimal design and operation of NV using a global optimization algorithm, by applying thermal mass distribution, by employing air distribution principles, and by developing a new ventilation control strategy.

1.4. OUTLINE OF THE THESIS

Chapter 1 introduces the research background and objective of this thesis, of which the night ventilation principle and air distribution principles are addressed.

Chapter 2 reviews the NV performance indicators and conducts the Monte Carlo simulations to identify the significance of various parameters on those indicators based on the global sensitivity analysis and evaluate the usefulness of those indicators.

Chapter 3 describes the experiments on the convective heat transfer of NV. Two air distribution principles (MV and DCV) and various thermal mass distribution schemes, ACHs, and supply temperatures are designed to develop CHTC correlations tailored for NV.

Chapter 4 validates the proposed CHTC correlations from experiments before simulating and comparing the performance of NV with DCV and MV in BES tools. Moreover, an optimization method is proposed to improve the performance in the field of energy-saving potential and indoor thermal comfort.

Chapter 5 summarizes the conclusions of the work demonstrated.

Chapter 6 closes the thesis with recommendations for future work.

CHAPTER 2. INFLUENTIAL PARAMETERS ON NIGHT VENTILATION PERFORMANCE THROUGH SENSITIVITY ANALYSIS

Before evaluating or predicting the NV performance, it is necessary to have a basic knowledge about the available indicators. This chapter firstly reviews the performance indicators for NV. A global sensitivity analysis method is then adopted to identify the influential parameters on different performance indicators. At last, the usefulness of performance indicators is evaluated. This chapter aims to find the crucial parameters for NV design and operation as well as the useful indicators for subsequent research.

2.1. REVIEW OF PERFORMANCE INDICATORS

The performance indicators for evaluating NV can be categorized into four types, which are (1) heat removal effectiveness, (2) energy efficiency, (3) reduction in cooling energy use, and (4) thermal comfort improvement [37]. The first type quantifies the effectiveness of purging the stored excess heat. The second type indicates the ability to provide cooling energy. The third type represents the energy-saving potential for mechanical cooling. The last type is the ability to reduce the uncomfortable percentage during the occupied period. Table 2-1 summarizes the NV performance indicators from the literature. The meaning of symbols can be seen in Nomenclature. For more detailed information about performance indicators, please refer to [37].

Table 2-1 Summary of NV performance indicators.

Type of indicators	Indicator	Equation	Brief definition	Source
Heat removal effectiveness	Ventilation effectiveness for heat removal (VEHR)	$\frac{T_{out} - T_{in}}{T_m - T_{in}}$	Depends on air distribution systems, temperature difference between supply and exhaust air, airflow rate, and location of internal heat source	[8]
	Temperature difference ratio (TDR)	$\frac{T_{o,max} - T_{i,max}}{T_{o,max} - T_{o,min}}$	A higher TDR implies a greater difference between indoor and outdoor temperatures and a more efficient NV.	[38]
	Temperature efficiency (TE)	$\frac{T_{out} - T_{in}}{T_{surface} - T_{in}}$	Yields from the measurement and mainly depends on the airflow rate and air distribution principles.	[9]
	Decrement factor (DF)	$\frac{T_{i,max} - T_{i,min}}{T_{o,max} - T_{o,min}}$	The ratio of indoor temperature variation to outdoor temperature variation.	[39]
Energy efficiency	Coefficient of performance (COP)	$\frac{\int_{t_s}^{t_e} \dot{m}_{air} c_p (T_i(t) - T_o(t)) dt}{\int_{t_s}^{t_e} P_e(t) dt}$	The ratio of the cooling energy supplied to the electricity use of fans. A higher COP implies a greater energy saving contributed by NV.	[10]

	Potential energy efficiency (PEE)	$\frac{\int_{t_s}^{t_e} \dot{m}_{air} c_p (T_o(t) - T_{out}(t)) dt}{\int_{t_s}^{t_e} P_e(t) dt}$	The ratio of energy removal to the electricity use of fans. A higher PEE may be attributed to the tuning of NV system.	[40]
	Seasonal energy efficiency ratio (SEER)	$\frac{Q_{t,c}^{ref} - Q_{t,c}^{scen}}{Q_{el,v}}$	The ratio of the saved cooling demand to electricity use of fans. A higher SEER implies a greater energy-saving benefit.	[5]
	Ventilative cooling advantage (ADV)	$\frac{Q_{el,c}^{ref} - Q_{el,c}^{scen}}{Q_{el,v}}$	The ratio of the saved cooling energy use to the electricity use of fans. A higher ADV implies a great energy-saving benefit.	[5]
	Life cycle efficiency ratio (LCER)	$\frac{OI_{ref} - OI}{EI - EI_{ref}}$	Evaluates the environmental benefit of NV with different thermal inertia systems. A higher LCER implies a larger life cycle benefit.	[41]
Reduction in cooling energy use	Cooling requirements reduction (CRR)	$\frac{Q_{t,c}^{ref} - Q_{t,c}^{scen}}{Q_{t,c}^{ref}}$	The ratio of saved cooling demand to the reference case's cooling demand. A positive CRR implies an energy-saving benefit, not vice versa.	[5]
	Degree-hours criterion (DhC)	$\sum_{t=1}^{oh} (w f_i \cdot h_i)$	The accumulation of hours that the indoor operative temperature above 26°C during the occupied period. A lower DhC implies better thermal comfort.	[11]
Thermal comfort improvement	Percentage outside the range (POR)	$\frac{\sum_{t=1}^{oh} (w f_i \cdot h_i)}{\sum_{t=1}^{oh} (h_i)}$	The percentage of thermal comfort parameters outside a prescribed level. Different thermal comfort models can be applied. A lower POR implies better thermal comfort.	[42]
	Weighted discomfort temperature index (DI)	$\sum (T_i - T_{comf,sup})^2$	Discomfort weighted on the distance of calculated indoor temperature from the acceptable temperature interval (e.g., 28°C). A lower DI implies better thermal comfort.	[12]

NV should be evaluated by selecting the appropriate performance indicators according to the application conditions (e.g., experiment or simulation). It is worth noting that the NV performance usually cannot be evaluated well with a single indicator, which needs to integrate different indicators. Quantifying the influence of various parameters on the indicators allows architects, engineers, or researchers to pay more attention to the crucial parameters for the selected performance indicators. This study selects nine representative performance indicators that can be adopted in the simulation research for the sensitivity analysis, which are TE, TDR, DF, COP, ADV, CRR, POR, DhC, and DI.

2.2. GLOBAL SENSITIVITY ANALYSIS

2.2.1. MODEL AND SENSITIVITY ANALYSIS DESCRIPTION

To conduct the global sensitivity analysis using BES, a case room in a three-story office building located in Aarhus, Denmark, is selected and constructed in a BES tool, EnergyPlus. Figure 2-1 shows the case room model and the plan of the office building. The case room (zone 1W) is located on the second floor, with a floor area of 51.3 m². The adiabatic boundary conditions are set for the internal walls between room 1W and

adjacent zones to assume identical thermal conditions for eliminating the heat conduction between adjacent zones. Room 1W is set with six occupants [43].

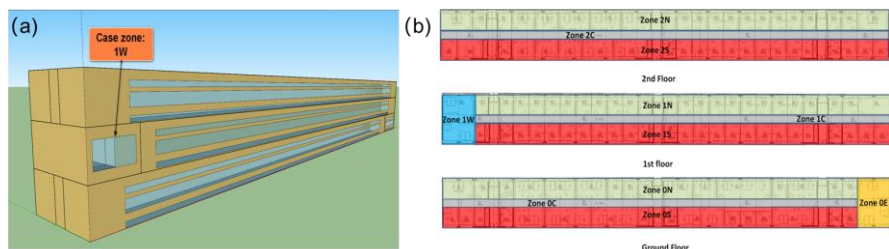
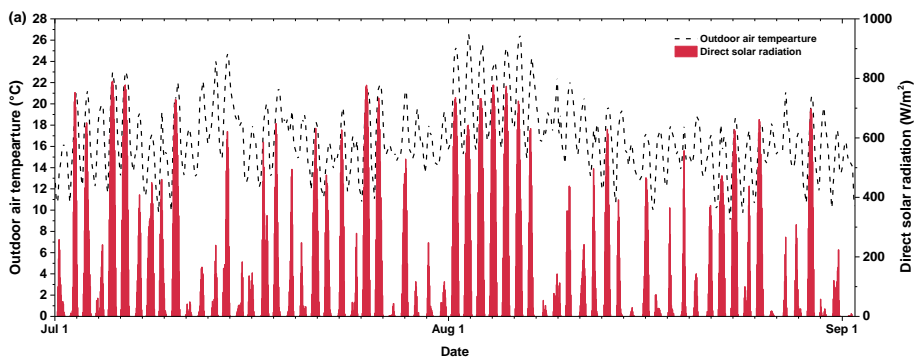


Figure 2-1(a) Case room model (b) plan of the three-story office building [44].

The typical meteorological year (TMY3) data [45] in summer (July 1 to September 1) of Copenhagen 061800 (IWEC), Geneva 067000 (IWEC), and Rome 162420 (IWEC) are selected to study the impact of climate conditions on NV performance. Copenhagen represents the cold climate regions, while Geneva and Rome represent the medium and hot climate regions, respectively. Figure 2-2 shows the outdoor dry-bulb air temperature and direct solar radiation between July 1 and September 1 of three cities. Table 2-2 summarizes the statistics on the direct solar radiation and outdoor air temperature of three cities. It indicates a gradient difference between the climate data in the three cities.



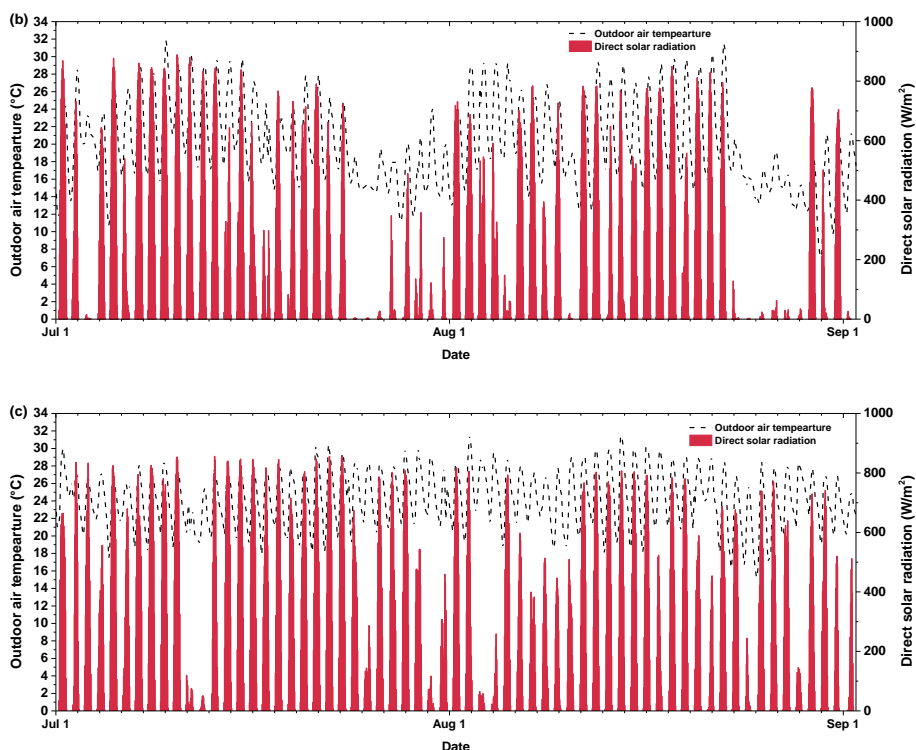


Figure 2-2 Outdoor air temperature and direct solar radiation of (a) Copenhagen, (b) Geneva, and (c) Rome from July 1 to September 1.

Table 2-2 Statistics on the direct solar radiation and outdoor air temperature of three cities.

City	Maximum daily direct solar radiation range (W/m ²)	Average daily outdoor air temperature range (°C)
Copenhagen	9.2 W/m ² – 790.8 W/m ²	10.4 °C – 21.7 °C
Geneva	15.1 W/m ² – 888.4 W/m ²	13.9 °C – 24.7 °C
Rome	50.7 W/m ² – 858.2 W/m ²	21.0 °C – 26.4 °C

Different cooling systems are also equipped with room 1W for comprehensive research. For daytime cooling methods, air conditioner (AC), natural ventilation, and mechanical ventilation are selected separately. While for the NV, natural and mechanical systems are chosen. Therefore, there are five cooling systems to be investigated, which can be abbreviated as (1) “Daytime AC + Night MecVent”, (2) “Daytime AC + Night NatVent”, (3) “All Day NatVent”, (4) “All Day MecVent”, (5) “Daytime MecVent + Night NatVent”. The daytime cooling method operates during the 08:00 – 17:00 on summer weekdays, while the NV system works during 17:00 – 08:00 on summer weekdays. Nine design parameters are selected and equipped with discrete, uniform, and triangular distribution, respectively. For more detailed

information about cooling systems and design parameters, please refer to Appendix A [44].

Global sensitivity analysis can simultaneously vary all the input variables, demonstrating the outputs' variations considered by the input factors compared to the local sensitivity analysis [46]. It might be time-consuming and impossible to conduct all parametric simulations, especially when there are continuous input variables. Therefore, the most widely used Monte Carlo analysis (MCA) method is adopted. Latin hypercube sampling (LHS) is then used to produce samples from nine design parameters with a sample size of 400 [47]. The parametric simulations based on the generated sample are conducted by coupling EnergyPlus with the parametric simulation manager jEPlus. After obtaining the results (i.e., values of performance indicators) from parametric simulations, the regression method is then applied. The software SimLab v2.2 is used for the regression method to calculate the standardized regression coefficient (SRC) of each input variable (i.e., design parameter). A positive value of SRC denotes that the indicator's value increases as the associated design parameter's value grows. A greater absolute value of SRC indicates that the associated design parameter is more significant.

2.2.2. SENSITIVITY ANALYSIS RESULTS

Figure 2-3 depicts the SRC of design parameters for the temperature efficiency (TE) in different cooling systems and climate conditions. It is worth noting that P6 has two sub-parameters, of which the discharge coefficient is the sub-parameter for the window opening under the natural ventilation scenario, and the night ACH is the sub-parameter for night mechanical ventilation. The top three significant parameters are colored with red, yellow, and green.

It can be seen that the SRC of design parameters differs a lot for temperature efficiency in diverse cooling systems and climate conditions. The internal CHTC ranks first in most cases. Even for the "All Day MecVent" system, the internal CHTC is the second influential parameter. With the increase of internal CHTC, the TE grows. For P6, the night ACH has a large SRC for night mechanical ventilation systems, while the SRC of discharge coefficient for night natural ventilation systems is small. The reason should be that the range of discharge coefficient is relatively narrow, which does not make a great difference in the airflow rate. Increasing the ACH tends to reduce the temperature efficiency. It is worth noting that TE is often applied in a mathematical model in combination with building information, ACH, and climate cooling potential to estimate the heat removed by NV [9]. The window-wall ratio is also a significant parameter for the temperature efficiency, which ranks second or third among all the parameters in most scenarios. The increase in window-wall ratio tends to decrease the temperature efficiency. In the "Daytime MecVent+Night NatVent" system, the internal thermal mass is influential and gets more important in a cold climate.

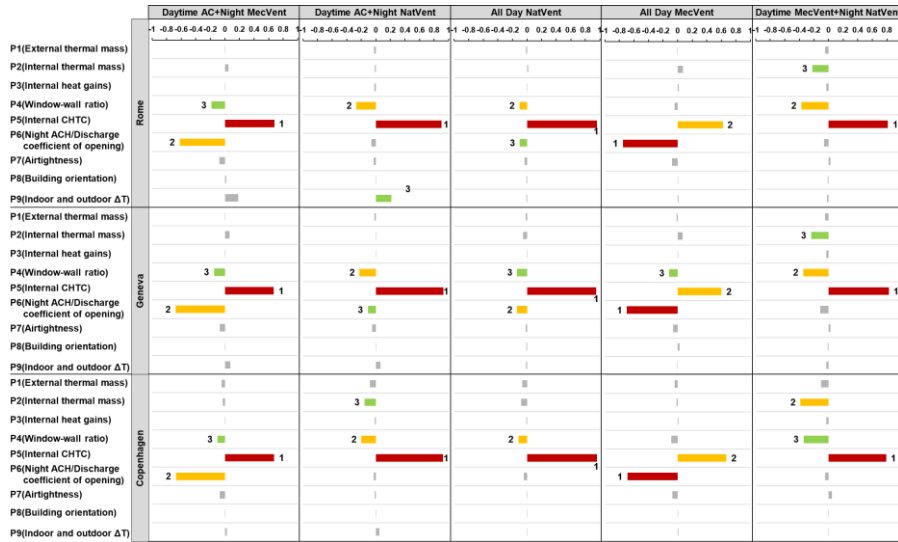


Figure 2-3 SRC of design parameters for the temperature efficiency [44].

The sensitivity analysis results of the remaining performance indicators with the similar interpolation method in Figure 2-3 can be referred to Appendix A [44]. Finally, the top three influential parameters for each indicator are counted to demonstrate the composition of the top three important parameters (see Figure 2-4). Window-wall ratio is the most influential parameter for more than half of the performance indicators, followed by the internal CHTC, internal thermal mass, and night ACH [44]. Those four parameters also account for more than 90% in the second important parameter composition and about 70% in the third important parameter composition. The building airtightness and internal heat, external thermal mass, and DeltaT (i.e., NV activation threshold temperature) should be paid attention to in some scenarios [44]. All the performance indicators are not sensitive to the remaining two design parameters (i.e., discharge coefficient of the opening and building orientations).

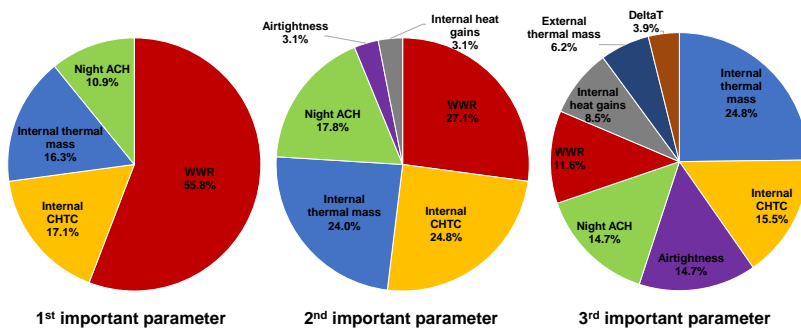


Figure 2-4. Composition of the top three influential parameters [44].

2.3. EVALUATION OF PERFORMANCE INDICATORS

The usefulness and unavailability of performance indicators are evaluated based on the sensitivity analysis results and parametric simulations' outputs. The indicators of heat removal effectiveness should be carefully adopted. For instance, TE is only applicable to compare the NV performance under the same ACH scenario directly. Otherwise, it needs to combine other parameters like climate cooling potential, building parameters, and ACH in a simple model [8] to estimate the amount of heat removed. Similarly, DF is suitable for the evaluation of different NV systems with the same building parameters. Moreover, TDR is only suitable to compare the NV performance under the same climate condition since the definition of TDR is based on the ambient temperature fluctuation.

ADV and CRR are appropriate indicators to evaluate the mechanical NV and natural NV systems, respectively. The value and sign of ADV and CRR can directly indicate whether the NV can save energy or not. The COP in this study originates from the definition of "COP" for AC performance. However, a COP larger than 1 does not necessarily save the total (i.e., daytime + night cooling systems) cooling energy. Therefore, the COP is only suitable for the evaluation of ventilation energy efficiency during the nighttime.

Among the thermal comfort improvement indicators, POR is the best indicator as it provides a straightforward explanation of percentages beyond the comfort range between 0 and 100%. It is also applicable to compare different NV systems under various climate conditions. More importantly, different thermal comfort models (e.g., Fanger, Adaptive) or parameters (e.g., operative temperature) can be used with POR. In contrast, DhC and DI both have their disadvantages and limitations. For instance, the threshold temperature for thermal comfort is too simple, either the indoor air temperature (e.g., 28°C) or the operative temperature (e.g., 26°C). Besides, the two indicators are cumulative indexes, which might not demonstrate thermal comfort intuitively without comparison.

2.4. CONCLUSION

This chapter firstly reviews the NV performance indicators in the literature. A holistic method integrating the global sensitivity analysis with Monte Carlo simulations is then adopted to identify the crucial parameters for NV performance. Finally, the usefulness and constraints of the indicators are evaluated. The following conclusions can be drawn:

The influence of design parameters on selected indicators depends significantly on climatic conditions and NV principles [44]. The four most influential design parameters are window-wall ratio, internal CHTC, internal thermal mass level, and night ACH [44]. The building airtightness, internal heat gains, external thermal mass,

and NV activation threshold temperature are influential for a few performance indicators under certain scenarios [44]. All the performance indicators are not sensitive to the discharge coefficient of the opening and building orientations.

There are limitations and disadvantages to some performance indicators. TE is only applicable to compare the NV performance under the same ACH scenario directly, and DF is suitable for evaluating different NV systems with the same building parameters. TDR is only suitable to compare the NV performance under the same climate condition. DhC and DI might be simplistic with the thermal comfort threshold temperature and not demonstrate thermal comfort intuitively without comparison. COP is only applicable to evaluate the ventilation energy efficiency during the nighttime. In summary, ADV (for mechanical NV), CRR (for natural NV), and POR are recommended for NV performance evaluation.

CHAPTER 3. EXPERIMENTS ON CONVECTIVE HEAT TRANSFER FOR NIGHT VENTILATION

Chapter 2 demonstrates that the internal CHTC, internal thermal mass, and night ACH are influential parameters for NV performance [44]. The internal CHTC in BES tools is calculated by the empirical CHTC correlations developed from the steady-state full-scale or flat plate experiments. Those correlations are not tailored for NV, which might cause an error in calculating the CHTC and cause a large error in predicting NV performance. Therefore, two air distribution principles of mixing ventilation (MV) and diffuse ceiling ventilation (DCV) are integrated with NV in a guarded hot box for dynamic full-scale experiments, respectively. Different supply temperatures, airflow rates, and thermal mass distribution schemes are designed for the experiments to develop the CHTC correlations tailored for NV.

3.1. EXPERIMENTAL DESCRIPTIONS

A guarded hot box is leveraged for night cooling experiments with MV (see Figure 3-1) and DCV (see Figure 3-2). The hot box contains the guarding zone, upper zone, test room. The upper zone and test room are covered by the guarding zone that is conditioned by an air handling unit (AHU) with a constant zone air temperature of 22 °C [48]. The conditioned air is supplied to the test room directly (MV) or to the upper zone firstly (DCV) by another AHU to simulate the night cooling. The test room acts as an office room without any internal heat gains. Besides, the envelope in the hot box is well insulated. The main difference between the MV experiment and the DCV experiment is the test room's ceiling material. For the MV experiment, the ceiling is made up of 12 mm wood panels and 50 mm foam boards. For the DCV experiment, the porous wood-cement boards that allow the air to penetrate are adopted. Moreover, the inlet's position is different for the two experiments. While the outlet for the two experiments is the same, locating in the lower right corner of the test room's front wall [48].

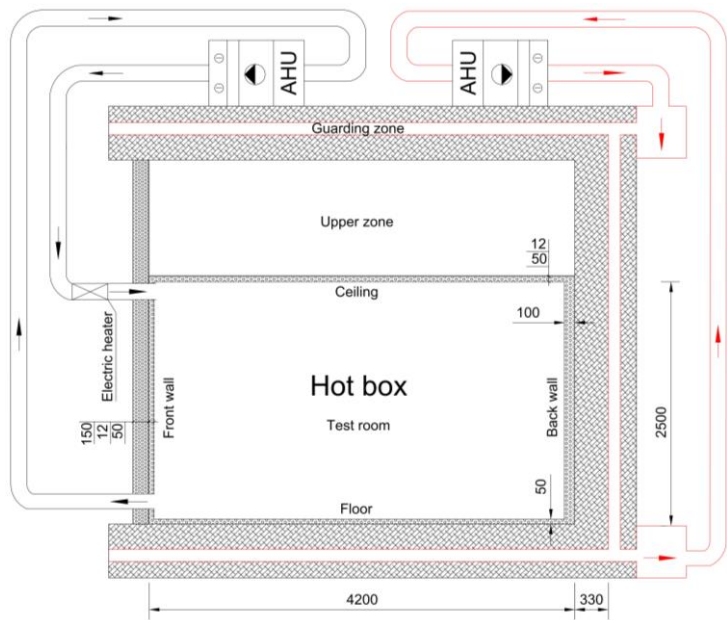


Figure 3-1 Cutaway view of guarded hot box for the MV experiment [48].

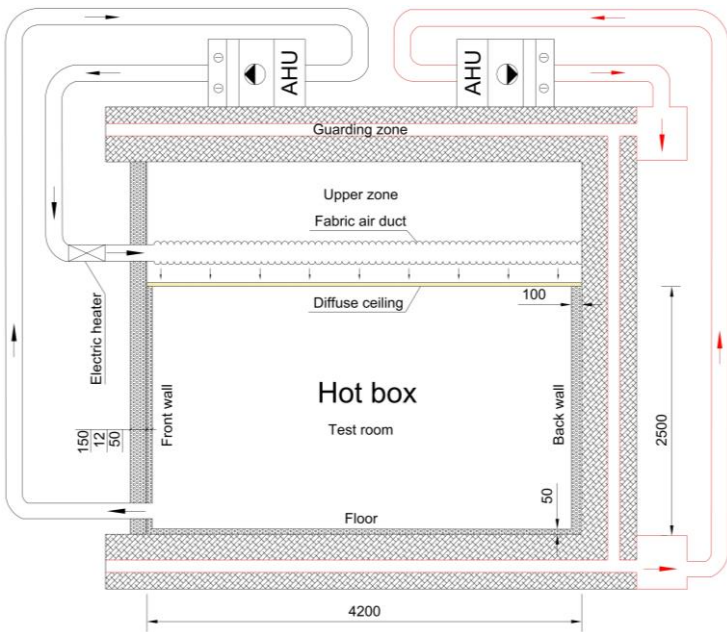


Figure 3-2 Cutaway view of guarded hot box for the DCV experiment [49].

The 18 mm fermacell® fiber plasterboards with a high dynamic heat capacity are placed on the test room's interior surface to form different thermal mass distribution schemes. Moreover, four indoor tables (furniture) made up of fiber plasterboards are also placed in different positions in the test room (see Figure 3-3). There are 48 design cases for the MV experiment and 25 design cases for the DCV experiment. Those design cases contain different thermal mass distribution schemes, supply ACHs, and initial difference (ΔT_0) between the supply and indoor temperatures. For each design case, the conditioned air at the specified airflow rate and the temperature is continuously supplied to the steady-state test room (indoor air and surface temperatures are 22 °C) for eight hours for cooling.

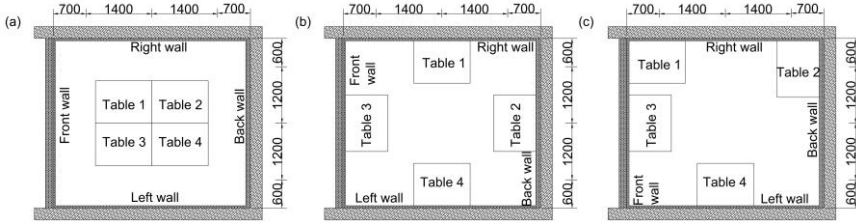


Figure 3-3 Tables (a) in the middle of the room, (b) close to walls, and (c) close to corners or walls [48].

The measured parameters in the two experiments include surface temperatures, air temperatures, temperature differences between interior and exterior surfaces, airflow rate, and air velocities. Each interior surface is equally divided into nine parts, of which the centre of each part is installed with the temperature (by type K thermocouples) and temperature difference (by thermopiles) measuring points. Hot-sphere anemometers are also placed in special movable columns to measure the local air velocity 50 mm away from the aforementioned measuring points. FTMU UltraLink airflow sensor is used to measure the airflow. All the data are recorded every 10s. For more detailed information about the experiment setup, please refer to Appendix B [48] and Appendix C [49].

3.2. Data processing method

3.2.1. CALCULATION OF CHTC AND UNCERTAINTY ANALYSIS

Equation (3-1) is used to calculate the CHTC at surface i .

$$h_{conv,i} = \frac{q_{conv,i}}{(T_{ref} - T_{surf,i})} = \frac{q_{cond,i} - q_{rad,i}}{(T_{ref} - T_{surf,i})} \quad (3-1)$$

where $q_{conv,i}$ is the convective heat flux of surface i , T_{ref} is the reference temperature, and $T_{surf,i}$ is the surface i temperature. $q_{conv,i}$ is then derived based on the conductive heat flux ($q_{cond,i}$) and radiative heat flux ($q_{rad,i}$). A 1D transient finite difference

model (FDM) [50] is adopted to calculate the $q_{\text{cond},i}$. The measured surface temperatures are the boundary conditions for 1D transient FDM. On the other hand, the radiosity method [51] is selected to calculate the $q_{\text{rad},i}$. The view factor between surfaces for the radiative heat transfer is calculated by the adaptive integration method (for design cases with tables) [52] and perpendicular and parallel rectangular plates method (for design cases without tables) [53].

Similar to the global sensitivity analysis introduced in Section 2.2, the MCA method is also adopted to estimate the uncertainty of results considering the uncertainties of the material properties the accuracy of measurement equipment, which are assumed with the normal distribution. According to those uncertainties and accuracy, the LHS method is also leveraged to produce the input variable with a sample size of 300. After experimental results (e.g., CHTC) based on the generated sample are obtained, total uncertainties of experiment results are then calculated. For more detailed information about the data processing method, please refer to Appendix B [48] and Appendix C [49].

3.2.2. GENERAL FORM OF DEVELOPED CHTC CORRELATION

The Equation (3-2) originates from Fisher [54] is selected as the general form for developing the CHTC correlations tailored for NV. The reason is that NV usually drives the forced convection regime in the enclosure [20]. For detailed information about the general form, please refer to Appendix B [48].

$$h = C_1 + C_2 \cdot ACH^m, \quad 0.5 \leq m \leq 0.8 \quad (3-2)$$

where C_1 and C_2 are two constants, the m is the exponent. The exponent of 0.5 and 0.8 denotes the general form is for laminar flow and turbulent flow, respectively. When the exponent lies between 0.5 and 0.8, the general form is for the transitional flow.

The surface-averaged experimental CHTC selects the supply reference temperature. Apart from the reason that forced convection correlations usually select the supply temperature as reference [18]. It is difficult to accurately determine the average indoor temperature because of the uneven air distribution in MV and DCV. Moreover, compared to other reference temperatures (e.g., outlet, local and indoor), the supply temperature can contribute to the lowest uncertainty of CHTC due to the highest temperature difference in Equation (3-1).

3.3. EXPERIMENTAL RESULTS OF MIXING VENTILATION

The experimental CHTCs are also compared with the predicted CHTCs by existing empirical CHTC correlations. The comparable correlations developed using a radial ceiling diffuser by Fisher & Pedersen [55] and a sidewall inlet by Fisher [54] are

selected, as shown in Table 3-1 and Table 3-2. The correlations are available when ACH ranges between 3 and 12 h⁻¹. It should be noticed that the Fisher's ceiling correlation also depends on the Archimedes number, which is not selected for comparison in this Chapter.

Table 3-1 Radial ceiling diffuser CHTC correlations [55].

Surface	Correlations
Ceiling	$h = 0.49ACH^{0.8}$
Floor	$h = 0.13ACH^{0.8}$
Walls	$h = 0.19ACH^{0.8}$

Table 3-2. Sidewall inlet CHTC correlations [54].

Surface	Correlations
Floor	$h = 0.698 + 0.173ACH^{0.8}$
Walls	$h = -0.109 + 0.135ACH^{0.8}$

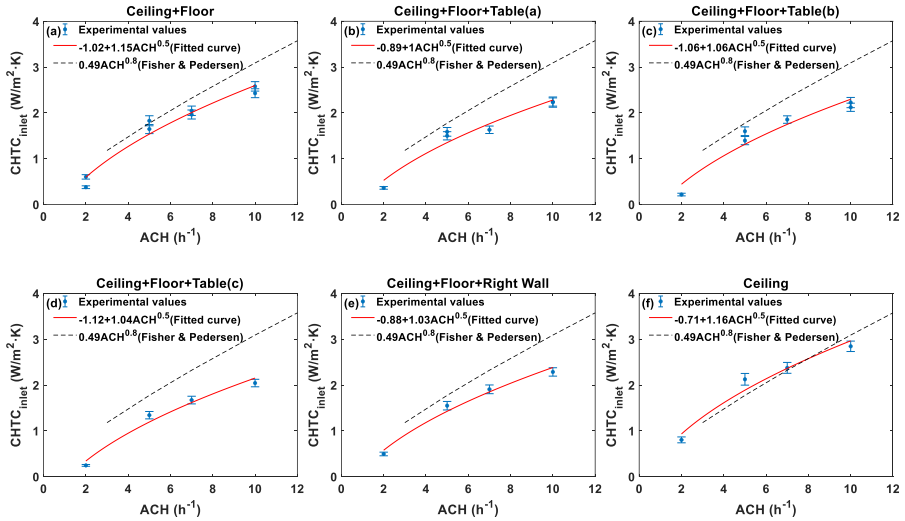
3.3.1. CHTC AT THE CEILING

To develop the correlations based on the experimental CHTC, the curve fitting toolboxTM [56] in MATLAB is adopted using the nonlinear least square method. Figure 3-4 illustrates the experimental CHTCs at the ceiling, developed correlations, and empirical radial ceiling diffuser ceiling correlation. The titles above sub-figures represent the thermal mass (i.e., fiber plasterboards) distribution scheme. For instance, “Ceiling + Floor + Table(a)” means that the ceiling and floor have thermal mass, and four indoor tables are in the middle of the room. The R^2 (coefficient of determination) of developed correlations (i.e., fitted curves) is between 0.93 and 0.99. The uncertainty of experimental value ranges between $\pm 4\%$ and $\pm 10\%$.

It is worth noting that several ACH points in Figure 3-4a, b, c have a pair of experimental values. The pair of values is derived from the design cases with two different ΔT_0 (5 or 10 °C) with the aim of initial trials that whether the ΔT_0 is influential on the experimental value. It can be seen that the pair of experiment values under the same ACH is very close, indicating that CHTC is almost not dependent on ΔT_0 . This can be explained that the inlet momentum is the main source to drive the forced convection under the NV scenario. However, it can be observed in Figure 3-4a, the discrepancy between the pair of experiment values at the ACH of 2 h⁻¹ is a little bit high (37%). It indicates that the flow over the ceiling should be laminar at low ACH. Thus, the exponent m of developed correlations is the lower bound (i.e., 0.5). Whereas the absolute difference between the pair of values is 0.22 W/m²·K, which should be tolerable for the NV performance simulation in BES tools.

By comparing the experimental values with predicted values by the empirical correlation, the experimental values are smaller than those in most cases. When only the ceiling has thermal mass (Figure 3-4f), those two correlations overlap a lot. Compared to the ceiling without thermal mass (Figure 3-4g to j), the ceiling with thermal mass (Figure 3-4a to f) has a much greater CHTC. One reason is that the thermal mass offers a greater dynamic heat capacity to store and release more heat. Another reason should be that the thermal mass reduces the congruence of local air temperature and interior surface temperature, which retains a larger temperature difference for a longer time for the thermal mass to release more heat [48].

For design cases that the ceiling has thermal mass (Figure 3-4a – f), the developed correlations are slightly different from each other. This phenomenon can also be found in the design cases that the ceiling does not have the thermal mass (Figure 3-4g – j). The reason is that other interior surface's (i.e., floor, wall) thermal mass level lead to a different surface temperature that affects the radiative heat flux over the ceiling. Similarly, Dréau et al. [20] indicated that surfaces' emissivity could affect the radiative heat transfer in the room; thus, impacting the CHTC at other individual surfaces. It should be noticed that the empirical correlations do not reflect this discrepancy since they were deduced from the isothermal and steady-state experiments, which almost eliminated the radiative heat transfer between interior surfaces. At last, it can be observed that the developed correlations for design cases with indoor tables (Figure 3-4b, c, d) are similar, indicating that the position of indoor tables has a negligible effect on the experiment CHTC at the ceiling.



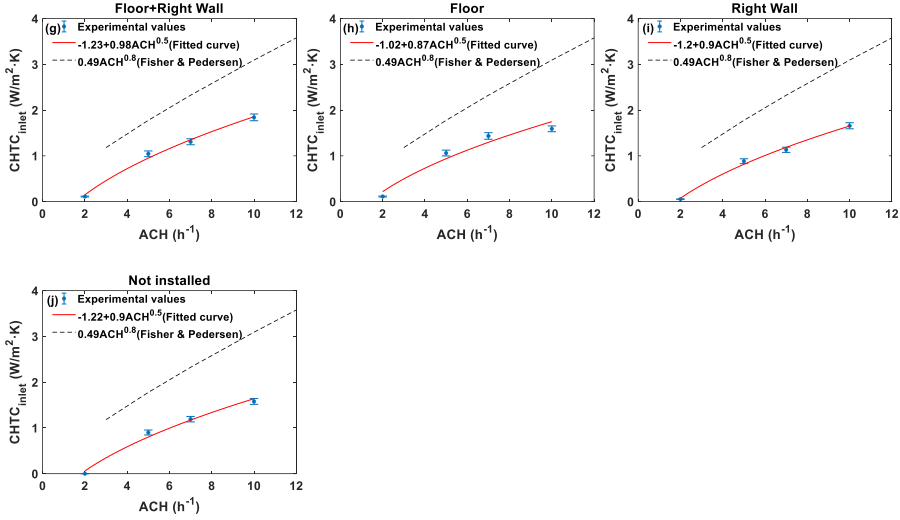


Figure 3-4. Experimental values at the ceiling in the MV experiment [48].

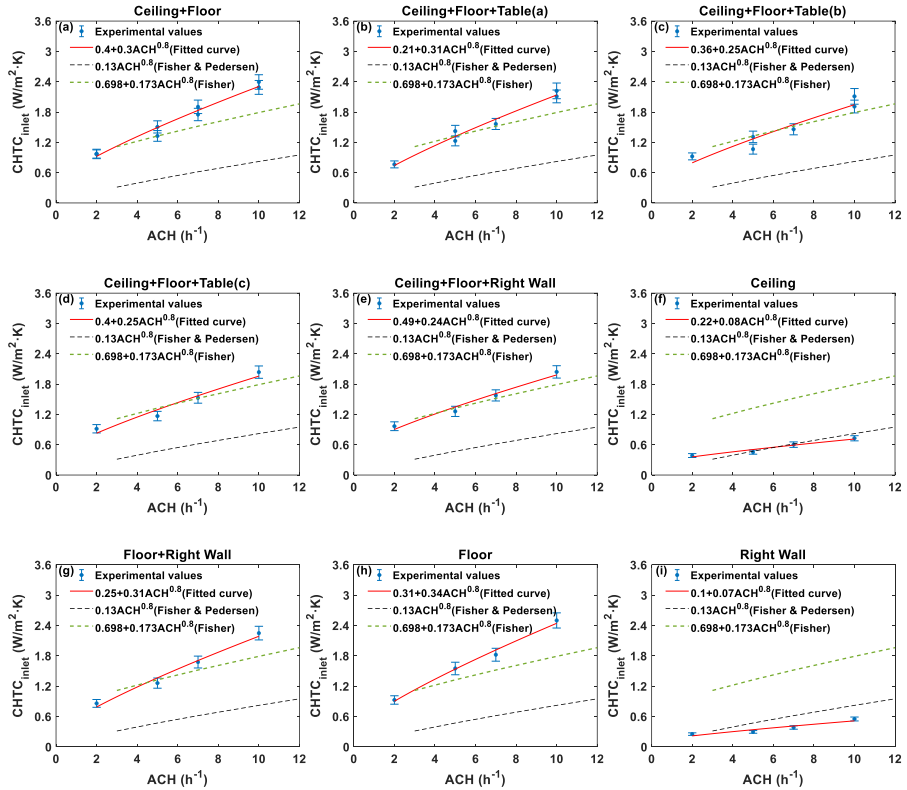
3.3.2. CHTC AT THE FLOOR

Figure 3-5 illustrates the experimental values at the floor, developed correlations, and two empirical floor correlations. The R^2 of developed correlations is between 0.91 and 0.99. The uncertainty of experimental value ranges between $\pm 6\%$ and $\pm 10\%$.

By comparing the design cases in Figure 3-5f, i, j with the remaining design cases, the floor with thermal mass has a quite larger CHTC than the floor without thermal mass under the same ACH. It indicates that the thermal mass also augments the CHTC on the floor. The sidewall inlet (i.e., Fisher) floor correlation predicts larger CHTC than the radial ceiling diffuser (i.e., Fisher & Pedersen) floor correlation when the ACH is the same. The reason is that the sidewall inlet (middle of a wall) delivers a free horizontal jet that covers a larger area of the floor than the radial ceiling diffuser and has a higher velocity.

By comparing the experimental values with the empirical correlations, the sidewall inlet floor correlation overestimates the experimental values of design cases that the floor without thermal mass. However, it predicts the CHTCs of design cases with thermal mass relatively accurately, especially the design cases in Figure 3-5e. On the contrary, radial ceiling diffuser floor correlation predicts relative accurately when the floor has thermal mass but underestimates the CHTCs when floor without thermal mass. The correlations of design cases with indoor tables (Figure 3-5b, c, d) are similar, indicates that the position of indoor tables also has a minor effect on the experimental CHTCs at the floor.

The exponent m in the developed correlations is 0.8, which indicates that the flow is turbulent over the floor even at the ACH of 2 h^{-1} . Thus, the experimental values of design cases with different ΔT_0 are almost the same at the ACH of 2 h^{-1} (see Figure 3-5a), which is different from the ceiling situation. Figure 3-6 shows the ceiling and floor's local air velocity contour after two hours for design case 4 in the MV experiment (i.e., ACH of 2 h^{-1} , ΔT_0 of 10°C , “Ceiling + floor”). The velocity contour is interpolated and extrapolated based on the measured air velocities 50 mm away from the ceiling and floor. The red arrow signifies the direction of the airflow. It can be seen at the ACH of 2 h^{-1} , the inlet jet covers a small area of the ceiling before evolving into a free horizontal jet downwards (Figure 3-6a). Figure 3-6b illustrates that the free horizontal jet directs towards the back wall and then drops down and sweeps over the floor towards the outlet. Due to the outlet's location, the average air velocity over the floor is higher than the ceiling. Moreover, CHTCs at the floor are larger than the ceiling under the ACH of 2 h^{-1} (cf. Figure 3-5a and Figure 3-4a), which can also be explained by Figure 3-6.



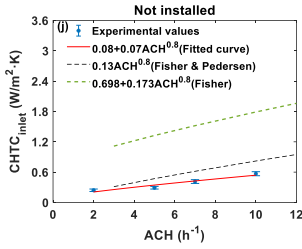


Figure 3-5. Experimental values at the floor in the MV experiment [48].

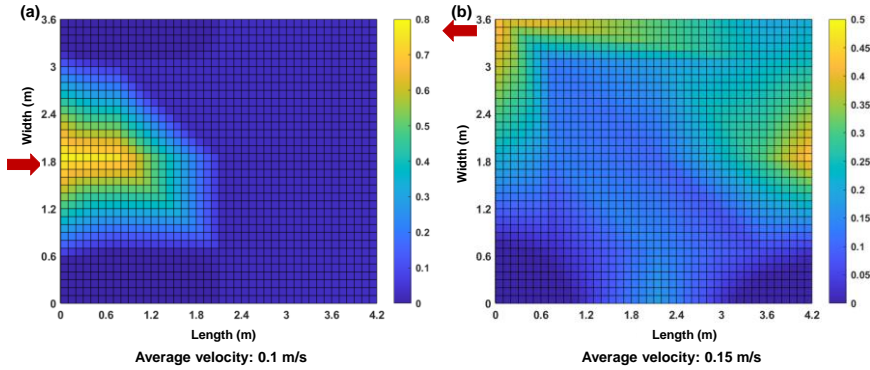


Figure 3-6 Local air velocity contour of the (a) ceiling and (b) floor after two hours for design case 4 in the MV experiment [48].

3.3.3. CHTC AT WALLS

Figure 3-7 illustrates the experimental values at the walls and two empirical wall correlations. The developed correlations ($0.91 \leq R^2 \leq 0.98$) are shown separately in a table, which can be referred to Appendix B [48]. The exponent m of all developed wall correlations is 0.8, indicating the turbulent flow over the walls. The uncertainty of experimental value at walls ranges between $\pm 6\%$ and $\pm 10\%$.

In contrast to the comparison between the two empirical floor correlations, sidewall inlet wall correlation (i.e., Fisher) predicts smaller values than the radial ceiling diffuser (i.e., Fisher & Pedersen) wall correlation when the ACH is the same. The reason is that the radial jet skims over more areas of walls than the free horizontal jet. The two empirical wall correlations give accurate CHTCs for specific cases. For example, the ceiling diffuser wall correlation predicts the CHTC at the back wall (Figure 3-7c) quite well. In comparison, sidewall inlet wall correlation can be used to predict the CHTCs at the front wall and left wall of design cases with the “Ceiling+Floor+Right wall” scheme (Figure 3-7a, d).

As shown in Figure 3-7b, the right wall with thermal mass has almost twice the experimental values compared to the right wall without thermal mass. As a result of the air distribution characteristic (cf. Figure 3-6), the CHTCs at the back wall are highest, followed by the right wall. The CHTCs at the front wall and left wall are similar. The presence and position of indoor tables have a limited impact on the experimental values at walls.

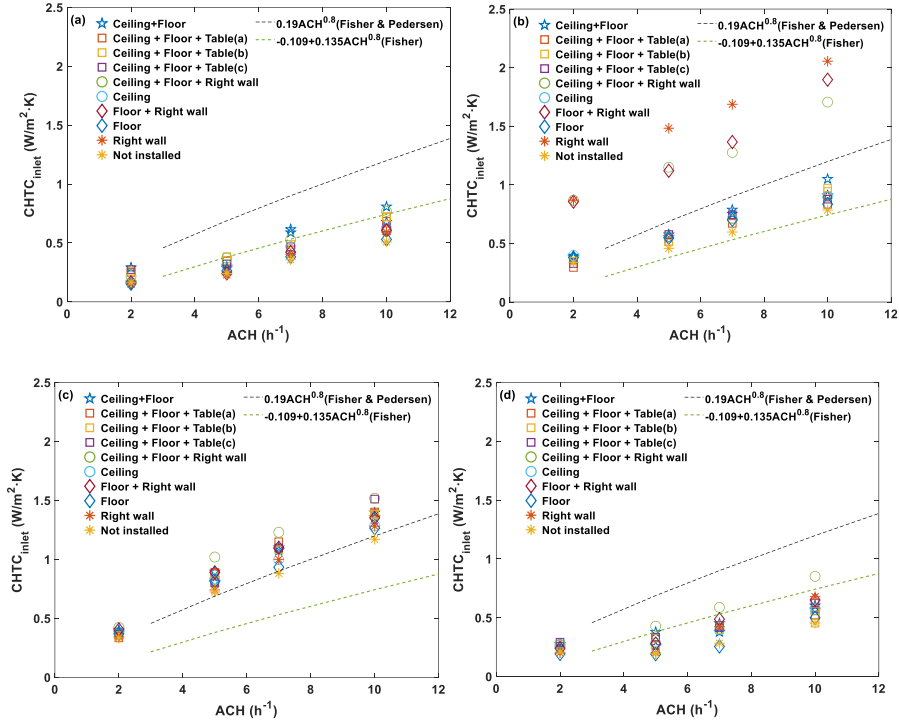


Figure 3-7. Experimental values at (a) front, (b) right, (c) back, (d) left walls in the MV experiment [48].

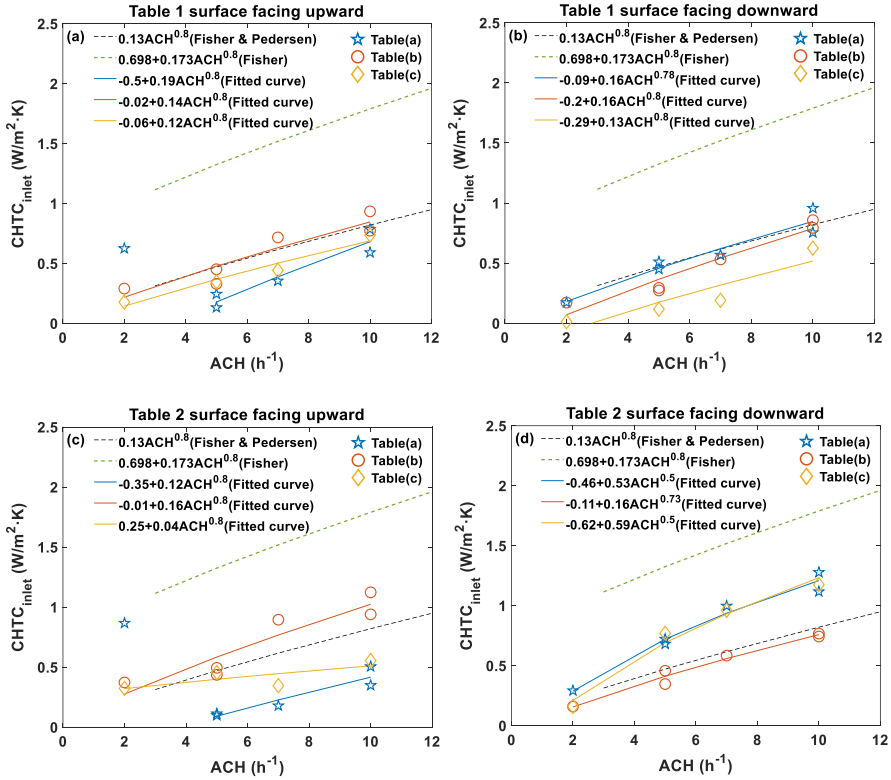
3.3.4. CHTC AT TABLES

The empirical floor correlations are selected for the comparison because there are no correlations specific to indoor tables, and the furniture is treated as the upward-facing and horizontal surface in BES tools [21]. Figure 3-8 illustrates the experimental values at the tables, developed correlations, and two empirical floor correlations. The uncertainty of experimental value ranges between $\pm 4\%$ and $\pm 9\%$.

Unlike the sidewall inlet floor correlation (i.e., Fisher) underestimates all experimental values, the radial ceiling diffuser (i.e., Fisher & Pedersen) floor correlation gives relative accurate results for many design cases. Due to the various

air distributions, each table's two surfaces have different experimental values. The CHTC at the indoor table surface is impacted differently by the position of indoor tables and air distribution. For example, the upward-facing surface of indoor table 2 has quite different values at three positions, while the opposite is true for the downward-facing surface of indoor table 3.

Interestingly, indoor tables' upward-facing surfaces have a larger CHTC at the ACH of 2 h^{-1} than at other ACHs, particularly for indoor tables located in "Table(a)" (i.e., in the middle of the room, cf. Figure 3-3). The reason is that the inlet flow sweeps through the ceiling and falls right down to those upward-facing surfaces at the ACH of 2 h^{-1} (cf. Figure 3-6a). Therefore, the experimental values at "Table(a)" position under the ACH of 2 h^{-1} are not included in the correlation development.



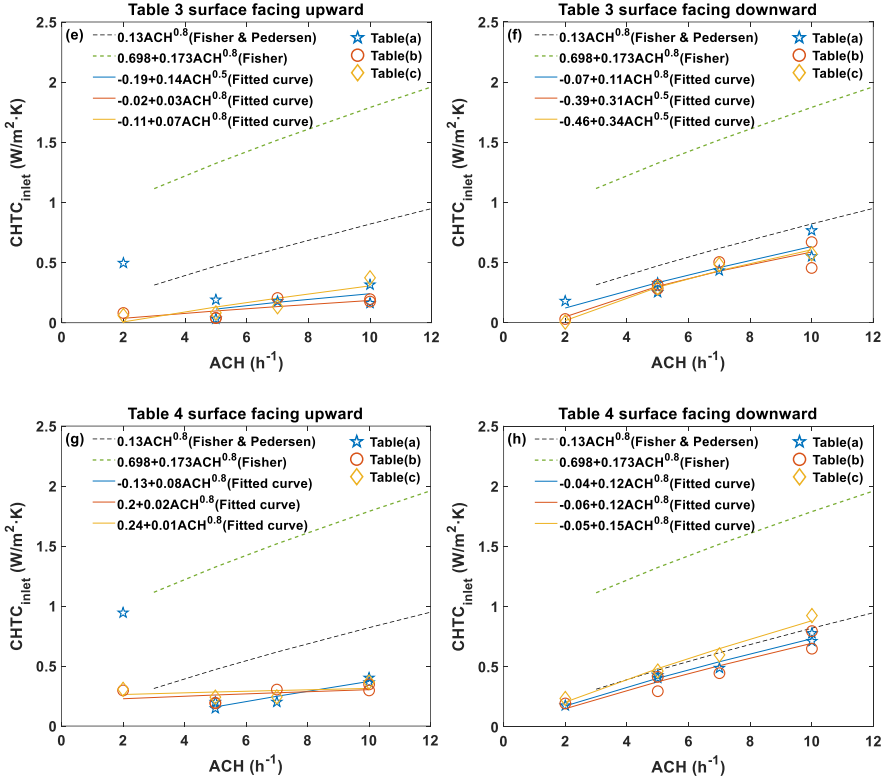


Figure 3-8. Experimental values at table surfaces in the MV experiment [48].

3.4. EXPERIMENTAL RESULTS OF DIFFUSE CEILING VENTILATION

The empirical correlations listed in Table 3-1 and Table 3-2 are also selected for comparison in the DCV experiment. In addition, the correlation developed by Novoselac et al. [57] for the floor ($h = 0.48ACH^{0.8}$) with a displacement ventilation (DV) diffuser is selected for comparison. Because a DV effect was found in the occupied zone when the internal heat load was low under the DCV scenario [58].

Unlike the MV experiment, the supply reference temperature for deriving the CHTC under the DCV is the mean air temperature calculated and measured by the nine shielding ventilated thermocouples 50 mm above the suspended diffuse ceiling. It is worth noting that the correlation for the diffuse ceiling is not developed due to the two reasons below. The first is that the conductive and convective heat transfer fluxes over the diffuse ceiling are partly converted into radiative heat transfer flux in the porous wood-cement material [31], making it difficult to derive the convective heat flux accurately. The second is that the dynamic heat capacity and heat capacitance of the

diffuse ceiling are very low, which has a negligible effect on the whole space's energy use. The CHTC correlation for the suspended ceiling panel under DCV will be investigated using BES tools by comparing the measured and simulated data in the subsequent Chapter 5.

3.4.1. CHTC AT THE FLOOR

Figure 3-9 illustrates the experimental values at the floor, developed correlations, and three empirical floor correlations. The R^2 of developed correlations is between 0.90 and 0.94. The uncertainty of experimental value ranges between $\pm 6\%$ and $\pm 10\%$. Same with the MV experiment, there are initial trails for some design cases with two different ΔT_0 under the same ACH. In Figure 3-9a, b, c, f, those experimental values under the same ACH are close, indicating that ΔT_0 also has a negligible effect on the experimental CHTCs at the floor.

By comparing the three empirical floor correlations, the DV diffuser (i.e., Novoselac et al.) floor correlation predicts the highest CHTC, followed by the sidewall inlet (i.e., Fisher) and radial ceiling diffuser (i.e., Fisher & Pedersen) floor correlations. This is because the DV diffuser is located on the floor to supply an inlet jet that sweeps over a larger area of the floor than the inlet jets. The sidewall inlet floor correlation gives quite accurate results for the design cases that the floor has thermal mass. When the floor has no thermal mass, the radial ceiling diffuser floor correlation predicts the CHTC relatively well. Furthermore, by comparing the experimental values of design cases with and without indoor tables, it turns out that the presence and positions of indoor tables have a negligible influence on the experimental values.

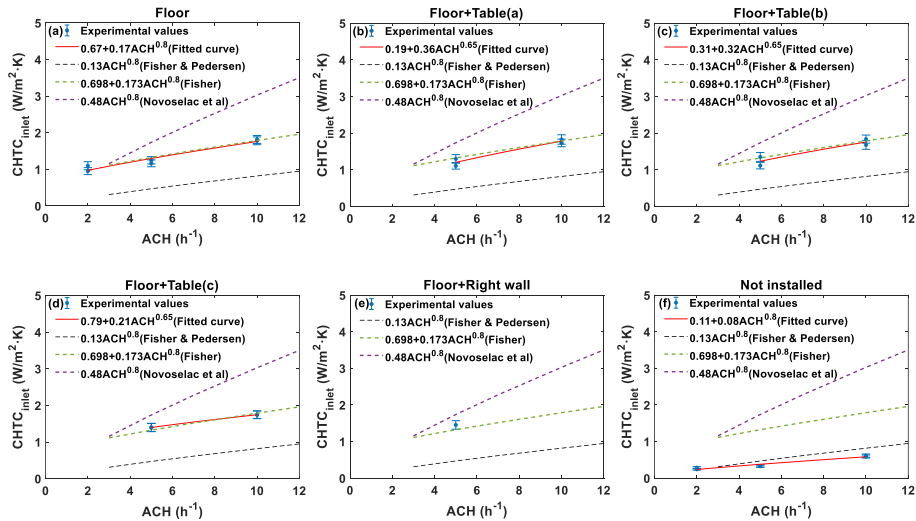


Figure 3-9. Experimental values at the floor in the DCV experiment [49].

3.4.2. CHTC AT WALLS

Figure 3-10 illustrates the experimental values at walls and two empirical wall correlations. The uncertainty of experimental value ranges between $\pm 5\%$ and $\pm 10\%$.

Sidewall inlet (i.e., Fisher's) wall correlation gives larger CHTC at walls fits with the experimental values relatively better than the radial ceiling diffuser (i.e., Fisher & Pedersen's) wall correlation. The experimental values at four walls at the same ACH are close since the air is relatively uniformly distributed under DCV. Nevertheless, the CHTCs at the front wall are slightly larger than at the other three walls for most cases due to the outlet's location is in the front wall. Figure 3-11 shows the front wall's local air velocity contour after two hours for design case 1 in the DCV experiment (i.e., ACH of 10 h^{-1} , ΔT_0 of $10 \text{ }^\circ\text{C}$, "Floor"). The velocity contour is interpolated and extrapolated using the measured nine local air velocity 50 mm away from the front wall by the hot sphere anemometers, which backs up the reasons mentioned above. Figure 3-10b shows that the thermal mass also increases the CHTC at the right wall.

For design cases without indoor tables, the pair of experimental values with two ΔT_0 is close. The corresponding developed correlations ($0.91 \leq R^2 \leq 0.95$) for those design cases are listed in Table 3-3. The presence and position of indoor tables impact the experimental values at walls to some extent. Thus, for design tables with indoor tables, two ΔT_0 under the ACH of 10 h^{-1} contributes to a relatively large difference up to $0.5 \text{ W/m}^2\cdot\text{K}$ (see "Floor+Table(b)" in Figure 3-12a) between the corresponding pair of experimental values. The reason should be that the indoor tables change the direction of the airflow that should have been flowing downwards, causing it to turn towards a nearby wall and a change in the airflow pattern at different supply temperatures. Therefore, the developed correlations for the design cases with the same position of indoor tables have a small R^2 as low as 0.47. It might be difficult to accurately predict the CHTC at walls under high ACH when indoor tables present.

An alternative approach is to derive the correlations for walls based on all the experimental values without taking into account the indoor tables' position. Then the "simplified" correlations ($0.49 \leq R^2 \leq 0.79$) are developed using the same curve fitting method. The correlations are shown as the solid red lines in Figure 3-10. The root mean squared error (RMSE) between the experimental and predicted (by simplified wall correlations) values ranges between $0.06 \text{ W/m}^2\cdot\text{K}$ and $0.12 \text{ W/m}^2\cdot\text{K}$, which should be tolerable for the NV performance simulation in BES tools.

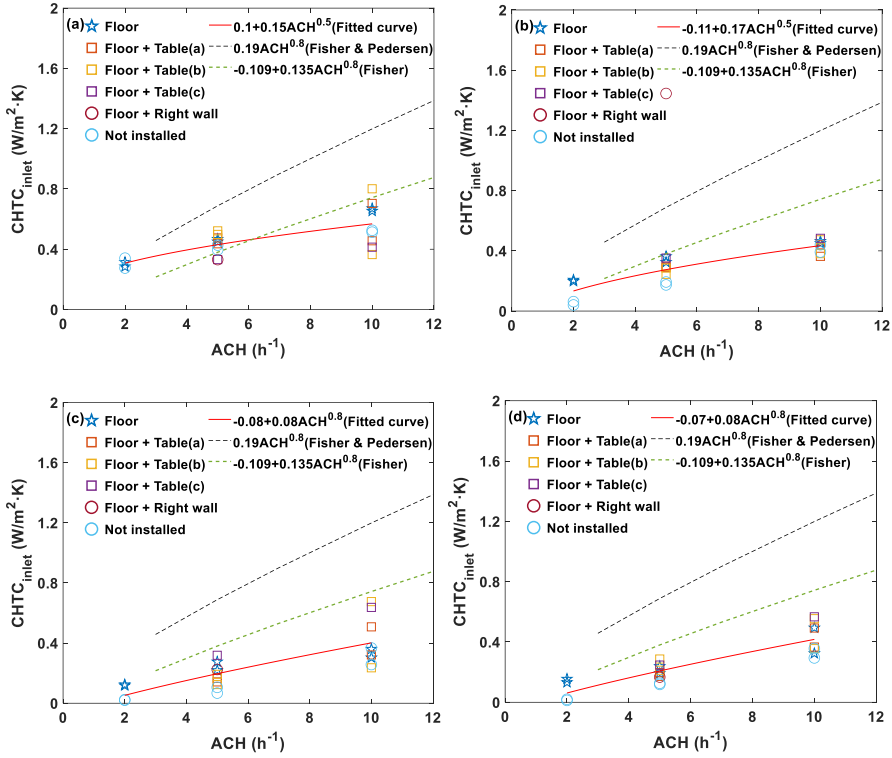


Figure 3-10. Experimental values at (a) front, (b) right, (c) back, (d) left walls in the DCV experiment [49].

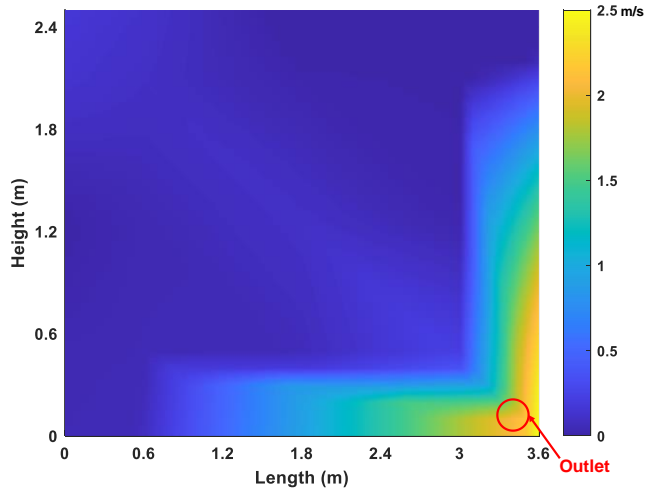


Figure 3-11 Local air velocity over the front wall after two hours for design case 1 in the DCV experiment [49].

Table 3-3 Developed wall correlations under DCV [49].

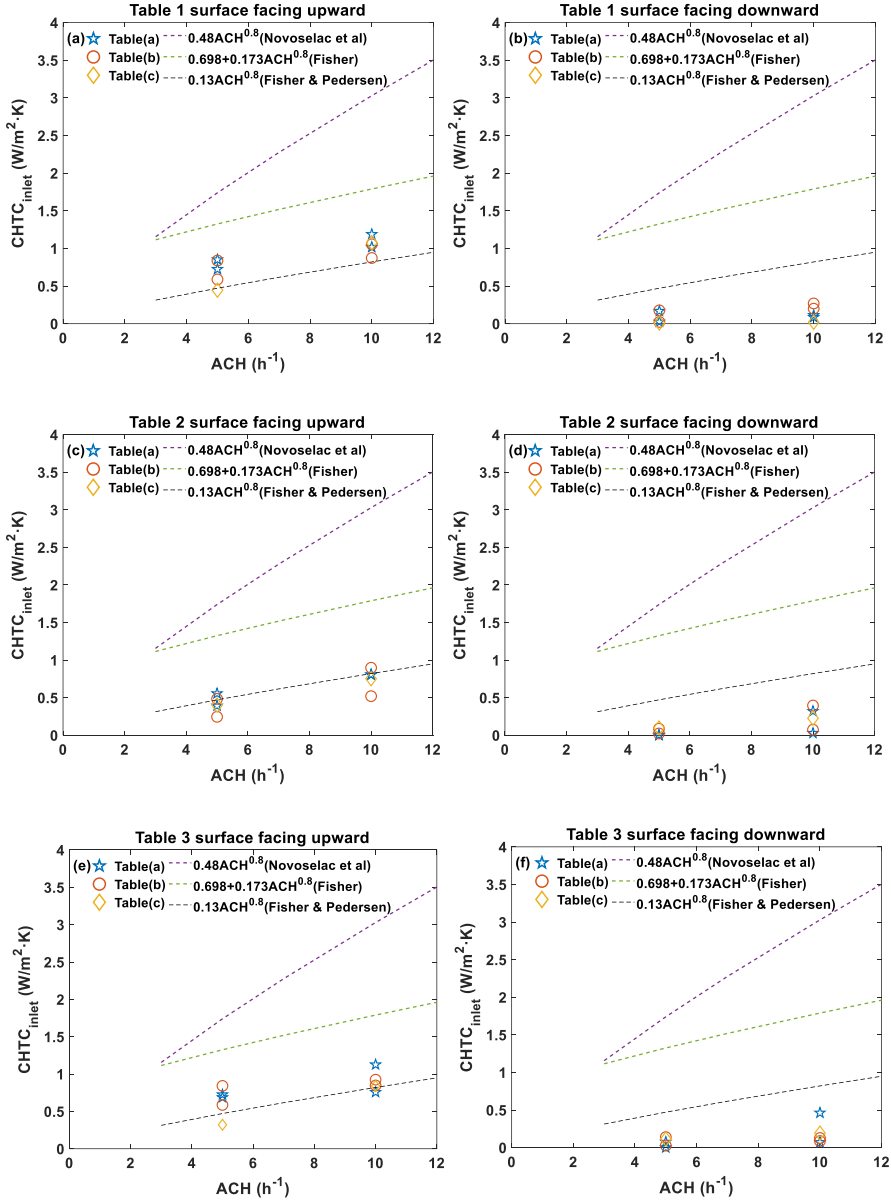
Thermal mass distribution	Front wall	Right wall	Back wall	Left wall
Floor	$0.14 + 0.08ACH^{0.8}$	$0.01 + 0.15ACH^{0.8}$	$-0.04 + 0.12ACH^{0.5}$	$0.03 + 0.06ACH^{0.8}$
Not installed	$0.14 + 0.12ACH^{0.5}$	$-0.1 + 0.08ACH^{0.8}$	$-0.15 + 0.07ACH^{0.8}$	$-0.2 + 0.08ACH^{0.8}$

3.4.3. CHTC AT TABLES

Figure 3-12 illustrates the experimental values at tables, developed correlations. The uncertainty of experimental value ranges between $\pm 7\%$ and $\pm 12\%$. Same as the comparison for the CHTC at tables in the MV experiment, the two empirical floor correlations (cf. Table 3-1 and Table 3-2) as well as the DV diffuser floor (i.e., Novoselac et al.) correlation, are selected for comparison. The radial ceiling diffuser (i.e., Fisher & Pedersen) floor correlation gives relatively accurate results for the upward-facing surfaces of indoor tables. All empirical correlations vastly overestimate the CHTC at downward-facing surfaces of indoor tables.

The CHTCs at the table upward-facing surfaces are much larger than the downward-facing surfaces under the same ACH. This is because the inlet jet from the suspended ceiling first pours down towards the upward-facing surfaces and flows over them, while the downward-facing surfaces are relatively unaffected by the jet.

Same with the situation of experimental CHTCs at walls, it is difficult to develop the correlations with a high R^2 (more than 0.90) for each position of indoor tables. The “simplified” correlations are then developed for the upward-facing and downward-facing surfaces rather than taking into account the position of indoor tables. Table 3-4 shows the simplified correlations for tables. The RMSE between the experimental and predicted (by simplified table correlations) values ranges between $0.13 \text{ W/m}^2 \cdot \text{K}$ and $0.21 \text{ W/m}^2 \cdot \text{K}$, which should be tolerable for the NV performance simulation in BES tools.



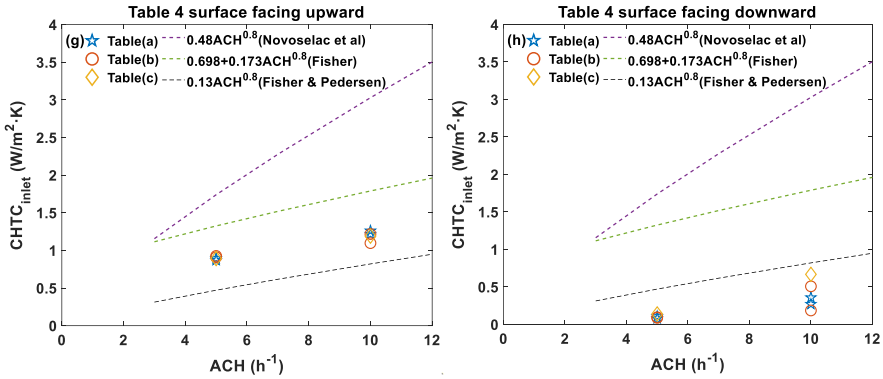


Figure 3-12. Experimental values at table surfaces in the DCV experiment [49].

Table 3-4. Developed table correlations under DCV [49].

Table surface	Correlation
Upward-facing	$0.11 + 0.19ACH^{0.65}$
Downward-facing	$-0.21 + 0.1ACH^{0.65}$

3.5. DEVELOPMENT OF SIMPLIFIED CHTC CORRELATIONS

The CHTC correlations developed in Sections 3.3 and 3.4 are expected to be adopted in BES tools to simulate NV performance. The developed correlations for all interior surfaces in MV and the floor under DCV are based on the explicit thermal mass distribution schemes, which might be complicated for simulation. Even though the CHTC at any one interior surface can be affected somewhat by the other surfaces' conditions, it would be easier to develop the "simplified" correlation for one surface only with the criteria of whether or not this surface has thermal mass for BES. Thus, the "simplified" CHTC correlations for interior surface are developed using the same curve fitting method mentioned in Section 3.3.1 and the corresponding experimental values, as shown in Table 3-5 and Table 3-6. The R^2 of those simplified correlations is between 0.82 and 0.96, which should be tolerable. In combination with the correlations for indoor tables under MV (cf. Figure 3-7) and DCV (cf. Table 3-4), the simplified correlations offer the possibility of studying more thermal mass distribution schemes.

Table 3-5. Simplified CHTC correlations for interior surfaces under NV with MV.

With thermal mass or not	Ceiling	Floor	Front wall	Right wall	Back wall	Left wall
Yes	- $0.94+1.07ACH^{0.5}$	$0.36+0.28ACH^{0.8}$	-	$0.13+0.12ACH^{0.8}$	-	-
No	- $1.17+0.92ACH^{0.5}$	$0.2+0.06ACH^{0.8}$	- $0.01+0.1ACH^{0.8}$	$0.46+0.22ACH^{0.8}$	- $0.41+0.55ACH^{0.5}$	$0.07+0.08ACH^{0.8}$

Table 3-6. Simplified CHTC correlations for interior surfaces under NV with DCV.

With thermal mass or not	Floor	Front wall	Right wall	Back wall	Left wall
Yes	$0.67+0.17ACH^{0.8}$	-	-	-	-
No	$0.11+0.08ACH^{0.8}$	$0.1+0.15ACH^{0.5}$	- $0.11+0.17ACH^{0.5}$	- $0.08+0.08ACH^{0.8}$	- $0.07+0.08ACH^{0.8}$

3.6. CONCLUSION

MV and DCV are integrated with NV to experimentally investigate the convective heat transfer under different supply temperatures, ACHs, and thermal mass distribution schemes. The surface-averaged CHTCs at the test room's interior surfaces and indoor tables (furniture) are calculated based on the supply reference temperature. The derived CHTCs are then used to develop the CHTC correlations specific to NV and compared with predicted CHTC by existing empirical CHTC correlations.

The empirical correlations cannot predict the CHTC accurately for most design cases [48][49]. The CHTC at a surface can be greatly augmented with the increase of thermal mass level and can be somewhat affected by the thermal mass distribution of other surfaces. The simplified correlation for the interior surface is also developed only with the criteria of whether or not this surface has thermal mass.

For MV, the presence and position of indoor tables have a negligible effect on the CHTCs at the test room's interior surfaces but a great impact on the CHTCs at the indoor table surfaces. For DCV, the conditions of indoor tables impact the CHTCs at walls and CHTCs at indoor table surfaces to some extent.

CHAPTER 4. SIMULATION AND OPTIMIZATION OF NIGHT VENTILATION PERFORMANCE

Chapter 3 develops the CHTC correlations tailored for MV and DCV, which provides the potential to simulate accurately and optimize the NV performance in BES. In this chapter, the experimentally proposed correlations are validated in a BES tool (EnergyPlus) based on the experimental test conditions. Then, the performance of NV with MV and DCV is simulated and compared using the validated correlations in a real office building. Finally, the NV performance is improved using a genetic optimization algorithm.

4.1. VALIDATION OF PROPOSED CORRELATIONS

4.1.1. VALIDATION SETUP

The guarded hot box model is built based on the experiment setup introduced in Section 3.1. Figure 4-1 shows the hot box model that involves the plenum (i.e., upper zone in the experiments), room (i.e., test room in the experiments), and guarding zone, and principles of MV and DCV. The hot box model's envelope is the same as the real hot box in [48][49]. A variable air volume (VAV) AC system is set to supply the cold conditioned air to the room, while an ideal load AC systems is set to maintain the guarding zone temperature at 22 °C. The simulation cases have the same supply ACH, supply temperature, and thermal mass distribution as the experimental design cases in [48][49].

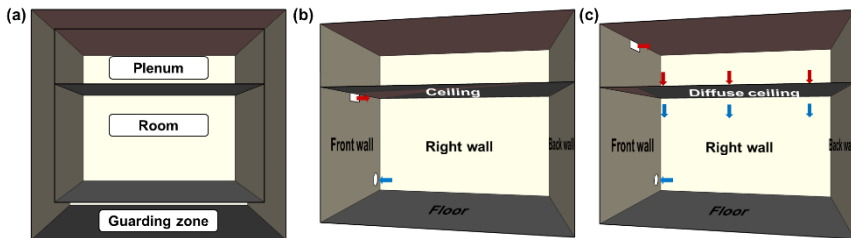


Figure 4-1. (a) Vertical perspective drawing of the hot box model, (b) MV principle, and (c) DCV principle [59].

The mean bias error (MBE) in Equation (4-1) is selected as the indicator for CHTC correlation validation by comparing the simulated surface temperatures with measured surface temperatures.

$$\text{MBE (\%)} = \frac{\sum_{j=1}^{N_p} (m_j - s_j)}{\sum_{j=1}^{N_p} (m_j)} \quad (4-1)$$

where m_j and s_j are the measured and simulated data points for each model instance i , respectively. N_p is the number of data points at interval p .

It is worth noting that before validating the CHTC correlations for DCV, the CHTC correlations for the surfaces in the plenum and diffuse ceiling need to be identified or developed. For the plenum, the existing empirical convection algorithms (i.e., a set of CHTC correlations) in EnergyPlus are selected one after the other to identify the appropriate one that provides the minimum MBE between the simulated and measured plenum air temperature. Design cases 1 to 6 of the DCV experiment are selected because all ranges of supply ACH and supply temperatures are included. The existing empirical correlations embedded in EnergyPlus might not be applicable for the suspended diffuse ceiling since the air exchange between adjacent zones is modeled as the convection in BES tools [21]. We assume the general form of CHTC correlation (cf. Equation (3-2)) is also applicable to the diffuse ceiling. The optimization with the genetic algorithm is then adopted by coupling MATLAB with EnergyPlus to develop the correlation to minimize the objective. The sum of the absolute value of MBE (see Equation (4-2)) between the simulated and measured diffuse ceiling temperature of six selected design cases is the objective for optimization.

$$\min \sum_{k=1}^6 |\text{MBE}_i| \quad (4-2)$$

After the models are constructed in EnergyPlus, the proposed CHTC correlations summarized in Section 3.5 are set for the corresponding interior surfaces, and the design cases are simulated in EnergyPlus. For more detailed information about the validation setup in EnergyPlus, please refer to Appendix E [59].

4.1.2. VALIDATION RESULTS

After simulating the design cases and comparing the measured data with simulated data, it is found that the ceiling diffuser convection algorithm is suitable for the plenum under DCV, which provides the minimum MBE with an average absolute value of 1.1% between the measured and simulated plenum air temperatures. The CHTC correlation $(-2.23\text{ACH}^{0.75} + 2.37)$ developed by the genetic algorithm offers the minimum MBE with an average absolute value of 2.8% between the measured and simulated diffuser ceiling temperatures. Figure 4-2 shows the measured and simulated temperatures under the correlation mentioned above, demonstrating the good agreement between those temperatures. The “m” and “s” in the legends of Figure 4-2 represent the measured and simulated data, respectively.

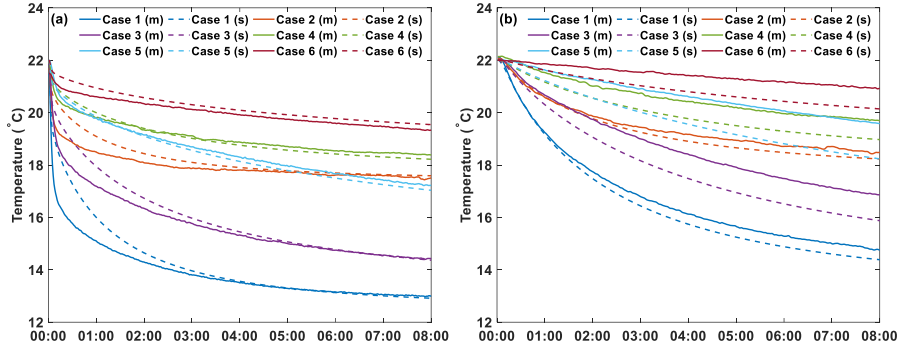


Figure 4-2 Measured and simulated (a) plenum air temperature and (b) diffuse ceiling temperature for design case 1 to 6 in DCV experiment [59].

Figure 4-3 shows the boxplot of the MBE between simulated and measured surface temperatures with the proposed correlations. The MBE ranges between -0.5% and 10.9% for all simulation cases, demonstrating that the proposed correlations are applicable for predicting the surface temperature in BES.

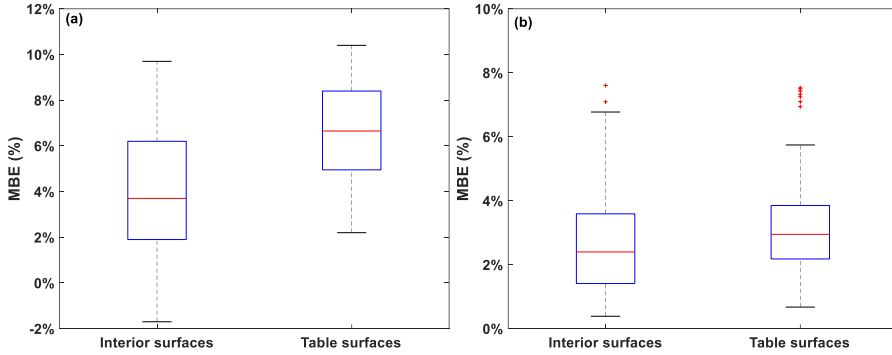


Figure 4-3 MBE between simulated and measured surface temperatures under NV with (a) MV and (b) DCV [59].

4.2. SIMULATION OF NIGHT VENTILATION PERFORMANCE

4.2.1. SIMULATION SETUP

The office building introduced in Section 2.2.1 is selected. However, the case room in this section is zone 1NC (see Figure 4-4), a typical room located on the building's middle floor. The case room has the same size as the plenum and room model (without guarding zone) mentioned in Section 4.1.1. The exterior wall facing north is the “front wall” (cf. Figure 4-1) with an energy-efficient window (area 1.44 m²) introduced in [44]. Adiabatic boundary conditions are also set for the internal partitions between zone 1NC and adjacent zones.



Figure 4-4. Layout of case room INC.

The VAV fan in the VAV AC system also serves the night mechanical ventilation system. A general NV scheme with the ACH setpoint of 10 h^{-1} , minimum indoor temperature setpoint of 18°C , and activation threshold temperature of 3°C is adopted. The TMY3 data of Copenhagen (cf. Figure 2-2a) in summer is used as the weather inputs for simulation. The reasons why this cooling system is selected are twofold: (1) prior studies [44][60] indicated that the daytime AC and NV system could result in an overcooling penalty in the cold climate regions, leading to a larger potential for simulation and optimization research. (2) BES tools currently only allow users to set the custom CHTC correlations with supply reference temperature for mechanical cooling, limiting the application of validated correlations in night natural ventilation.

The same thermal mass distribution schemes for MV and DCV should be selected as the simulation cases for comparison. According to the thermal mass distribution schemes of design cases for DCV [49], “Not installed”, “Floor”, “Floor+Table” schemes are selected.

When AC operates during the daytime, we assume that AC’s supply outlet to the room is a radial diffuser. Therefore, the ceiling diffuser convection algorithm (cf. Table 3-1) is adopted for the room during the daytime, while the validated and identified correlations in Section 4.2 are adopted during the nighttime. Furthermore, to evaluate NV performance discrepancy between validated correlations and previous empirical correlations, the reformulated ceiling diffuser algorithm embedded in EnergyPlus [21] is selected both all the day as the comparison simulation case. It is worth noting that the reformulated correlations are based on the exhaust (indoor) temperature for a fully mixed room in EnergyPlus, as shown in Table 4-1. For more detailed information about the simulation setup, please refer to Appendix E [59].

Table 4-1. Reformulated ceiling diffuser convection algorithm in EnergyPlus [21].

Surface type	Correlations
Ceiling	$h = 1.012ACH^{0.604} + 1.208$
Floor	$h = 0.082ACH^{0.98} + 3.873$
Walls	$h = 4.099ACH^{0.503} + 2.234$

4.2.2. SIMULATION RESULTS

Figure 4-5 shows the simulated HVAC electricity use and percentage outside the range (POR) during the working hours of MV cases. The Fanger's thermal comfort model [61] is applied in POR.

For the cases shown in Figure 4-5a, the night cooling saves HVAC electricity use by 8.2 kWh (16.0%) to 13.7 kWh (26.0%) but increases the POR by 2.6% – 9.4% compared to the corresponding cases without NV. The POR of most cases is over 10%, indicating that the general NV scheme could result in an overcooling penalty. For cases shown in Figure 4-5b, NV reduces HVAC electricity use by 4.1 kWh (8.0%) – 8.2 kWh (15.3%) but increases the POR by 2.4% – 6.4%. The ceiling diffuser algorithm overestimates the night energy-saving potential by 4.1 kWh (8.0%) – 5.5 kWh (10.7%) and yields a difference in POR between -0.9% and 1.5%, compared to the validated CHTC correlations for MV. The reason causes the prediction discrepancy should be that the validated correlations induce a smaller night ACH. By comparing the night cooled MV cases, it is found that NV saves the most energy and provides the highest POR when the floor has thermal mass and indoor tables present, and the opposite is true for the case without thermal mass. A higher thermal mass contributes to more energy-saving potential but worsens indoor thermal comfort.

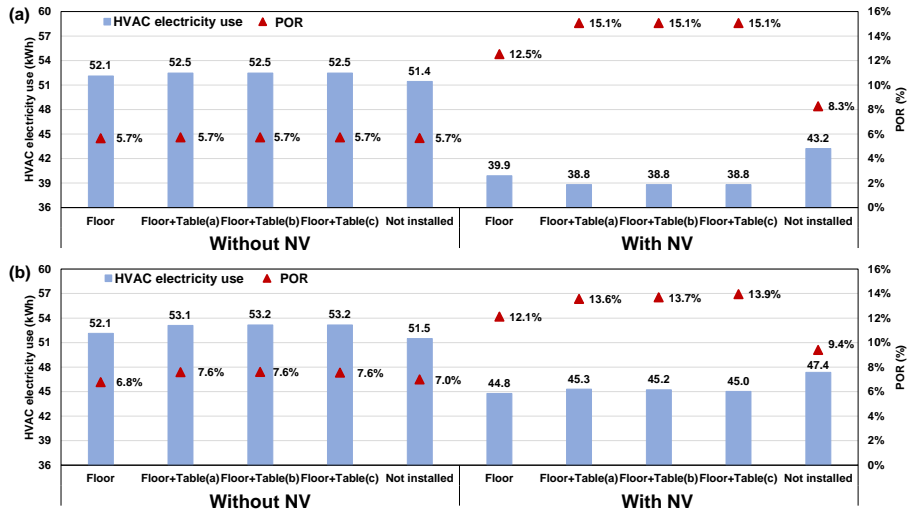


Figure 4-5. HVAC electricity use and POR of MV cases with (a) ceiling diffuser algorithm and (b) validated correlations at night [59].

Figure 4-6 shows the simulated results of DCV cases. For the cases shown in Figure 4-6a, NV saves HVAC electricity use by 11.8 kWh (20.9%) to 16.8 kWh (29.6%) but raises the POR by 1.7% – 6.4%, compared to respective cases without NV. Whereas in Figure 4-6b, NV cuts the cooling energy by 7.5 kWh (13.4%) to 10.9 kWh (19.0%),

while the POR rises by 1.7% – 3.8%. The ceiling diffuser algorithm overestimates the night energy-saving potential by 4.3 kWh (7.5%) to 5.9 kWh (10.6%) and yields a difference in POR between -0.9% – 1.3%, compared to the validated CHTC correlations for DCV.

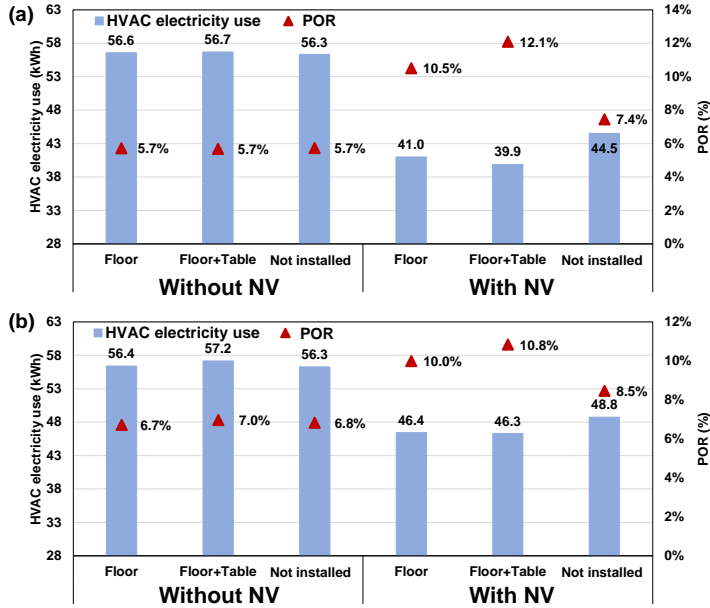


Figure 4-6 HVAC electricity use and POR of DCV cases with (a) ceiling diffuser algorithm and (b) validated correlations at night [59].

For the conditioned room without NV, DCV consumes 4.0 kWh – 4.8 kWh more cooling energy than MV (cf. Figure 4-5b, Figure 4-6b) due to the internal heat load in the plenum is taken by the HVAC system with DCV. On the contrary, night cooling with DCV saves 2.7 kWh to 3.4 kWh more HVAC electricity than that with MV. This is because the plenum is also cooled down by the outdoor air at night, which can be a cooling source for the room during the daytime. Apart from the energy performance, the DCV contributes to a lower POR of 0.9% – 3.1% compared to MV, especially under the NV scenario. The reasons are twofold: (1) The air velocity under DCV in the occupied zone (0.08 m/s) is smaller than the velocity (0.2 m/s) under MV. (2) Night cooling with DCV cools down both the plenum and room, resulting in relatively high indoor temperatures and a small overcooling penalty, compared to the same case with MV.

4.3. OPTIMIZATION OF NIGHT VENTILATION PERFORMANCE

4.3.1. OPTIMIZATION SETUP

The simulation results in Section 4.2 reveal that the general NV scheme reduces cooling energy use and increases POR in Copenhagen. The optimization is adopted to save more cooling energy while maintaining thermal comfort within a certain range [60]. The optimization problem is the single objective with a single constraint type. The objective is to minimize the HVAC electricity use (Equations (4-3)), and the recommended category II of PPD (<10%) in EN 15251 [43] for designing the buildings with mechanical cooling is selected as the constraint (Equations (4-4)).

$$\min \text{ HVAC electricity use} \quad (4-3)$$

$$\text{subject to } \text{POR} < 10\% \quad (4-4)$$

The genetic algorithm is also leveraged to minimize the objective and fulfill the constraint by integrating MALAB with EnergyPlus. The MV and DCV cases without thermal mass distribution (i.e., 'Not installed') are selected as the base cases. Four parameters are optimized: NV hourly ACH setpoint, minimum indoor temperature setpoint, AC temperature setpoint, and thermal mass level. For more detailed information about the optimization setup in EnergyPlus and MATLAB, please refer to Appendix E [59].

4.3.2. OPTIMIZATION RESULTS

Figure 4-7 shows the parameters of the optimal cases as well as the base cases with a general NV scheme. Both the optimal MV and DCV cases have the respective maximum thermal mass level and have the maximum allowed temperature setpoint (i.e., 27 °C) for daytime AC. The optimal DCV case has a lower minimum indoor air temperature setpoint (i.e., 16 °C) than MV. The two optimal cases' hourly night ACH setpoints vary significantly and are smaller than the general NV scheme (i.e., 10 h⁻¹).

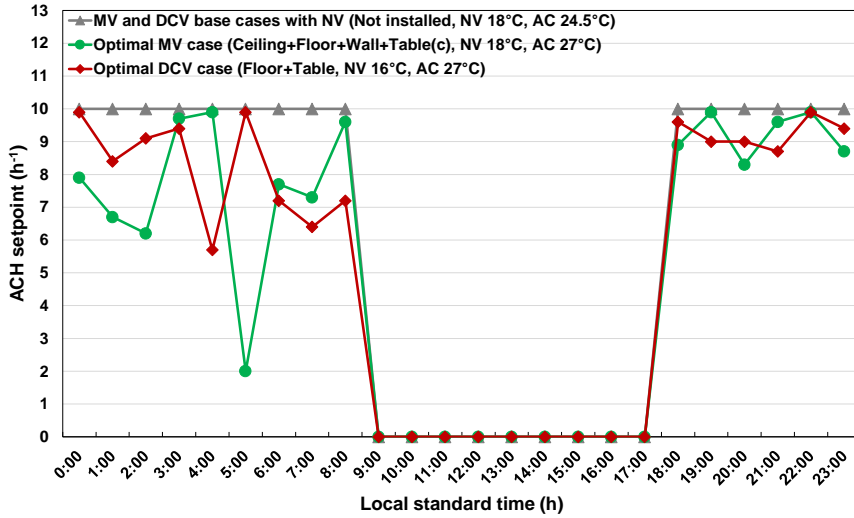


Figure 4-7 Parameters of the optimal cases and base cases [59].

Figure 4-8 shows the simulated results of relevant simulation cases. Compared with the respective base cases (i.e., without thermal mass and NV), the optimal MV and DCV case can significantly save energy use by 14.4 kWh (27.6%) and 17.3 kWh (30.7%), respectively, while maintaining the POR within 10%. The performance of DCV improves more after the optimization.

Compared to the base cases with the general NV scheme, optimal cases can further save energy by 9.7 kWh (20.5%) for MV and 17.3 kWh (20.1%) for DCV, respectively. The MV and DCV cases under the respective maximum thermal mass levels with the general NV scheme both save the cooling energy but lead to a cold thermal environment compared to respective base cases. Then optimization not only improves the thermal comfort by reducing the POR but also goes on saving the HVAC electricity use by 5.3 kWh (12.3%) for MV and 7.3 kWh (15.8%) for DCV.

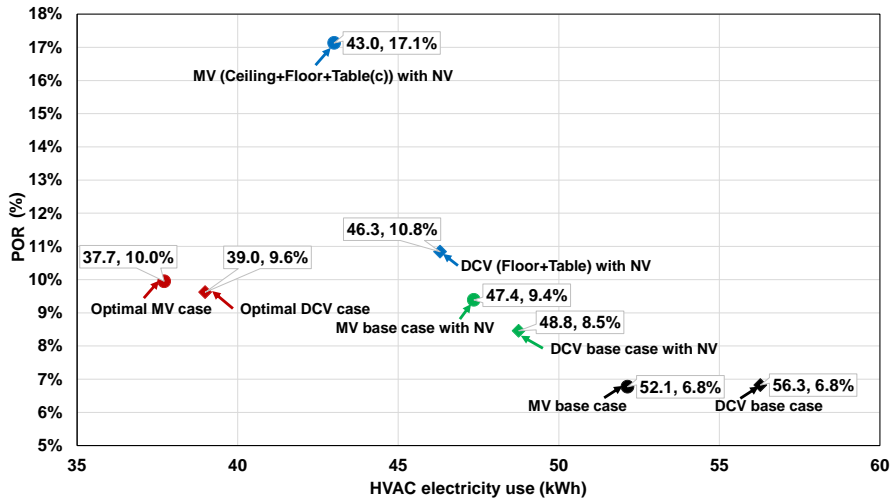


Figure 4-8 Simulated HVAC electricity use and POR of relevant simulation cases [59].

4.4. CONCLUSION

This chapter puts forward a systematic approach using EnergyPlus to i) validate the experimentally proposed CHTC correlations, ii) identify and develop the suitable correlations for the surfaces in the plenum and diffuse ceiling under DCV, iii) simulate, and iv) optimize the NV performance with MV and DCV considering the energy and thermal comfort.

The MBE between the simulated and measured temperatures of interior surfaces and indoor tables ranges between -0.5% and 10.9% when the proposed correlations are adopted. The ceiling diffuser convection algorithm is suitable for the plenum under DCV, which provides the minimum MBE with an average absolute value of 1.1% between the measured and simulated plenum air temperatures. The developed correlation for the diffuse ceiling offers an MBE with an average absolute value of 2.8% between the simulated and measured diffuse ceiling temperature.

For the conditioned room without NV, DCV consumes 4.0 kWh (7.5%) to 4.8 kWh (9.3%) more HVAC electricity than MV. A general night cooling scheme with DCV offers a larger energy-saving potential and better indoor thermal comfort, saving more HVAC electricity by 2.7 kWh – 3.4 kWh and contributing to a lower POR of 0.9% – 3.1% than that with MV.

Compared to the validated correlations, the empirical ceiling diffuser convection algorithm overestimates NV energy-saving potential up to 10.6% for MV and 10.7% for DCV, respectively. Moreover, the empirical algorithm yields a difference in POR up to 1.5% for MV and 1.3% for DCV, respectively.

Optimal MV and DCV cases show that the thermal mass and AC cooling setpoints should be as high as possible. The optimal DCV case allows a lower minimum indoor temperature setpoint than the optimal MV case. The hourly night ACH setpoints of optimal cases fluctuate significantly and are smaller than the general NV scheme. Compared with the respective base cases, the optimal MV and DCV case can significantly save energy use by 14.4 kWh (27.6%) and 17.3 kWh (30.7%), respectively, while maintaining the POR less than 10%. The performance of DCV improves more after the optimization.

CHAPTER 5. CONCLUSIONS OF THE THESIS

This thesis proposes a holistic method integrating sensitivity analysis, full-scale experiment, building energy simulation, and optimization to accurately simulate and improve night ventilation (NV) performance. The results are expected to support a more efficient design and wider application of NV.

The NV performance indicators are firstly reviewed and categorized into four types: (1) heat removal effectiveness, (2) energy efficiency, (3) reduction in cooling energy use, and (4) thermal comfort improvement [44]. The influence of design parameters on the performance indicators depends significantly on the climatic conditions and NV principles [44]. The four most influential design parameters are window-wall ratio, internal CHTC, internal thermal mass level, and night ACH [44]. The building airtightness, internal heat gains, external thermal mass, and NV activation threshold temperature are influential for a few performance indicators under certain scenarios [44]. The building orientation and discharge coefficient of the opening have negligible influences on all performance indicators.

There are limitations and disadvantages to some performance indicators. The temperature efficiency (TE) is only applicable to compare the NV performance under the same ACH scenario directly, and the decrement factor (DF) is suitable for evaluating different NV systems with the same building parameters. The temperature difference ratio (TDR) is only suitable to compare the NV performance under the same climate condition. The coefficient of performance (COP) is only applicable to evaluate the ventilation energy efficiency during the nighttime. Weighted discomfort temperature index (DI) and degree-hours criterion (DhC) might be simplistic with the thermal comfort threshold temperature and not demonstrate thermal comfort intuitively without comparison. In summary, ventilative cooling advantage (ADV), cooling requirement reduction (CRR), and percentage outside the range (POR) are recommended [44].

After experimentally investigating the convective heat transfer for mixing ventilation (MV) and diffuser ceiling ventilation (DCV) under the NV scenario, the new CHTC correlations are developed based on the experimental surface-averaged CHTCs (supply reference temperature) at interior surfaces and indoor tables (furniture). Comparing the experimental CHTC with values predicted by empirical correlations shows that the CHTC for most design cases cannot be precisely predicted by empirical correlations. Increasing any surface thermal mass level can significantly enhance the CHTC at this surface. Moreover, the CHTC at any surface can be affected somewhat by other surfaces' thermal mass distribution. For MV, the presence and position of indoor tables have a negligible effect on the CHTCs at the test room's interior surfaces

but a great effect on the CHTCs at the indoor table surfaces. For DCV, the presence and position of indoor tables impact the CHTCs at walls, and indoor table surfaces to some extent.

The developed correlations are then validated using a building energy simulation tool. For night cooling with DCV, the ceiling diffuser convection algorithm is appropriate to predict the plenum air temperature accurately. In addition, the CHTC correlation for the diffuse ceiling is developed using genetic algorithm optimization.

For the conditioned room without NV, DCV consumes 4.0 kWh to 4.8 kWh more HVAC electricity than MV. When a general NV scheme is adopted, the DCV provides a greater energy-saving potential and better indoor thermal comfort. It saves HVAC electricity use by up to 3.4 kWh and contributing to a lower percentage outside the range (POR) during working hours up to 3.1% than night cooling with MV. The empirical ceiling diffuser convection algorithm overestimates NV energy-saving potential up to 10.6% for MV and 10.7% for DCV, respectively. Moreover, the empirical algorithm results in a discrepancy of POR up to 1.5% for MV and 1.3% for DCV, respectively.

Optimal MV and DCV cases show that the thermal mass and AC cooling setpoints should be as high as possible. The optimal DCV case allows a lower minimum indoor temperature setpoint than the optimal MV case. The hourly night ACH setpoints of optimal cases fluctuate significantly and are smaller than the general NV scheme. Compared with the respective base cases, optimization can significantly save energy use by 14.4 kWh (27.6%) for MV and 17.3 kWh (30.7%) for DCV, respectively, while maintaining the POR less than 10%. The performance of DCV improves more after the optimization.

CHAPTER 6. RECOMMENDATION FOR FUTURE WORK

Despite the promising findings of this thesis, further investigation is required to leverage night ventilation fully.

In the present experiments, only one thermal mass material is investigated. The relationship between the dynamic heat capacity of materials and CHTC at the material surface needs further study, especially the phase change material (PCM). It is worth studying the applicability of developed correlation in other enclosure dimensions by a real office room experiment.

The current correlations select the supply reference temperature. However, most of the current building energy simulation tools only allow users to set custom correlations for mechanical cooling, limiting the application of those correlations in natural ventilation. One way is to use other tools like the Modelica language, which may provide a more flexible way to set the custom correlations for CHTC calculation or contact the developer of EnergyPlus to report this issue. Another way is to validate the correlations using computational fluid dynamics (CFD) and develop other correlations by selecting the calculated (by the CFD model) indoor temperature as reference. Moreover, the impact of the room's height or plenum's height on night cooling performance with DCV needs further simulation or experiment research.

The optimization in this thesis selects the typical meteorological year (TMY3) data in the summer of Copenhagen, which can be expanded to other climate regions and other mechanical cooling systems. Furthermore, whether the optimal NV design is resilient under extreme weather conditions or predicted weather conditions in the future is interesting. Finally, the model predictive control based on validated correlations for night cooling control is another research direction.

LITERATURE LIST

- [1] T.R. Whiffen, G. Russell-Smith, S.B. Riffat, Active thermal mass enhancement using phase change materials, *Energy Build.* 111 (2016) 1–11. doi:10.1016/j.enbuild.2015.09.062.
- [2] M. Santamouris, Cooling the buildings – past, present and future, *Energy Build.* 128 (2016) 617–638. doi:10.1016/j.enbuild.2016.07.034.
- [3] N. Artmann, H. Manz, P. Heiselberg, Climatic potential for passive cooling of buildings by night-time ventilation in Europe, *Appl. Energy.* 84 (2007) 187–201. doi:10.1016/j.apenergy.2006.05.004.
- [4] M. Kolokotroni, P. Heiselberg, Ventilative Cooling: State-of-the-Art Review, Aalborg Univ. Aalborg, Denmark. (2015). <https://www.buildup.eu/en/node/52462>.
- [5] A. O'Donnavan, A. Belleri, F. Flourentzou, G.-Q. Zhang, G.C. da Graca, H. Breesch, M. Justo-Alonso, M. Kolokotroni, M.Z. Pomianowski, P. O'Sullivan, others, Ventilative Cooling Design Guide: Energy in Buildings and Communities Programme. March 2018, Aalborg University, Department of Civil Engineering, 2018. <https://venticool.eu/wp-content/uploads/2016/11/VC-Design-Guide-EBC-Annex-62-March-2018.pdf> (accessed April 15, 2019).
- [6] Thermal mass and summer nights cooling, (2014). <https://www.youtube.com/watch?v=UHQnDYCC6w> (accessed March 3, 2021).
- [7] E. Solgi, Z. Hamedani, R. Fernando, H. Skates, N.E. Orji, A literature review of night ventilation strategies in buildings, *Energy Build.* 173 (2018) 337–352. doi:10.1016/j.enbuild.2018.05.052.
- [8] H.B.H. Awbi, G. Gan, Evaluation of the overall performance of room air distribution, *Proc. 6th Int. Conf. Indoor Air Qual. Clim. Helsinki.* 5 (1993) 283–288. <https://www.aivc.org/resource/evaluation-overall-performance-room-air-distribution>.
- [9] N. Artmann, R.L. Jensen, H. Manz, P. Heiselberg, Experimental investigation of heat transfer during night-time ventilation, *Energy Build.* 42 (2010) 366–374. doi:10.1016/j.enbuild.2009.10.003.
- [10] J. Pfafferott, S. Herkel, M. Jäschke, Design of passive cooling by night ventilation: Evaluation of a parametric model and building simulation with

- measurements, *Energy Build.* 35 (2003) 1129–1143. doi:10.1016/j.enbuild.2003.09.005.
- [11] N. Artmann, H. Manz, P. Heiselberg, Parameter study on performance of building cooling by night-time ventilation, *Renew. Energy.* 33 (2008) 2589–2598. doi:10.1016/j.renene.2008.02.025.
- [12] S.P. Corgnati, A. Kindinis, Thermal mass activation by hollow core slab coupled with night ventilation to reduce summer cooling loads, *Build. Environ.* 42 (2007) 3285–3297. doi:10.1016/j.buildenv.2006.08.018.
- [13] D.P. Finn, D. Connolly, P. Kenny, Sensitivity analysis of a maritime located night ventilated library building, *Sol. Energy.* 81 (2007) 697–710. doi:10.1016/j.solener.2006.10.008.
- [14] H. Breesch, A. Janssens, Performance evaluation of passive cooling in office buildings based on uncertainty and sensitivity analysis, *Sol. Energy.* 84 (2010) 1453–1467. doi:10.1016/j.solener.2010.05.008.
- [15] H. Breesch, A. Janssens, M.C. Gameiro Da Silva, Uncertainty and sensitivity analysis of the performances of natural night ventilation, in: *Roomvent 2004 Conf.*, 2004: p. ISBN 972-97973-2-3. <https://www.aivc.org/resource/uncertainty-and-sensitivity-analysis-performances-natural-night-ventilation>.
- [16] K. Goethals, H. Breesch, A. Janssens, Sensitivity analysis of predicted night cooling performance to internal convective heat transfer modelling, *Energy Build.* 43 (2011) 2429–2441. doi:10.1016/j.enbuild.2011.05.033.
- [17] J. Ran, M. Tang, Passive cooling of the green roofs combined with night-time ventilation and walls insulation in hot and humid regions, *Sustain. Cities Soc.* 38 (2018) 466–475. doi:10.1016/j.scs.2018.01.027.
- [18] L. Peeters, I. Beausoleil-Morrison, A. Novoselac, Internal convective heat transfer modeling: Critical review and discussion of experimentally derived correlations, *Energy Build.* 43 (2011) 2227–2239. doi:10.1016/j.enbuild.2011.05.002.
- [19] W. Ji, Q. Luo, Z. Zhang, H. Wang, T. Du, P.K. Heiselberg, Investigation on thermal performance of the wall-mounted attached ventilation for night cooling under hot summer conditions, *Build. Environ.* 146 (2018) 268–279. doi:10.1016/j.buildenv.2018.10.002.
- [20] J. Le Dréau, P. Heiselberg, R.L. Jensen, Experimental investigation of

- convective heat transfer during night cooling with different ventilation systems and surface emissivities, *Energy Build.* 61 (2013) 308–317. doi:10.1016/j.enbuild.2013.02.021.
- [21] U.S. Department of Energy, EnergyPlus 9.3 Engineering Reference, (2020). <https://bigladdersoftware.com/epx/docs/9-3/engineering-reference/>.
- [22] L.-X.X. Wu, J.-N.N. Zhao, Z.-J.J. Wang, Night ventilation and active cooling coupled operation for large supermarkets in cold climates, *Energy Build.* 38 (2006) 1409–1416. doi:10.1016/j.enbuild.2006.02.011.
- [23] M. Kolokotroni, A. Aronis, Cooling-energy reduction in air-conditioned offices by using night ventilation, *Appl. Energy.* 63 (1999) 241–253. doi:10.1016/S0306-2619(99)00031-8.
- [24] P. Roach, F. Bruno, M. Belusko, Modelling the cooling energy of night ventilation and economiser strategies on façade selection of commercial buildings, *Energy Build.* 66 (2013) 562–570. doi:10.1016/j.enbuild.2013.06.034.
- [25] J.E. Braun, Z. Zhong, Development and evaluation of a night ventilation precooling algorithm, *HVAC R Res.* 11 (2005) 433–458. doi:10.1080/10789669.2005.10391147.
- [26] A.T. Nguyen, S. Reiter, P. Rigo, A review on simulation-based optimization methods applied to building performance analysis, *Appl. Energy.* 113 (2014) 1043–1058. doi:10.1016/j.apenergy.2013.08.061.
- [27] B. Yang, A.K. Melikov, A. Kabanshi, C. Zhang, F.S. Bauman, G. Cao, H. Awbi, H. Wigö, J. Niu, K.W.D. Cheong, K.W. Tham, M. Sandberg, P.V. Nielsen, R. Kosonen, R. Yao, S. Kato, S.C. Sekhar, S. Schiavon, T. Karimipannah, X. Li, Z. Lin, A review of advanced air distribution methods - theory, practice, limitations and solutions, *Energy Build.* 202 (2019) 109359. doi:10.1016/j.enbuild.2019.109359.
- [28] G. Cao, H. Awbi, R. Yao, Y. Fan, K. Sirén, R. Kosonen, J. (Jensen) Zhang, A review of the performance of different ventilation and airflow distribution systems in buildings, *Build. Environ.* 73 (2014) 171–186. doi:10.1016/j.buildenv.2013.12.009.
- [29] C. Zhang, T. Yu, P. Heiselberg, M. Pominaowski, P. Nielsen, Diffuse Ceiling Ventilation – Design Guide, 2016. https://vbn.aau.dk/ws/portalfiles/portal/243057526/Diffuse_ceiling_ventilation_Design_guide.pdf (accessed June 5, 2019).

- [30] C. Zhang, P. Heiselberg, P. V. Nielsen, Diffuse ceiling ventilation - A review, *Int. J. Vent.* 13 (2014) 49–63. doi:10.1080/14733315.2014.11684036.
- [31] W. Wu, N. Yoon, Z. Tong, Y. Chen, Y. Lv, T. Aerenlund, J. Benner, Diffuse ceiling ventilation for buildings: A review of fundamental theories and research methodologies, *J. Clean. Prod.* 211 (2019) 1600–1619. doi:10.1016/j.jclepro.2018.11.148.
- [32] C. Zhang, M.H. Kristensen, J.S. Jensen, P.K. Heiselberg, R.L. Jensen, M. Pomianowski, Parametrical analysis on the diffuse ceiling ventilation by experimental and numerical studies, *Energy Build.* 111 (2016) 87–97. doi:10.1016/j.enbuild.2015.11.041.
- [33] P. V Nielsen, E. Jakubowska, The Performance of Diffuse Ceiling Inlet and other Room Air Distribution Systems, *Cold Clim. HVAC.* (2009) 7.
- [34] C.A. Hviid, S. Petersen, Integrated ventilation and night cooling in classrooms with diffuse ceiling ventilation, in: 11Th Ökosan, 2011. <https://orbit.dtu.dk/en/publications/integrated-ventilation-and-night-cooling-in-classrooms-with-diffu> (accessed October 30, 2020).
- [35] C.A. Hviid, S. Terkildsen, Experimental study of diffuse ceiling ventilation in classroom, in: 33rd AIVC Conf. 2nd TightVent Conf., 2012. <https://orbit.dtu.dk/en/publications/experimental-study-of-diffuse-ceiling-ventilation-in-classroom> (accessed October 30, 2020).
- [36] T. Yu, P. Heiselberg, B. Lei, M. Pomianowski, C. Zhang, A novel system solution for cooling and ventilation in office buildings: A review of applied technologies and a case study, *Energy Build.* 90 (2015) 142–155. doi:10.1016/j.enbuild.2014.12.057.
- [37] G. Rui, H. Yue, P. Heiselberg, A review of the performance indicators of night-time ventilation, 39th AIVC Conf. (2018) 14. <https://vbn.aau.dk/en/publications/f7e0ddc6-0fcc-469b-8f3d-279febddd589> (accessed May 17, 2019).
- [38] B. Givoni, Comfort, climate analysis and building design guidelines, *Energy Build.* 18 (1992) 11–23. doi:10.1016/0378-7788(92)90047-K.
- [39] A. Gagliano, F. Patania, F. Nocera, C. Signorello, Assessment of the dynamic thermal performance of massive buildings, *Energy Build.* 72 (2014) 361–370. doi:10.1016/j.enbuild.2013.12.060.
- [40] P. Blondeau, M. Spérandoio, F. Allard, Night ventilation for building cooling

- in summer, *Sol. Energy*. 61 (1997) 327–335. doi:10.1016/S0038-092X(97)00076-5.
- [41] A. Brambilla, J. Bonvin, F. Flourentzou, T. Jusselme, Life cycle efficiency ratio: A new performance indicator for a life cycle driven approach to evaluate the potential of ventilative cooling and thermal inertia, *Energy Build.* 163 (2018) 22–33. doi:10.1016/j.enbuild.2017.12.010.
 - [42] S. Carlucci, L. Pagliano, A review of indices for the long-term evaluation of the general thermal comfort conditions in buildings, *Energy Build.* 53 (2012) 194–205. doi:10.1016/j.enbuild.2012.06.015.
 - [43] EN 15251, Indoor environmental input parameters for design and assessment of energy performance of buildings addressing indoor air quality, thermal environment, lighting and acoustics, (2007). <https://webshop.ds.dk/Default.aspx?ID=219&GroupID=91.040.01&ProductID=M204572>.
 - [44] R. Guo, Y. Hu, M. Liu, P. Heiselberg, Influence of design parameters on the night ventilation performance in office buildings based on sensitivity analysis, *Sustain. Cities Soc.* 50 (2019) 101661. doi:10.1016/j.scs.2019.101661.
 - [45] WMO Country Profile Database, World Meteorological Organization, (2018). <https://www.wmo.int/cpdb/>.
 - [46] A. Saltelli, Sensitivity analysis: Could better methods be used?, *J. Geophys. Res. Atmos.* 104 (1999) 3789–3793. doi:10.1029/1998JD100042.
 - [47] European Commission - IPSC, Simlab 2.2: Reference Manual, (2008). <https://ec.europa.eu/jrc/en/samo/simlab>.
 - [48] R. Guo, P. Heiselberg, Y. Hu, H. Johra, R.L. Jensen, K.T. Jønsson, P. Peng, Experimental investigation of convective heat transfer for night ventilation in case of mixing ventilation, *Build. Environ.* 193 (2021) 107670. doi:10.1016/j.buildenv.2021.107670.
 - [49] R. Guo, P. Heiselberg, Y. Hu, H. Johra, C. Zhang, R.L. Jensen, K.T. Jønsson, P. Peng, Experimental investigation of convective heat transfer for night cooling with diffuse ceiling ventilation, *Build. Environ.* 193 (2021) 107665. doi:10.1016/j.buildenv.2021.107665.
 - [50] G.D. Smith, Numerical solution of partial differential equations: finite difference methods, Oxford university press, 1985. <https://anujitspenjoymath.files.wordpress.com/2019/02/g.-d.-smith->

numerical-solution-of-partial-differential-equations_-finite-difference-methods.pdf.

- [51] A.J. Chapman, Fundamentals of heat transfer, Macmillan, 1987.
- [52] G. Walton, Calculation of obstructed view factors by adaptive integration, Gaithersburg, MD, 2002. doi:10.6028/NIST.IR.6925.
- [53] J.R. Ehlert, T.F. Smith, View factors for perpendicular and parallel rectangular plates, J. Thermophys. Heat Transf. 7 (1993) 173–175. doi:10.2514/3.11587.
- [54] D.E. Fisher, An experimental investigation of mixed convection heat transfer in a rectangular enclosure, University of Illinois at Urbana-Champaign, 1995. <https://www.ideals.illinois.edu/handle/2142/22513>.
- [55] D.E. Fisher, C.O. Pedersen, Convective heat transfer in building energy and thermal load calculations, ASHRAE Trans. 103 (1997) 137–148. <https://citeseerx.ist.psu.edu/viewdoc/download?doi=10.1.1.616.9820&rep=rep1&type=pdf>.
- [56] Mathworks®, Curve Fitting Toolbox™: User's Guide (R2019b), 2019. <https://www.mathworks.com/help/curvefit/>.
- [57] A. Novoselac, B.J. Burley, J. Srebric, Development of new and validation of existing convection correlations for rooms with displacement ventilation systems, Energy Build. 38 (2006) 163–173. doi:10.1016/j.enbuild.2005.04.005.
- [58] S. Petersen, N.U. Christensen, C. Heinsen, A.S. Hansen, Investigation of the displacement effect of a diffuse ceiling ventilation system, Energy Build. 85 (2014) 265–274. doi:10.1016/j.enbuild.2014.09.041.
- [59] R. Guo, Y. Hu, P. Heiselberg, C. Zhang, H. Johra, P. Peng, Simulation and optimization of night cooling with mixing ventilation and diffuse ceiling ventilation in a cold climate region, Build. Environ. Submitted (2021).
- [60] R. Guo, P. Heiselberg, Y. Hu, C. Zhang, S. Vasilevskis, Optimization of night ventilation performance in office buildings in a cold climate, Energy Build. 225 (2020) 110319. doi:10.1016/j.enbuild.2020.110319.
- [61] P.O. Fanger, others, Thermal comfort: Analysis and applications in environmental engineering, Appl. Ergon. 3 (1972) 181. doi:10.1016/s0003-6870(72)80074-7.

PUBLICATION FOR THE THESIS

Thesis Title: Performance improvement of night ventilation for passive cooling of office buildings

Name of Ph.D. Student: Rui Guo

Name of Supervisor: Professor Per K. Heiselberg

List of Publications:

1. Guo, R., Hu, Y., Liu, M., & Heiselberg, P. (2019). Influence of design parameters on the night ventilation performance in office buildings based on sensitivity analysis. *Sustainable Cities and Society*, 50, 101661.
2. Guo, R., Heiselberg, P., Hu, Y., Johra, H., Jensen, R. L., Jønsson, K. T., & Peng, P. (2021). Experimental investigation of convective heat transfer for night ventilation in case of mixing ventilation. *Building and Environment*, 107670.
3. Guo, R., Heiselberg, P., Hu, Y., Johra, H., Zhang, C., Jensen, R. L., ... & Peng, P. (2021). Experimental investigation of convective heat transfer for night cooling with diffuse ceiling ventilation. *Building and Environment*, 107665.
4. Guo, R., Heiselberg, P., Hu, Y., Zhang, C., & Vasilevskis, S. (2020). Optimization of night ventilation performance in office buildings in a cold climate. *Energy and Buildings*, 225, 110319.
5. Guo, R., Hu, Y., Heiselberg, P., Zhang, C., Johra, H., & Peng, P. Simulation and optimization of night cooling with mixing ventilation and diffuse ceiling ventilation in a cold climate. Submitted to *Building and Environment*.

Other publications:

1. Guo, R., Heiselberg, P., & Hu, Y. (2018). A review of the performance indicators of nighttime ventilation. In 39th AIVC Conference: "Smart ventilation for buildings".
2. Guo, R., Hu, Y., Liu, M., & Heiselberg, P. (2019). Optimal night mechanical ventilation control strategy in office buildings. X IAQVEC Conference. In *IOP Conference Series: Materials Science and Engineering* (Vol. 609, No. 3, p. 032013). IOP Publishing.
3. Guo, R., Gao, Y., Zhuang, C., Heiselberg, P., Levinson, R., Zhao, X., & Shi, D. (2020). Optimization of cool roof and night ventilation in office buildings: A case study in Xiamen, China. *Renewable Energy*, 147, 2279-2294.
4. Hu, Y., Guo, R., & Heiselberg, P. K. (2020). Performance and control strategy development of a PCM enhanced ventilated window system by a

- combined experimental and numerical study. *Renewable Energy*, 155, 134-152.
5. Hu, Y., Guo, R., Heiselberg, P. K., & Johra, H. (2020). Modeling PCM Phase Change Temperature and Hysteresis in Ventilation Cooling and Heating Applications. *Energies*, 13(23), 6455.
 6. Hu, Y., Heiselberg, P. K., & Guo, R. (2020). Ventilation cooling/heating performance of a PCM enhanced ventilated window-an experimental study. *Energy and Buildings*, 214, 109903.
 7. Hu, Y., Heiselberg, P. K., Johra, H., & Guo, R. (2020). Experimental and numerical study of a PCM solar air heat exchanger and its ventilation preheating effectiveness. *Renewable Energy*, 145, 106-115.

This thesis has been submitted for assessment in partial fulfillment of the Ph.D. degree. The thesis is based on the submitted or published scientific papers which are listed above. Parts of the papers are used directly or indirectly in the extended summary of the thesis. As part of the assessment, co-author statements have been made available to the assessment committee and are also available at the Faculty.

APPENDICES

Appendix A. Paper 1..... 75

Appendix B. Paper 2..... 93

Appendix C. Paper 3..... 112

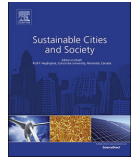
Appendix D. Paper 4..... 127

Appendix E. Paper 5..... 141

Appendix A. Paper 1

Guo, R., Hu, Y., Liu, M., & Heiselberg, P. (2019). Influence of design parameters on the night ventilation performance in office buildings based on sensitivity analysis. *Sustainable Cities and Society*, 50, 101661. <https://doi.org/10.1016/j.scs.2019.101661>

Reprinted by permission from Elsevier.



Influence of design parameters on the night ventilation performance in office buildings based on sensitivity analysis

Rui Guo*, Yue Hu, Mingzhe Liu, Per Heiselberg

Department of Civil Engineering, Aalborg University, Thomas Manns Vej 23, Aalborg, 9220, Denmark

ARTICLE INFO

Keywords:

Night ventilation
Performance indicators
Design parameters
Sensitivity analysis
Parametric simulation

ABSTRACT

Overheating and energy-extensive consumption in buildings, especially in office buildings, are emerging challenges. Night ventilation (NV) is a promising technique. The performance of NV can be evaluated by a series of performance indicators. As many design parameters affect those indicators, it is beneficial to choose suitable indicators and identify the most important design parameters to develop more efficient design solutions at the early design stage. Sensitivity analysis makes it possible to identify the most important design parameters in relation to NV performance and to focus design and optimization of NV on these fewer, but most important, parameters. A holistic approach integrating sensitivity analysis and parametric simulation analysis is developed to explore the key design parameters on night cooling performance indicators and evaluate the applicability and limitations of those indicators. The results show that the climatic conditions and NV modes strongly affect the influence of design parameters on the performance indicators. The window-wall ratio, internal thermal mass level, internal convective heat transfer coefficient, and night mechanical air change rate are the most important design parameters. The indicators of ventilative cooling advantage, cooling requirement reduction, and percentage outside the range are recommended for the night cooling performance evaluation.

1. Introduction

During the last decades, there has been a trend of increasing cooling demand in buildings. This has especially been the case for commercial buildings, where high internal loads in combination with high solar gains through extensive glazing have led to considerable cooling loads, even in moderate and cold climates (Artmann, Manz, & Heiselberg, 2008). An additional rise of the cooling demand is caused by global climate warming, which is expected to increase summertime temperatures significantly (Artmann, Gyalistras, Manz, & Heiselberg, 2008; Artmann, Manz, & Heiselberg, 2007). Night ventilation is a promising way to alleviate or solve the foregoing problem. The basic concept is to utilize the relatively low-temperature ambient air during the night time by the natural or mechanical ventilation systems to cool down the indoor air as well as the building construction components to provide a heat sink for the following day (Belmonte, Eguía, Molina, & Almendros-Ibáñez, 2015; Santamouris, Santamouris, & Asimakopoulos, 1996).

Numerous night cooling projects have been successfully undertaken in the past decades (Geros, Santamouris, Tsangrasoulis, & Guaracino, 1999; Ji et al., 2018; Solgi, Hamedani, Fernando, Skates, & Orji, 2018; Strith et al., 2018; Wang, Yi, & Gao, 2009). Despite the simplicity of the concept, architects and engineers are hesitant to apply this low-energy

technology (Breesch, Bossaer, & Janssens, 2005). One reason is that the efficiency of night-time cooling is affected by many parameters, which makes the performance predictions uncertain. Another reason is that there are many different performance indicators used for night ventilation design and evaluation, which confuse designers. Some of these indicators focus on temperature performance, others evaluate the energy balance, and several of them pay attention to thermal comfort. The heat removal effectiveness of night ventilation is evaluated by the temperature performance of the building and its relationship to the outdoor temperature profile. Several researchers have proposed different indicators for heat removal, including ventilation effectiveness for heat removal (Awbi & Gan, 1993), temperature efficiency (Artmann, Jensen, Manz, & Heiselberg, 2010), temperature difference ratio (Givoni, 1992), decrement factor, and daily time lag (Gagliano, Patania, Nocera, & Signorello, 2014). The energy efficiency of night ventilation is evaluated by the ratio of ventilation energy saving and ventilation equipment energy use. The indicators for energy efficiency proposed by researchers are the coefficient of performance (Pfafferott, Herkel, & Jäschke, 2003), potential energy efficiency index (Blondeau, Spérandoio, & Allard, 1997), ventilative cooling advantage, cooling requirement reduction (O'Donnavan et al., 2018), etc. For thermal comfort evaluation when applying night ventilation, there are indicators like the

* Corresponding author.

E-mail address: rg@civil.aau.dk (R. Guo).

<https://doi.org/10.1016/j.scs.2019.101661>

Received 16 March 2019; Received in revised form 23 May 2019; Accepted 13 June 2019

Available online 20 June 2019

2210-6707/© 2019 Elsevier Ltd. All rights reserved.

Nomenclature		$T_{conf,sup}$ Upper comfort temperature limit (°C)	
T_{out} Outlet air temperature (°C)		Abbreviations	
T_{in} Inlet air temperature (°C)		NV	Night ventilation
$\bar{T}_{surface}$ Average building indoor surface temperature (°C)		TE	Temperature efficiency
$T_{o,max}$ Maximum ambient air temperature (°C)		TDR	Temperature difference ratio
$T_{o,min}$ Minimum ambient air temperature (°C)		DF	Decrement factor
$T_{i,max}$ Maximum building indoor air temperature (°C)		COP	Coefficient of performance
$T_{i,min}$ Minimum building indoor air temperature (°C)		ADV	Ventilative cooling advantage
$T_i(t)$ Building indoor air temperature at time t (°C)		CRR	Cooling requirements reduction
$T_o(t)$ Ambient air temperature at time t (°C)		POR	Percentage outside the range
\dot{m}_{air} Airflow rate (kg/s)		DhC	Degree-hours criterion
c_p Specific heat capacity (kJ/kg.°C)		DI	Weighted discomfort temperature index
P_e Electric power of fan (W)		SHGC	Solar heat gain coefficient
t_i Start time of night-time ventilation (h)		CHTC	Convective heat transfer coefficient
t_f End time of night-time ventilation (h)		MCA	Monte Carlo analysis
$Q_{el,c}^{ref}$ Cooling system electrical energy consumption of the scenario without ventilative cooling (kWh/m ²)		LHS	Latin hypercube sampling
$Q_{el,c}^{scen}$ Cooling system electrical energy consumption of the scenario with ventilative cooling (kWh/m ²)		SRC	Standardized regression coefficient
$Q_{el,v}$ Electrical energy use of the night ventilation system		SA	Sensitivity analysis
$Q_{t,c}^{ref}$ Cooling demand of the reference scenario (kWh)		ACH	Air change rate per hour
$Q_{t,c}^{scen}$ Cooling demand of the analyzed scenario (kWh)		WWR	Window-wall ratio
wf_i Weighting factor		AC	Air conditioner
h_i Occupied hours (h)			

degree-hours criterion (Artmann, Manz et al., 2008) and the weighted discomfort temperature index (Corgnati & Kindinis, 2007). Some of the indicators are independent of each other, others have a different level of dependency between each other. It is necessary to choose multiple indicators to have an overall evaluation of the night ventilation performance.

Sensitivity analysis is a useful tool to identify the most important parameters for the building design and energy analysis (Tian, 2013). The methods for sensitivity analysis can be sorted into local sensitivity methods and global sensitivity methods (Saltelli, Ratto, Tarantola, & Campolongo, 2005). Local sensitivity analysis is based on only varying one design parameter at a time, while the global sensitivity analysis is based on changing all the design parameters at the same time (Mara & Tarantola, 2008). Therefore, the global method is more reliable but with a high computational calculation effort compared to the local method. Both local (Firth, Lomas, & Wright, 2010; Lam, Wan, & Yang, 2008; Lomas & Eppel, 1992; Petersen & Svendsen, 2010) and global methods (Breesch & Janssens, 2010; Goethals, Breesch, & Janssens, 2011; Heiselberg et al., 2009; Hopfe & Hensen, 2011; Hygh, DeCarolis, Hill, & Ranji Ranjithan, 2012) have been widely used in investigating the most important variables related to building energy performance. Among those, few research are about night ventilation performance. Artmann, Manz et al. (2008) conducted a local sensitivity analysis to investigate the most influential design parameters for night mechanical ventilation in an office room located in a moderate climatic location with the indicator of the number of overhear degree hours. The conclusion was that the climatic conditions and air flow rate at night-time were the most important parameters. Finn, Connolly, and Kenny (2007) examined the design and operational parameters in a night ventilated library building located in a maritime type climate. The result showed the building mass as the most significant parameter, followed by the internal heat gains and night air flow rates. Breesch and Janssens (2010), Breesch, Janssens, and Gameiro Da Silva (2004) analyzed the input parameters causing the uncertainty on the thermal comfort for a single-sided night natural ventilation in the moderate climate. The results showed that the top 3 important design parameters were the internal heat gains, the solar heat gain coefficient of the sun blinds, and the internal convective heat transfer coefficient. Encinas and De Herde

(2013) found that for night cooling of a real estate market in a warm climate region, the most important input parameter for summer comfort is solar and light transmittance of the solar protection devices, followed by the night ventilation flow rate. Goethals et al. (2011) investigated the sensitivity of convection algorithms on the night ventilation performance, showing that the selection of the convection algorithm strongly affects the energy and thermal comfort predictions. Ran and Tang (2018) adopted the local sensitivity analysis method to investigate the influence of external wall insulation level, night ventilation airflow rate on the indoor air temperature reduction, showing that the increase of the insulation level and night airflow rate will enhance the night cooling performance.

The aforementioned sensitivity analyses for night ventilation performance are mostly only focused on one night ventilation mode with one daytime cooling method or limited to the amount of performance indicators and climate regions. To get an overall design guideline of night ventilation design parameters, research should include various night ventilation systems and performance indicators in different climatic conditions.

This paper firstly selects nine performance indicators for night ventilation performance evaluation. Then it investigates the performance of night mechanical and natural ventilation integrated with three different daytime cooling systems (air conditioning, mechanical ventilation, and natural ventilation) to do a global sensitivity analysis for an office room located in three climate zones (cold, medium, and hot climate regions). The night cooling performance is analyzed based on the parametric simulation results in consideration of the thermal comfort evaluation and energy-saving benefit. Finally, the evaluation of the applicability of performance indicators is conducted to propose the recommendation.

2. Methodology

2.1. Outline of the quantitative study

A systematic approach is proposed to evaluate and quantify the influence of different design parameters on the night ventilation performance alongside the evaluation of performance indicators as shown

in Fig. 1. In the first step, a suitable series of performance indicators for night cooling are reviewed and selected. In the second step, a software designed for uncertainty and sensitivity analysis by Monte Carlo method-SimLab v2.2 (EU Science Hub, 2008) generates samples based on the input design parameters and sends the scenarios to the parametric simulation manger jEPlus (Zhang & Korolija, 2016). Then, the jEPlus uses the model built by EnergyPlus to do parametric simulations before transferring the simulation results back again to SimLab. Follow on, a global sensitivity analysis is conducted in SimLab by regression method to investigate the influence of design parameters on performance indicators. Finally, the parametric simulation results of night cooling performance indicators are used to propose the application recommendations for those performance indicators by mathematical analysis.

2.2. Performance indicators of night ventilation

Appropriate performance indicators should be chosen according to the application conditions of the night ventilation, in order to provide guidelines for the measurement or simulation in the design process to achieve those goals. It should be noted that the performance of night ventilation cannot be well represented by a single indicator. It needs a combination of different types of indicators. The performance of night ventilation can be quantified by the thermodynamical effect (energy balance) and by its cooling effect (room temperature). Night ventilation performance indicators can be sorted into the following four categories: 1) Heat removal effectiveness, 2) Energy efficiency, 3) Ability to reduce cooling energy use, and 4) Thermal comfort improvement (Rui, Yue, & Heiselberg, 2018). Heat removal effectiveness quantifies the ability of the night cooling system to remove excess heat stored in the building. Energy efficiency quantifies the energy use required to reduce cooling demand. The ability to reduce cooling energy use represents the ability of the night cooling system to provide energy saving for the daytime mechanical cooling. Thermal comfort improvement shows the ability of the night cooling system to reduce periods of thermal discomfort during the occupied time.

Some indicators are more suitable for simulation analysis because they can be easily calculated by post-processing outcomes of building energy simulation runs of a reference scenario (e.g. mechanically cooled building) and a ventilative cooling scenario (e.g. natural night cooling and daytime mechanical cooling). However, other indicators are more suitable for experimental analysis, since some data is easier to obtain in field studies. In addition, in experimental studies, the thermal comfort improvement indicators are much more prevalent than the energy efficiency indicators, probably because the indoor conditions

are easier obtained than energy data, which is often challenging to measure directly.

In this paper, we select nine performance indicators in total from the four categories mentioned above to evaluate the influences of different design parameters. Table 1 summarizes the selected performance indicators.

2.3. Case study

2.3.1. Building model

The EnergyPlus v.8.9 software was selected in this study to build a model and simulate its heat, energy, and thermal comfort performance. An office building located in Aarhus, Denmark was used for this study, as shown in Fig. 2(a). The building is 103.7 m long and 9.5 m wide, with 3 stories and a total area of 2924.1 m². The layout of the office building can be seen in Fig. 2(b), in which N, W, S, and C indicate the orientation as north, west, south, and center respectively. A typical office room 1 W occupied by 6 persons was selected as the case zone, whose floor area is 51.3 m² and height is 2.8 m (Vidrih, Arkar, & Medved, 2016). Internal partitions between the concerned zone 1 W and adjacent zones were set as adiabatic to assume the similar conditions in all adjacent zones. The case was simulated in the hot (Rome), medium (Geneva), and cold (Copenhagen) climates respectively to investigate the climate influence on night ventilation performance. The weather data for the three locations originated from the World Meteorological Organization (WMO, 2018).

In order to evaluate the influence of building orientation on night ventilation performance, the orientation was set with a uniform distribution from 0° to 360°. The European ventilation standard for office building recommends that the airtightness should be below 1.0 h⁻¹ in case of buildings with more than three stories (EN 16798-3, 2017). The infiltration of building airtightness was set with triangular distribution with a minimum value of 0.1 h⁻¹, maximum 1.0 h⁻¹, and mean value 0.6 h⁻¹.

2.3.2. Thermal mass models

Thermal mass can be sorted as external and internal thermal mass. External thermal mass, such as an external wall or roof, is affected by the ambient air temperature and solar radiation directly. Internal thermal mass, such as internal walls or interior furniture, influences the indoor air temperature through the process of absorbing and releasing heat (Zhou, Zhang, Lin, & Li, 2008). For the concerned zone 1 W, the external thermal mass is the external wall, while the internal thermal mass contains an internal wall, ceiling, floor, and interior furniture.

Three different levels (light, medium, heavy) were defined for

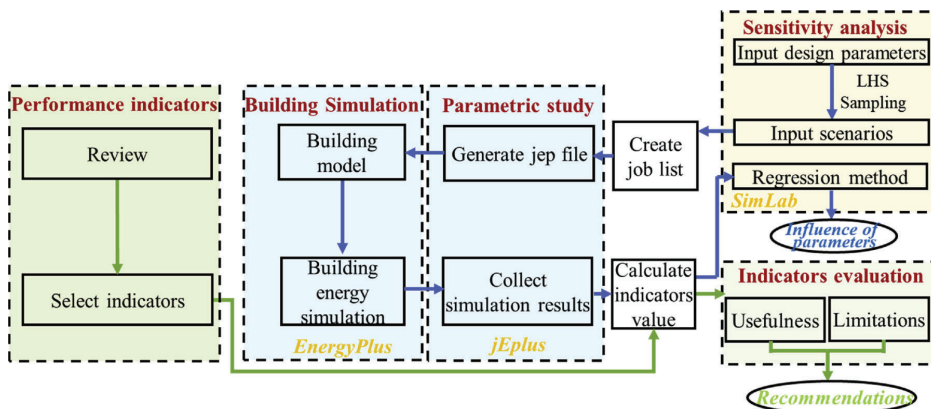


Fig. 1. Flow chart of the systematic approach.

Table 1
Summary of the selected performance indicators.

Family of indices	Indicator name	Expression	Explanation	Source
Heat removal effectiveness	Temperature efficiency (TE)	$TE = \frac{T_{out} - T_{in}}{T_{surface} - T_{in}}$	Originates from experimental studies. Mainly depends on the air distribution concept and the airflow rate. For mixing ventilation, the value of temperature efficiency is limited to 1, while in displacement ventilation the temperature stratification can result in an efficiency exceeding 1.	(Armann et al., 2010)
	Temperature difference ratio (TDR)	$TDR = \frac{T_{o,max} - T_{i,max}}{T_{o,max} - T_{o,min}}$	Used with good results to compare passive cooling systems with different configurations. A higher value of TDR indicates a larger temperature difference between indoors and outdoors and thus a more efficient night cooling strategy.	(Givoni, 1992)
	Decrement factor (DF)	$DF = \frac{T_{i,max} - T_{i,min}}{T_{o,max} - T_{o,min}}$	Means the ratio of indoor air temperature fluctuation to the ambient air temperature fluctuation.	(Gagliano et al., 2014)
	Coefficient of performance (COP)	$COP = \frac{\int_{t_0}^{t_1} \dot{m}_{air} \rho (T_1(t) - T_0(t)) dt}{\int_{t_0}^{t_1} \dot{Q}_{ch} dt}$	The ratio of the cooling energy delivered into the building to the auxiliary electric consumption by mechanical machines during the night period. The higher the COP, the better the performance for night-time ventilation.	(Pfaferott et al., 2003)
Energy efficiency	Ventilative cooling advantage (ADV)	$ADV_{VC} = \frac{Q_{ch}^{ref} - Q_{ch}^{gen}}{Q_{ch}^{ref}}$	Defines the benefit of the night ventilative cooling in case which ventilation rates are provided mechanically. If ADV_{VC} is lower than 1, the electrical energy use of the scenario is higher than the reference scenario. If ADV_{VC} is higher than 1, the electrical energy use of the scenario is lower than the reference scenario.	(O'Domavan et al., 2018)
	Cooling requirements reduction (CRR)	$CRR = \frac{Q_{ch}^{ref} - Q_{ch}^{gen}}{Q_{ch}^{ref}}$	Expresses the percentage of reduction of the cooling demand of a scenario with night cooling in respect to the cooling demand of the reference scenario. The value of CRR can range between -1 and +1. If CRR is positive, it means that the night ventilative cooling system reduces the cooling need of the building. If the value of CRR is negative or 0, it means that the night ventilative cooling system does not reduce the cooling requirements	(O'Domavan et al., 2018)
Thermal comfort improvement in daytime	Percentage outside the range (POR)	$POR = \frac{\sum_{i=1}^{N_h} (w_i \cdot h_i)}{\sum_{i=1}^{N_h} h_i}$	Accumulate the percentage of occupied hours when the thermal comfort parameters are outside a specified range. The comfort range can be expressed in terms of PMV when referring to the Panger model or in terms of operative temperature when referring to the adaptive comfort model. If the thermal comfort parameters exceed the corresponding comfort range, the w_i would be 1, or the w_i would be 0. The lower value of POR is, the better thermal comfort improvement is provided by night ventilative cooling.	(Carlucci & Pagliano, 2012)
	Degree-hours criterion (DhC)	$DhC = \sum_{i=1}^{N_h} (w_i \cdot h_i)$	Accumulate overheating degree hours of the operative room temperature above 26°C during the occupied period. w_i here is calculated as the module of the difference between actual and calculated operative temperature. The lower the value of DhC is, the better the thermal comfort improvement is provided by night ventilation.	(Armann, Manz et al., 2008)
Weighted discomfort temperature index (DI)		$DI = \sum (T_i - T_{comf,sup})$	Discomfort weighted on the distance of calculated operative temperature from the comfort temperature upper limit which is fixed at 28 °C. The lower the value of DI is, the better thermal comfort improvement is provided by night ventilation.	(Gorgnati & Kindinis, 2007)

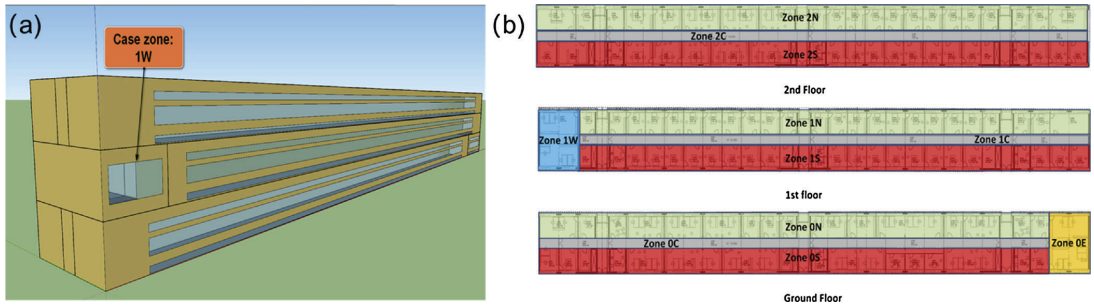


Fig. 2. (a) View of the building model and (b) Layout of the case office building.

external and internal thermal mass, respectively. Table 2 shows the detailed composition of the thermophysical properties of building materials and the thermal mass of the building components. The last column of Table 2 is the dynamic heat capacity per unit floor area, indicating the thermal mass level. The dynamic heat capacity c_{dyn} is the ability to store energy per area when the building component is exposed to a sinusoidal temperature variation for a period of 24 h with surface resistance, as defined by EN ISO (13786, 2017). It should be noticed that for light, medium, and heavy internal thermal mass levels, the interior furniture surface area is 10, 30, 50 m² respectively.

2.3.3. Internal heat gain models

Similar to the thermal mass, internal heat gains were also defined by three different levels, cf. Table 3. The hourly operational schedules for people, lights, and electric equipment were always 1.0 during the occupied hours (08:00–17:00) and 0 for the other hours. The people clothing insulation was set to 0.5 clo in summer (EN 15251, 2007).

2.3.4. Window models

The windows in zone 1W were modeled as energy-efficient windows with a double pane construction made by 3 mm glass and a 13 mm gap filled with argon. The window U-value is 1.062 W/m²K, while the glass solar heat gain coefficient (SHGC) and visible transmittance are 0.579 and 0.698 respectively. In order to evaluate the influence of window-wall ratio on night ventilation performance, the design parameter of the window-wall ratio for north and south windows of zone 1W was set with a discrete distribution from 10%, 20%, ..., 90%.

2.3.5. Night ventilation systems

Two typical concepts of night ventilation were selected for the investigation, which are mechanical ventilation and natural ventilation. The night venting schedule is during 17:00–08:00 (+1) from 1st July to 1st September, except for weekends.

The night mechanical ventilation system is a balanced system with a supply fan and an exhaust fan. The night natural ventilation has been modeled using a wind and stack model in EnergyPlus, in which the ventilation air flow rate is a function of wind speed and thermal stack effect, along with the area of the opening being modeled (U. Department of Energy, 2017).

To prevent the overcooling and to store more cooling energy in building thermal mass, the minimum indoor air temperature setpoint for both night ventilation systems was 18°C (M.A. J, 1995). Night ventilation is only activated when the indoor air temperature exceeds the ambient temperature at a certain temperature which was set with a discrete value of 1, 2, and 3 °C.

Because the maximum airflow rate for the design of night ventilation should be further increased corresponding to an air change rate of 10 h⁻¹ (O'Donnovan et al., 2018), the design air flow rate for night mechanical ventilation was set with uniform distribution from 1 to 10 h⁻¹. For night natural ventilation, the opening area is 0.4 m², and

the discharge coefficient of the opening was set with a typical uniform distribution from 0.5 to 0.7 (Flourentzou, Van der Maas, & Roulet, 2002). The opening effectiveness for natural ventilation was calculated automatically in EnergyPlus so that the window can be assumed to adjust its angle to make the most use of wind under different wind direction. Table 4 shows the detailed setup information of night ventilation.

2.3.6. Daytime cooling systems

Three typical methods were selected to cool the building at daytime, which are air conditioner (AC), mechanical ventilation, and natural ventilation. The operating period for daytime cooling is 08:00–17:00 on weekdays from 1st July to 1st September.

A packaged thermal heat pump with a dedicated outdoor air system was modeled as the air conditioning system with COP (coefficient of performance) 3.0 for cooling in summer with the HVAC template module of EnergyPlus. The setpoint for the air conditioning system is 24.5°C which is a middle point of the temperature range for cooling, EN 15251 (EN 15251, 2007). The outdoor air flow rate was set to 30 m³/h per person (EN 15251, 2007).

The setups for daytime mechanical ventilation and natural ventilation are similar to that of night mechanical and natural ventilation systems respectively, but with some differences. The first difference is the design flow rate for daytime mechanical ventilation and maximum flow rate for daytime natural ventilation is 6 h⁻¹. It is because the typical maximum air flow rate used in the design of daytime ventilative cooling is 6 h⁻¹ (O'Donnovan et al., 2018). The second difference is that when the indoor and outdoor air temperature difference is smaller than 2°C, the outdoor air flow rate is 30 m³/h per person to fulfill the human hygiene requirements. Table 5 shows the detailed setup information of daytime cooling methods.

2.3.7. Internal convective heat transfer coefficient

Several research indicated different convective heat transfer coefficient (CHTC) correlations or values for different types of the internal surface (Alamdari & Hammond, 1983; Lomas, 1996). According to the EN ISO (13791, 2012), the standard convective heat transfer coefficient for vertical, horizontal (upward), and horizontal (downward) are 2.5, 5.0, 0.7 W/m²K respectively. As a consequence, the CHTC of internal surfaces were both set with uniform distribution from 0.5 to 5 W/m²K.

2.3.8. Summary of the independent design parameters

Table 6 summarizes the independent design parameters for night mechanical/natural ventilation. P6 has two meanings, of which night air change rate per hour (ACH) is for mechanical ventilation and discharge coefficient for the opening of natural ventilation.

2.4. Sensitivity analysis

Sensitivity analysis (SA) can be divided into three different types:

Table 2
Detailed composition of the thermal mass and thermophysical properties of building materials.

External thermal mass								
	<i>d</i> (mm)	ρ (kg/m ³)	<i>c</i> (J/kg·K)	λ (W/m·K)	Total $c_{\text{ext}}/A_{\text{ext}}$ (kJ/m ² ·K)			
External wall (Heavy)								
Plaster	15	1400	936	0.7	77.5			
Sand-lime	150	2000	936	1.1				
Exp-polystyrene	120	40	1200	0.035				
Plaster ext.	20	1600	1000	0.87				
External wall (Medium)								
Plasterboard (fire-resisting)	160	900	1000	0.25	42.0			
Concrete 200	200	2385	800	1.2				
PUR 210	210	40	1400	0.021				
Cement plate	15	2000	1500	0.35				
External wall (Light)								
Gypsum board	25	1000	792	0.4	24.0			
Exp-polystyrene	120	40	1200	0.035				
Concrete 180	180	2400	1080	1.8				
Internal thermal mass								
	<i>d</i> (mm)	ρ (kg/m ³)	<i>c</i> (J/kg·K)	λ (W/m·K)	$R_{\text{userdefined}}$ (m ² ·K/W)	Total $c_{\text{ext}}/A_{\text{ext}}$ (kJ/m ² ·K)		
Internal wall (heavy)								
Plaster	15	1400	936	0.7	238.1			
Sand-lime	150	2000	936	1.1				
Plaster	15	1400	936	0.7				
Ceiling (Heavy)								
Concrete 180	180	2400	1080	1.8				
Floor (Heavy)								
Concrete 180	180	2400	1080	1.8				
Sound insulation	40	30	1404	0.04				
Plaster floor	80	2200	1080	1.5				
Carpet	5	80	930	0.05				
Interior furniture (Heavy)								
Wood 6inch	150	540	1210	0.12				
Internal wall (Medium)								
Gypsum board	25	1000	792	0.4				
Mineral wool	70	1750	1000	0.56				
Gypsum board	25	1000	792	0.4				
Ceiling (Medium)								
Cast concrete	120	1800	1000	1.13				
Floor (Medium)								
Linoleum	3	1200	1470	0.17				
Cement screed (fiber reinforced)	50	1400	1000	0.8				
Acoustic insulation	9	556	1700	0.15				
OSB panels	25	600	2150	0.13				
Insulation glass wool	200	28	1030	0.032				
Wooden panels	60	250	2100	0.047				
Interior furniture (Medium)								
Wood 6inch	150	540	1210	0.12				
Internal wall (Light)								
Gypsum board	25	1000	792	0.4		160.1		
Mineral wool	70	90	612	0.036				

(continued on next page)

Table 2 (continued)

Internal thermal mass					Total $c_{cpr}/A_{q_{cpr}}$ (kJ/m ² ·K)
	d (mm)	ρ (kg/m ³)	c (J/kg·K)	λ (W/m·K)	
Gypsum board	25	1000	792	0.4	0.16
Suspend ceiling (Light)					
Acoustic panel	20	800	900	0.21	
Air gap	250				
Floor (Light)					
Linoletum	3	1200	1470	0.17	
Acoustic insulation	9	556	1700	0.15	
OSB panels	25	600	2150	0.13	
Insulation glass wool	200	28	1030	0.032	
Wooden panels	60	250	2100	0.047	
Interior furniture (Light)					63.3
Wood 6inch	150	540	1210	0.12	

Table 3
Internal heat gains per unit floor area in zone 1 W.

Internal heat gains		Low	Medium	High
People	W/pers.	70	75	80
Lights	W/m ²	4	6	8
Electric equipment	W/m ²	6	8	10
Total	W/m ²	18.2	22.8	27.4

Table 4
Detailed setup information of night ventilation systems.

<i>Night mechanical ventilation</i>	
System	Supply fan + exhaust fan
Design pressure rise	600 Pa (Both for supply and exhaust fan)
Fan total efficiency	0.9
Design flow rate	U[1-10]
Minimum indoor temperature	18°C
Activation requirements	T _{in} -T _{out} > D[1,2,3]°C
<i>Night natural ventilation</i>	
System	Natural ventilation driven by wind and stack effect
Minimum indoor temperature	18 °C
Activation requirements	T _{in} -T _{out} > D[1,2,3]°C
Opening area	0.4 m ²
Discharge coefficient	U[0.5-0.7]
Opening effectiveness	Automatic calculation by EnergyPlus

T_{in}: indoor air temperature (°C); T_{out}: ambient temperature (°C); D: discrete distribution (levels); U: uniform distribution (lower value, upper value).

Table 5
Detailed setup information about daytime cooling methods.

<i>Daytime air conditioning</i>	
System	Packaged terminal heat pump + dedicated outdoor air system
Setpoint	24.5 °C
Design fan pressure rise	75 Pa
Outdoor air flow rate	30 m ³ /h/person
<i>Daytime mechanical ventilation</i>	
System	Supply fan + exhaust fan
Design fan pressure rise	1000 Pa (Both for supply and exhaust fan)
Fan total efficiency	0.9
Minimum indoor temperature	24.5°C
Design flow rate	6 h ⁻¹ or 30 m ³ /h/person
Control strategy	If T _{in} -T _{out} > 2 °C air flow = 6 h ⁻¹ or flow = 30 m ³ /h /person
<i>Daytime natural ventilation</i>	
System	Natural ventilation driven by wind and stack effect
Minimum indoor temperature	24.5°C
Opening area	0.4 m ²
Discharge coefficient	U[0.5-0.7]
Control strategy	If T _{in} -T _{out} > 2°C air flow < 6 ACH or flow = 30 m ³ /h /person
Opening effectiveness	Automatic calculation by EnergyPlus

screening methods, local sensitivity methods, and global sensitivity methods (Saltelli, Chan, & Scott, 2000). In this paper, the global sensitivity analysis methods were selected to quantify the influence of a single input variable on the outputs while all other input variables also vary simultaneously. Monte Carlo Analysis (MCA) is the most prevalent variance-based method because it provides approximate solutions only with a restricted number of simulations and the input variables have uncertainties of a different order of magnitude (Breesch & Janssens, 2010). Different sampling methods exist in MCA studies: random sampling, importance sampling, quasi-random sampling, and Latin hypercube sampling (LHS). The LHS method was selected because this method is a powerful tool in building performance analysis and it fully covers the range of each variable (Tian, 2013). The sample size based on LHS was chosen to be 400 as the minimum number of model

Table 6

Design parameters for sensitivity analysis, their range, and distribution.

Parameter	Unit	Distribution
P1 External thermal mass	$\text{kJ/m}^2\text{K}$	D[24.0, 42.0, 77.5]
P2 Internal thermal mass	$\text{kJ/m}^2\text{K}$	D[63.3, 160.1, 238.1]
P3 Internal heat gains	W/m^2	D[18.2, 22.8, 27.4]
P4 Window-wall ratio (WWR)	%	D[10, 20, 30, 40, 50, 60, 70, 80, 90]
P5 Internal CHTC	$\text{W/m}^2\text{K}$	U[0.7-5]
P6 Night ACH	h^{-1}	U[1-10]
Discharge coefficient for opening	–	U[0.5-0.7]
P7 Building airtightness	h^{-1}	T[0.1, 0.6, 1]
P8 Building orientation	°	U[0-360]
P9 Indoor and outdoor ΔT	°C	D[1,2,3]

Note: D: discrete distribution (levels); U: uniform distribution (lower value, upper value); T: triangular distribution (lower value, mode, upper value).

executions should be higher than 10 times the number of variables (European Commission - IPSC, 2008). SimLab v2.2 generated the 400 samples by LHS method (European Commission - IPSC, 2008), then those samples were sent to jEPlus to do parametric simulations before transferring the simulation results back again to SimLab to do the sensitivity analysis. The Standardized Regression Coefficient (SRC) based on regression analysis was used as the global sensitivity analysis indicator when the input variables are independent. The sign of SRC indicates whether the output increases (positive value) or decreases (negative value) with the related input variable increases. The bigger the absolute value of SRC, the more influential the input variable is. Calculating the SRCs involves a linear multidimensional model based on an $m \times k$ samples, with m the total number of samples and k the total number of input variables:

$$\hat{y}_i = \beta_0 + \sum_{j=1}^k \beta_j x_j \quad (1)$$

where \hat{y}_i represents the estimate of the output y_i , x_j the input variable, i is the sample size, j is the number of variables and β_j the regression coefficient. This regression model can be standardized by subtracting the mean value from each input and output factor and successively dividing this result by its standard deviation:

$$\frac{\hat{y}_i - \bar{y}}{\hat{\sigma}} = \sum_{j=1}^k \frac{\beta_j \hat{\sigma}_j}{\hat{\sigma}} \frac{(x_j - \bar{x}_j)}{\hat{\sigma}_j}$$

where

$$\bar{y} = \sum_{i=1}^m \frac{y_i}{m}, \bar{x}_j = \sum_{i=1}^m \frac{x_{ij}}{m}, \hat{\sigma} = \sqrt{\left[\sum_{i=1}^m \frac{(y_i - \bar{y})^2}{m-1} \right]}, \hat{\sigma}_j = \sqrt{\left[\sum_{i=1}^m \frac{(x_{ij} - \bar{x}_j)^2}{m-1} \right]} \quad (2)$$

The SRC for the input variable j is defined as:

$$\text{SRC}_j = \frac{\beta_j \hat{\sigma}_j}{\hat{\sigma}} \quad (3)$$

The model coefficient of determination R_y^2 measures how well the linear regression model matches the data, which can be calculated by:

$$R_y^2 = \frac{\sum_{i=1}^m (\hat{y}_i - \bar{y})^2}{\sum_{i=1}^m (y_i - \bar{y})^2} \quad (4)$$

where R_y^2 represents the fraction of the variance of the output explained by the regression. The closer it is to 1, the better the model performance is.

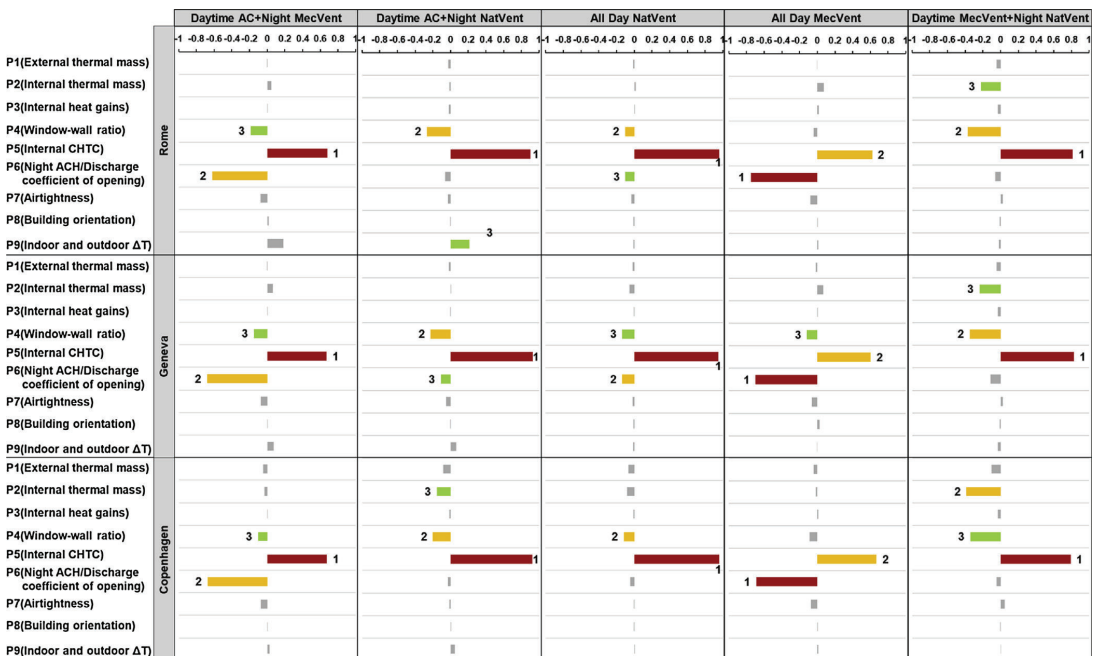


Fig. 3. Sensitivity analysis for TE.

3. Results

3.1. SA for temperature efficiency (TE)

Fig. 3 illustrates the results of the sensitivity analysis ($R^2 = 0.95$) for TE where the three top (and the absolute value of SRC greater than 0.1) influential parameters are labeled. It can be concluded that the internal CHTC is the most influential parameter for all climates and systems, except for the all-day mechanical ventilation system, but still ranking second. P6 (Night ACH) is important for the systems with night mechanical ventilation, while P6 (Discharge coefficient of opening) is not obvious in cases with night natural ventilation. The risk of this happening for the range of discharge coefficient is relatively small and will not influence the level of night natural ventilation rate. However, it is acceptable because the range has been defined according to the bibliography. Increasing window-wall ratio (WWR) always decreases the value of this indicator considerably, except for the all-day mechanical ventilation system. In the daytime mechanical ventilation with night natural ventilation system, the internal thermal mass becomes more influential. Additionally, the colder the weather is, the larger the influence of the internal thermal mass on TE.

It may confuse people that the higher the night ACH is, the lower the value of TEs. Artmann updated the indicator by multiplying TE with daily climatic cooling potential, ACH, and physical parameters of room and air to evaluate the amount of heat removed by night ventilation, demonstrating that increasing ACH will remove more heat (Artmann et al., 2010). Therefore, the temperature efficiency is not suitable to evaluate the heat removal effectiveness affected by different night ACH, but available to evaluate the performance of night ventilation for different scenarios with the same air flow rate.

3.2. SA for temperature difference ratio (TDR)

Fig. 4 shows that the WWR is the most important design parameter

for TDR for all systems in all climates. Similar to the SA for TE, P6 is important for the systems with night mechanical ventilation, while not obvious for the systems with night natural ventilation. In cases with the daytime AC system, the internal CHTC tends to have a large influence with a positive SRC. Moreover, the TDR appears to be sensitive to the building airtightness for the systems with night natural ventilation. Increasing the infiltration rate will raise the value of TDR, as it can lower the maximum indoor air temperature. As expected, the colder the weather is, the more influential the building airtightness. For the all-day natural ventilation system and all-day mechanical ventilation system, the internal thermal mass becomes influential, but the sign of its SRC is negative for the former system while positive for the latter system. The reason is that for the former system, the increase of internal thermal mass raises the maximum indoor air temperature while decreases it for the latter system.

3.3. SA for decrement factor (DF)

Fig. 5 shows the sensitivity analysis for the DF. Generally, the most influential design parameters are the internal thermal mass and WWR, whose rank vary slightly in some cases. The increase of WWR raises the fluctuation of indoor air temperature, while the augment of the internal thermal mass level decreases the fluctuation. P6 is also important for the systems with night mechanical ventilation systems and insignificant in the systems with night natural ventilation. Moreover, the value of SRC ranges from -0.4 to -0.2 , indicating that the internal CHTC generally has a big influence on DF. Even though the external thermal mass does not have the same obvious influence with the internal thermal mass, some attention should be paid on it, as the value of its SRC ranges from -0.4 to -0.1 .

In general, the lower the value of DF is, the less the indoor air is affected by the local weather, which is beneficial for the climate region with high diurnal temperature range and has a great potential for night ventilation. Although the night ventilation can lower the indoor air

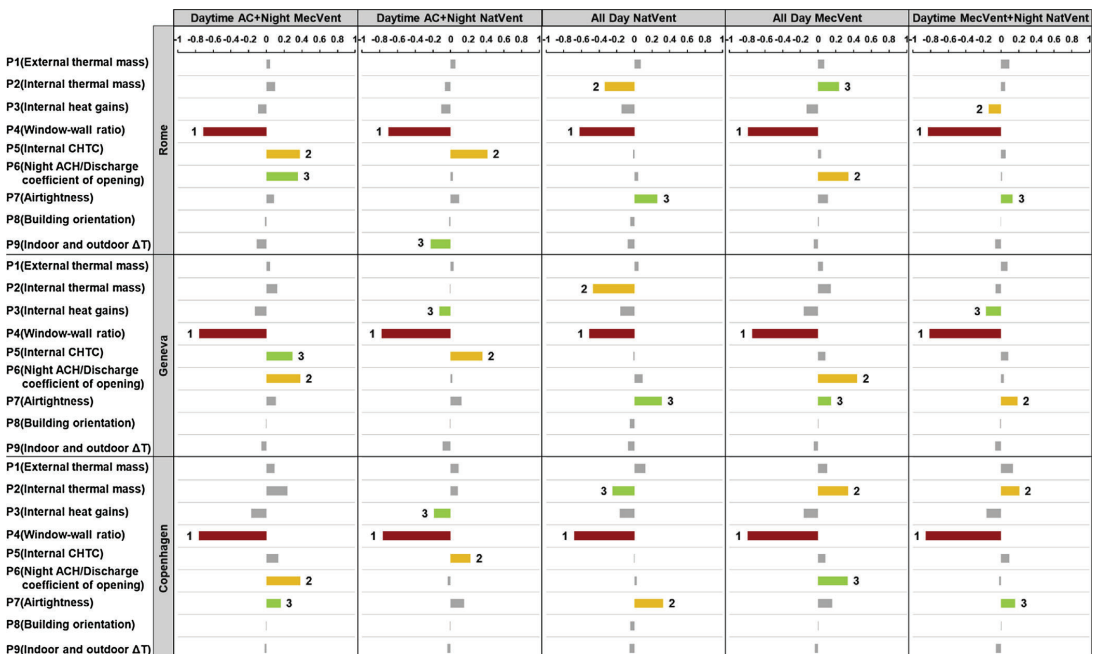


Fig. 4. Sensitivity analysis for TDR.

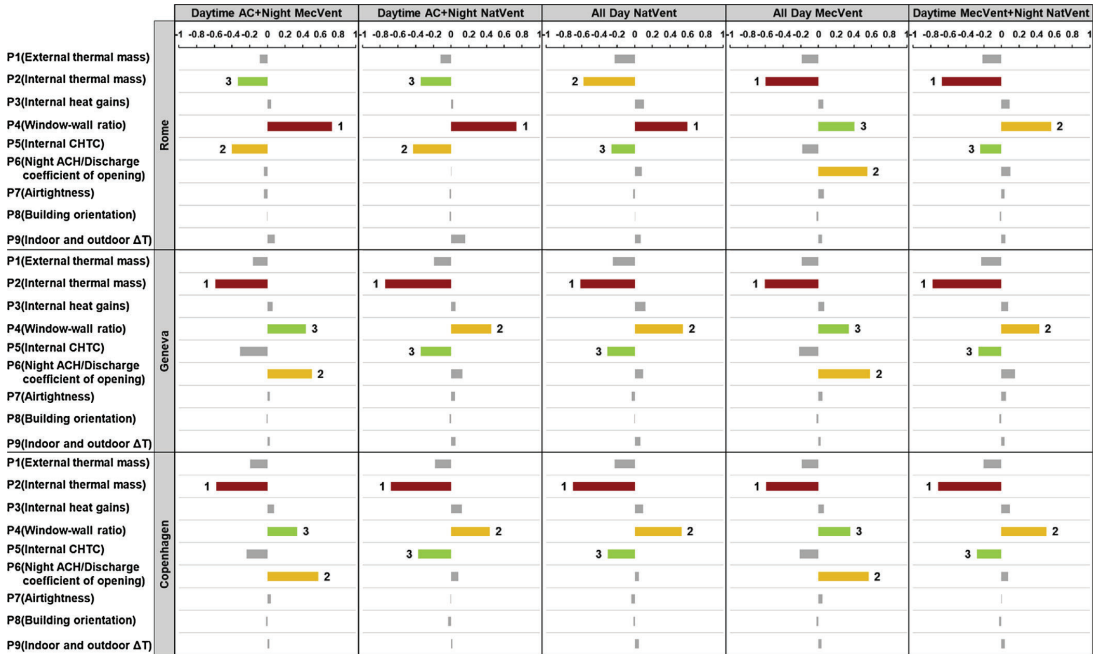


Fig. 5. Sensitivity analysis for DF.

temperature, it also enlarges the indoor air temperature fluctuation which increases the value of DF since the minimum indoor air temperature reduces more.

In such cases, it may be also confusing whether the bigger the value of DF means a better night ventilation performance. Therefore, the DF may be only suitable for the cases with the same building information to compare the scenarios with and without night ventilation or the scenarios with different night airflow rates.

3.4. SA for coefficient of performance (COP) and ventilative cooling advantage (ADV)

Fig. 6 shows the influence of design parameters on COP (Fig. 6(a)) and ADV (Fig. 6(b)). The COP and ADV are only available for the systems with night mechanical ventilation. It can be concluded that the influence of parameters on COP is almost the same for the two systems. The night ACH is the most important design parameter with a negative SRC, followed by the WWR and internal thermal mass whose signs of SRC are both positive. The reason why the night ACH has a negative SRC on COP is that increasing the air flow rate result in more fan electric consumption, while the amount of cooling energy supplied by the fan does not increase linearly with the fan electric consumption. When increasing the WWR and internal thermal mass level, there will be more excess heat stored during the daytime to be removed by the same night ventilation consumption. Attention should be paid on the building airtightness, as its SRC value is about -0.2 , indicating that this parameter has some influence on COP.

The influence of design parameters on ADV varies a lot for different systems and locations. The WWR is important for both systems. However, it has a positive SRC on ADV for daytime AC with night mechanical ventilation system while has a negative SRC for the all-day mechanical ventilation system. Undoubtedly, increasing the WWR will increase the cooling system electrical energy consumption of both the scenarios without and with night ventilative cooling which are $Q_{el,c}^{ref}$ and

$Q_{el,c}^{scen}$ respectively. The reason why the WWR has a different effect on ADV for two systems may be that increasing WWR will increase $Q_{el,c}^{ref}$ more for the former system while increase $Q_{el,c}^{scen}$ more for the latter system. Night ACH plays an important role in the former system, especially in the medium and cold climate regions, but it is not influential for the latter system. Internal thermal mass ranks second among all design parameters for the former system but is not important for the latter system. It should be noticed that the P2 has a negative SRC on ADV for the former system in Rome, while has a positive SRC for the former system in Geneva and Copenhagen. This indicates that in hot climates, the internal thermal mass level should not be increased without limit, because the night cooling with relatively high-temperature ambient air may not be able to remove all the stored excess heat in the thermal mass during the daytime. Additionally, internal CHTC and internal heat gains have a limited effect on ADV for both systems.

3.5. SA for cooling requirements reduction (CRR)

CRR is not available for the all-day natural ventilation system, because this system does not have daytime mechanical cooling method. Fig. 7 shows that the design parameters have various effects on CRR for different systems and locations. WWR is the most influential parameter in the systems with daytime mechanical ventilation, but not the same influential in the cases with daytime AC. The colder the weather is, the more influential the WWR is for systems with daytime mechanical ventilation. This is probably due to the increasing P4 leads to a different cooling demand increment of the reference scenario without ventilation and the analyzed scenario with ventilation. Generally, the internal thermal mass has a big influence on CRR for the systems with daytime AC, but the influence varies a lot in different locations. It indicates that the internal thermal mass should be arranged properly based on climate conditions and system configurations. Similar to other indicators, the P6 is only significant in the cases with night mechanical ventilation, with a positive SRC. Moreover, the internal CHTC always has a small



Fig. 6. Sensitivity analysis for (a) COP and (b) ADV.

negative SRC on CRR.

3.6. SA for percentage outside the range (POR)

Two comfort models from EN 15251 Category II (EN 15251, 2007) and ASHRAE 55 (ASHRAE 55-2004, 2004) were applied to calculate POR. EN 15251 adaptive model category II refers to whether the operative temperature falls into the 80% acceptability limits, while ASHRAE 55 simple model indicates whether the combination of humidity ratio and the operative temperature is in the ASHRAE 55-2004 summer clothes region. Fig. 8 shows the sensitivity analysis for the POR based on the two comfort models. The PORE and PORA refer to the POR with CEN 15251 Category II and ASHRAE 55 simple model respectively.

For EN 15251 model, the WWR is most influential for the last three systems, while its influence is not as obvious for the first two systems which have daytime AC, especially in the cold climate region. The effect of the internal thermal mass on POR varies a lot for different systems and locations. In general, P2 is more influential in medium or cold climate regions, but whether its SRC for the indicator is positive or negative depends on the systems. On the contrary, the PORE is more sensitive to the internal CHTC in non-cold climate regions, and the POR always declines with increasing the internal CHTC. P6 can only make a great difference in this indicator for the all-day mechanical ventilation system. Additionally, some attention should be paid for the building airtightness in the all-day natural ventilation system, as its SRC value ranges from -0.3 to -0.2.

Generally, the influence of design parameters on the ASHRAE 55 simple model is similar to those in EN 15251 adaptive model in most scenarios. However, the influences of WWR, internal CHTC, and night

ACH on PORA are quite different or even reverse between the two comfort models for the systems with daytime AC and mechanical ventilation system in Copenhagen. The WWR does not play the same important role in PORA for the last three systems but is more influential for the first two systems when in comparison with PORE in Copenhagen, shown in Fig. 8(b). This might be because the ASHRAE 55 simple model takes the humidity ratio into account, while the EN 15251 adaptive model only considers operative temperature.

3.7. SA for degree-hours criterion (DhC) and weighted discomfort temperature index (DI)

As the influence of design parameters on DI are quite similar to those on DhC, the SA results for DI in Fig. 9 are also represented for DhC. The difference between the SA results of DI and DhC is mainly the magnitude of SRC value for some design parameters in some scenarios. Generally, for the two thermal comfort indicators, the WWR is most influential, followed by the internal CHTC. The influence of internal thermal mass on DhC and DI varies a lot in different systems and locations, indicating that the internal thermal mass should be designed properly. P6 is important for the systems with night mechanical ventilation but not obvious for the systems with night natural ventilation. For all-day natural ventilation system, the building airtightness has some impact on the two indicators with negative SRCs. Besides, as expected, the colder the weather is, the larger the influence of the building airtightness is.



Fig. 7. Sensitivity analysis for CRR.

4. Discussions

4.1. Importance of design parameters

Fig. 10 shows the proportions of the design parameters in the corresponding first, second, third important design parameter for all performance indicators. The 1st important parameter results show that the WWR, internal CHTC, internal thermal mass, and night mechanical ACH are the most important design parameters. The 2nd important parameter results mean that building airtightness and internal heat gains should be taken into consideration when concerning some performance indicators. Apart from the aforementioned six parameters, the results of the 3rd important parameter show that the external thermal mass and threshold temperature ΔT for night ventilation should be paid some attention in certain cases.

In the perspective of the influence of each design parameter on all night cooling performance indicators based on sensitivity analysis results from Section 3, it can be concluded that the WWR always has significant negative SRCs on TE and TDR, but positive SRCs on DF, COP, and the thermal comfort indicators. But there is an exception that WWR has a negative SRC on the PORA for the systems with daytime AC and the all-day mechanical ventilation system in cold climate region. Meanwhile, the signs and values of SRC of WWR on ADV and CRR vary a lot depending on the climates or system configurations. Increasing the WWR will raise the value of ADV and CRR for the systems with daytime AC, while reduces those value for the systems with daytime mechanical ventilation.

The internal CHTC have uniform signs of SRCs for each indicator.

Increasing the internal CHTC will decrease the value of thermal comfort indicators to improve thermal comfort, as well as the value of DF to keep the indoor air temperature steadier. On the other hand, increasing the internal CHTC will augment heat removal effectiveness (TE & TDR), energy efficiency (COP & ADV), and cooling energy use reduction (CRR). It means that increasing the CHTC is always beneficial, which can be achieved by selecting appropriate night ventilation mode or optimizing the indoor air distribution to enhance the heat transfer area between the cold air and building elements.

The external thermal mass is much less influential than the internal thermal mass. The former one is only slightly important on the CRR, POR, and DI in some scenarios. The latter one has positive SRCs for COP and negative SRCs on the DF all the time. But the signs of its SRCs for the rest of indicators vary a lot based on the night cooling solutions and climates.

Night ACH always has positive SRCs on TDR, DF, and CRR, but negative SRCs on TE, COP, DhC, DI, PORE, and PORA except for the daytime AC with night mechanical ventilation system in cold climate region. Commonly, increasing the night ACH will reduce the value of ADV. However, the ADV of the all-day mechanical ventilation system in the medium and hot climate regions will benefit from the increase of night ACH.

The building airtightness is only important on the TDR, COP, ADV, CRR, and the thermal comfort improvement indicators in some cases. In general, the colder the weather is, the more influential the building airtightness is. The internal heat gains always have negative SRCs on TDR. Moreover, it will influence the ADV, CRR, and POR for several scenarios a lot. ΔT only has a limited influence on the TE, TDR, and

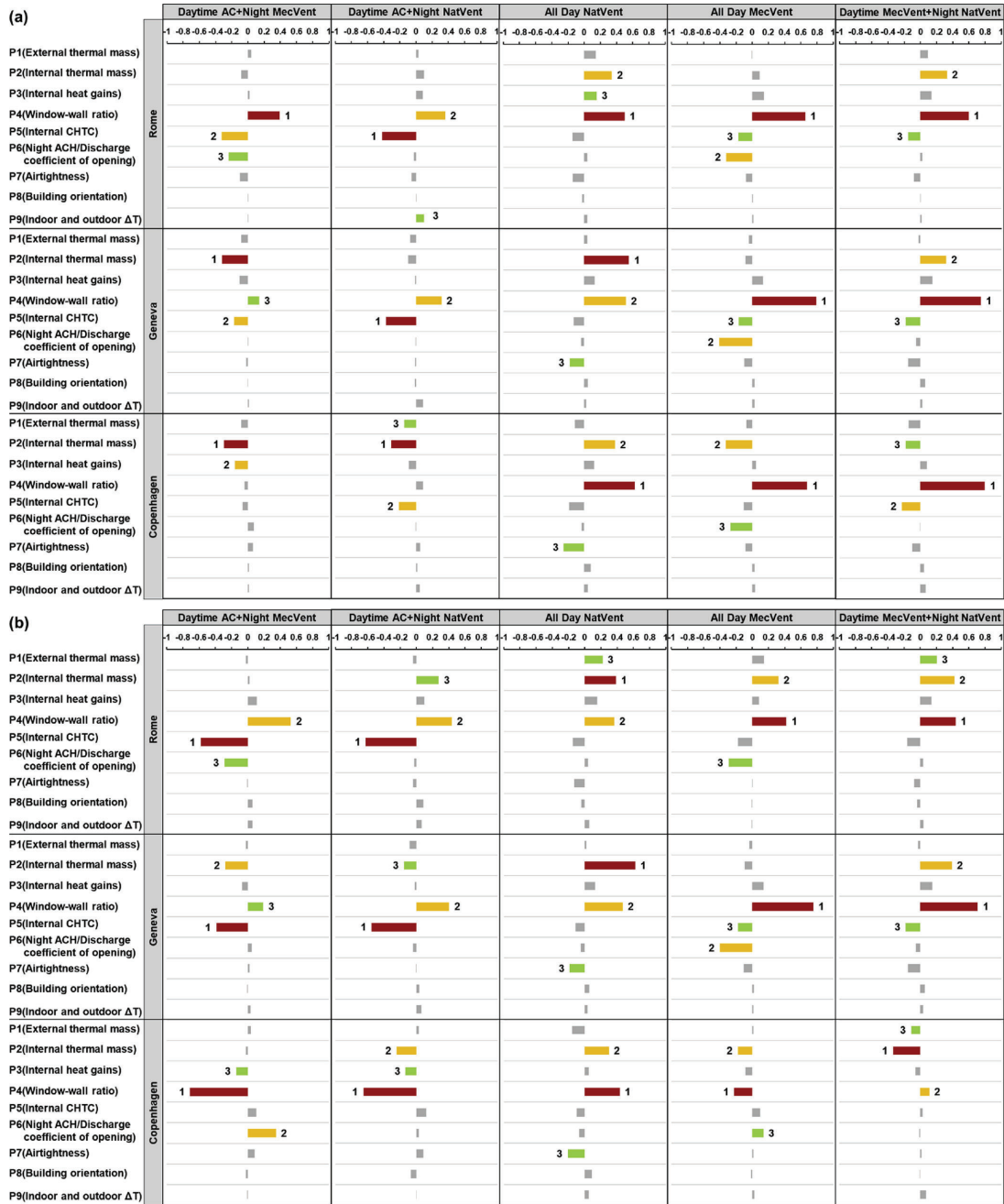


Fig. 8. Sensitivity analysis for (a) POR EN 15251 model and (b) POR ASHRAE 55 model.

thermal comfort improvement indicators for the daytime AC with night natural ventilation system in the hot or medium climate regions. Increasing the ΔT will raise the value of thermal comfort improvement indicators and TE, but reduce the value of TDR.

Building orientation can affect the solar heat gains of the room, and

the air flow rate of natural ventilation. However, the influence of building orientation on the night cooling performance is quite low, because the solar heat gains were generally low when compared with the internal heat gains, and the air flow rate does not have a big difference with the orientation changing (shown in Fig. 11). The reason

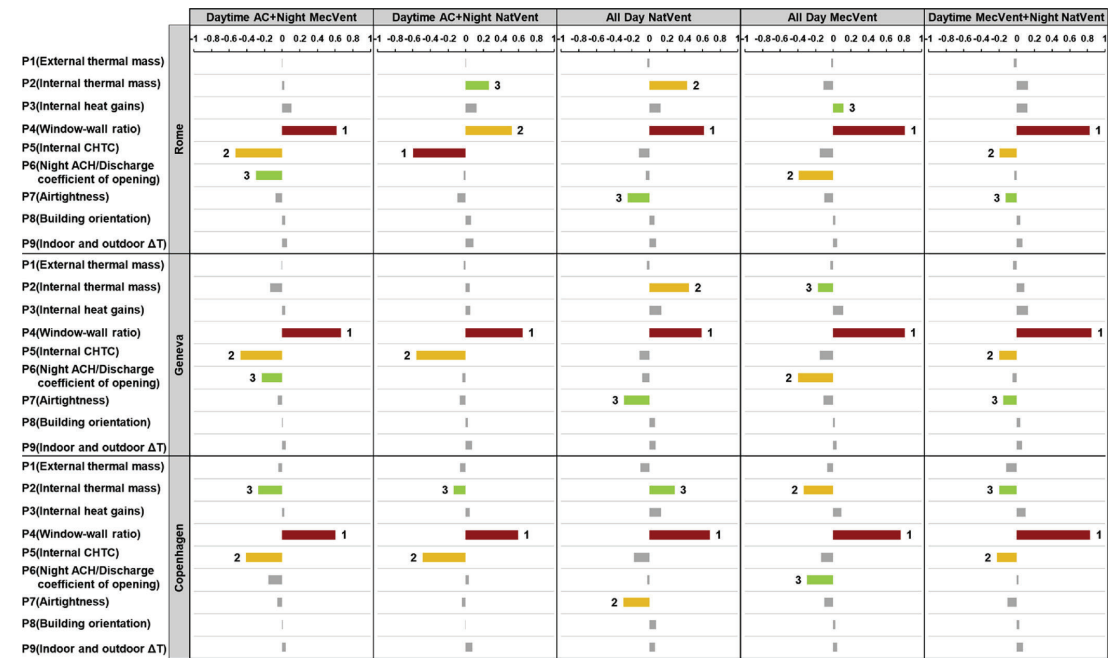


Fig. 9. Sensitivity analysis for DhC and DI.

why the orientation has little influence on the change of air flow rate is that the opening effectiveness in natural ventilation model is calculated automatically in EnergyPlus, which assumes the window can adjust its angle to make the most of wind under different wind directions.

4.2. Night cooling performance

4.2.1. Thermal comfort evaluation

The ability of night cooling to improve thermal comfort performance depends on the night cooling solutions as well as the climate. As the magnitude of DhC and DI for different night cooling solutions varies a lot, the Fig. 12 only shows an overview of the PORE and PORA for the modeled cases. The numbers 1, 2, and 3 represent Rome, Geneva, and Copenhagen, respectively.

The comparison of the mean and median value of POR between different night cooling solutions demonstrates that the all-day natural ventilation system has the highest POR, followed by the daytime mechanical ventilation system with night natural ventilation system, all-day mechanical ventilation system, daytime AC with night natural ventilation system, and daytime AC with night mechanical ventilation system. It also can be concluded that the night mechanical ventilation can provide better thermal comfort with lower POR than night natural ventilation. Both for night natural and mechanical cooling solutions the best performance in the EN 15251 model are obtained with the daytime AC system in Rome, reaching 0%. While in the ASHARE55 model the best performance of night natural and mechanical ventilation are also obtained with the daytime AC system, but in Copenhagen, close to 0% and 5% respectively.

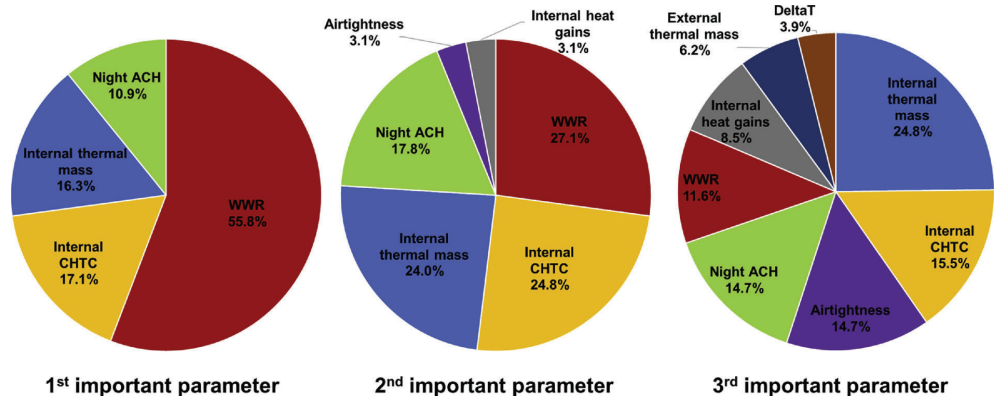


Fig. 10. Pie chart for the top three influential parameters.

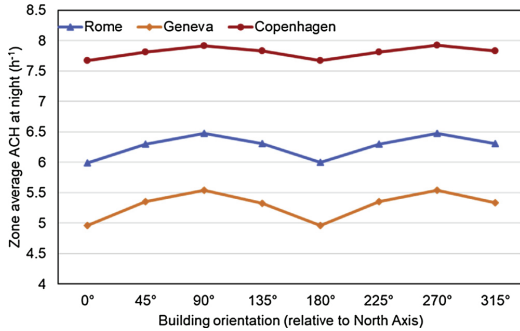


Fig. 11. Zone average ACH at night under different orientations for the daytime AC with night natural ventilation system in three cities.

The value difference between PORE and PORA for the same system in the same climate region shows that the thermal comfort criterion selected will come to different results. The ASHRAE 55 model seems stricter than EN 15251 model, as the PORA is higher than PORE for the same system in the same city. There is a clear trend that the PORE for all systems and PORA for the latter three systems decrease with the location varying from Rome to Copenhagen. This indicates that night ventilation has more application potential in cold climate regions. However, no clear trend exists for the PORA for the first two systems in the same condition. The lowest median and average value of PORA is in Geneva rather than in Copenhagen. One reason may be that the system with daytime AC leaves less excess heat during daytime than other night cooling solutions, leading to the overcooling phenomenon caused by night cooling in cold climate region. Another reason is that the summer comfort range in ASHRAE 55 simple is fixed. Consequently, the zone operative temperature in Rome tending to be higher than the comfort range but lower than the comfort range in Copenhagen.

4.2.2. Energy-saving benefit

The energy efficiency and ability to reduce the cooling energy use of the different night cooling solutions are also very different. Fig. 13 shows the values of COP, ADV, and CRR for different night ventilation solutions. Night mechanical ventilation with daytime AC system tends to have a lower COP but higher ADV than with daytime mechanical ventilation system. This is due to the fact that the daytime AC system can remove more heat and maintain the indoor temperature at the designed level when compared with the daytime mechanical ventilation

system. Therefore, less excess heat stored at daytime with AC system will lead to lower COP and higher ADV for night mechanical cooling. ADV can evaluate directly whether the night mechanical cooling is energy saving or not. However, through the comparison of COP with ADV for all-day mechanical ventilation in different climate regions, it can be concluded that high COP does not result in high ADV. COP is not the key indicators to determine whether the night cooling can save energy or not. The result of CRR clearly demonstrates that there is a trend that the value of CRR increases with the climate becoming colder.

For night natural cooling solutions, the best performance for CRR is obtained with the daytime mechanical ventilation system in Copenhagen, reaching 97.1%. For night mechanical cooling solutions, the best performance for ADV and CRR are obtained with the daytime AC system in Copenhagen, reaching 2.4 and 73.8% respectively. While for the COP of night mechanical cooling, the best performance is obtained with daytime mechanical ventilation in Rome, reaching 13.9.

In hot climate region, even though the all-day mechanical ventilation can get a value of COP higher than 10, the night mechanical ventilation does not save energy. Because the ADV is less than 1. However, the CRR of night natural cooling system indicates that this system can be energy-saving, with the highest value of more than 60% for the all-day mechanical ventilation system. While in the cold climate region, all the night ventilation systems can achieve better performance with a higher value of COP, ADV, and CRR, except for the COP of the all-day mechanical ventilation system in Copenhagen. Besides, it is easier to save energy for night mechanical ventilation, with highest and mean value of ADV is 2.4 and 1.1 respectively. For the medium climate region of Geneva, all the values of three indicators are between that in Rome and Copenhagen. The result indicates that the colder the climate, the better performance the night cooling can achieve. However, it should be noticed that the ADV of daytime AC with night mechanical ventilation could be higher than 1 even in Rome, while close to 0 in Copenhagen. Therefore, the night ventilation system should be designed properly based on the climate in order to maximize the energy-saving benefit.

4.3. Applicability of the different performance indicators

The heat removal effectiveness indicators should be used with caution. Firstly, the lack of modeling of the temperature distribution in spaces leads to inaccurate values of the temperature efficiency. Secondly, a comparison of night cooling performance can only be carried out for systems with similar airflow rates by the indicator of TE or with similar building information by the indicator of DF. Under the application conditions, the higher the value of TE or DF, the better the

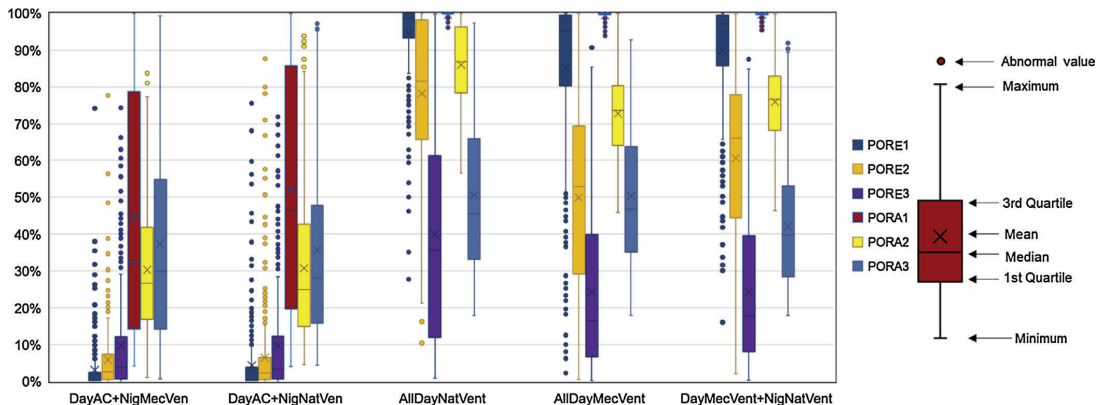


Fig. 12. Box-and-whisker plot of POR for different night cooling solutions.

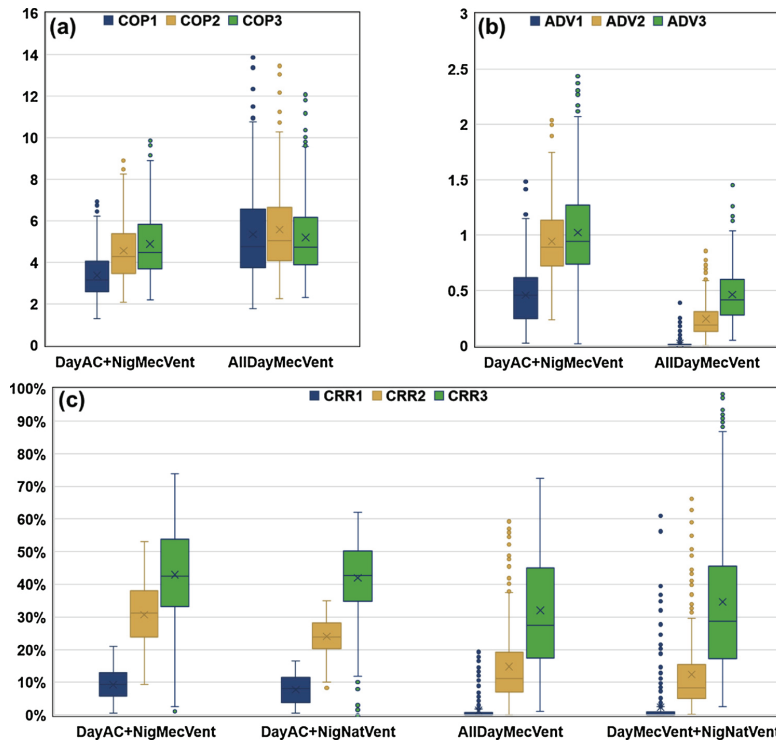


Fig. 13. Box-and-whisker plot of COP (a), ADV (b) and CRR (c) for different night cooling solutions.

performance of night cooling. According to the definition of TDR, the denominator is the ambient temperature swing which is dependent on the local climate condition. Therefore, the TDR is not suitable for the same night cooling system to compare the heat removal effectiveness in different climate regions, but only suitable for the comparison of different system configurations in the same climate region.

The energy-related indicators of COP, ADV, and CRR are used to evaluate energy efficiency and cooling energy use of night cooling. ADV is very useful for night mechanical ventilation systems, while CRR is useful for night natural ventilation systems. Though COP provides a first evaluation of the thermal behavior, the night ventilation energy-saving effect cannot be quantified. Because for the all-day mechanical ventilation system, the high COP does not result in high ADV. Therefore, the COP only evaluates the energy efficiency of ventilation at night time, rather than the energy efficiency for an entire day.

For evaluation of the thermal comfort improvement in the daytime, the best performance indicator is POR because it gives a direct explanation of the percentage outside the comfort range. Furthermore, it can accompany different thermal comfort models or parameters, such as PMV, operative temperature, and dry resultant temperature. Both DhC and DI have some limitations and disadvantages. The biggest limitation is that the thermal comfort threshold value is too simple, such as the operative temperature 26°C or the indoor air temperature 28°C. In addition, the two indicators belong to the cumulative index, of which it may be difficult to evaluate the thermal comfort intuitively.

5. Conclusion

This paper applies a global sensitivity analysis to identify the key design parameters affecting the night ventilation performance. Besides,

the applicability and limitations of the performance indicators are evaluated by the results from the parametric simulation. Based on the results of the case study, conclusions can be made as follows.

- The sensitivity analysis shows that the influence of design parameters depends much on the climate conditions and night ventilation system modes. The WWR, internal CHTC, internal thermal mass level, and night mechanical ACH of are the most important design parameters. However, the building airtightness, internal heat gains, external thermal mass level, and threshold temperature ΔT also have limited effect on some indicators in several scenarios. Small differences on the night cooling performance can be noticed for various building orientations and different discharge coefficients of the opening.
- The parametric simulation results show that the way to get the best thermal comfort and energy-saving benefit for night ventilation is equipped with daytime AC. The colder the climate, the better performance the night cooling can achieve. Nevertheless, some measures should be taken to avoid the overcooling effect in cold climate region for the night ventilation with the daytime AC system.
- Some performance indicators have limitations and disadvantages. TE is only suitable to evaluate the performance of different scenarios with similar night ACH, while the DF can be only applied to evaluate the performance of different night ventilation with similar building information. TDR is only available to compare the different night cooling systems in the same climate region. COP is not able to evaluate the energy-saving benefit. DhC and DI are too simple and not able to evaluate the thermal comfort intuitively. Therefore, the ADV, CRR, and POR are recommended to evaluate the night ventilation performance.

Acknowledgment

This work gratefully acknowledges the financial support from the Chinese Scholarship Council (CSC No. 201706050001).

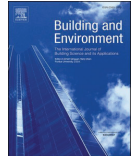
References

- Alamdari, F., & Hammond, G. P. (1983). *Improved data correlations for buoyancy-driven convection in rooms*. London, England: SAGE Publications Sage UK <https://doi.org/10.1177/014362448300400304>.
- Armann, N., Manz, H., & Heiselberg, P. (2007). Climatic potential for passive cooling of buildings by night-time ventilation in Europe. *Applied Energy*, 84, 187–201. <https://doi.org/10.1016/j.apenergy.2006.05.004>.
- Armann, N., Jensen, R. L., Manz, H., & Heiselberg, P. (2010). Experimental investigation of heat transfer during night-time ventilation. *Energy and Buildings*, 42, 366–374. <https://doi.org/10.1016/j.enbuild.2009.10.003>.
- Armann, N., Gyalistras, D., Manz, H., & Heiselberg, P. (2008). Impact of climate warming on passive night cooling potential. *Building Research & Information*, 36, 111–128. <https://doi.org/10.1080/09613210701621919>.
- Armann, N., Manz, H., & Heiselberg, P. (2008). Parameter study on performance of building cooling by night-time ventilation. *Renewable Energy*, 33, 2589–2598. <https://doi.org/10.1016/j.renene.2008.02.025>.
- ASHRAE 55-2004 (2004). *Thermal environmental conditions for human occupancy*. American Society of Heating, Refrigerating and Air-Conditioning Engineers https://www.techstreet.com/ashrae/standards/ashrae-55-2004?gateway_code=ashrae&product_id=1160905.
- Awbi, H. B. H., & Gan, G. (1993). Evaluation of the overall performance of room air distribution. In: *Proc. 6th Int. Conf. Indoor Air Qual. Clim. Helsinki*, 5, 283–288. <https://www.aivc.org/resource/evaluation-overall-performance-room-air-distribution>.
- Belmonte, J. F., Eguía, P., Molina, A. E., & Almendros-Ibáñez, J. A. (2015). Thermal simulation and system optimization of a chilled ceiling coupled with a floor containing a phase change material (PCM). *Sustainable Cities and Society*, 14, 154–170. <https://doi.org/10.1016/j.scs.2014.09.004>.
- Blondeau, P., Spérando, M., & Allard, F. (1997). Night ventilation for building cooling in summer. *Solar Energy*, 61, 327–335. [https://doi.org/10.1016/S0038-092X\(97\)00076-5](https://doi.org/10.1016/S0038-092X(97)00076-5).
- Breesch, H., & Janssens, A. (2010). Performance evaluation of passive cooling in office buildings based on uncertainty and sensitivity analysis. *Solar Energy*, 84, 1453–1467. <https://doi.org/10.1016/j.solener.2010.05.008>.
- Breesch, H., Janssens, A., & Gameiro Da Silva, M. C. (2004). *Uncertainty and sensitivity analysis of the performances of natural night ventilation*. Roomvent 2004 Conf., p. ISBN 972-97973-2-3. <https://www.aivc.org/resource/uncertainty-and-sensitivity-analysis-performances-natural-night-ventilation>.
- Breesch, H., Bossaer, A., & Janssens, A. (2005). *Passive cooling in a low-energy office building*. Sol. energy, Pergamon 682–696. <https://doi.org/10.1016/j.solener.2004.12.002>.
- Carlucci, S., & Pagliano, L. (2012). A review of indices for the long-term evaluation of the general thermal comfort conditions in buildings. *Energy and Buildings*, 53, 194–205. <https://doi.org/10.1016/j.enbuild.2012.06.015>.
- Corgnati, S. P., & Kindin, A. (2007). Thermal mass activation by hollow core slab coupled with night ventilation to reduce summer cooling loads. *Building and Environment*, 42, 3285–3297. <https://doi.org/10.1016/j.buildenv.2006.08.018>.
- EN 15251 (2007). *Indoor environmental input parameters for design and assessment of energy performance of buildings addressing indoor air quality, thermal environment, lighting and acoustics*. <https://webshop.dk/Default.aspx?ID=2198&GroupID=19.040.01&ProductID=M204572>.
- EN 16798-3 (2017). *Energy performance of buildings – Ventilation for buildings – Part 3: For non-residential buildings – Performance requirements for ventilation and room-conditioning systems (Modules M5-1, M5-4)*. <https://webshop.dk/en-gb/search/ds-en-16798-32017>.
- EN ISO 13786 (2017). *Thermal performance of building components – Dynamic thermal characteristics – Calculation methods*. <https://webshop.dk/Default.aspx?ID=2198&GroupID=91.120.10&ProductID=M289824>.
- Encinas, F., & De Herde, A. (2013). Sensitivity analysis in building performance simulation for summer comfort assessment of apartments from the real estate market. *Energy and Buildings*, 65, 55–65. <https://doi.org/10.1016/j.enbuild.2013.05.047>.
- EU Science Hub (2008). *Simlab v2.2*. <https://ec.europa.eu/jrc/en/samo/simlab>.
- European Commission - IPCC (2008). *Simlab 2.2: Reference manual*. <https://ec.europa.eu/jrc/en/p/samo/simlab>.
- Finn, D. P., Connolly, D., & Kenny, P. (2007). Sensitivity analysis of a maritime located night ventilated library building. *Solar Energy*, 81, 697–710. <https://doi.org/10.1016/j.solener.2006.10.008>.
- Firth, S. K., Lomas, K. J., & Wright, A. J. (2010). Targeting household energy-efficiency measures using sensitivity analysis. *Building Research & Information*, 38, 24–41. <https://doi.org/10.1080/09613210903236706>.
- Flourentzou, F., Van der Maas, J., & Roulet, C.-A. (2002). Natural ventilation for passive cooling: Measurement of discharge coefficients. *Energy and Buildings*, 27, 283–292. [https://doi.org/10.1016/s0378-7788\(97\)00043-1](https://doi.org/10.1016/s0378-7788(97)00043-1).
- Gagliano, A., Patania, F., Nocera, F., & Signorello, C. (2014). Assessment of the dynamic thermal performance of massive buildings. *Energy and Buildings*, 72, 361–370. <https://doi.org/10.1016/j.enbuild.2013.12.060>.
- Geros, V., Santamouris, M., Tsangrasoulis, A., & Guarracino, G. (1999). Experimental evaluation of night ventilation phenomena. *Energy and Buildings*, 29, 141–154. [https://doi.org/10.1016/S0378-7788\(98\)00056-5](https://doi.org/10.1016/S0378-7788(98)00056-5).
- Givoni, B. (1992). Comfort, climate analysis and building design guidelines. *Energy and Buildings*, 18, 11–23. [https://doi.org/10.1016/0378-7788\(92\)90047-K](https://doi.org/10.1016/0378-7788(92)90047-K).
- Goethals, K., Breesch, H., & Janssens, A. (2011). Sensitivity analysis of predicted night cooling performance to internal convective heat transfer modelling. *Energy and Buildings*, 43, 2429–2441. <https://doi.org/10.1016/j.enbuild.2011.05.033>.
- Heiselberg, P., Brohus, H., Hesselholt, A., Rasmussen, H., Seire, E., & Thomas, S. (2009). Application of sensitivity analysis in design of sustainable buildings. *Renewable Energy*, 34, 2030–2036. <https://doi.org/10.1016/j.renene.2009.02.016>.
- Hopfe, C. J., & Hensen, J. L. M. (2011). Uncertainty analysis in building performance simulation for design support. *Energy and Buildings*, 43, 2798–2805. <https://doi.org/10.1016/j.enbuild.2011.06.034>.
- Hygh, J. S., DeCarolis, J. F., Hill, D. B., & Ranji Ranjithan, S. (2012). Multivariate regression as an energy assessment tool in early building design. *Building and Environment*, 57, 165–175. <https://doi.org/10.1016/j.buildenv.2012.04.021>.
- ISO 13791 (2012). *Thermal performance of buildings – Calculation of internal temperatures of a room in summer without mechanical cooling – General criteria and validation procedures*. <https://www.iso.org/standard/51614.html>.
- Ji, W., Luo, Q., Zhang, Z., Wang, H., Du, T., & Heiselberg, P. K. (2018). Investigation on thermal performance of the wall-mounted attached ventilation for night cooling under hot summer conditions. *Building and Environment*, 146, 268–279. <https://doi.org/10.1016/j.buildenv.2018.10.002>.
- Lam, J. C., Wan, K. K. W., & Yang, L. (2008). Sensitivity analysis and energy conservation measures implications. *Energy Conversion and Management*, 49, 3170–3177. <https://doi.org/10.1016/j.enconman.2008.05.022>.
- Lomas, K. J. (1996). The U.K. applicability study: An evaluation of thermal simulation programs for passive solar house design. *Building and Environment*, 31, 197–206. [https://doi.org/10.1016/0360-1323\(95\)00050-X](https://doi.org/10.1016/0360-1323(95)00050-X).
- Lomas, K. J., & Eppel, H. (1992). Sensitivity analysis techniques for building thermal simulation programs. *Energy and Buildings*, 19, 21–44. [https://doi.org/10.1016/0378-7788\(92\)90033-D](https://doi.org/10.1016/0378-7788(92)90033-D).
- M.A. J (1995). *Control of natural ventilation*. <https://www.bsria.co.uk/information-membership/bookshop/publication/control-of-natural-ventilation/>.
- Mara, T. A., & Tarantola, S. (2008). Application of global sensitivity analysis of model output to building thermal simulations. *Building Simulation*, 1, 290–302. <https://doi.org/10.1007/s12273-008-8129-5>.
- O'Donnovan, A., Belleri, A., Flourentzou, F., Zhang, G.-Q., da Graca, G. C., Breesch, H., et al. (2018). *Ventilative cooling design guide: Energy in buildings and communities programme*. March 2018 Aalborg University, Department of Civil Engineering <https://www.vicool.eu/wp-content/uploads/2016/11/VC-Design-Guide-EBC-Annex-62-March-2018.pdf>.
- Petersen, S., & Svendsen, S. (2010). Method and simulation program informed decisions in the early stages of building design. *Energy and Buildings*, 42, 1113–1119. <https://doi.org/10.1016/j.enbuild.2010.02.002>.
- Pfaffert, J., Herkel, S., & Jäschke, M. (2003). Design of passive cooling by night ventilation: Evaluation of a parametric model and building simulation with measurements. *Energy and Buildings*, 35, 1129–1143. <https://doi.org/10.1016/j.enbuild.2003.09.005>.
- Ran, J., & Tang, M. (2018). Passive cooling of the green roofs combined with night-time ventilation and walls insulation in hot and humid regions. *Sustainable Cities and Society*, 38, 466–475. <https://doi.org/10.1016/j.scs.2018.01.027>.
- Rui, G., Yue, H., & Heiselberg, P. (2018). A review of the performance indicators of night-time ventilation. *39th AIVC Conf.14*. <https://www.aivc.org/resource/review-performance-indicators-night-time-ventilation?volume=37602>.
- Saltelli, A., Chan, K., Scott, E. M., et al. (2000). *Sensitivity analysis*. New York: Wiley. <https://www.wiley.com/en-us/Sensitivity+Analysis-p-9780470743829>.
- Saltelli, A., Ratto, M., Tarantola, S., & Campolongo, F. (2005). Sensitivity analysis for chemical models. *Chemical Reviews*, 105, 2811–2828. <https://doi.org/10.1021/cr040659d>.
- Santamouris, D. A. M., Santamouris, M., & Asimakopoulos, D. (1996). *Passive cooling of buildings*. Earthscan https://books.google.dk/books/about/Passive_Cooling_of_Buildings.html?id=tHsJ0-veKjC&redir_esc=y.
- Solgi, E., Hamedani, Z., Fernando, R., Skates, H., & Orji, N. E. (2018). A literature review of night ventilation strategies in buildings. *Energy and Buildings*, 173, 337–352. <https://doi.org/10.1016/j.enbuild.2018.05.052>.
- Strith, U., Charvat, P., Koželj, R., Klimes, L., Osterman, E., Ostry, M., et al. (2018). PCM thermal energy storage in solar heating of ventilation air – Experimental and numerical investigations. *Sustainable Cities and Society*, 37, 104–115. <https://doi.org/10.1016/j.scs.2017.10.018>.
- Tian, W. (2013). A review of sensitivity analysis methods in building energy analysis. *Renewable and Sustainable Energy Reviews*, 20, 411–419. <https://doi.org/10.1016/j.rser.2012.12.014>.
- U. Department of Energy (2017). *EnergyPlus, simulation program v8.9*. <https://energypplus.net/documentation>.
- Vidrih, B., Arkar, C., & Medved, S. (2016). Generalized model-based predictive weather control for the control of free cooling by enhanced night-time ventilation. *Applied Energy*, 168, 482–492. <https://doi.org/10.1016/j.apenergy.2016.01.109>.
- Wang, Z., Yi, L., & Gao, F. (2009). Night ventilation control strategies in office buildings. *Solar Energy*, 83, 1902–1913. <https://doi.org/10.1016/j.solener.2009.07.003>.
- WMO (2018). *WMO country profile database*. World Meteorological Organization <https://www.wmo.int/cpd/>.
- Zhang, Y., & Korolija, I. (2016). *JEPlus-An EnergyPlus simulation manager for parametrics*. <http://www.jeplus.org/wiki/doku.php>.
- Zhou, J., Zhang, G., Lin, Y., & Li, Y. (2008). Coupling of thermal mass and natural ventilation in buildings. *Energy and Buildings*, 40, 979–986. <https://doi.org/10.1016/j.enbuild.2007.08.001>.

Appendix B. Paper 2

Guo, R., Heiselberg, P., Hu, Y., Johra, H., Jensen, R. L., Jønsson, K. T., & Peng, P. (2021). Experimental investigation of convective heat transfer for night ventilation in case of mixing ventilation. *Building and Environment*, 107670. <https://doi.org/10.1016/j.buildenv.2021.107670>

Reprinted by permission from Elsevier.



Experimental investigation of convective heat transfer for night ventilation in case of mixing ventilation

Rui Guo^{*}, Per Heiselberg, Yue Hu, Hicham Johra, Rasmus Lund Jensen, Kim Trangbæk Jønsson, Pei Peng

Department of the Built Environment, Aalborg University, Thomas Manns Vej 23, Aalborg, 9220, Denmark

ARTICLE INFO

Keywords:

Night ventilation
Mixing ventilation
Convective heat transfer coefficient
Thermal mass
Dynamic full-scale experiment

ABSTRACT

The purpose of night ventilation (NV) is to improve building energy and thermal comfort performance. The key to accurately predicting NV performance is selecting the appropriate convective heat transfer coefficient (CHTC) at different surfaces of the built environment. The current CHTC correlations used in building energy simulation tools are limited and prevent accurate modeling of NV strategies. The building thermal mass activation is also an important factor to influence the efficiency of NV. A series of dynamic full-scale experiments with ten thermal mass distribution schemes, four air change rates per hour (ACH), and two inlet air temperatures was conducted to derive the CHTCs at test room surfaces during NV in case of mixing ventilation. The results show that the existing correlations did not accurately predict the CHTC for most cases. Therefore, the new surface-averaged CHTC correlations with inlet temperature as reference were developed for different thermal mass distribution schemes and ACH. Installing the thermal mass on one surface can significantly enhance its CHTC and affect the CHTC at other surfaces. The mean CHTC of the test room was independent of the inlet air temperature but increased together with ACH and thermal mass level of interior surfaces. Finally, the presence and locations of tables had limited influence on the CHTC at interior surfaces but reduced the mean CHTC.

1. Introduction

1.1. Background

An emerging challenge at the design stage and during operation is the increasing cooling demand and overheating period in buildings, especially in commercial buildings [1]. Night ventilation (NV) is a promising way to reduce the cooling demand in buildings and provide better indoor thermal comfort. The basic concept of NV consists of utilizing the relatively cold ambient air at night by means of natural or mechanical force to cool down the indoor air and building elements that have stored excess heat during the daytime. The cooled building elements can then act as a heat sink during the occupied period of the next day to absorb the heat gains and reduce risks of overheating [2]. In past decades, many researchers have experimentally or numerically investigated the building performance improvement offered by NV [3–14]. However, architects and engineers still hesitate to adopt NV in building design due to the high uncertainty in predicting its performance by using building energy simulation (BES) tools.

One of the factors contributing to this problem is the complexity and diversity of NV flow rates, leading to inaccurate convective heat transfer coefficient (CHTC) at the interior surfaces of the built environment. The purpose of daytime cooling (e.g., air conditioning) is to maintain the indoor air temperature within a certain range. This type of system usually has limited airflow rates to avoid risks of draft. Unlike daytime cooling in office buildings, night cooling can employ a high air change rate per hour (ACH) up to 10 h^{-1} or more if applicable [15]. Therefore, accurate CHTC is more critical to predict night cooling performance rather than for daytime cooling performance. Previous research conducted a series of sensitivity analyses to demonstrate that the internal CHTC is a crucial parameter in energy and thermal comfort prediction for NV [16–18].

Since it is impossible to analyze the airflow around and in the building in detail for the yearly BES, the empirical correlations are used to calculate the CHTC. For the past 60 years, researchers have developed numerous CHTC correlations based on experiments or theoretical analyses [19–28]. However, most of these correlations were deduced from the flat plate or steady state full-scale experiments. They are thus only applicable under specific conditions of ventilation principles and airflow

^{*} Corresponding author.

E-mail address: rgu@build.aau.dk (R. Guo).

<https://doi.org/10.1016/j.buildenv.2021.107670>

Received 24 October 2020; Received in revised form 24 December 2020; Accepted 1 February 2021

Available online 8 February 2021

0360-1323/© 2021 Elsevier Ltd. All rights reserved.

Nomenclature			
<i>Latin symbols</i>		β	Coefficient of thermal expansion
A	Area	λ	Thermal conductivity
c	Heat capacity	<i>Subscript</i>	
C	Constant	<i>conv</i>	Convective
C_p	Specific heat capacity	<i>cond</i>	Conductive
E_b	Black body emissive power	<i>rad</i>	Radiative
F	View factor	<i>surf</i>	Surface
g	Gravitational acceleration	i, j	Index for surface i and j
h	Surface heat transfer coefficient	<i>Acronyms</i>	
k	Air thermal conductivity	ACH	Air change rate per hour
L	Characteristic length	AHU	Air handling unit
q	Heat flux	Ar	Archimedes number
Q	Heat flow	BES	Building energy simulation
T	Temperature	CFD	Computational fluid dynamics
u	Airflow speed	CHTC	Convective heat transfer coefficient
\dot{V}	Air volume flow rate	Gr	Grashof number
<i>Greek symbols</i>		LHS	Latin Hypercube Sampling
Δ	Change in a variable	MCA	Monte Carlo analysis
δ	Kronecker symbol	NV	Night ventilation
ε	Emissivity	Re	Reynolds number
ρ	Density	Ri	Richardson number
ν	Air dynamic viscosity	Nu	Nusselt number

regimes. The inappropriate selection of CHTC correlations makes a difference in ventilation performance prediction. The CHTC correlations themselves may also result in high uncertainty in predicting building energy use when forced convection is considered. Beausoleil-Morrison [29] proposed comprehensive, adaptive CHTC correlations for mixed convection, which blended the natural and forced convection correlations from the literature. Nevertheless, it was observed that high uncertainty of 20–40% occurred in predicting heating and cooling energy use. Several studies [13,30,31] conducted dynamic full-scale experiments to investigate the heat transfer for NV with different air distribution systems (mixing ventilation, displacement ventilation, and wall-mounted attached ventilation). However, those studies only looked at the convective heat flow of different surfaces and were only based on one thermal mass distribution. Moreover, they did not focus on characterizing CHTC or developing CHTC correlation.

Another factor that may impede the application of NV is the thermal mass activation. The thermal mass capacity accumulates the heat gain in the daytime and determines the cooling potential for NV; in turn, the capacity to release the heat at night affects the NV performance [32]. If coupling the thermal mass activation with NV to achieve the best performance for office buildings, it is necessary to account for the amount and location of thermal mass. Goethals et al. [33] investigated the influence of different inlet and exhaust configurations as well as the thermal mass on the heat transfer of two mixed convection regimes. The results revealed that when the inlet was close to the floor with thermal mass (concrete tiles) rather than near the ceiling, NV released 11% more heat. More convective heat flow occurred when the floor was installed with concrete tiles. This study only calculated the convective heat flow of surfaces and investigated a limited set of eight designed cases, of which only four cases had night cooling. Apart from the thermal mass on the building elements, several studies investigated the impact of internal thermal mass (e.g., furniture) on the convective heat transfer. Wallentén [34] experimented on a full-scale with and without furniture (a desk, two chairs, and a small chest). It was found that the furniture had little effect on the convective heat transfer along with the window and wall around the window. Spitler et al. [22] compared the airflow of an empty room and a furnished room (one table and six chairs or two cabinets),

indicating that the furniture impacted the flow. Those studies only investigated the heat transfer of some room interior surfaces rather than the indoor furniture. The impact of the amount of indoor furniture and its location on the heat transfer in the room needs further study. Besides, none of the researchers deduced the CHTC at the interior surfaces with thermal mass.

In BES tools, it is easy to consider the thermal mass capacity in the room interior surfaces by setting the construction composition in detail. Modeling the internal mass (particularly furniture) accurately is cumbersome due to the difficulty of measuring internal mass geometry and quantifying its amount [35]. One approach to modeling the internal mass in BES software is simplifying the internal mass as a virtual equivalent planar element (i.e., a horizontal and upward-facing surface) [36]. The internal mass is involved in the zone air heat balance and the longwave radiant exchange with other surfaces. If both sides of the internal mass exchange energy with the zone, the user should double the mass area. The BES software switches algorithms applicable to the horizontal upward-facing surface for the internal mass based on the flow regime. One possible way to accurately model the furniture in BES is by adopting the specific CHTC algorithm. However, no specific correlations for internal mass were founded in the existing studies.

1.2. Novelty and main contributions

Regarding the current state-of-the-art, this study proposes experimental research that focuses on heat transfer, especially the CHTC of night cooling with mixing ventilation. A series of dynamic full-scale experiments involving 48 designed cases with ten thermal mass distribution schemes, four ACH, and two inlet temperatures were conducted. The original contributions of this study are briefly summarized in the following:

- 1) The influence of ACH, inlet temperature, and thermal mass (especially the indoor furniture) distribution on the CHTC at surfaces and the mean CHTC of the test room were comprehensively investigated.

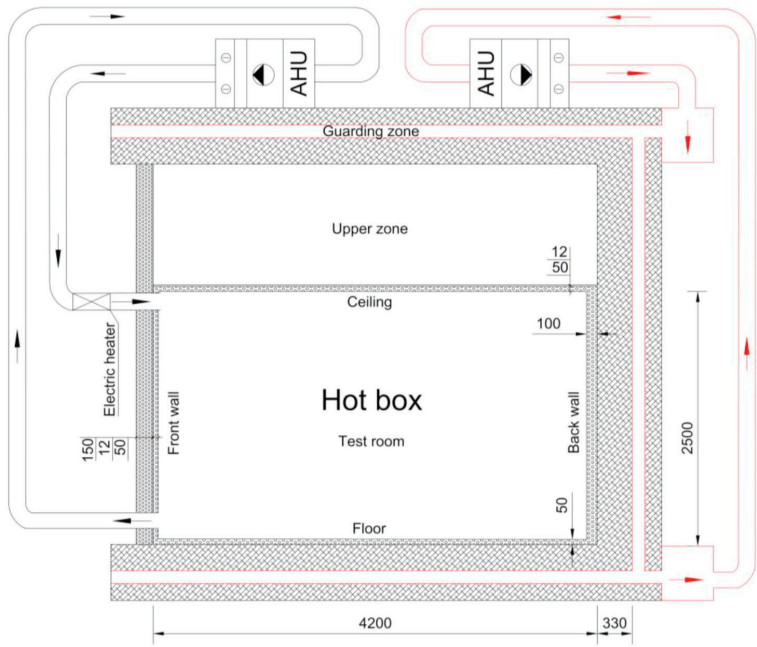


Fig. 1. Vertical section view of the hot box.

Table 1
Specification of the measurement equipment.

Equipment	Measured parameter	Range	Accuracy	Remark	Reference
FTMU UltraLink	Airflow rate	0–507 m ³ /h	±5%	Ø = 160 mm	[39]
Type K thermocouple	Surface temperature	0–50 °C	±0.09 °C	–	[40]
	Local, indoor, inlet, and outlet air temperature				
PT 100	Supply air temperature, air temperature from AHUs	0–50 °C	±0.1 °C	–	[41]
Thermopile	Temperature difference between interior and exterior surface	–	±0.058 °C	Formed by three thermocouples connected in series	[42]
Hot-sphere anemometer	Air velocity	0–5 m/s	±0.01 m/s	–	[43]

- 2) The experimental CHTCs with the inlet temperature or local air temperature as reference were deduced and compared with existing CHTC correlations.
- 3) New CHTC correlations tailored for NV were developed, which provides architects and engineers with possibilities to design or optimize the NV system.

The organization of this paper is as follows. Section 2 describes the experimental setup. Section 3 introduces the data analysis method for the derivation of CHTC, uncertainty analysis, and energy balance criteria. Section 4 presents CHTCs at different surfaces under different designed cases. Section 5 summarizes the conclusion and suggestions for future work.

2. Experimental descriptions

2.1. Hot box setup

The so-called “Large Guarded Hot Box” located in the Aalborg

University laboratory was used as a guarded test chamber to conduct the dynamic full-scale experiment. The hot box in this study was designed and constructed based on the guarded hot box concept [37]. Fig. 1 shows the vertical sectional view of the hot box. It consisted of the upper zone, the test room, and the guarding zone. A 12 mm wood panel separated the upper zone and test room. The upper zone was a plenum. The test room represents an office room with dimensions of 4.2 m (L) × 3.6 m (W) × 2.5 m (H). The guarding zone enclosed both the upper zone and the lower zone.

The original insulations between different zones of the hot box were made by a sandwich element (i.e., 15 mm wood panel + 225 mm expanded polystyrene + 15 mm wood panel). It should be noticed that the original insulation for the front side of the hot box was not the sandwich element but a combined element consisting of a 150 mm foam board and a 12 mm wood panel. Apart from the original insulation of the hot box, 50 mm foam boards ($\rho = 14.5 \text{ kg/m}^3$, $C_p = 1500 \text{ J/kg}\cdot\text{K}$, $\lambda = 0.038 \text{ W/m}\cdot\text{K}$) were installed on the test room interior surfaces for better insulation. Due to the open position of the door to the hot box, the back wall of the room was insulated with 100 mm foam boards. An air

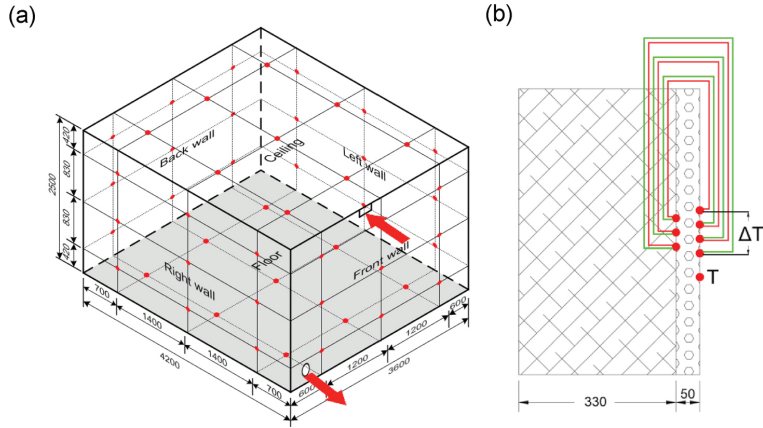


Fig. 2. (a) Positions of thermocouple/thermopile measuring points in interior surfaces, (b) the location of thermocouple and thermopile in a wall.

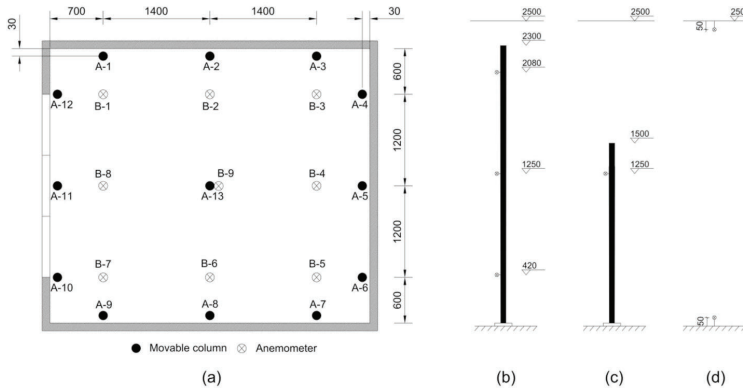


Fig. 3. (a) Horizontal positions of anemometers in the test room, (b) anemometers in the columns close to the room surface (A1-A12), (c) anemometer in the column in the middle of the room (A-13), (d) anemometers fixed close to the ceiling or floor (B1-B9).

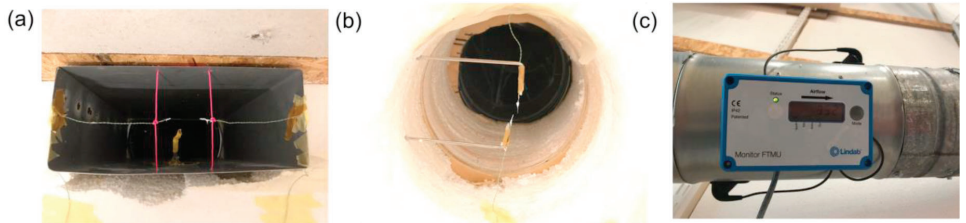


Fig. 4. Thermocouples for the (a) inlet, (b) outlet, and (c) orifice with airflow sensor.

handling unit (AHU) recirculated the air in the guarding zone to keep the zone air temperature identical to the stable laboratory air temperature (22 °C). The temperature of 22 °C was also a representative temperature for an office at the end of the summer working day [38]. Another AHU provided the conditioned air to the test room through a rectangular inlet to simulate the NV and exhausted the room air away through a round outlet. The inlet was located in the middle-upper portion of the front wall with a size of 250 mm (W) × 100 mm (H).

The outlet was located in the bottom right corner of the front wall with a diameter of 215 mm. A 1000 W electrical heater located before the inlet was turned on to heat the conditioned air with predefined cooling temperature (e.g., 12 °C) to 22 °C for creating the steady state for the test room and was turned off when NV started so that the inlet air temperature for the room can reach the predefined cooling temperature quicker than the temperature adjustment by AHU.

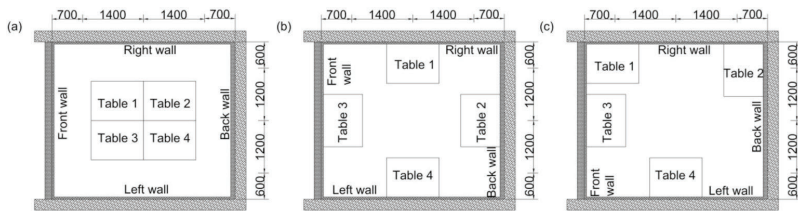


Fig. 5. Positions of tables (a) in the middle, (b) close to walls, and (c) close to the corners or the walls.

Table 2
Designed cases and the corresponding thermal mass level.

Case No.	Thermal mass distribution	ACH (h ⁻¹)	ΔT ₀ (°C)	Total c_{dyn}/A_{floor} (kJ/m ² ·K)
Case 1 to 8	Ceiling + Floor	10, 7, 5, 2	10, 5	72.2
Case 9 to 12	Ceiling + Floor + Table(a)	10, 7, 5, 2	10	97.5
Case 13 to 14	Ceiling + Floor + Table(a)	10, 5	5	97.5
Case 15 to 18	Ceiling + Floor + Table(b)	10, 7, 5, 2	10	97.5
Case 19 to 20	Ceiling + Floor + Table(b)	10, 5	5	97.5
Case 21 to 24	Ceiling + Floor + Table(c)	10, 7, 5, 2	10	97.5
Case 25 to 28	Ceiling + Floor + Right wall	10, 7, 5, 2	5	84.2
Case 29 to 32	Ceiling	10, 7, 5, 2	5	55.0
Case 33 to 36	Floor + Right wall	10, 7, 5, 2	5	67.0
Case 37 to 40	Floor	10, 7, 5, 2	5	55.0
Case 41 to 44	Right wall	10, 7, 5, 2	5	49.8
Case 45 to 48	Not installed	10, 7, 5, 2	5	37.8

2.2. Measurement equipment and location of sensors

The measured parameters are temperatures, temperature differences between the interior (facing to the test room) and exterior surfaces, and air velocities. Table 1 presents the specification of the measurement equipment.

Each interior surface in the room was evenly divided into nine sections, and the center of each section was the measuring point for thermocouples or thermopiles (see Fig. 2a). All measuring points were coated with thermal paste to ensure good thermal contact between the temperature sensor and the surface. The temperature difference was used to calculate the conductive heat flux through the interior surface. Fig. 2b shows the location of the thermopile and thermocouple in a wall.

Hot-sphere anemometers were used to measure the local air velocities close to the interior surfaces for evaluating the flow regime near the surfaces. Some anemometers were fixed on the special movable columns labeled as “A1 – A13” in Fig. 3a or fixed close to the ceiling and floor of the test room labeled as “B1 – B9” in Fig. 3a. Twelve columns (A1 – A12) holding three anemometers were close to the internal walls with a 50 mm distance (see Fig. 3b). In addition, one column (A13) holding one anemometer was in the middle of the room (see Fig. 3c), and the rest of the anemometers were located in the positions (B1 – B9) shown in Fig. 3d. It should be noticed that B9 and A13 were in the same position in the plan.

The indoor air temperatures were measured by two thermocouples located in the middle of the test room and 1.2 m away from the floor. The inlet air temperatures and outlet air temperatures were measured by

two thermocouples placed in the middle of the inlet (Fig. 4a) and outlet (Fig. 4b), respectively. The outlet was connected to an orifice with an FTMU UltraLink airflow sensor (Fig. 4c). All thermocouples and thermopiles were connected to two Fluke Helios Plus 2287A dataloggers. The conditioned air temperatures from AHUs were measured by PT 100 sensors. All the data was logged at a sampling rate of 0.1 Hz (every 10 s). The moving average of 15 values (2.5 min) was applied for temperature and temperature difference data to reduce the noise in the measurement signals.

2.3. Designed cases and experimental procedure

According to EN ISO 13786 [44], the dynamic heat capacity c_{dyn} defines the amount of energy that can be stored per surface area when the surface is exposed to a sinusoidal temperature variation with a 24 h period. The total dynamic heat capacity per unit floor area c_{dyn}/A_{floor} determines the building thermal mass level. The hot box construction described in Section 2.1 provided the test room with a low thermal mass level ($c_{dyn}/A_{floor} = 37.8 \text{ kJ/m}^2\cdot\text{K}$). To investigate the influence of thermal mass distribution on the surface heat transfer, 18 mm fermacell® fiber plasterboards ($\rho = 1150 \text{ kg/m}^3$, $C_p = 1100 \text{ J/kg}\cdot\text{K}$, $\lambda = 0.32 \text{ W/m}\cdot\text{K}$) were installed on the different interior surfaces that were foam boards. Installing the fiber plasterboard increased the c_{dyn} of one original interior surface from 8.5 to 26.0 kJ/m²·K. For the sake of simplification, the fiber plasterboard is called “thermal mass” in the following sections. Moreover, four tables assembled by the fiber plasterboards were also included to test different furniture distribution schemes. Each table contained two fiber plasterboards (of 36 mm thickness) and four metal columns. The height of the table was 700 mm. Fig. 5 shows the positions of indoor tables. Four air change rates per hour (ACH) and two initial temperature differences (ΔT_0) between the inlet and indoor air were set for different designed cases. Table 2 lists the designed cases and corresponding thermal mass level. The designed cases are referred to by abbreviations in later sections. For instance, “10 ACH 10 °C Ceiling + Floor” represents case 1, meaning that the ACH is 10 h⁻¹, ΔT_0 is 10 °C, and the thermal mass is installed on the ceiling and floor. It should be noticed that the designed cases in Table 1 depended on initial trials and were updated based on primary results. The experiment started with the hypothesis that the initial temperature difference between the inlet and indoor air would make a difference for the CHTC. The preliminary results showed that the CHTCs (inlet temperature as reference) of the cases with the same ACH but different inlet temperatures were similar (cf. Section 4). It indicated that the initial temperature difference was not the case since the forced convection dominates during NV. Thus, the experiment only focused on the variation of ACH and thermal mass distribution.

The experiment procedures were: (1) supplying the air temperature with 22 °C until the steady state was reached (i.e., interior surfaces and indoor air temperature were close to 22 °C, the average temperature difference between the interior and exterior surfaces less than 0.1 °C) and (2) supplying the cold air continuously with the predefined temperature for 8 h to simulate NV. Steps 1 and 2 were then repeated for the next case.

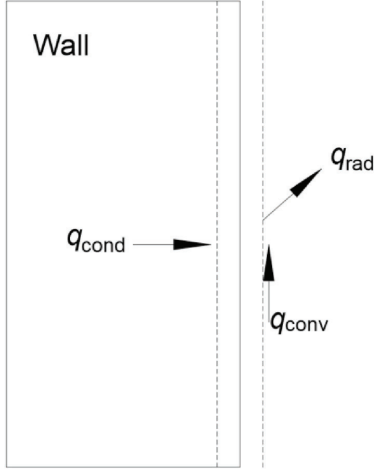


Fig. 6. The interior surface energy balance.

$$h_{\text{conv},i} = \frac{q_{\text{conv},i}}{(T_{\text{ref}} - T_{\text{surf},i})} \quad (1)$$

Table 3
Properties of materials used in the test room.

Material	λ (W/m·K)	ρ (kg/m ³)	C_p (J/kg·K)	ε (—)
Foam	0.038 ± 0.001	14.5 ± 0.1	1500 ± 100	0.96 ± 0.03
Fermcell	0.32 ± 0.01	1150 ± 10	1100 ± 100	0.95 ± 0.03

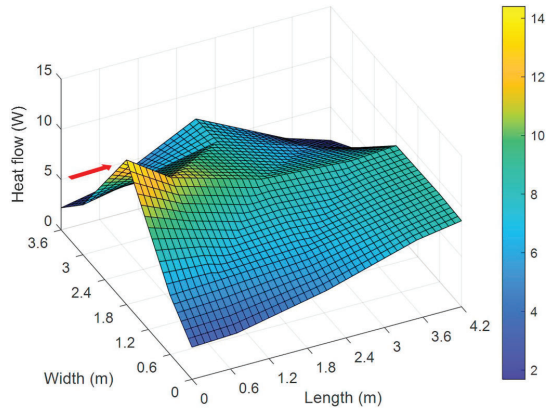


Fig. 7. The conductive heat flow of the ceiling in case 29 after 5 h and 30 min.

3. Methods of data analysis

3.1. Derivation of CHTC

The CHTC is derived from the energy balance of the interior surface energy balance (see Fig. 6). The convective heat flux (q_{conv}) is equal to the difference of the conductive (q_{cond}) and radiative heat flux (q_{rad}). The CHTC for the surface i ($h_{\text{conv},i}$) can thus be derived from Eq. (1). T_{ref} and $T_{\text{surf},i}$ are the reference temperature and the surface i temperature,

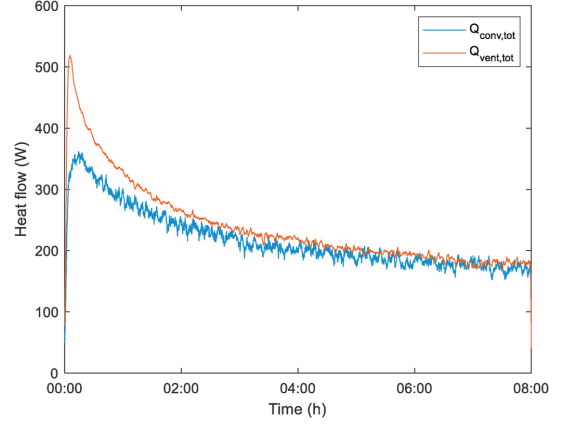


Fig. 8. Total heat flow removed from the room obtained from direct measurements and from integrating the convective heat flows over all surfaces for case 29.

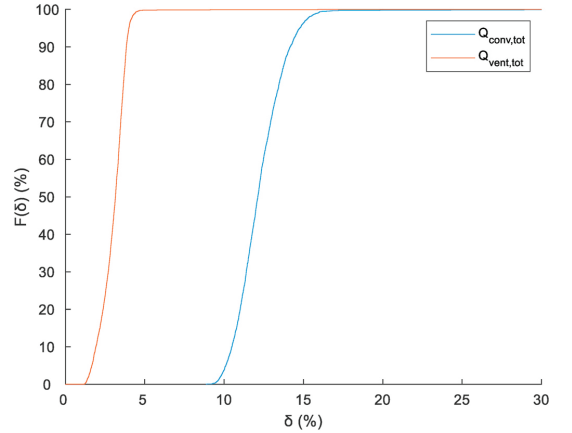


Fig. 9. Cumulative distribution function of the uncertainty in the total ventilative heat flow and total convective heat flow of case 29 due to measurement errors.

Table 4
CHTC correlations for the radial ceiling diffuser configuration (ACH: 3 to 100 h⁻¹) [24].

Surface type	Correlations
Ceiling	$h = 0.49ACH^{0.8}$
Floor	$h = 0.13ACH^{0.8}$
Walls	$h = 0.19ACH^{0.8}$

respectively.

The conductive heat flux for each surface was calculated by a transient 1D finite-difference model with an explicit scheme [45]. The interior and exterior surface temperatures were used as boundary conditions for the finite-difference model. The exterior surface temperature was calculated by subtracting the measured temperature difference between the interior and exterior surface from the measured interior surface temperature.

Table 5

CHTC correlations for the radial ceiling diffuser configuration (ACH: 3 to 12 h⁻¹) [23].

Surface type	Correlations
Ceiling	$h = -0.165 + 0.497ACH^{0.8}$
Floor	$h = 0.158 + 0.119ACH^{0.8}$
Walls	$h = -0.198 + 0.195ACH^{0.8}$

Table 6

CHTC correlations for the sidewall inlet configuration (ACH: 3 to 12 h⁻¹) [23].

Surface type	Correlations
Ceiling	$h = 0.038 + 599.3ACH^{0.8}/Ar_e$
Floor	$h = 0.698 + 0.173ACH^{0.8}$
Walls	$h = -0.109 + 0.135ACH^{0.8}$

The radiosity method was chosen to calculate the radiative heat flow of each surface [46]. This method is based on the equivalent network of building construction to represent the interaction between surfaces and has been widely adopted in BES software like EnergyPlus and IDA-ICE.

$$\left[\frac{\delta_{ij} - (1 - \epsilon_i) \cdot F_{i-j}}{\epsilon_i} \right] [J_i] = [E_{bi}] \quad (2)$$

$$q_{rad, i} = \frac{\epsilon_i}{(1 - \epsilon_i)} [E_{bi} - J_i] \quad (3)$$

where δ is the Kronecker symbol, ϵ is the emissivity, F_{i-j} is the view factor from surface i to surface j , and E_b is the black body emissive power. For the cases without tables, the view factors F_{i-j} between interior surfaces were determined according to Ref. [47]. For cases with tables, F_{i-j} between tables and other interior surfaces was calculated using the adaptive integration method [48].

3.2. Uncertainty analysis

To evaluate the accuracy of results, the uncertainty analysis was conducted by considering the accuracy of equipment (cf. Table 2) and the uncertainties of the material properties shown in Table 3. The material properties, excluding the emissivity, were given by the manufacturers. The material emissivity was measured with a TH9100MR thermo tracer. The accuracy of equipment and uncertainties of materials were assumed to be normally distributed and reported with a confidence interval of 95%.

Latin Hypercube Sampling (LHS) was applied as the sampling method in the uncertainty analysis [54]. The input scenarios based on the uncertainty of the main concerned parameters were generated by the

LHS sampling method. The LHS sample size was 300. Finally, the Monte Carlo analysis (MCA) was conducted to perform the total uncertainty on the derived heat flux and CHTC. The resulting uncertainty was given with a confidence interval of 95%.

3.3. Energy balance of the test room

To verify the accuracy of the experiment, the energy balance of the test room is established for designed cases. It is assumed that the heat input into the test room is positive, while the heat removed from the room is negative.

The total convective heat flow equals the total conductive heat flow ($Q_{cond, tot}$), as radiation heat is only transported from one surface to another ($Q_{rad, tot}=0$). They can be calculated by Eq. (4) and Eq. (5).

$$Q_{conv, tot} = \sum_i A_i \cdot q_{conv, i} \quad (4)$$

$$Q_{cond, tot} = \sum_i A_i \cdot q_{cond, i} \quad (5)$$

The total ventilative heat flow removed for the test room can be determined by the airflow volume rate (\dot{V}_{air}), the air density (ρ_{air}), the air heat capacity ($c_{p, air}$), and the temperature difference between the inlet (T_{outlet}) and outlet (T_{inlet}). It can be calculated by Eq. (6).

$$Q_{vent, tot} = \dot{V}_{air} \cdot \rho_{air} \cdot c_{p, air} \cdot (T_{outlet} - T_{inlet}) \quad (6)$$

Based on the above equations, the sensible heat balance of the test room can be evaluated by Eq. (7), and the heat unbalance rate is defined as Eq. (8).

$$\Delta Q = Q_{vent, tot} + Q_{cond, tot} \quad (7)$$

$$\bar{Q} = \frac{\Delta Q}{Q_{cond, tot}} \quad (8)$$

Because the jet flowed along with the ceiling, the conductive heat flow in the ceiling was inhomogeneous. Integrating the calculated heat flow of each section to derive the heat flow of the entire ceiling may result in a large error. To estimate the conductive heat flow of the entire ceiling accurately, the linear interpolation and extrapolation methods were used based on the conductive heat flow of each section. Fig. 7 shows the conductive heat flow of the ceiling in case 29 (10 ACH 5 °C Ceiling) after 5 h and 30 min. The red arrow in Fig. 7 indicates the inlet air direction.

Fig. 8 compares the total ventilative heat flow and total convective heat flow of a representative case (case 29). The two heat flows were in very good agreement. The large initial difference between the two heat flows was due to the thermal capacity of the air in the test room. Fig. 9 shows that during 95% of the cooling period, the uncertainties in $Q_{conv, tot}$ and $Q_{vent, tot}$ for case 29, were below $\pm 15\%$ and $\pm 4\%$, respectively. In other cases, a difference of up to 20% over the cooling period

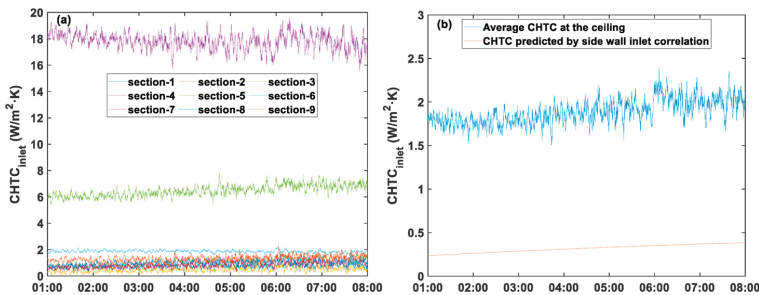


Fig. 10. (a) CHTCs of nine sections at the ceiling, and (b) average CHTC over the ceiling during NV for case 3 (first hourly data excluded).

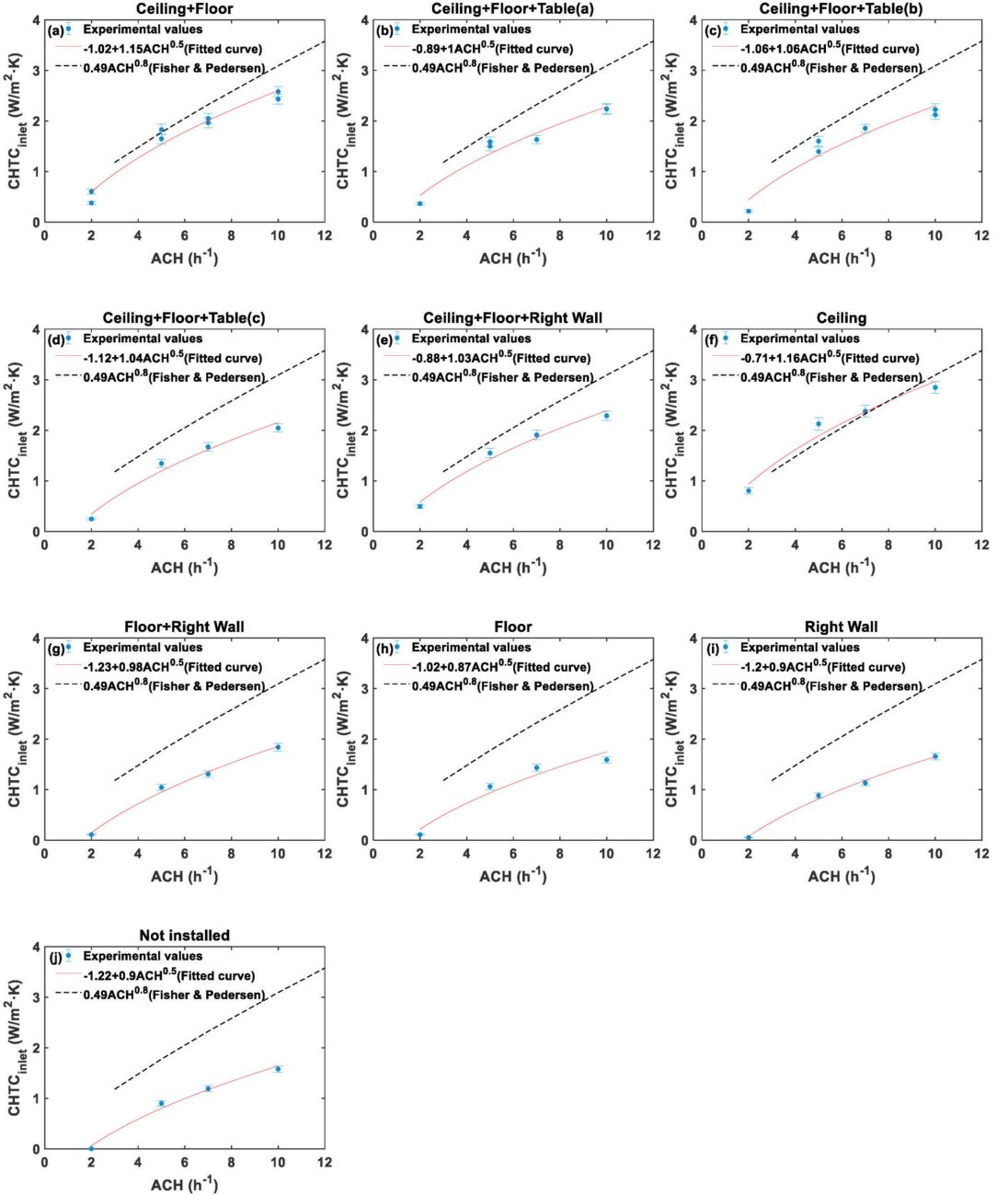


Fig. 11. Average CHTC at the ceiling for thermal mass (a) on the ceiling, (b) ceiling + floor + wall, (c) ceiling, (d) ceiling + floor + table (a), (e) ceiling + floor + table (b), (f) ceiling + floor + table (c), (g) floor + wall, (h) floor, (i) wall, and (j) thermal mass not installed.

(first hour excluded) was found due to experimental errors. While considering the uncertainties of $Q_{conv,tot}$ and $Q_{vent,tot}$, the two flows over the cooling period overlaps.

3.4. General form of CHTC correlation development

When the forced convection dominates in an enclosure, Eq. (9) shows the relationship between Reynolds number (Re) and Nusselt number

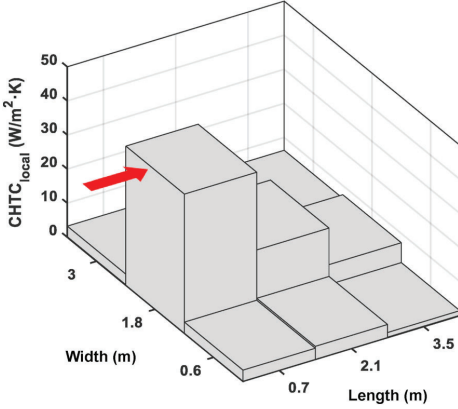


Fig. 12. Local CHTC at the ceiling for case 3 after 2 h.

(Nu) for the turbulent flow and laminar flow, respectively [49].

$$Nu = \begin{cases} C_1 \cdot Re^{0.5}, & \text{for laminar flow} \\ C_2 \cdot Re^{0.8}, & \text{for turbulent flow} \end{cases} \quad (9)$$

where C_1 and C_2 are the constant for different flow patterns, respectively. Nu and Re in an enclosure can be calculated by Eq. (10) and Eq. (11), respectively.

$$Nu = \frac{hL}{k} \quad (10)$$

$$Re = \frac{\dot{V}}{vL} \quad (11)$$

where h is the CHTC, L is the characteristic length, which can be expressed as the cubic root of the room volume ($V_{room}^{1/3}$). \dot{V} , k and v represent the air volume flow rate, air thermal conductivity, and air dynamic viscosity. Substituting Eq. (9) with (11), the CHTC can also be expressed as a function of $ACH = \dot{V}/V_{room}$ with another constant C_3 , by Eq. (12).

$$h = C_3 \cdot ACH^m \quad (12)$$

The exponent m is 0.5 for laminar flow, 0.8 for turbulent flow, and between these two values for transitional flow.

Fisher & Pedersen [24] investigated the forced CHTCs in an isothermal room with a radial ceiling diffuser. The supply ACH ranged from 3 to 12 h^{-1} , and the supply air temperature varied between 10 °C and 25 °C. The CHTC proved dependent on the jet mass flow rate rather than the inlet jet velocity and momentum. They then combined the experimental results with Spiliter's experimental results with high ACH from 15 to 100 h^{-1} [22] and developed the CHTC correlations with the turbulent flow pattern in Eq. (12) based on the inlet reference temperature summarized in Table 4.

Fisher [23] also mentioned that the CHTCs predicted at low flow rates by the correlations in Table 4 did not match the experimental CHTC very well. It may be because the flow pattern was not turbulent, or the inlet jet did not dominate the surface heat transfer at low ACH. Therefore, a modified correlation form for Nu and Re was developed, as shown in Eq. (13). It can also be transformed into the relationship between h and ACH , as shown in Eq. (14).

$$Nu = C_4 + C_5 \cdot Re^{0.8} \quad (13)$$

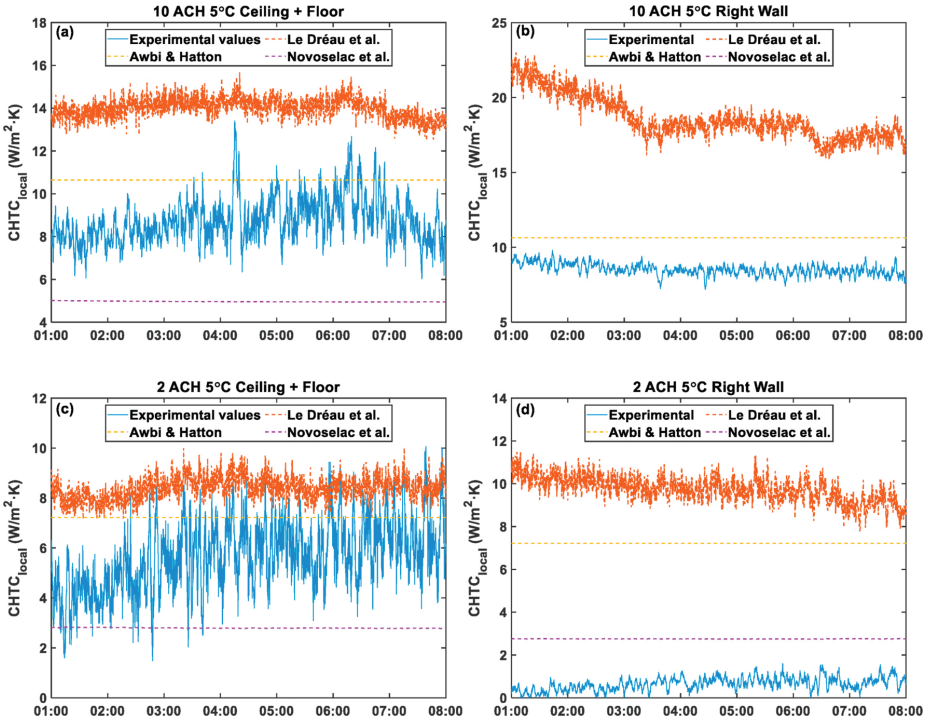


Fig. 13. Local CHTC at the ceiling for (a) case 2, (b) case 41, (c) case 8, and (d) case 44.

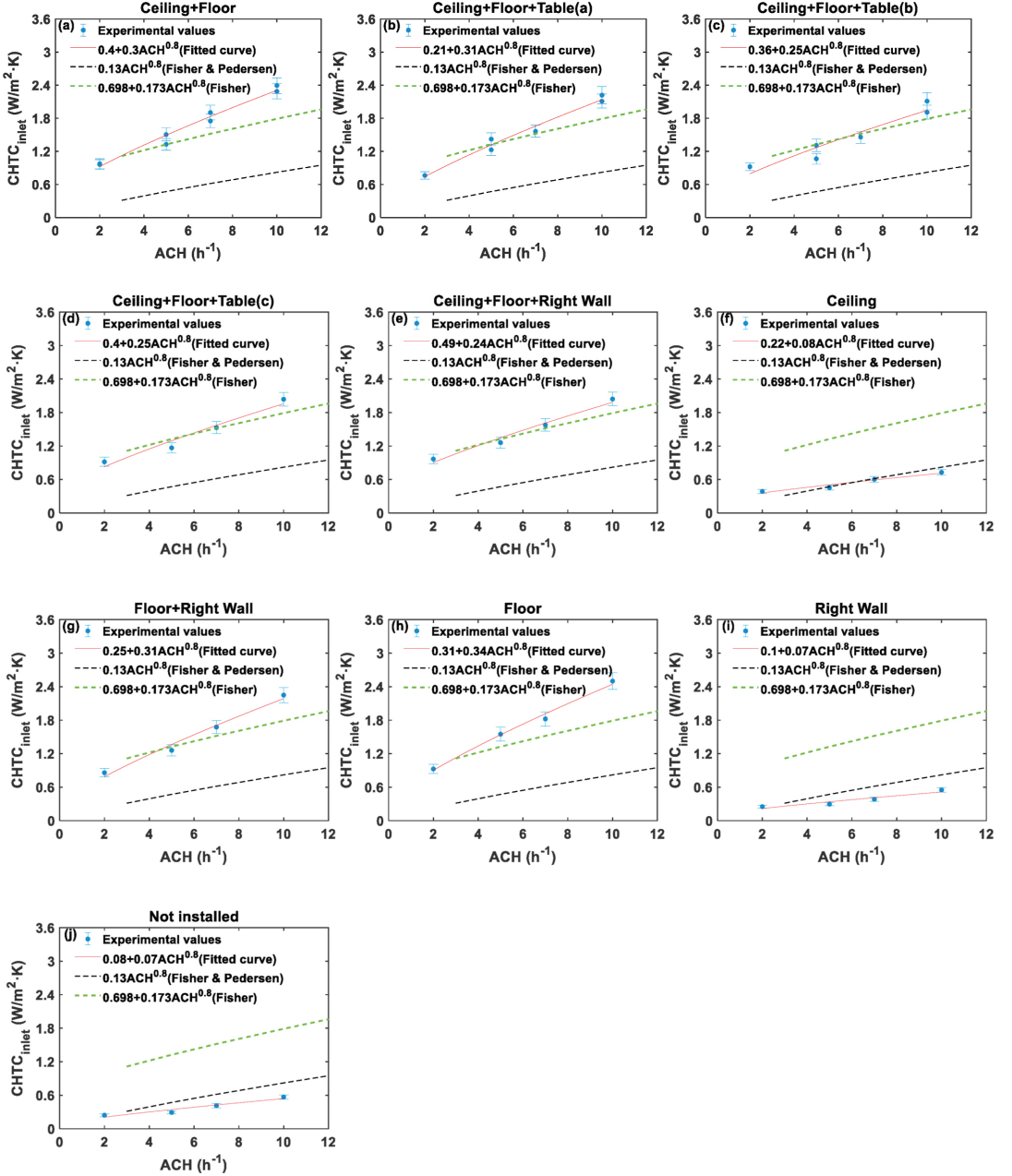


Fig. 14. Average CHTC at the floor for thermal mass (a) on the ceiling, (b) ceiling + floor + wall, (c) ceiling, (d) ceiling + floor + table (a), (e) ceiling + floor + table (b), (f) ceiling + floor + table (c), (g) floor + wall, (h) floor, (i) wall, and (j) thermal mass not installed.

$$h = C_6 + C_7 \cdot ACH^{0.8} \quad (14)$$

Table 5 summarizes the CHTC correlations for the radial ceiling diffuser configuration with Eq. (14) for ACH ranges from 3 to 12 h⁻¹.

Fisher [23] also used a vertical slot located midway up the wall (the

sidewall inlet) in an isothermal room to investigate the CHTCs caused by the free horizontal jet, which was summarized in Table 6. The Archimedes number, Ar_e was calculated by Eq. (15), where g is the gravitational acceleration, β is the coefficient of thermal expansion, L is the characteristic length. T_{outlet} and T_{inlet} are the outlet and inlet air

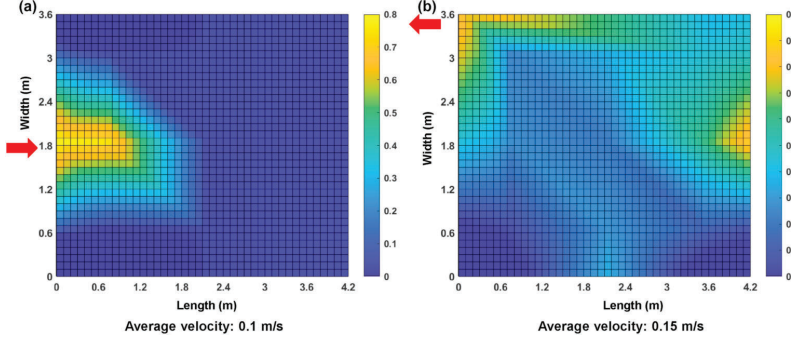


Fig. 15. Air velocity over the (a) ceiling and (b) floor for case 4 after 2 h.

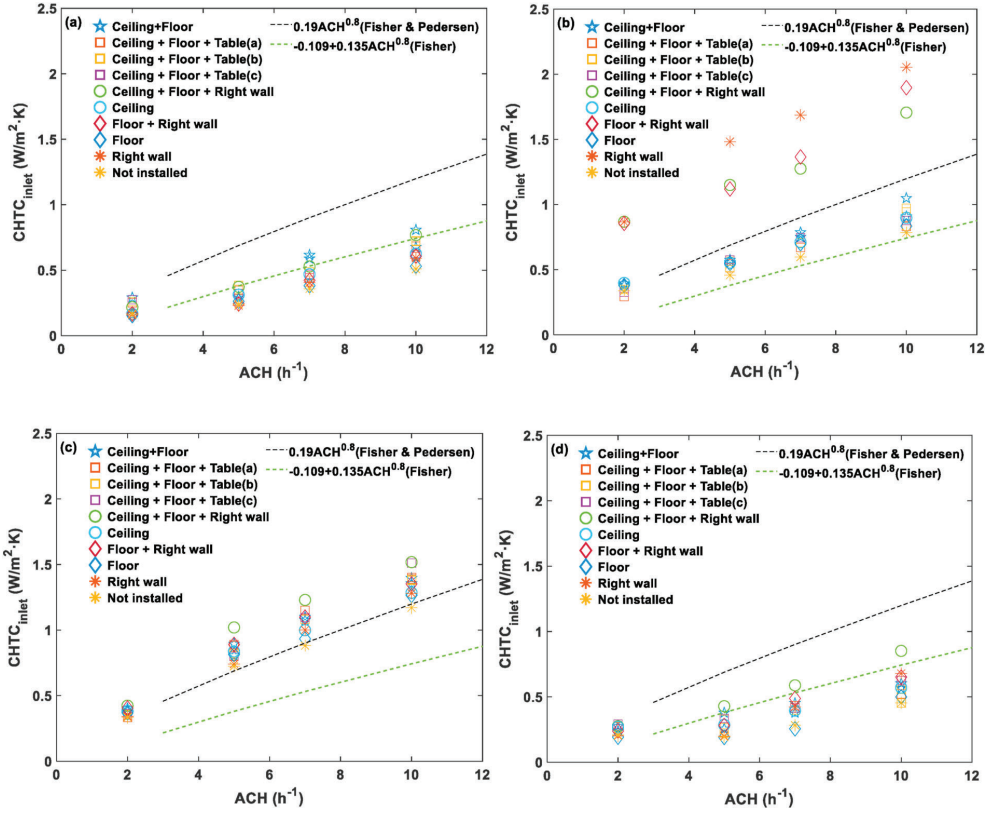


Fig. 16. Average CHTC for the (a) front wall, (b) right wall, (c) back wall, (d) left wall.

temperature, respectively.

$$Ar_c = \frac{g \cdot \beta \cdot L \cdot (T_{\text{outlet}} - T_{\text{inlet}})}{\bar{v}} \quad (15)$$

The surface flow regime can be assessed by the Richardson number (Ri), which is a dimensionless parameter expressed by combining the Grashof number (Gr) and Re , as shown in Eq. (16).

$$Ri = \frac{Gr}{Re^2} = \frac{g \cdot \beta \cdot (T_{\text{surf}} - T_{\text{ref}})}{u^2} \frac{L_{Gr}^3}{L} \quad (16)$$

where u is the airflow speed across the surface, and L_{Gr} is the characteristic length (usually room height) for Gr . Ri gives the ratio of the buoyant forces over the momentum forces and has been used in BES software such as EnergyPlus to switch the CHTC algorithms between natural, mixed, and forced flow regimes [36]. Typically, forced

Table 7

Fitted curve functions for different walls of designed cases.

Thermal mass distribution	Front wall	Right wall	Back wall	Left wall
Ceiling + Floor	-0.03 + 0.12ACH ^{0.8}	0.14 + 0.13ACH ^{0.8}	-0.4 + 0.56ACH ^{0.5}	0.1 + 0.07ACH ^{0.8}
Ceiling + Floor + Table(a)	0.04 + 0.09ACH ^{0.8}	0.07 + 0.13ACH ^{0.8}	-0.48 + 0.6ACH ^{0.5}	0.1 + 0.07ACH ^{0.8}
Ceiling + Floor + Table(b)	0.02 + 0.11ACH ^{0.8}	0.07 + 0.14ACH ^{0.8}	-0.28 + 0.42ACH ^{0.6}	0.11 + 0.06ACH ^{0.8}
Ceiling + Floor + Table(c)	0.09 + 0.08ACH ^{0.8}	-0.12 + 0.32ACH ^{0.8}	-0.09 + 0.25ACH ^{0.8}	0.12 + 0.07ACH ^{0.8}
Ceiling + Floor + Right wall	-0.02 + 0.12ACH ^{0.8}	0.52 + 0.18ACH ^{0.8}	-0.43 + 0.63ACH ^{0.5}	0.02 + 0.13ACH ^{0.8}
Ceiling	-0.03 + 0.1ACH ^{0.8}	0.19 + 0.11ACH ^{0.8}	-0.33 + 0.51ACH ^{0.5}	0.11 + 0.07ACH ^{0.8}
Floor + Right wall	-0.05 + 0.1ACH ^{0.8}	0.39 + 0.22ACH ^{0.8}	-0.35 + 0.54ACH ^{0.5}	0.03 + 0.09ACH ^{0.8}
Floor	-0.01 + 0.08ACH ^{0.8}	0.2 + 0.1ACH ^{0.8}	-0.21 + 0.4ACH ^{0.57}	0.02 + 0.06ACH ^{0.8}
Right wall	-0.05 + 0.1ACH ^{0.8}	-0.07 + 0.67ACH ^{0.8}	-0.15 + 0.31ACH ^{0.66}	-0.07 + 0.11ACH ^{0.8}
Not installed	-0.01 + 0.08ACH ^{0.8}	0.14 + 0.1ACH ^{0.8}	-0.15 + 0.31ACH ^{0.62}	0.06 + 0.05ACH ^{0.8}

convection dominates for $Ri < 0.1$, natural convection dominates for $Ri > 10$, and mixed convection exists for $0.1 < Ri < 10$ [50].

Calculating Ri for all cases by Eq. (16), where u was measured and averaged by anemometers 50 mm away from the interior surfaces, and T_{ref} was selected as the indoor air temperature measured and averaged by two thermocouples 1.2 m away from the floor. It can be concluded that for the cases with ACH of 2 h^{-1} , the average Ri during the cooling period for different surfaces ranged from 1.9 to 4.9, indicating that natural convection form cannot be neglected at the low ACH. For cases with ACH of 5, 7, and 10 h^{-1} , the average Ri for different surfaces were much below or close to 0.1, indicating that forced convection dominated. Thus, considering Eq. (14) and the meaning of exponent m in Eq. (12), the general form for the CHTC correlations developed in this study is shown by Eq. (17).

$$h = C_8 + C_9 \cdot \text{ACH}^m, \quad 0.5 \leq m \leq 0.8 \quad (17)$$

The constant C_8 , C_9 , and the exponent m were derived from curve fitting of experimental data. The lower bound and upper bound of m are 0.5 and 0.8, respectively. The existing correlations shown in Tables 4 and 6 were compared with the experimental CHTC. Table 4, instead of Table 5, was selected because the correlations in Table 4 were widely used. Other researchers also developed correlations for forced convection [22,28,51]. However, those correlations were used for the displacement ventilation or selected the outlet reference temperature; thus, those correlations were not considered in this study.

The inlet temperature was selected as the reference temperature to calculate CHTC in this study for the following reasons: (1) the convective heat flow in the room was mainly driven by the inlet airflow, especially the interior surfaces did not have heat gains (e.g., solar radiation on the part of the floor at daytime) at night, (2) the mean indoor air temperature was difficult to determine accurately due to the uneven air distribution, and (3) compared to other temperatures (outlet air

temperature, local air temperature, and indoor air temperature), the inlet temperature contributed to the highest temperature difference in Eq. (1), leading to the smallest uncertainty of CHTC.

4. Results and discussions

4.1. CHTC at the ceiling

4.1.1. Average values

The CHTCs of the nine sections with the inlet temperature as reference at the ceiling were very different due to the high gradient velocity and temperature. However, all CHTCs fluctuated moderately during the NV period for case 3 (7 ACH 10°C Ceiling + Floor) (see Fig. 10a). The first hourly data were excluded due to the high uncertainties at the beginning of the experiments. Along the inlet direction, section 4 had the highest CHTC (about $18 \text{ W/m}^2\cdot\text{K}$), followed by sections 5 and 6. The CHTCs at the remaining sections were below $2 \text{ W/m}^2\cdot\text{K}$. Directly averaging the nine CHTCs may overestimate the CHTC at the entire ceiling. Therefore, the same linear interpolation and extrapolation method introduced in Section 3.3 was adopted to calculate the convective heat flux and surface temperature of the ceiling. After that, Eq. (1) was used to calculate the surface-averaged CHTC over the night cooling period for different cases. Fig. 10b shows an example from case 3 in which the average CHTC at the ceiling was $1.97 \text{ W/m}^2\cdot\text{K}$ with a standard deviation of $0.14 \text{ W/m}^2\cdot\text{K}$ during the cooling period from 01:00 to 08:00.

The CHTC predicted by Fisher's correlation for the sidewall inlet configuration at the ceiling (cf. Table 6) was also compared with the experimental CHTCs. The results indicate that the correlation for the sidewall inlet configuration at the ceiling largely underestimated the experimental CHTC. Fig. 10b also shows an example from case 3, in which the CHTC calculated by the correlation for the sidewall inlet ranged from 0.25 to $0.4 \text{ W/m}^2\cdot\text{K}$, much less than the experimental CHTC over the cooling period. The mismatch may be because the sidewall inlet in Fisher's experiment was located in the midway of the west wall and induced a free horizontal jet, which subsequently did not impact the ceiling sufficiently.

Fig. 11 shows the experimental surface-averaged CHTCs and fitted curves with R^2 (coefficient of determination) between 0.93 and 0.99 for different designed cases, as well as Fisher & Pedersen's CHTC curve for the ceiling. The fitted curve is deduced by the nonlinear least square method with the trust-region-reflective algorithm [52]. The uncertainties estimated for the average CHTC at the ceiling range from $\pm 4\%$ to $\pm 10\%$ for different cases. It should be noticed that the title above the figures corresponds to the thermal mass distribution schemes listed in Table 2. In Fig. 11 a, b and c, the cases with two ΔT_0 (i.e., 5°C and 10°C) under the same ACH were for initial trials and had two experimental values. Those values were similar under the same ACH, indicating that CHTC at the ceiling was independent of the ΔT_0 . The reason was that the forced convection dominated during NV, which determines that the inlet momentum rather than the temperature difference between the surface and air drives the convective heat transfer. It should be noticed that for the cases with the ACH of 2 h^{-1} , the discrepancy between the two experimental values is a little high (36.7%). This can be explained by the fact that at low ACH, the flow over the ceiling might not be turbulent, which also leads to the value of exponent m to the lower bound (i.e., 0.5) for the fitted curves. However, considering that the absolute difference between the two experimental values at the ACH 2 h^{-1} was only $0.22 \text{ W/m}^2\cdot\text{K}$, the prediction error caused by the fitted curve at low ACH should be acceptable.

For most cases, the experimental values were smaller than those predicted by Fisher & Pedersen's correlation. The reason should be that

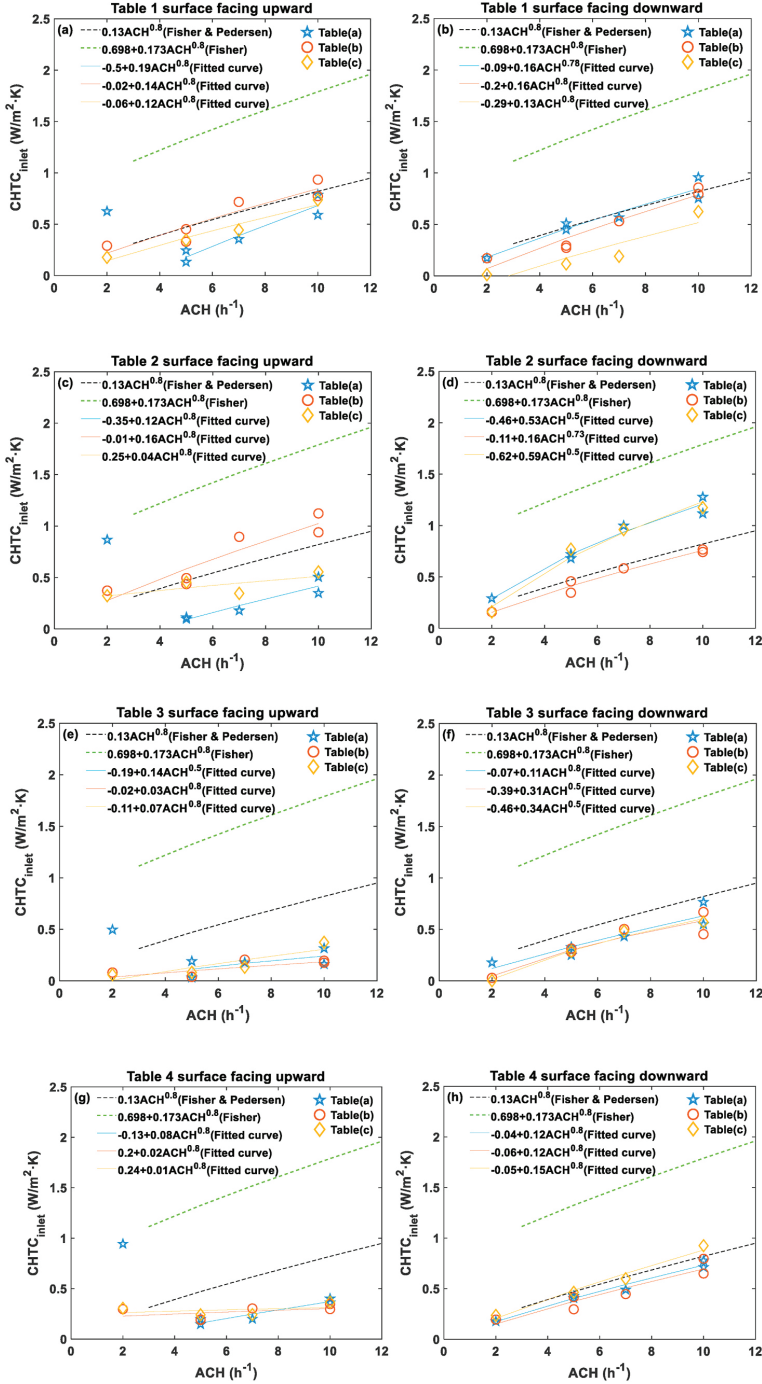


Fig. 17. Average CHTC at different table surfaces.

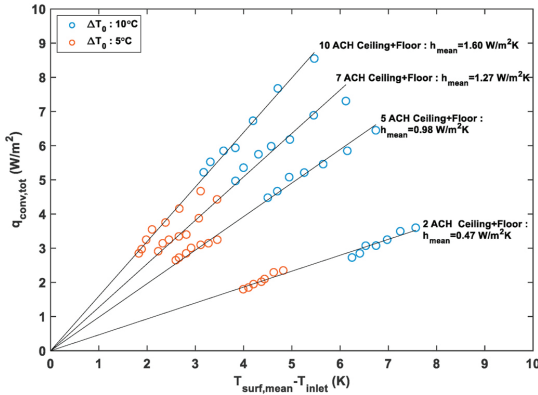


Fig. 18. Mean CHTCs of the test room for cases 1 to 8.

the air jet from the radial ceiling diffuser covered a larger area of the ceiling and the Coanda effect was strong to let the jet attached to the ceiling. For cases shown in Fig. 11f, the existing correlation predicted CHTC relatively well for the experimental values. Consequently, the fitted curve and the existing CHTC curve are in very good agreement. Compared to cases (Fig. 11a–f) where ceiling had thermal mass, the ceiling without thermal mass (Fig. 11g–j) had much lower CHTCs. There are two possible explanations: (1) installing the thermal mass on the original ceiling (i.e., foam boards) provided a larger dynamic heat capacity that can be a heat sink to store/release more heat, or (2) the thermal mass slowed down the congruence of the local air temperature and the surface temperature, resulting in a higher temperature difference for a longer period to release more energy from thermal mass. Comparing the cases that ceiling with thermal mass or without thermal mass also proved that the thermal mass distribution on other interior surfaces affected the average CHTC at the ceiling. The reason was that thermal mass on other surfaces affected the radiative heat transfer between surfaces. However, Fisher & Pedersen's correlations were derived from the isothermal experimental conditions that greatly eliminated the radiative heat transfer inside the enclosure. By comparing the cases with tables (Fig. 11b, c, d), it can be seen that the locations of tables had little impact on the average CHTC at the ceiling.

4.1.2. Local values

The existing mixed CHTC correlations with local air temperature as reference were also compared with experimental local CHTC. The local air temperatures measured by the thermocouples 50 mm away from the nine sections of the ceiling were selected as the reference temperatures. Fig. 12 shows an example of local CHTCs of nine sections at the ceiling for case 3 (7 ACH 10 °C Ceiling + Floor) after 2 h. The CHTC close to the inlet was the highest and gradually decreased along the length of the ceiling. The ratio between the highest CHTC and the lowest one was about 28.

Le Dréau et al. [31] developed a mixed correlation using local velocity, surface temperature, inlet air temperature, and indoor air temperature. We reformulated the correlation using the local air temperature as the indoor air temperature was difficult to be determined accurately and transformed the modified correlation for the entire ceiling by Eq. (18).

$$h_{local,1} = \left[\left(0.6 \cdot \left(\frac{T_{ceiling} - T_{local}}{D_h} \right)^{0.2} \right)^6 + \left(\frac{6.02 \cdot U^{0.8}}{D_h^{0.2}} \right)^6 \left(\frac{T_{ceiling} - T_{inlet}}{T_{ceiling} - T_{local}} \right)^6 \right]^{1/6} \quad (18)$$

Moreover, Awbi & Hatton [27] proposed a mixed convection

correlation for the ceiling by a fan box with an adjustable nozzle at the end of a heated ceiling by Eq. (19). Novoselac et al. [53] also developed a mixed convection correlation for the ceiling by configuring high aspiration ceiling diffusers with a cooled ceiling by Eq. (20). Both equations selected the local air temperatures as reference temperatures, which were measured 100 mm away from the ceiling.

$$h_{local,2} = \left[\left(0.704 \cdot \frac{(T_{ceiling} - T_{local})^{0.133}}{D_h^{0.601}} \right)^{3.2} + \left(1.35 \cdot W^{0.074} U^{0.772} \right)^{3.2} \right]^{1/3.2} \quad (19)$$

$$h_{local,3} = \left[\left(0.704 \cdot \frac{(T_{ceiling} - T_{local})^{0.133}}{D_h^{0.601}} \right)^3 + \left(2.0 \cdot ACH^{0.39} \right)^3 \right]^{1/3}, T_{ceiling} > T_{local} \quad (20)$$

where $T_{ceiling}$ and T_{local} are the ceiling surface temperature and the local air temperature, respectively. W is the width of the nozzle opening, U is the velocity at nozzle opening, and D_h is the hydraulic diameter of the ceiling, which is calculated by $4 \times \text{area/perimeter}$.

The three existing correlations were compared with the experimental local CHTC over the entire ceiling during the night cooling period. The results show that all three existing correlations cannot predict the local CHTC adequately. Fig. 13 shows the local CHTCs for four cases as examples. The CHTC in cases with thermal mass on the ceiling fluctuated more than in cases without thermal mass on the ceiling. The ceiling with thermal mass (Fig. 13a, c) also had higher local CHTC than the ceiling without thermal mass (Fig. 13b, d), especially at low ACH.

4.2. CHTC at the floor

Fig. 14 shows the surface-averaged CHTCs and fitted curves with R^2 between 0.91 and 0.99 for different designed cases, as well as two existing CHTC curves for the floor. The uncertainties estimated for the average CHTC values at the floor ranged from $\pm 6\%$ to $\pm 10\%$ for different cases. Like the CHTC at the ceiling, the CHTC at the floor increased when the floor has thermal mass.

Fisher's correlation (i.e., sidewall inlet) predicted higher CHTC at the floor than Fisher & Pedersen's correlation (i.e., radial ceiling diffuser) under the same ACH. The reason was that the free horizontal jet from the vertical slot located in the middle of a west wall covered a larger floor area with a higher air velocity compared to the radial ceiling diffuser. Fisher's correlation predicted CHTC relatively well for the cases with the thermal mass on the floor, especially for cases shown in Fig. 14e, but overestimated the experimental CHTC in cases without thermal mass. In contrast, Fisher & Pedersen's correlation underestimated the experimental values when the floor had thermal mass but gave relatively accurate results for the cases without thermal mass on the floor, especially for the cases in Fig. 14f. By comparing the cases with tables (Fig. 14b, c, d), it can be seen that the locations of tables had little impact on the average CHTC at the floor.

It is worth noticing that the exponent m for the floor is 0.8, indicating that flow at the floor was turbulent even at the low ACH, which is demonstrated by the similarity of experimental CHTCs of the cases at 2 ACH with two ΔT_0 in Fig. 14a. One reason why the flows over the ceiling and floor were different at low ACH could be that the inlet air evolved into the free horizontal jet and covered a small ceiling area. Another reason may be that the outlet located at the bottom of the front wall exhausted the air, which resulted in a relatively high local velocity at the floor level. Fig. 15 shows the local air velocity over the ceiling and floor with the linear interpolation and extrapolation method for case 4 (2 ACH 10 °C Ceiling + Floor) after 2 h, which further verifies the two reasons mentioned above. The red arrow represents the airflow direction. Furthermore, the CHTC at the floor was higher than the ceiling at low ACH when comparing the same cases in Fig. 14 with Fig. 11, which can also be explained by Fig. 15.

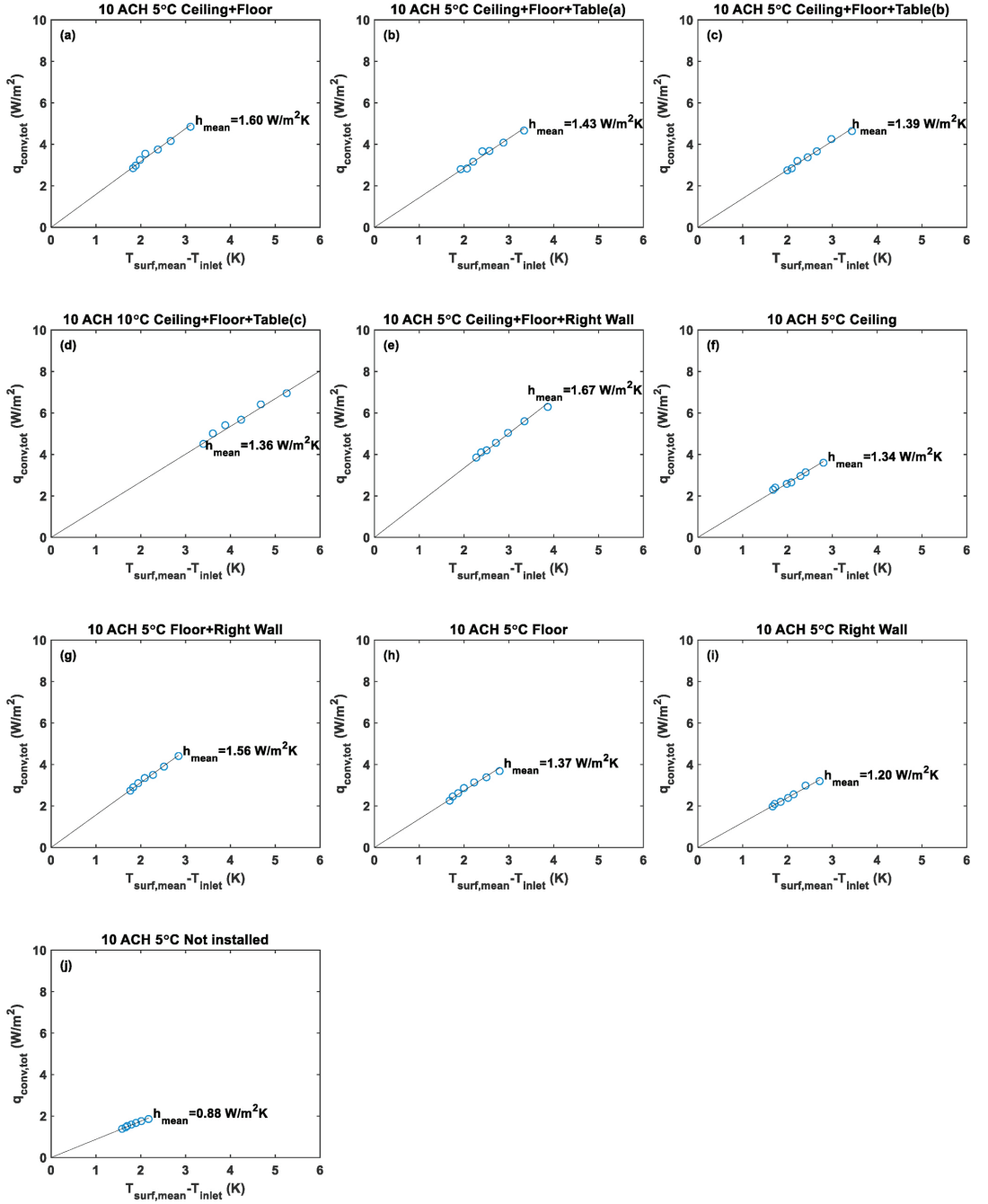


Fig. 19. Mean CHTC of room for (a) case 2, (b) case 9, (c) case 15, (d) case 21, (e) case 25, (f) case 29, (g) case 33, (h) case 37, (i) case 41, and (j) case 45.

4.3. CHTC at walls

Fig. 16 shows the surface-averaged CHTCs at walls and the two existing CHTC curves for walls. Table 7 shows the fitted curve functions with R^2 between 0.91 and 0.98 for different designed cases. The uncertainties estimated for the average CHTCs at walls ranged from $\pm 6\%$ to $\pm 10\%$ for different cases. Due to the inlet and outlet positions in the experiment, the inlet jet was not evenly distributed in the test room, resulting in different CHTCs at four walls. Contrary to the comparison between the two existing correlations at the floor, Fisher's correlation (i.e., sidewall inlet) predicted lower CHTC at walls than Fisher & Pedersen's correlation (i.e., radial ceiling diffuser) at the same ACH. The reason was that the ceiling jet from the radial ceiling diffuser attached a larger wall area than the free horizontal jet from the middle of a west wall. Both the correlations predicted CHTC well for some specific cases. For instance, Fisher & Pedersen's correlation matched quite well with the experimental CHTCs at the back wall without thermal mass (Fig. 16c). In comparison, Fisher's correlation predicted CHTC well for the front and left walls of cases with the thermal mass on the ceiling, floor, and right wall (Fig. 16a, d).

As shown in Fig. 16b, when the right wall had thermal mass, the CHTC at the right wall almost doubled, compared to the cases where the right wall was without thermal mass. The locations of tables had a small influence on the CHTCs at the walls by comparing the cases with tables and without tables. By comparing the walls without thermal mass, the back wall had the highest CHTCs (Fig. 16c), followed by the right wall (Fig. 16b). One reason was that after the inlet jet flowed away from the ceiling, it hit the back wall before falling onto the floor along the wall. Another reason was that the outlet was located on the right corner of the front wall, which caused the airflow to approach the right wall (cf. Fig. 15b). The front and left walls had similar CHTCs at the same ACH by comparing Fig. 16a and d. Thus, the corresponding fitted curve functions were similar, as shown in Table 7. It should be noticed that most of the exponent m for the back wall were between 0.5 and 0.6 because the back wall was affected relatively less by the inlet jet at the low ACH, which made the flow not turbulent at the back wall.

4.4. CHTC at tables

As there are no specific CHTC correlations for tables, the indoor furniture is usually regarded as a horizontal and upward-facing surface in BES software [36]. The existing CHTC correlations for the floor were used to compare the experimental CHTCs at tables and the fitted curves. Fig. 17 shows the surface-averaged CHTCs at walls, fitted curves, and corresponding existing CHTC correlations. The uncertainties estimated for the average CHTCs at tables ranged from 4% to 9% for different cases. Compared to Fisher's correlation that underestimated all experimental CHTCs, Fisher & Pedersen's correlation predicted CHTC relatively well for many cases.

Each table has two sides (surfaces facing upward and downward), and the two sides had different CHTCs due to the different air distribution above the surfaces. When comparing the CHTC at the same table surface with different locations, the locations of tables and air distribution had different influences on the value of CHTC. For instance, the CHTCs at table 2 surface facing upward were quite different at different locations, whereas the opposite was true for table 3 surface facing downward. It can seem surprising that the CHTCs at upward-facing surfaces of tables under 2 ACH were larger than at higher ACH, especially for tables in the middle of the room (Table(a), Fig. 2a). The reason was that, at 2ACH, the inlet jet flowed from the ceiling and fell onto the tables located in the middle of the room (cf. Fig. 15a), resulting in a higher airflow velocity and a larger area affected at the upward-facing surfaces. Thus, the CHTCs at 2 ACH of "Table(a)" location were not involved in the curve fitting.

4.5. Mean CHTC of the test room

The mean CHTC of the test room $h_{\text{mean}} = q_{\text{conv,tot}} / (T_{\text{surf,mean}} - T_{\text{inlet}})$ was also investigated. Fig. 18 shows the linear relationship between the hourly total convective heat flux ($q_{\text{conv,tot}}$) and the temperature difference between the mean interior surfaces and the inlet air ($T_{\text{surf,mean}} - T_{\text{inlet}}$) of cases 1 to 8 (i.e., thermal mass on the ceiling and floor). The first hourly data were excluded. The convective heat flux decreases with the reduction of the temperature difference. The mean CHTC of the room is not correlated to ΔT_0 but positively correlated to ACH. The reason is that the forced convection dominates during the night cooling; therefore, the inlet temperature has little effect on the mean CHTC of the test room.

Fig. 19 shows the mean CHTCs with R^2 between 0.94 and 0.98 for 10-ACH cases under different thermal mass distribution schemes. The uncertainties estimated for those mean values were $\pm 5\%$ for different cases. The mean CHTCs of three cases with tables (Fig. 19b, c, and d) were close to each other, indicating that the location of tables had little influence. While comparing the cases with tables with the first case (Fig. 19a) without tables, it can be seen that tables reduced the mean CHTC of the room. One possible reason was that the horizontal tables above the floor did not contribute more heat removed by NV than the sole floor. Another reason may be that the tables enlarged the total interior surface area, increasing the temperature difference ($T_{\text{surf,mean}} - T_{\text{inlet}}$). Apart from the cases with tables, the remaining figures reveal that the mean CHTC of case 25 (Fig. 19e) was the highest (1.67 W/m²·K), while case 45 (Fig. 19j) had the lowest mean CHTC (0.88 W/m²·K). The mean CHTC tends to increase with the thermal mass level when the thermal mass is installed on the surfaces.

5. Conclusions

This study analyzed dynamic full-scale experiments conducted in a test room with 10 thermal mass distribution schemes, which were cooled down by four constant air change rates per hour (ACH) and two inlet air temperatures for 8 h to simulate night cooling with mixing ventilation. The surface-averaged convective heat transfer coefficient (CHTC) at interior surfaces and local CHTC at the ceiling were derived from the experiment and compared with existing correlations. The mean CHTC of the test room was also calculated to investigate the impact of thermal mass, ACH, and inlet temperature. New correlations based on the experimental surface-averaged CHTCs were specifically developed for night ventilation.

The existing CHTC correlations did not accurately predict the average CHTC with the inlet temperature as reference at room interior surfaces for most designed cases, but only relatively well for a few cases. The existing local CHTC correlations also cannot give accurate results to the experimental local CHTC at the ceiling. The installation of thermal mass (i.e., fiber plasterboard) on one original surface with foam boards can significantly enhance its surface-averaged CHTC and affect the average CHTC at other surfaces due to radiative heat transfer. The presence and locations of tables had little influence on the CHTCs at the interior surfaces of the room but may greatly impact the CHTC at table surfaces due to the air distribution.

The mean CHTC of the test room with the inlet temperature as reference was not correlated to the inlet temperature but positively correlated to the ACH. When the thermal mass was installed on the room interior surfaces, a higher thermal mass level induced a higher mean CHTC. If tables were placed in the room, the mean CHTC decreased. The location of tables made no difference in the mean CHTC.

The developed correlations of this study can be adopted to build energy simulation (BES) tools, allowing users to set custom equations for interior surface CHTC to estimate mechanical or natural night ventilation performance accurately. These correlations also provide the potential to optimize the ACH and thermal mass distribution to improve

the night ventilation performance by yearly BES without coupling complex computational fluid dynamics (CFD) methods.

Declaration of competing interest

The authors declare that they have no known competing financial interests or personal relationships that could have appeared to influence the work reported in this paper.

Acknowledgements

The project is carried out as part of IEA EBC Annex 80 Resilient Cooling. The first author gratefully acknowledges the financial support from the China Scholarship Council (CSC No. 201706050001). The first author would also like to thank Lars Isbach Poulsen, Yanmin Wang, Bolong Wei, Baoming Su, Weiheng Zhang, and Min Liu for their great technical support. We would also like to thank Vivi Søndergaard for her help.

References

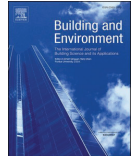
- [1] M. Kolokotroni, P. Heiselberg, Ventilative Cooling: State-Of-The-Art Review, Aalborg Univ. Aalborg, Denmark, 2015. <https://www.buildup.eu/en/node/52462>.
- [2] E. Solgi, Z. Hamedani, R. Fernando, H. Skates, N.E. Orji, A literature review of night ventilation strategies in buildings, *Energy Build.* 173 (2018) 337–352, <https://doi.org/10.1016/j.enbuild.2018.05.052>.
- [3] S.P. Corgnati, A. Kandinis, Thermal mass activation by hollow core slab coupled with night ventilation to reduce summer cooling loads, *Build. Environ.* 42 (2007) 3285–3297, <https://doi.org/10.1016/j.buildenv.2006.08.018>.
- [4] D.P. Albuquerque, N. Mateus, M. Avantaggiato, G. Carrilho da Graça, Full-scale measurement and validated simulation of cooling load reduction due to nighttime natural ventilation of a large atrium, *Energy Build.* 224 (2020) 110233, <https://doi.org/10.1016/j.enbuild.2020.110233>.
- [5] M. Lança, P.J. Coelho, J. Viegas, Enhancement of heat transfer in office buildings during night cooling – reduced scale experimentation, *Build. Environ.* 148 (2019) 653–667, <https://doi.org/10.1016/j.buildenv.2018.11.033>.
- [6] L.-X.X. Wu, J.-N.N. Zhao, Z.-J.J. Wang, Night ventilation and active cooling coupled operation for large supermarkets in cold climates, *Energy Build.* 38 (2006) 1409–1416, <https://doi.org/10.1016/j.enbuild.2006.02.011>.
- [7] R. Guo, Y. Gao, C. Zhuang, P. Heiselberg, R. Levinson, X. Zhao, D. Shi, Optimization of cool roof and night ventilation in office buildings: a case study in Xiamen, China, *Renew. Energy* 147 (2020) 2279–2294, <https://doi.org/10.1016/j.renene.2019.10.032>.
- [8] M. Kolokotroni, A. Aronis, Cooling-energy reduction in air-conditioned offices by using night ventilation, *Appl. Energy* 63 (1999) 241–253, [https://doi.org/10.1016/S0306-2619\(99\)00031-8](https://doi.org/10.1016/S0306-2619(99)00031-8).
- [9] V. Geros, M. Santamouris, A. Tsangrassoulis, G. Guarracino, Experimental evaluation of night ventilation phenomena, *Energy Build.* 29 (1999) 141–154, [https://doi.org/10.1016/S0378-7788\(98\)00056-5](https://doi.org/10.1016/S0378-7788(98)00056-5).
- [10] P. Blondeau, M. Spérando, F. Allard, Night ventilation for building cooling in summer, *Sol. Energy* 61 (1997) 327–335, [https://doi.org/10.1016/S0038-092X\(97\)00076-5](https://doi.org/10.1016/S0038-092X(97)00076-5).
- [11] Z. Wang, L. Yi, F. Gao, Night ventilation control strategies in office buildings, *Sol. Energy* 83 (2009) 1902–1913, <https://doi.org/10.1016/j.solener.2009.07.003>.
- [12] H. Sha, D. Qi, Investigation of mechanical ventilation for cooling in high-rise buildings, *Energy Build.* 228 (2020) 110440, <https://doi.org/10.1016/j.enbuild.2020.110440>.
- [13] W. Ji, Q. Luo, Z. Zhang, H. Wang, T. Du, P.K. Heiselberg, Investigation on thermal performance of the wall-mounted attached ventilation for night cooling under hot summer conditions, *Build. Environ.* 146 (2018) 268–279, <https://doi.org/10.1016/j.buildenv.2018.10.002>.
- [14] E. Solgi, Z. Hamedani, R. Fernando, B. Mohammad Kari, H. Skates, A parametric study of phase change material behaviour when used with night ventilation in different climatic zones, *Build. Environ.* 147 (2019) 327–336, <https://doi.org/10.1016/j.buildenv.2018.10.031>.
- [15] A. O'Donnovan, A. Belleri, F. Flourentzou, G.-Q. Zhang, G.C. da Graca, H. Breesch, M. Justo-Alonso, M. Kolokotroni, M.Z. Pomianowski, P. O'Sullivan, Others, Ventilative Cooling Design Guide: Energy in Buildings and Communities Programme. March 2018, Aalborg University, Department of Civil Engineering, 2018. <https://venticool.eu/wp-content/uploads/2016/11/VC-Design-Guide-EBC-Annex-62-March-2018.pdf> (accessed April 15, 2019).
- [16] N. Artmann, H. Manz, P. Heiselberg, Parameter study on performance of building cooling by night-time ventilation, *Renew. Energy* 33 (2008) 2589–2598, <https://doi.org/10.1016/j.renene.2008.02.025>.
- [17] R. Guo, Y. Hu, M. Liu, P. Heiselberg, Influence of design parameters on the night ventilation performance in office buildings based on sensitivity analysis, *Sustain. Cities Soc.* 50 (2019) 101661, <https://doi.org/10.1016/j.scs.2019.101661>.
- [18] K. Goethals, H. Breesch, A. Janssens, Sensitivity analysis of predicted night cooling performance to internal convective heat transfer modelling, *Energy Build.* 43 (2011) 2429–2441, <https://doi.org/10.1016/j.enbuild.2011.05.033>.
- [19] ASHRAE, ASHRAE Handbook Fundamentals 2017, ASHRAE Handb., 2017. <https://www.ashrae.org/technical-resources/ashrae-handbook/description-2017-ashrae-handbook-fundamentals>.
- [20] T.C. Min, L.F. Schutrum, G. V Parmelee, J.D. Vouris, Natural convection and radiation in a panel heated room, *Build. Eng.* 62 (1956) 337–358.
- [21] F. Alamdari, G.P. Hammond, Improved Data Correlations for Buoyancy-Driven Convection in Rooms, SAGE Publications Sage UK, London, England, 1983, <https://doi.org/10.1177/014362448300400304>.
- [22] J.D. Spitler, C.O. Pedersen, D.E. Fisher, Interior convective heat transfer in buildings with large ventilative flow rates, in: ASHRAE Trans., 1991, pp. 505–515. www.hvac.okstate.edu (accessed May 11, 2020).
- [23] D.E. Fisher, An Experimental Investigation of Mixed Convection Heat Transfer in a Rectangular Enclosure, University of Illinois at Urbana-Champaign, 1995. <https://www.ideals.illinois.edu/handle/2142/22513>.
- [24] D.E. Fisher, C.O. Pedersen, Convective heat transfer in building energy and thermal load calculations, *Build. Eng.* 103 (1997) 137–148. <https://citeseerx.ist.psu.edu/viewdoc/download?doi=10.1.1.616.9820&rep=rep1&type=pdf>.
- [25] H.B. Awbi, A. Hattori, Natural convection from heated room surfaces, *Energy Build.* 30 (1999) 233–244, [https://doi.org/10.1016/S0378-7788\(99\)00004-3](https://doi.org/10.1016/S0378-7788(99)00004-3).
- [26] I. Beausoleil-Morrison, The adaptive coupling of heat and air flow modelling within dynamic whole-building simulation. <http://www.esru.strath.ac.uk/Documents/PhD/beausoleil-morrison-thesis.pdf>, 2000 (accessed May 13, 2020).
- [27] H.B. Awbi, A. Hattori, Mixed convection from heated room surfaces, *Energy Build.* 32 (2000) 153–166, [https://doi.org/10.1016/S0098-8472\(99\)00063-5](https://doi.org/10.1016/S0098-8472(99)00063-5).
- [28] A. Novoselac, B.J. Burley, J. Srebric, Development of new and validation of existing convection correlations for rooms with displacement ventilation systems, *Energy Build.* 38 (2006) 163–173, <https://doi.org/10.1016/j.enbuild.2005.04.005>.
- [29] I. Beausoleil-Morrison, The adaptive simulation of convective heat transfer at internal building surfaces, *Build. Environ.* 37 (2002) 791–806, [https://doi.org/10.1016/S0360-1323\(02\)00042-2](https://doi.org/10.1016/S0360-1323(02)00042-2).
- [30] N. Artmann, R.L. Jensen, H. Manz, P. Heiselberg, Experimental investigation of heat transfer during night-time ventilation, *Energy Build.* 42 (2010) 366–374, <https://doi.org/10.1016/j.enbuild.2009.10.003>.
- [31] J. Le Dreau, P. Heiselberg, R.L. Jensen, Experimental investigation of convective heat transfer during night cooling with different ventilation systems and surface emissivities, *Energy Build.* 61 (2013) 308–317, <https://doi.org/10.1016/j.enbuild.2013.02.021>.
- [32] D. Olsthoorn, F. Haghighat, A. Moreau, G. Lacroix, Abilities and limitations of thermal mass activation for thermal comfort, peak shifting and shaving: a review, *Build. Environ.* 118 (2017) 113–127, <https://doi.org/10.1016/j.buildenv.2017.03.029>.
- [33] K. Goethals, M. Delghust, G. Flamant, M. De Paepe, A. Janssens, Experimental investigation of the impact of room/system design on mixed convection heat transfer, *Energy Build.* 49 (2012) 542–551, <https://doi.org/10.1016/j.enbuild.2012.03.017>.
- [34] P. Wallentén, Convective heat transfer coefficients in a full-scale room with and without furniture, *Build. Environ.* 36 (2001) 743–751, [https://doi.org/10.1016/S0360-1323\(00\)00070-6](https://doi.org/10.1016/S0360-1323(00)00070-6).
- [35] H. Johra, P. Heiselberg, Influence of internal thermal mass on the indoor thermal dynamics and integration of phase change materials in furniture for building energy storage: a review, *Renew. Sustain. Energy Rev.* 69 (2017) 19–32, <https://doi.org/10.1016/j.rser.2016.11.145>.
- [36] U.S. DoE, Energyplus engineering reference. <https://bigladdersoftware.com/epx/docs/9-3/engineering-reference/>, 2020.
- [37] ISO 8990-1996, Thermal Insulation — Determination of Steady-State Thermal Transmission Properties — Calibrated and Guarded Hot Box, International Standard, 1996. <https://www.iso.org/standard/16519.html>.
- [38] S. Leenknegt, R. Wagemakers, W. Bosschaerts, D. Saels, Improving the modelling of surface convection during natural night ventilation in building energy simulation models, in: Proc. Build. Simul. 2011 12th Conf. Int. Build. Perform. Simul. Assoc., 2011, pp. 2233–2240. https://limo.libis.be/primo-explore/fulldisplay?docid=LIRIAS156532&context=L&vid=Lirias&search_scope=Lirias&tab=default_tab&lang=en-US&fromSiteMap=1 (accessed September 26, 2020).
- [39] About FTMU Lindab.dk, (n.d.). <http://www.lindab.com/dk/pro/products/Pages/FTMU.aspx> (accessed July 25, 2020).
- [40] J. Le Dreau, P. Heiselberg, R.L. Jensen, Experimental Data from a Full-Scale Facility Investigating Radiant and Convective Terminals: Uncertainty and Sensitivity Analysis, Description of the Experimental Data, Department of Civil Engineering, Aalborg University, 2014. <http://vbn.aau.dk/en/publications/experimental-data-from-a-full-scale-facility-investigating-radiant-and-convective-terminals/1ce46b33-cfa8-4979-b112-cd9ab4879c7?html> (accessed October 22, 2020).
- [41] M.H. Kristensen, J.S. Jensen, R.L. Jensen, Air Temperature Measurements Using Dantec Draught Probes, Department of Civil Engineering, Aalborg University, 2015. <https://vbn.aau.dk/en/publications/air-temperature-measurements-using-dantec-draught-probes> (accessed July 25, 2020).
- [42] N. Artmann, R. Vonbank, R.L. Jensen, Temperature Measurements Using Type K Thermocouples and the Fluke Helios Plus 2287A Data Logger Thermocouples and the Fluke Helios Plus, 2008.
- [43] R.L. Jensen, O.K. Larsen, C.-E. Hylgård, On the use of hot-sphere anemometers in a highly transient flow in a double-skin facade, in: Int. Conf. Air Distrib. Rooms, Roomvent, 2007, pp. 13–15. <https://vbn.aau.dk/en/publications/on-the-use-of-hot-sphere-anemometers-in-a-highly-transient-flow-i> (accessed July 22, 2020).

- [44] EN ISO 13786, Thermal Performance of Building Components – Dynamic Thermal Characteristics – Calculation Methods, 2017. <https://webshop.ds.dk/Default.aspx?ID=219&GroupID=91.120.10&ProductID=M289824>.
- [45] G.D. Smith, Numerical Solution of Partial Differential Equations: Finite Difference Methods, Oxford university press, 1985. <https://anujitspenjoymath.files.wordpress.com/2019/02/g.-d.-smith-numerical-solution-of-partial-differential-equations-finite-difference-methods.pdf>.
- [46] A.J. Chapman, Fundamentals of Heat Transfer, Macmillan, 1987.
- [47] J.R. Ehlert, T.F. Smith, View factors for perpendicular and parallel rectangular plates, J. Thermophys. Heat Tran. 7 (1993) 173–175, <https://doi.org/10.2514/3.11587>.
- [48] G. Walton, Calculation of Obstructed View Factors by Adaptive Integration, Gaithersburg, MD, 2002, <https://doi.org/10.6028/NIST.IR.6925>.
- [49] A. Bejan, Convection Heat Transfer, John Wiley & Sons, 2013. <https://ebookcentral.proquest.com/lib/aalborguniv-ebooks/detail.action?docID=1161535&pq-origsite=primo>.
- [50] S. Leenknegt, D. Saelens, Assessing convection modelling in Building Energy Simulation models for night cooling, in: Proc. BS2013 13th Conf. Int. Build. Perform. Simul. Assoc. Chambery, Fr. August. 2013, 2010, pp. 1160–1167, in: <http://www.ibpsa.org/proceedings/BS2013/p.987.pdf> (accessed April 15, 2019).
- [51] Novoselac Atila, Combined Airflow and Energy Simulation Program for Building Mechanical System Design, 2005. http://www.ce.utexas.edu/prof/Novoselac/Atila_Novoselac_thesis.pdf (accessed May 13, 2020).
- [52] Curve Fitting Toolbox™. Mathworks®, User's Guide (R2019b), 2019. <https://www.mathworks.com/help/curvefit/>.
- [53] A. Novoselac, B.J. Burley, J. Srebric, New convection correlations for cooled ceiling panels in room with mixed and stratified airflow, HVAC R Res. 12 (2006) 279–294, <https://doi.org/10.1080/10789669.2006.10391179>.
- [54] C. Zhuang, K. Shan, S. Wang, Coordinated demand-controlled ventilation strategy for energy-efficient operation in multi-zone cleanroom air-conditioning systems, Build. Environ. 191 (2021) 107588, <https://doi.org/10.1016/j.buildenv.2021.107588>.

Appendix C. Paper 3

Guo, R., Heiselberg, P., Hu, Y., Johra, H., Zhang, C., Jensen, R. L., ... & Peng, P. (2021). Experimental investigation of convective heat transfer for night cooling with diffuse ceiling ventilation. *Building and Environment*, 107665. <https://doi.org/10.1016/j.buildenv.2021.107665>

Reprinted by permission from Elsevier.



Experimental investigation of convective heat transfer for night cooling with diffuse ceiling ventilation

Rui Guo^{*}, Per Heiselberg, Yue Hu, Hicham Johra, Chen Zhang, Rasmus Lund Jensen, Kim Trangbæk Jønsson, Pei Peng

Department of the Built Environment, Aalborg University, Thomas Manns Vej 23, Aalborg, 9220, Denmark

ARTICLE INFO

Keywords:

Convective heat transfer coefficient
Night ventilation
Diffuse ceiling ventilation
Dynamic full-scale experiments

ABSTRACT

The convective heat transfer coefficient (CHTC) is a crucial parameter for night ventilation performance estimation. This paper investigates the heat transfer of night ventilation with diffuse ceiling ventilation (DCV) concept in an office room. A series of dynamic full-scale experiments were conducted with different thermal mass distribution schemes, air change rates per hour (ACH), and supply temperatures. The CHTC at interior surfaces with the inlet and outlet temperatures as the reference and the temperature efficiency of DCV were then derived. In most cases, the experimental CHTCs differed significantly from the CHTCs predicted by existing correlations. The presence of furniture (tables), its location, and the thermal mass installed on the walls had little influence on the CHTC at the floor. However, increasing the thermal mass of one surface can significantly augment its own surface CHTC. New correlations based on experimental CHTCs were developed for potential application in building energy simulation tools. The temperature efficiency of DCV decreased with the increase of ACH, the initial temperature difference between the supply air and indoor air, and the thermal mass level. DCV had higher temperature efficiency than the mixing ventilation and displacement ventilation, except for the case with displacement ventilation at low ACH.

1. Introduction

Night ventilation (NV) is a promising way to alleviate the overheating in buildings and reduce the building cooling demand by using cold outdoor air to cool down the building's thermal mass. The cooled thermal mass then acts as a heat sink on the next day to absorb the heat gain and stabilize the indoor air temperature [1]. During the daytime, the purpose of cooling methods is to maintain the indoor air temperature within the thermal comfort range, limiting the airflow rate and inlet temperature decrease to avoid draught. The purpose of NV is to purge out the diurnal excess heat stored in the thermal mass by convection when the office building is not occupied. The added benefit of NV is that the indoor air temperature limit of NV can be as low as 18 °C, and the air change rate per hour (ACH) can be high up to 10 h⁻¹ [2].

Although NV has the benefits mentioned above and has been investigated widely in experimental or simulation research [3–8], architects or engineers still hesitate to adopt this solution due to the high uncertainty in performance prediction caused by the inaccurate CHTC at interior surfaces. Several studies identified the convective heat transfer

(CHTC) as a critical parameter necessary to predict the NV performance [9–11]. Numerous empirical CHTC correlations have been developed based on the steady flat plate or steady full-scale experiments [12] and widely adopted in building energy simulation (BES) tools [13]. Nevertheless, those correlations are only applicable to specific conditions (e.g., radial ceiling diffuser or displacement ventilation), which may not be adequate for NV and cause a large error in NV simulations. Previous studies [14–16] investigated the heat transfer of NV with mixing ventilation, displacement ventilation, and wall-mounted attached ventilation by dynamic full-scale experiments. However, those studies did not focus on characterizing CHTC or developing CHTC correlation.

Thermal mass activation also plays a decisive role in NV efficiency [17]. Goethals et al. simulated surrogate models based on CFD [18] and tested the conditions [19] in a modified PASLINK cell (an outdoor climate chamber) to investigate the convective heat flux in a night cooled office room with different ventilation concepts, thermal mass distributions, and room geometries. The results showed that the thermal mass could augment the convective heat flux on the surface. Besides the thermal mass on the interior surfaces of buildings, a few studies investigated the impact of furniture (a kind of internal thermal mass) on the

^{*} Corresponding author.

E-mail address: rgu@build.aau.dk (R. Guo).

<https://doi.org/10.1016/j.buildenv.2021.107665>

Received 20 November 2020; Received in revised form 22 January 2021; Accepted 2 February 2021

Available online 6 February 2021

0360-1323/© 2021 Elsevier Ltd. All rights reserved.

Nomenclature			
<i>Latin symbols</i>		ν	Air dynamic viscosity
A	Area	λ	Thermal conductivity
c	Heat capacity	<i>Subscript</i>	
C	Constant	<i>conv</i>	Convective
C_p	Specific heat capacity	<i>cond</i>	Conductive
E_b	Black body emissive power	<i>rad</i>	Radiative
F	View factor	<i>surf</i>	Surface
g	Gravitational acceleration	i, j	Index for surface i and j
h	Surface heat transfer coefficient	<i>Acronyms</i>	
H	Height of walls	ACH	Air change rate per hour
k	Air thermal conductivity	AHU	Air handling unit
L	Characteristic length	BES	Building energy simulation
\dot{m}	Air volume flow rate	CCP	Climatic cooling potential
q	Heat flux	CFD	Computational fluid dynamics
Q	Heat flow	CHTC	Convective heat transfer coefficient
T	Temperature	CTF	Conduction transfer function module
u	Airflow speed	DCV	Diffuse ceiling ventilation
<i>Greek symbols</i>		HAMT	Combined heat and moisture transfer module
Δ	Change in a variable	LHS	Latin Hypercube Sampling
δ	Kronecker symbol	MCA	Monte Carlo analysis
ε	Emissivity	NV	Night ventilation
ρ	Density	Re	Reynolds number
		Nu	Nusselt number

heat transfer in the room. Wallentén [20] conducted a full-scale experiment involving a desk, two chairs, and a small chest. The impact of furniture on the convective heat transfer was found to be small. Spitzer et al. [21] indicated that the furniture (one table and six chairs/two cabinets) impacted the airflow by comparing the airflow of the room with and without furniture. Those studies focused more on the convective heat flux or airflow rather than analyzing the CHTC at surfaces.

Diffuse ceiling ventilation (DCV) is an air distribution concept originally developed for livestock buildings but attracting growing interest for buildings with human occupancy in recent years [22]. This air distribution system comprises three components: the air plenum, the suspended ceiling, and the ventilated room. The basic principle of DCV is to induce outdoor air or supply conditioned air to the plenum before air diffuses through the suspended ceiling panel into the occupied zone [23]. The plenum acts as the “air duct” to distribute the air; thus, reducing or replacing the common duct. The large suspended ceiling panel is characterized as an air diffuser that supplies the air to the occupied zone with very low velocity, which can utilize extremely low-temperature air without increasing the risk of draught. Furthermore, the pressure drop through the suspended ceiling panel is much lower than conventional diffusers and air ducts, saving fan energy use and providing natural ventilation potential [24]. Several studies have investigated the DCV performance in buildings concerning thermal comfort [25–28] and energy performance [29–32] by full-scale experiments or numerical simulations.

Taking account of the advantages mentioned above, DCV should also have a high night cooling potential. Indeed, the outdoor air is circulated throughout the building to effectively remove the stored heat in building components, especially the ceiling slab in which the plenum is directly exposed to the ambient air [33]. However, only a few studies have investigated the night cooling potential using DCV. Hviid [34] simulated the local CHTC in the plenum by computational fluid dynamics (CFD) and input those values in BES to evaluate the night cooling potential. The simulated combined CHTC (i.e., convective + radiative) at the ceiling slab in the plenum was 11 W/m²·K, only 1 W/m²·K higher than the prescribed value in the Danish standard for building heat transfer

calculations [35]. NV with DCV significantly reduced the overheating hours and lowered the peak temperature. Hviid and Lessing [36] derived the total CHTC of the plenum by a full-scale experiment and used the results in a BES tool to simulate NV's cooling effect. Compared to the room without DCV, the total CHTC of the plenum was greatly increased, and the occupied zone temperature reduced 1–1.5 °C, which showed the free cooling potential by utilizing the thermal mass in the ceiling slab. Those studies focused on the heat transfer in the plenum rather than the ventilated room, which has a larger interior surface area that directly affects human thermal comfort and the energy use by absorbing the heat gain during the daytime.

Furthermore, few studies have modeled the building energy performance with DCV only. According to the authors' knowledge and literature review, only one thermally activated building system integrated with DCV was modeled in BES tools [31]. The results showed that unlike the surfaces in the plenum cooled day and night by conditioned air or cold ambient air, the surfaces in the ventilated room absorb internal and solar heat gains and impact human comfort by radiation directly. Zhang et al. [37] demonstrated that for DCV, the buoyancy flow from heat sources controls the room's airflow pattern when the ACH is not higher than 10 h⁻¹. NV usually drives a predominately forced convection heat flow because there is no heat source or solar irradiance in the office room at night [14]. The heat transfer of the ventilated room with DCV at night cooling scenario needs further study.

To the best of the authors' knowledge, this paper aims to analyze the CHTC at surfaces in a ventilated room and the temperature efficiency of DCV under the NV scenario. The study also investigates the impact of thermal mass distribution on the CHTC, compares the CHTC with existing correlations, and develops CHTC correlations. The dynamic full-scale experiments were conducted in 25 design cases involving 6 thermal mass distribution schemes, 3 constant ACH, and 2 supply air temperatures. Section 2 describes the experimental setup. Section 3 introduces the data analysis methods for the derivation of CHTC and uncertainty analysis. Section 4 presents the experimental CHTCs at surfaces of the ventilated room. Section 5 summarizes the conclusions and closes the article with suggestions for future work.

2. Experimental descriptions

2.1. Guarded hot box setup

The Standard EN ISO 8990 defines two types of hot box apparatuses: the guarded hot box and the calibrated hot box [38]. A guarded hot box was used as a test chamber to conduct the dynamic full-scale experiments (see Fig. 1). The hot box was divided into three zones: a guarding zone, an upper zone, and a test room. The upper zone was an air plenum that represents the space between the room ceiling and diffuse ceiling in a real building, while the test room represents the office room with dimensions of 4.2 m (L) \times 3.6 m (W) \times 2.5 m (H). The guarding zone enclosed the upper zone and test room with the constant air temperature (22 °C) by an air handling unit (AHU) to simulate a stable outdoor environment for ensuring that the heat loss of envelope was only caused by NV. The temperature of 22 °C is a representative temperature for the office building at the end of the summer working day [39]. Another AHU supplied the conditioned air into the upper zone and exhausted the air in the test room by a circular outlet with a diameter of 215 mm located in the bottom right corner of the front wall shown in Fig. 2a. A duct with an airflow sensor was connected to the outlet to measure the airflow rate (see Fig. 2d). A fabric air duct with a diameter of 300 mm in the upper zone was applied to distribute the air in the upper zone uniformly (see Fig. 2c). The diffuse ceiling panels made by wood-cement boards ($\rho = 359 \text{ kg/m}^3$, $C_p = 923 \text{ J/kg}\cdot\text{K}$, $\lambda = 0.085 \text{ W/m}\cdot\text{K}$, porosity = 65%) with a thickness of 25 mm separated the upper zone and test room (see Fig. 2d).

The original construction of three walls (right, back, and left) and floor in the test room was sandwich elements (i.e., 15 mm wood panel+225 mm expanded polystyrene+15 mm wood panel). The front wall comprised 150 mm foam boards ($\rho = 14.5 \text{ kg/m}^3$, $C_p = 1500 \text{ J/kg}\cdot\text{K}$, $\lambda = 0.038 \text{ W/m}\cdot\text{K}$) and 12 mm wood panels. The front wall was in contact with the indoor laboratory environment, conditioned at a constant temperature of 22 °C. To achieve better insulation, 50 mm foam boards were installed on the test room's interior surfaces. Due to the practical door open position in the room, 100 mm foam boards were installed on the back wall.

2.2. Design cases and experimental procedure

The total dynamic heat capacity per unit floor area (c_{dyn}/A_{floor}) defines the building's thermal mass level. c_{dyn} represents the amount of energy stored per surface area when the surface is exposed to a

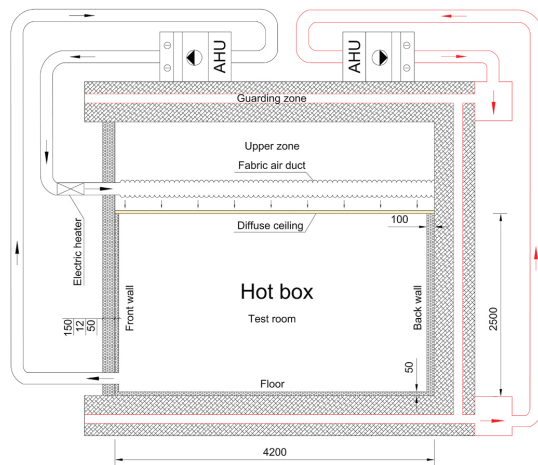


Fig. 1. Vertical section view of the hot box.

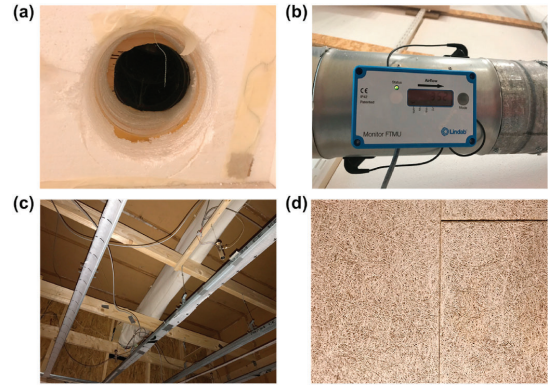


Fig. 2. (a) Outlet, (b) air distribution duct with airflow sensor, (c) fabric air duct and suspension brackets, and (d) diffuse ceiling panel.

sinusoidal temperature variation over one periodic cycle and can be calculated by EN ISO 13786 [40]. The original test room's thermal mass level was low, with the c_{dyn}/A_{floor} of $31.6 \text{ kJ/m}^2\cdot\text{K}$. In order to investigate the influence of thermal mass distribution on the heat transfer in the test room, 18 mm Fermacell® fiber plasterboards ($\rho = 1150 \text{ kg/m}^3$, $C_p = 1100 \text{ J/kg}\cdot\text{K}$, $\lambda = 0.32 \text{ W/m}\cdot\text{K}$) were installed on the different surfaces of the test room or were used to assemble four tables in the room. Each table comprised two fiber plasterboards (i.e., 36 mm thickness) and was supported with four metal columns with a height of 700 mm. Fig. 3 shows the locations of tables. Three different constant air change rates per hour (ACH) and two initial temperature differences (ΔT_0) between the supply air (i.e., the conditioned air before entering the plenum) and test room indoor air were designed for different experimental cases. Table 1 lists the design cases and the corresponding thermal mass level of the test room. For the sake of simplification, the fiber plasterboard is called "thermal mass" in later sections. The design cases are referred to by abbreviations in later sections. For example, '10ACH 10 °C Floor' represents case 1 with ACH of 10 h^{-1} , ΔT_0 of 10 °C, and thermal mass installed on the floor.

The experiment procedures are: (1) supplying the air temperature with 22 °C until the steady state was reached (i.e., interior surfaces and indoor air temperature were close to 22 °C, the average temperature difference between the interior and exterior surfaces less than 0.1 °C); (2) supplying the conditioned cold air with the predefined temperature to the upper zone and exhaust the air from the test room by AHU for 8 h to simulate NV. Steps 1 and 2 were then repeated for the next case. An automatic control system was developed using the LabVIEW programming language to identify the steady state and control AHUs. It is worth noting that an electrical heater with a power of 1000 W was installed before the inlet of the upper zone (cf. Fig. 1). The heater was turned on to heat the conditioned air with predefined temperature (e.g., 12 °C) to 22 °C to ensure steady state condition. Then the heater to start the NV case study. This is done to save the time to turn the temperature from 22 °C to the predefined temperature by AHU.

2.3. Measurements

Table 2 shows the specifications of measurement equipment and the measured parameters. Every surface in the test room was evenly divided into nine parts, and the center of each part was the measuring point for thermocouples or thermopiles (see Fig. 4a). A thermal paste ensured good thermal contact between the thermocouples and surfaces. Fig. 4b and c detail the locations of the thermocouples and thermopiles in one wall.

Local air temperatures above and below the diffuse ceiling were

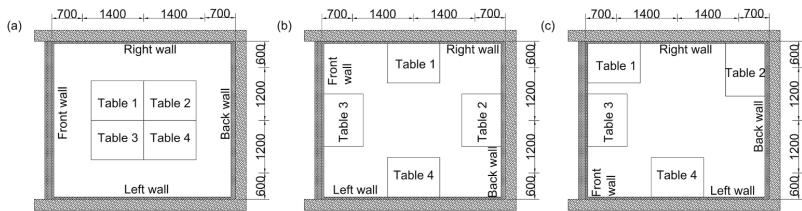


Fig. 3. Tables (a) in the middle, (b) close to walls, and (c) close to corners or walls.

Table 1
Design cases and the corresponding thermal mass level of the test room.

Case No.	Thermal mass distribution	ACH (h ⁻¹)	ΔT_0 (°C)	Total c_{dyn}/A_{floor} (kJ/m ² ·K)
Case 1 to 6	Floor	10, 5, 2	10, 5	50.6
Case 9 to 12	Floor + Table(a)	10, 5	10, 5	75.9
Case 13 to 16	Floor + Table(b)	10, 5	10, 5	75.9
Case 17	Floor + Table(c)	10	10	75.9
Case 18	Floor + Table(c)	5	5	75.9
Case 19	Floor + Right wall	5	5	62.6
Case 20 to 25	Not installed	10, 5, 2	10, 5	31.6

measured by thermocouples. Fig. 5a and b shows the horizontal section and vertical section of the temperature measuring points, respectively. The thermocouples shielded inside a ventilated tube (see Fig. 5c), which

Table 2
Specification of measurement equipment.

Instrument	Measured parameter	Range	Accuracy	Remark	Reference
FTMU UltraLink	Airflow rate	0–507 m ³ /h	±5%	Ø = 160 mm	[41]
Type K thermocouple	Surface temperature, indoor air, and outlet temperature	0–50 °C	±0.09 °C		[42]
	Local air temperatures above and below the diffuse ceiling			With shielding ventilated tube	[43]
PT 100	Supply air temperature, air temperature from AHUs	0–50 °C	±0.1 °C		[44]
TH9100MR Thermo tracer	Diffuse ceiling temperature	–20 to 100 °C	±2 °C		[45]
Thermopile	Temperature difference between interior and exterior surface	–	±0.058 °C	Formed by 3 thermocouples connected in series	[46]
Hot-sphere Anemometer	Air velocity	0–5 m/s	±0.05 m/s	–	[47]

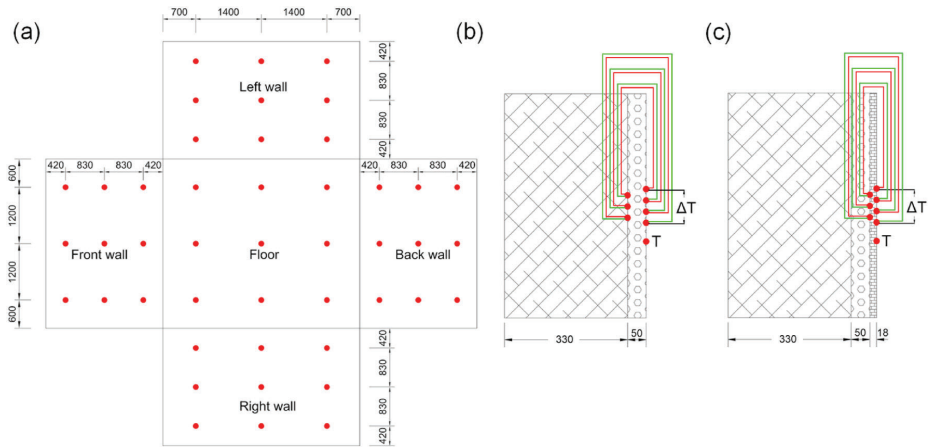


Fig. 4. (a) Positions of thermocouples/thermopiles measuring points in the surface, location of thermocouple and thermopile in (b) the original wall, (c) the original wall with fiber plasterboard.

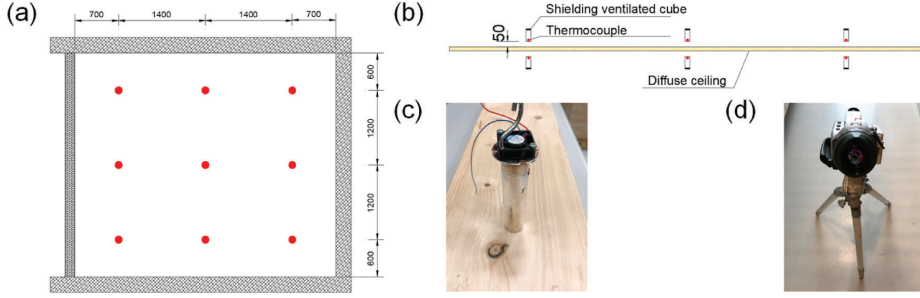


Fig. 5. (a) Horizontal section of measuring points below and above the diffuse ceiling, (b) vertical section of measuring points, (c) shielding ventilated tube, (d) thermo tracer.

represents the positions of columns, and “B1 – B9” means the positions of anemometers placed on the ceiling and floor. The columns (A1 – A12) hold three anemometers, while the column (A13) only had one, as shown in Fig. 6b and c. Each position (B1 – B9) had two anemometers installed on the ceiling and floor, respectively. The distances of anemometers away from surfaces were 50 mm.

One thermocouple located in the middle of the test room measured the indoor air temperature, while another one placed in the middle of the outlet recorded the outlet air temperature. Fluke Helios Plus 2287A dataloggers acquired analog signals from all thermocouples and thermopiles. PT100 monitoring the supply air temperature for the upper zone was logged with a data acquisition modules NI-9216 from National Instruments. The sampling rate of 0.1 Hz (every 10 s) was selected to log all the data. To reduce the noise in the measurement signals, the moving average of 15 values (2.5 min) was applied.

3. Data analysis

3.1. Derivation of CHTC

The convective heat flux ($q_{conv,i}$) on surface i is derived by the corresponding calculated conductive heat flux ($q_{cond,i}$) and radiative heat flux ($q_{rad,i}$) based on the inside surface heat balance, as shown in Eq. (1), assuming that heat flux from outside to inside is positive. Then, the convective heat transfer coefficient (CHTC) $h_{conv,i}$ at surface i is calculated by Eq. (2).

$$q_{conv,i} = q_{cond,i} - q_{rad,i} \quad (1)$$

$$h_{conv,i} = \frac{q_{conv,i}}{(T_{ref} - T_{surf,i})} \quad (2)$$

where T_{ref} and $T_{surf,i}$ are the reference temperature and surface i temperature, respectively. $q_{cond,i}$ was calculated by a transient 1D finite difference model with an explicit scheme [48]. The boundary conditions for the 1D model were the interior and exterior surface temperatures, respectively. For the surfaces (i.e., four walls and the floor), the interior surface temperature was measured by the thermocouple, and the exterior surface temperature was derived by the temperature difference measured by the thermopile and the measured interior surface temperature. For the four tables, the interior and exterior surface temperatures were measured by the thermocouples. $q_{rad,i}$ was calculated using the radiosity method [49] that is widely used in BES tools like EnergyPlus and IDA-ICE. Eqs. (3) and (4) show the calculation method.

$$\left[\frac{\delta_{ij} - (1 - \epsilon_i) n F_{i-j}}{\epsilon_i} \right] [J_i] = [E_{bi}] \quad (3)$$

$$q_{rad,i} = \frac{\epsilon_i}{(1 - \epsilon_i)} n [E_{bi} - J_i] \quad (4)$$

where δ is the Kronecker symbol, ϵ is the emissivity, F_{i-j} is view factor from surface i to surface j and E_b is the black body emissive power. For cases without indoor tables, F_{i-j} was calculated by the method for perpendicular and parallel rectangular plates [50]. While for cases with tables, F_{i-j} was considered as the obstructed view factor and was calculated using the adaptive integration method [51].

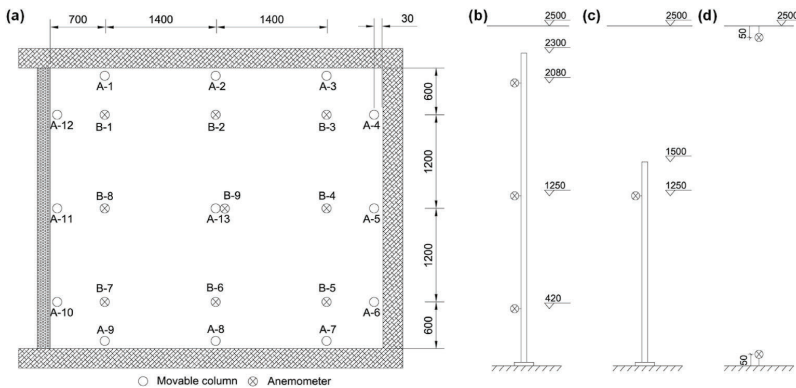


Fig. 6. (a) Horizontal positions of anemometers in the test room, (b) anemometers in the columns close to the room surface (A1-A12), (c) anemometer in the column in the middle of the room (A-13), (d) anemometers fixed close to the ceiling or floor (B1-B9).

3.2. Uncertainty analysis

The uncertainty analysis based on the most widely used uncertainty propagation method-Monte Carlo analysis (MCA) was conducted to estimate the uncertainty of result concerning the accuracies of equipment (cf. Table 1) and the uncertainties of the material properties that were assumed to be normally distributed and given with a confidence interval of 95%, as shown in Table 3. The thermal conductivity, density, and specific heat capacity originated from the manufacture, while the emissivity was deduced by comparing the material surface temperature to the temperature of black tape with high emissivity using the TH9100MR thermo tracer. Latin Hypercube Sampling (LHS) was adopted as the sampling method to generate the input scenarios according to the uncertainties of parameters mentioned above. The benefit of LHS is that results can be converged easily with a considerably small reduced number of samples for the MCA [52,53]; thus, the sample size by LHS was set as 300. After generating input scenarios by LHS, MCA was then conducted to determine the total uncertainty with a confidence interval of 95% for the derived results, including the CHTC.

3.3. General form of CHTC correlation development

Forced convection is the driving force of NV. For a flat plate with dominated forced convection, the Nusselt number (Nu_H) can be written as a function of the Reynolds number (Re_H) by Eq. (5) [54].

$$\frac{hH}{k} = Nu_H \sim \begin{cases} Re_H^{0.5}, & \text{for laminar flow} \\ Re_H^{0.8}, & \text{for turbulent flow} \end{cases} \quad (5)$$

$$Re_H = \frac{U_\infty H}{\nu} \quad (6)$$

where h is the CHTC, U_∞ represents the fluid free stream velocity, H is the plate length, k is the fluid thermal conductivity, ν is the air dynamic viscosity.

Fisher & Pedersen [55] conducted the steady-state experiment in an isothermal room with a radial ceiling diffuser that supplied air with ACH from 3 to 12 h^{-1} and with the temperature from 10 °C to 25 °C to derive the CHTCs with the inlet temperature as the reference at interior surfaces. They then combined the experimental results with the high ACH from 15 to 100 h^{-1} [21] to develop the correlations for forced convection in the enclosure by the scale analysis of the boundary layer for the flat plate in Eq. (5). Table 4 shows these correlations for forced convection.

Fisher [56] also noticed that correlations in Table 4 gave a relatively large error in predicting the CHTC at low ACH due to the flow pattern not being fully turbulent. Then, a relationship between Nu_e and Re_e was expressed in Eq. (7).

$$Nu_e = C_2 + C_3 \cdot Re_e^m \quad (7)$$

$$Nu_e = \frac{hL}{k} \quad (8)$$

$$Re_e = \frac{\dot{m}}{\rho \nu L} \quad (9)$$

where L is the characteristic length that can be the cubic root of the room volume ($V_{room}^{1/3}$), and \dot{m} is the air volume flow rate. Combining Eqs. (7)–

Table 4

CHTC correlations for the radial ceiling diffuser configuration (ACH: 3 to 100 h^{-1}) [55].

Surface type	Correlations
Ceiling	$h = 0.49ACH^{0.8}$
Floor	$h = 0.13ACH^{0.8}$
Walls	$h = 0.19ACH^{0.8}$

(9), the CHTC can be expressed by Eq. (10).

$$h = C_4 + C_5 \cdot ACH^m, \quad 0.5 \leq m \leq 0.8 \quad (10)$$

Eq. (10) was used as the general form for the CHTC correlation development. The reference temperature for the correlation development was the inlet temperature for the test room (i.e., the temperature measured by shielding ventilated thermocouple above the diffuse ceiling panel, cf. Fig. 5b). It should be noticed that the CHTC at the diffuse ceiling lower surface (i.e., the ceiling for the test room) was not investigated. The reasons are listed below: (1) the convective heat flux at the diffuse ceiling surface is difficult to be derived because the porous matrix of wood-cement ceiling converts part of the conductive and convective heat transfer into radiative heat transfer [22]; (2) the diffuse ceiling made by the wood-cement has very low thermal mass and heat capacitance, which has little influence on the energy use of DCV with respect of the whole space; (3) the heat transfer through the porous material in BES tools like EnergyPlus cannot be modeled by the most commonly used Conduction Transfer Function (CTF) module. While the Combined Heat and Moisture Transfer (HAMT) Model needs another input of moisture in all the building materials and does not fit the heat transfer equations for the diffuse ceiling panel mentioned in Ref. [22]. This is because EnergyPlus treats the air exchange and interchange between zones as convective heat gain [13]. A possible approach to select the suitable CHTC correlation for the diffuse ceiling is to adopt different existing correlations to find the one that minimizes the discrepancy between the measured values (e.g., interior surface temperature) and simulated values by BES.

After integrating the conductive and radiative heat flux at nine sections of each surface and calculating the mean surface temperature, Eq. (2) was used to calculate the surface-averaged CHTCs with the inlet temperature as the reference over the night cooling period. It is worth noting that the first hour data of the whole 8-h night cooling period is excluded due to the initial transient effect at the beginning of NV.

The forced CHTC correlations for the floor and walls in Table 4 as well as the correlations in Table 5 that were derived from the same test chamber with a sidewall inlet, were used to compare with the experimental CHTCs. Petersen et al. [57] found that DCV tends to have the displacement ventilation effect within the occupied zone at low internal heat loads. Therefore, the forced convection correlation for the floor ($h = 0.48ACH^{0.8}$) without heat patches under the displacement ventilation was also selected for comparison [58].

Furthermore, adaptive CHTC correlations that blended the natural and forced convection correlations [59] were also used for comparison. Those correlations may be the most comprehensive model for CHTC available and have been widely implemented in BES tools. For the NV scenario (i.e., cold air above or close to interior surfaces), the correlations for the buoyant floor and the walls with opposing forces were selected, as shown in Eq. (11) and Eq. (12), respectively.

Table 5

CHTC correlations for the sidewall inlet configuration (ACH: 3 to 12 h^{-1}) [56].

Surface type	Correlations
Floor	$h = 0.698 + 0.173ACH^{0.8}$
Wall	$h = -0.109 + 0.135ACH^{0.8}$

Table 3

Properties of materials used in the test room.

Material	λ (W/m·K)	ρ (kg/m ³)	C_p (J/kg·K)	ε (–)
Wood-cement	0.085 ± 0.001	359 ± 10	923 ± 100	0.95 ± 0.03
Foam boards	0.038 ± 0.001	14.5 ± 0.1	1500 ± 100	0.96 ± 0.03
Fiber plasterboards	0.32 ± 0.01	1150 ± 10	1100 ± 100	0.95 ± 0.03

gradient in the ventilated room [37]. Therefore, the surfaced-average CHTCs with the outlet temperature as the reference were deduced to compare with the predicted values by adaptive correlations. The

$$h_{\text{floor,adaptive}} = \left[\left[\left(1.4 \left(\frac{\Delta T}{D_h} \right)^{1/4} \right)^6 + (1.63 \Delta T^{1/3})^6 \right]^{3/6} + \left[\left(\frac{T_{\text{surf}} - T_{\text{inlet}}}{\Delta T} \right) (0.159 + 0.116 ACH^{0.8}) \right]^3 \right]^{1/3} \quad (11)$$

where ΔT is the temperature difference between the surface and the indoor air, H is the wall height, and D_h is the hydraulic diameter of the

discrepancy between the two values was evaluated by the mean absolute percentage error (MAPE) using Eq. (13).

$$h_{\text{wall,adaptive}} = \max \left\{ \begin{aligned} & \left[\left[\left(1.5 \left(\frac{\Delta T}{H} \right)^{1/4} \right)^6 + (1.23 \Delta T^{1/3})^6 \right]^{3/6} - \left[\left(\frac{T_{\text{surf}} - T_{\text{inlet}}}{\Delta T} \right) (-0.199 + 0.19 ACH^{0.8}) \right]^3 \right]^{1/3} \\ & 80\% \left[\left(1.5 \left(\frac{\Delta T}{H} \right)^{1/4} \right)^6 + (1.23 \Delta T^{1/3})^6 \right]^{1/6} \\ & 80\% \left[\left(\frac{T_{\text{surf}} - T_{\text{inlet}}}{\Delta T} \right) (-0.199 + 0.19 ACH^{0.8}) \right] \end{aligned} \right. \quad (12)$$

floor, which is calculated by $4 \times \text{area/perimeter}$. It is worth noting that the outlet air temperature is selected to represent the test room's average indoor air temperature due to the small air temperature

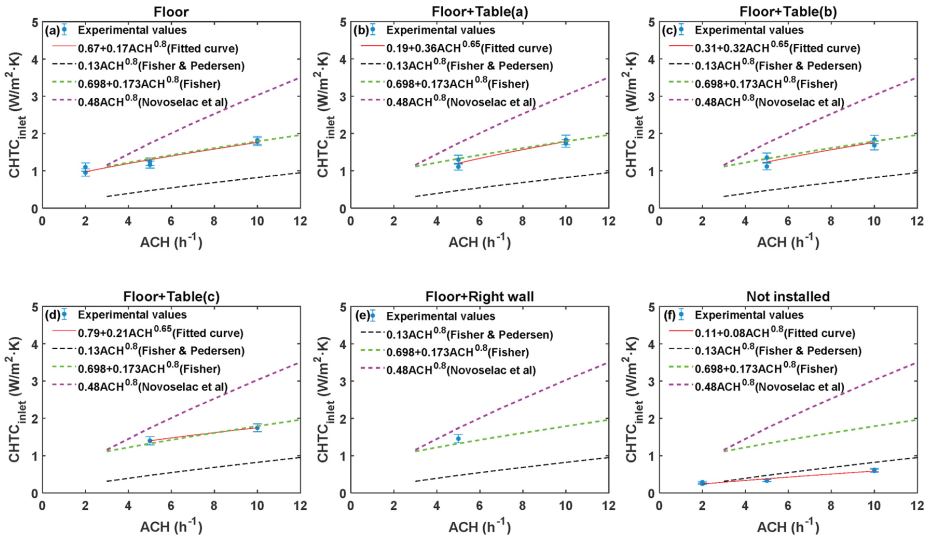


Fig. 7. Experimental CHTC at the floor for thermal mass on the (a) floor, (b) floor + table(a), (c) floor + table(b), (d) floor + table(c), (e) floor + right wall, and (j) thermal mass not installed.

$$\text{RMSE} = \sqrt{\frac{\sum_{i=1}^n (E_i - P_i)^2}{n}} \quad (14)$$

$$\text{MAPE} = \frac{1}{n} \sum_{i=1}^n \left| \frac{E_i - P_i}{E_i} \right| \quad (13)$$

where E_i and P_i are the experimental value and predicted value at point i , respectively. n is the number of data points (i.e., 2520 points from 7 h data with 10 s interval). MAPE was also used to evaluate the discrepancy between the experimental CHTC (inlet temperature as reference) with predicted values by forced correlations at ACH of 5 and 10 h^{-1} .

The indoor furniture was usually regarded as a horizontal and upward-facing surface in BES software [34] because no specific CHTC correlations were developed for the furniture. Therefore, the forced correlations and adaptive correlations for the floor were also used for comparison, respectively.

4. Results and discussion

4.1. CHTC at the floor

Fig. 7 shows the experimental surface-averaged CHTCs at the floor (inlet temperature as reference) and the corresponding existing CHTC correlations. The nonlinear least square method with the trust-region-reflective [60] algorithm is adopted to deduce the fitted curve based on the experimental values. For different design cases, the R^2 (coefficient of determination) of fitted curves is between 0.90 and 0.94, and the uncertainties estimated for the surface-averaged CHTCs range from $\pm 6\%$ to $\pm 10\%$. It is worth noting that there are two experimental values at the same ACH, representing the values are from two different inlet temperatures. Those values are very close to each other, indicating ΔT_0 has little influence on the average CHTC at the floor; thus, demonstrating the inlet jet momentum by NV drives the forced convection at the floor.

It can be seen that at the same ACH, Novoselac et al.'s correlation [58] (i.e., displacement ventilation) predicts the highest CHTC, followed by Fisher's correlation [56] (i.e., sidewall inlet) and Fisher & Pedersen's correlation [55] (i.e., radial ceiling diffuser). The reason is that the displacement ventilation diffuser located on the floor covered a larger floor area with the cool inlet jet compared to the free horizontal jet from the vertical slot located in the middle of a west wall and the downward jet from the radial ceiling diffuser. When the thermal mass (i.e., fiber plasterboard) was installed on the floor (except Fig. 7f), the experimental values at ACHs of 5 and 10 h^{-1} fit quite well with Fisher's correlation, while the other two existing correlations either overestimate or underestimate the experimental values. It seems that the presence of

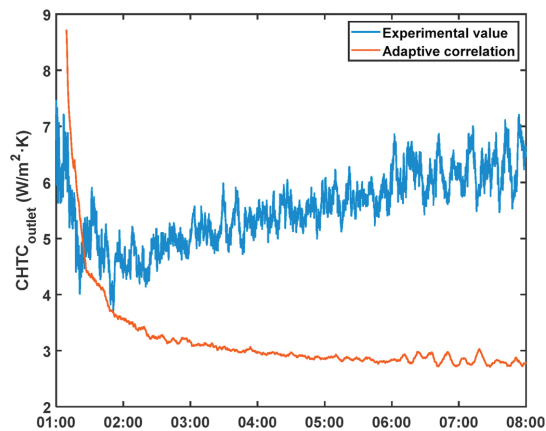


Fig. 8. Comparison between the experimental CHTC at the floor and CHTC predicted by adaptive correlation for the floor for case 11.

tables, locations of tables, and the thermal mass installed on the right wall has negligible impact on the average CHTC at the floor. Even though the number of experimental values for cases shown in Fig. 7b–e is smaller than the case with the thermal mass on the floor, it can infer that the fitted curve in Fig. 7a is also applicable for those cases with ACH ranging from 2 to 10 h^{-1} . Compared to the floor with thermal mass, the floor without thermal mass had much lower surface-averaged CHTCs (Fig. 7f). The possible reasons are: (1) the dynamic heat capacity of the floor increases a lot from 8.5 to 26.0 $\text{kJ/m}^2\cdot\text{K}$ by installing the thermal mass on the original foam boards, which provides a larger heat sink to store/release more heat; (2) the temperature congruence of the local air and floor surface is slowed down by the thermal mass which leads to a higher temperature difference for a longer period to extract more heat by NV. When no thermal mass is installed on the floor, all three existing correlations overestimate the average CHTC at the floor, of which Fisher & Pedersen's correlation predicted the results relatively well with the mean absolute percentage error (MAPE) of 38.7%, and root mean squared error (RMSE) calculated by Eq. (14) of 0.18 $\text{W/m}^2\cdot\text{K}$ at high ACH (i.e., 5 and 10 h^{-1}).

The comparison between the experimental CHTCs at the floor (outlet temperature as reference) and the predicted CHTCs by the corresponding adaptive correlation is also conducted. Generally, the adaptive correlation for the floor underestimated the experimental values. The MAPE between those two values ranges from 42% to 221% for different design cases. The lowest MAPE (i.e., 42%) occurs in case 11 (5ACH 10 °C Floor + Table(a)), as shown in Fig. 8.

4.2. CHTC at walls

Fig. 9 shows the experimental surface-averaged CHTCs at four walls (inlet temperature as reference) and the corresponding two existing CHTC correlations. The experimental values with the same symbols at the same ACH represent those values are from two different inlet temperatures. The text of "Floor" or "Floor + Table(a)" in the legend of Fig. 9 represents the thermal mass distribution. The uncertainties estimated for the experimental CHTCs range from $\pm 5\%$ to $\pm 10\%$. Fisher's correlation gives higher values for walls than Fisher & Pedersen's correlation at the same ACH because the jet from the radial ceiling diffuser covered a larger wall area than the free horizontal jet from the middle of a west wall. Fisher's correlation fits relatively better with the experimental values than Fisher & Pedersen's correlation, but the errors are still large with MAPE ranging from 28% to 131%, and RMSE ranging from 0.17 to 0.34 $\text{W/m}^2\cdot\text{K}$ for different walls at high ACH.

Fig. 10 shows the mean vertical air velocity measured by anemometers on columns A-1 to A-13 and anemometers in position B-9 (cf. Fig. 6) for case 1 (10ACH 10 °C Floor) over the night cooling period. The vertical velocity changed little for most locations, indicating a relatively uniform air distribution in the test room. The velocity in the height of 0.42 m of column A-12 was larger than other measured velocities because the anemometer was close to the outlet. Due to the relatively uniform air distribution, the experimental CHTCs at four walls under the same ACH were similar, except the front wall had slightly higher CHTC than the other three walls for most cases. The reason could be that the outlet was located in the bottom right corner of the front wall that induced more airflow near the outlet, resulting in a higher average velocity over the entire front wall than other walls. Fig. 11 shows the local air velocity over the whole front wall with the linear interpolation and extrapolation method by the local velocities measured by nine anemometers on the columns A-10, A-11, and A-12 in Fig. 6 and the outlet velocity deduced by the airflow rate and outlet area for case 1 (10ACH 10 °C Floor) after 2 h, which supports the reasons mentioned above.

In Fig. 9b, it can be seen that the right wall with the thermal mass had a much higher average CHTC than the right wall without thermal mass, indicating the thermal mass enhanced the convective heat transfer at the surface. For cases without tables, the experimental values at the same ACH and under the same thermal mass distribution were almost

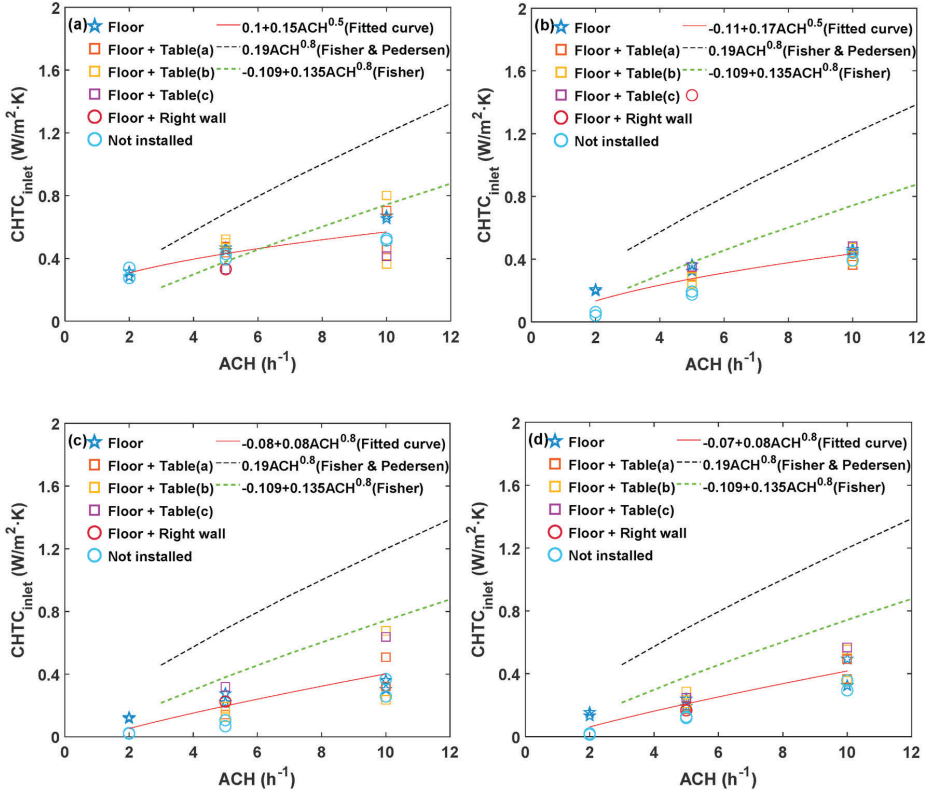


Fig. 9. Experimental CHTC at the (a) front wall, (b) right wall, (c) back wall, (d) left wall.

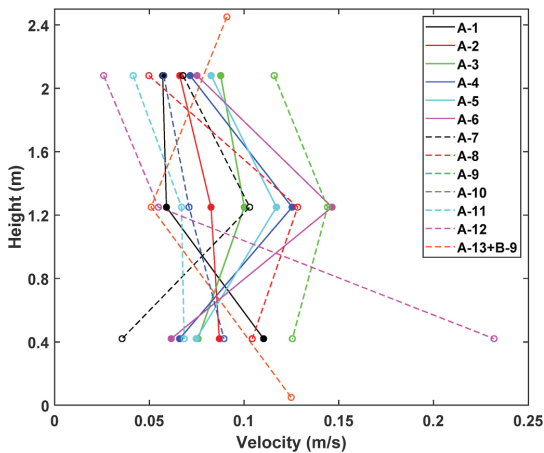


Fig. 10. Vertical air velocity measured by anemometers on columns A-1 to A-13 and anemometers in position B-9.

independent of the inlet temperatures. The corresponding fitted curves with R^2 ranging from 0.91 to 0.95 (see Table 6). The presence of tables and the location of tables seem to have some influence on the average

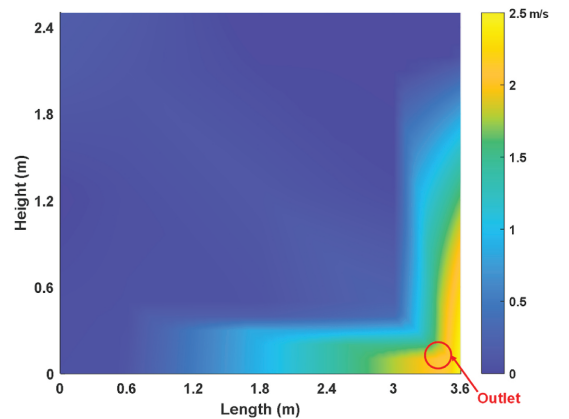


Fig. 11. Local air velocity over the front wall for case 1 after 2 h.

CHTC at walls. For cases with tables, the discrepancy between the experimental values with different inlet temperatures under the same locations of tables at the ACH of $10 h^{-1}$ is large, with the absolute error up to $0.5 W/m^2 \cdot K$, resulting in a small R^2 as low as 0.47. This may be explained that tables obstructed the downward airflow to turn more airflow horizontal to walls or just reduced the downward airflow along

Table 6

Fitted curve functions for CHTCs at different walls of two thermal mass distribution.

Thermal mass distribution	Front wall	Right wall	Back wall	Left wall
Floor	0.14 + 0.08ACH ^{0.8}	0.01 + 0.15ACH ^{0.8}	-0.04 + 0.12ACH ^{0.5}	0.03 + 0.06ACH ^{0.8}
Not installed	0.14 + 0.12ACH ^{0.5}	-0.1 + 0.08ACH ^{0.8}	-0.15 + 0.07ACH ^{0.8}	-0.2 + 0.08ACH ^{0.8}

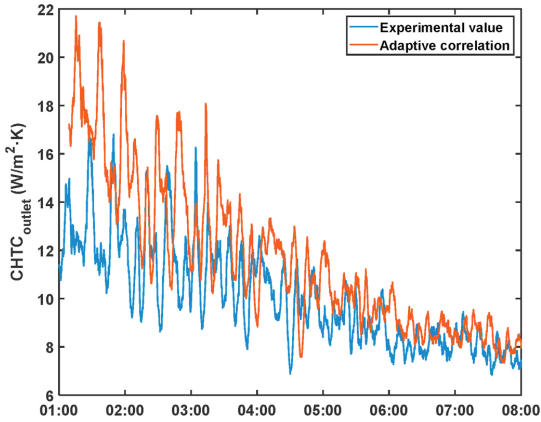


Fig. 12. Comparison between the experimental CHTC at the front wall and CHTC predicted by adaptive correlation for the wall for case 9.

the walls, changing the airflow pattern on the walls with different inlet temperatures. Therefore, the average CHTCs at walls are difficult to be predicted when tables are placed in the room.

An alternative easier way is to derive the fitted curve for each wall based on all experimental CHTCs regardless of the tables' parameters. The solid red lines in Fig. 9 are the fitted curves with R^2 ranging from 0.49 to 0.79. The R^2 of those fitted curves is small, leading to the MAPE between the experimental values and predicted values range from 17% to 51%. However, the RMSE between those two values ranges from 0.06 to 0.12 W/m²·K, which should be acceptable in BES.

The comparison between the experimental CHTCs at four walls (outlet temperature as reference) and the predicted CHTCs by the corresponding adaptive correlation shows that the MAPE between those two values ranges from 14% to 3229%. The reason that the MAPE can be up to 3229% was that the experimental values of cases at low ACH were small, but the values predicted by adaptive correlations were large, leading to a small denominator and a large numerator for calculating the MAPE by Eq. (13). Either the adaptive correlation for the wall underestimated or overestimated the experimental values for different design cases. The lowest MAPE (i.e., 14%) occurs in case 9 (10ACH 10 °C Floor + Table(a)) for the front wall, as shown in Fig. 12.

4.3. CHTC at tables

Fig. 13 shows the surface-averaged CHTCs at tables (inlet temperature as reference) and the corresponding three existing correlations. The experimental values with the same symbols at the same ACH represent those values are from two different inlet temperatures. The uncertainties estimated for the surface-averaged CHTCs range from $\pm 7\%$ to $\pm 12\%$. Fisher & Pedersen's correlation predicts relatively well for CHTCs at table surfaces facing upward, while all three correlations largely overestimate the experimental values at table surfaces facing downward.

For the same table of all design cases, the CHTC at the table surface facing upward was higher than that for the table surface facing downward. Because the inlet jet poured down the table surface facing upward firstly and flowed over the table surface facing upward, while the table surface facing downward was affected relatively less by the cold air. Another reason that can contribute to the difference between the CHTCs at two surfaces of one table was the different view factor of the two surfaces, resulting in different radiative heat transfer fluxes, which can impact the CHTC. The CHTCs at tables were dependent on the locations of tables. However, it is difficult to develop an accurate CHTC correlation (i.e., R^2 exceeds 0.90) using the curve fitting method for specific locations of tables since the discrepancy between the experimental values at the same ACH with different inlet temperatures is high. The possible reason is that the boundary conditions for the 1D finite-difference model to calculate the transient conductive heat flux of table surfaces were temperatures measured by two thermocouples, causing higher uncertainty for the results than the other interior surfaces (e.g., floor) whose temperature difference was measured by thermopiles.

A feasible way is to derive the fitted curves (even with the small R^2 of 0.28 and 0.37, respectively) for table surfaces facing upward and for table surfaces facing downward based on the corresponding experimental values without concerning the location of tables, as shown in Table 7. The MAPE and RMSE between the experimental CHTCs at table surfaces facing upward and the CHTCs calculated by the fitted curves are 29% and 0.21 W/m²·K. For table surfaces facing downward, the MAPE between the experimental values and predicted values are very large (up to 7014%) because some experimental values are close to 0, but the RMSE between those two values is 0.13 W/m²·K, which should also be acceptable in BES.

The MAPE between the experimental CHTC at tables (outlet temperature as reference) and the predicted CHTC by the adaptive correlation for the floor range from 18% to 31,512%. Either the adaptive correlation for the floor underestimated or overestimated the experimental values for different design cases. The lowest MAPE (i.e., 18%) occurs in case 17 (10ACH 10 °C Floor + Table(c)) for surfaces facing upward of table 1 (see Fig. 14). The MAPE is up to 31,512% because the experimental CHTCs (outlet temperature as the reference) at the table surfaces facing downward were too small.

4.4. Temperature efficiency

Apart from modeling the NV for performance estimation by adopting CHTC correlations in BES tools, the NV performance in terms of the surface cooling effectiveness can also be calculated in a simple model with the climatic cooling potential (CCP), temperature efficiency, and other parameters at the design stage [15]. The CCP for passive cooling of buildings by NV in Europe can be found in Ref. [61], while the temperature efficiency can be calculated by Eq. (15).

$$\eta = \frac{T_{\text{outlet}} - T_{\text{inlet}}}{\bar{T}_{\text{surface}} - T_{\text{inlet}}} \quad (15)$$

where T_{outlet} and T_{inlet} are the outlet and inlet temperatures, respectively. \bar{T}_{surface} is the average interior surface temperature. Because the value of temperature efficiency oscillated during the cooling period, the η for each case can be yielded by averaging the values over the cooling period (the first hour data excluded). Fig. 15 shows the temperature efficiencies of cases with the thermal mass on the floor and without thermal mass and corresponding fitted curves ($R^2 > 0.94$) based on the quadratic polynomial form. The fitted curves can be used to estimate the η at other ACH. The uncertainties estimated for the η range from $\pm 3\%$ to $\pm 5\%$. It can be seen that η can be higher than 1 at low ACH. The temperature efficiency decreases with the increase of ACH, ΔT_0 (i.e., the initial temperature difference between the supply air and indoor air), and thermal mass level. When comparing to the derived η of the displacement ventilation and mixing ventilation in literature [15], the

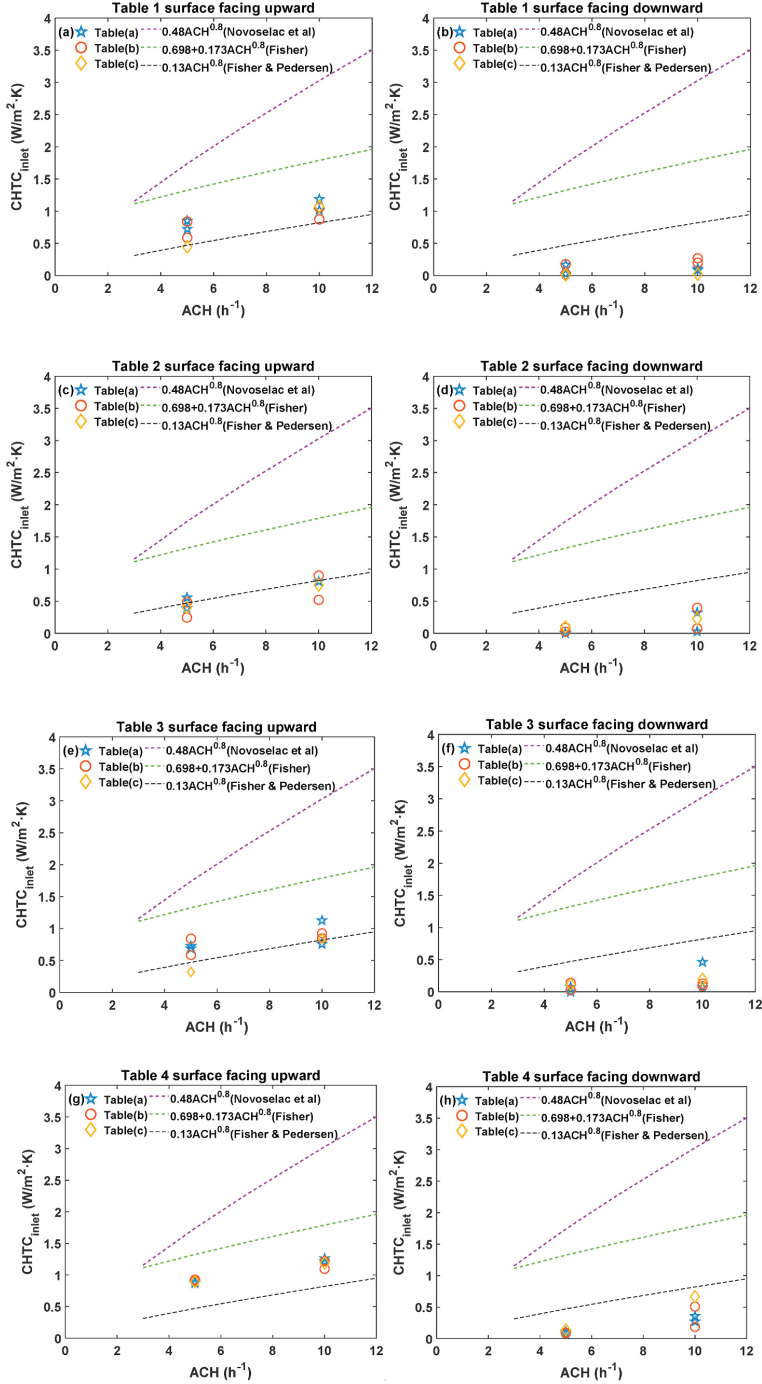


Fig. 13. Experimental CHTC at different table surfaces.

Table 7

Fitted curve functions for the table surface facing upward and downward.

Table surface	Fitted curve function
Facing upward	$0.11 + 0.19ACH^{0.65}$
Facing downward	$-0.21 + 0.1ACH^{0.65}$

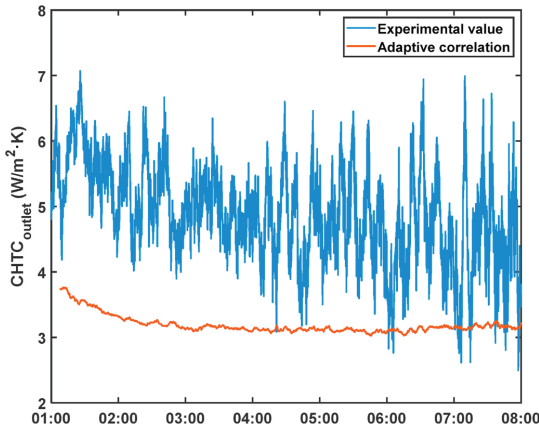


Fig. 14. Comparison between the experimental CHTC at surface facing upward of table 1 and CHTC predicted by adaptive correlation for the floor for case 17.

temperature efficiency of DCV is higher than those two ventilation concepts, except for the case with displacement ventilation at low ACH whose η is higher than 1.10.

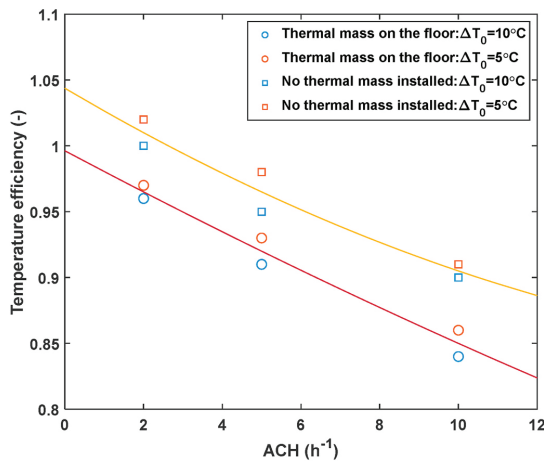


Fig. 15. Temperature efficiency depending on the ACH for DCV.

5. Conclusions and future work

The heat transfer of night ventilation (NV) using the diffuse ceiling ventilation (DCV) concept was investigated by conducting a series of dynamic full-scale experiments. The design cases comprised 6 thermal mass distributions, 3 constant air change rates per hour (ACH), and 2 supply air temperatures. The surface-averaged convective heat transfer coefficient (CHTC) with the inlet temperature and outlet temperature as the reference at the floor, walls, and tables were derived from the experiments and compared with existing CHTC correlations. New CHTC correlations (inlet temperature as reference) specific to DCV with NV were developed. The temperature efficiency of DCV was also derived to compare with that of the mixing ventilation and displacement ventilation.

For the surface-averaged CHTCs with the outlet temperature as the reference, the adaptive correlations predict accurately for some cases with a mean absolute percentage error (MAPE) between the experiment and the prediction as low as 14%. However, for most cases, large error was observed with MAPE up to 31.512%. For the surface-averaged CHTCs with the inlet temperature as the reference, existing forced correlations also do not predict well except Fisher's correlation (i.e., side-wall inlet configuration) for the floor [56], which predicts quite well for the floor with thermal mass. The presence of furniture (tables), its location, and the thermal mass installed on the wall have little influence on the CHTC at the floor. Increasing the thermal mass level of one surface can significantly augment the CHTC at the surface.

The temperature efficiency of DCV decreases with the increase of ACH, the initial temperature difference between the supply air and indoor air, and the thermal mass level. Compared to the temperature efficiency of mixing ventilation and displacement ventilation in literature, DCV has higher temperature efficiency in most cases, except the case with displacement ventilation at low ACH.

The developed CHTC correlations can be adopted in building energy simulation (BES) tools that enable the user to set custom functions for interior CHTC to simulate the building energy use and indoor thermal comfort quickly and more accurately without coupling complex computational fluid dynamics (CFD). Furthermore, the developed correlations also enable the user to optimize the ACH and thermal mass distribution to achieve low building energy use and good thermal comfort.

The study is limited because only two surface materials were used. The CHTC of the interior surface with other materials include PCM, needs to be investigated in the future. The influence of the plenum's height on the CHTCs of room interior surfaces also needs further study. CFD simulations can be used to calculate the indoor temperature accurately. The latter can be regarded as the reference temperature to calculate the experimental CHTC and compare the adaptive correlations in this way. Due to the lack of CHTC correlation development for the suspended ceiling panel in this study, the suitable correlation for the diffuse ceiling in BES needs further research.

Declaration of competing interest

The authors declare that they have no known competing financial interests or personal relationships that could have appeared to influence the work reported in this paper.

Acknowledgements

The project is carried out as part of IEA EBC Annex 80 Resilient Cooling. The first author gratefully acknowledges the financial support from the China Scholarship Council (CSC No. 201706050001). The first author would also like to thank Lars Isbach Poulsen, Yanmin Wang, Bolong Wei, Baoming Su, Weiheng Zhang, and Min Liu for their great technical support.

References

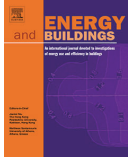
- [1] E. Solgi, Z. Hamedani, R. Fernando, H. Skates, N.E. Orji, A literature review of night ventilation strategies in buildings, *Energy Build.* 173 (2018) 337–352, <https://doi.org/10.1016/j.enbuild.2018.05.052>.
- [2] M. Kolokotroni, P. Heiselberg, Ventilative Cooling: State-Of-The-Art Review, Aalborg Univ. Aalborg, Denmark, 2015. <https://www.buildup.eu/en/node/52462>.
- [3] E. Solgi, Z. Hamedani, R. Fernando, B. Mohammad Kari, H. Skates, A parametric study of phase change material behaviour when used with night ventilation in different climatic zones, *Build. Environ.* 147 (2019) 327–336, <https://doi.org/10.1016/j.buildenv.2018.10.031>.
- [4] S.P. Corgnati, A. Kindin, Thermal mass activation by hollow core slab coupled with night ventilation to reduce summer cooling loads, *Build. Environ.* 42 (2007) 3285–3297, <https://doi.org/10.1016/j.buildenv.2006.08.018>.
- [5] E. Solgi, Z. Hamedani, R. Fernando, B. Mohammad Kari, A parametric study of phase change material characteristics when coupled with thermal insulation for different Australian climatic zones, *Build. Environ.* (2019), <https://doi.org/10.1016/j.buildenv.2019.106317>.
- [6] R. Lapisa, E. Bozonnet, P. Salagnac, M.O. Abadie, Optimized design of low-rise commercial buildings under various climates – energy performance and passive cooling strategies, *Build. Environ.* (2018), <https://doi.org/10.1016/j.buildenv.2018.01.029>.
- [7] E. Shaviv, A. Yezioro, I.G. Capeluto, Thermal mass and night ventilation as passive cooling design strategy, *Renew. Energy* 24 (2001) 445–452, [https://doi.org/10.1016/S0960-1481\(01\)00027-1](https://doi.org/10.1016/S0960-1481(01)00027-1).
- [8] R. Guo, P. Heiselberg, Y. Hu, C. Zhang, S. Vasilievskis, Optimization of night ventilation performance in office buildings in a cold climate, *Energy Build.* 225 (2020) 110319, <https://doi.org/10.1016/j.enbuild.2020.110319>.
- [9] N. Artmann, H. Manz, P. Heiselberg, Parameter study on performance of building cooling by night-time ventilation, *Renew. Energy* 33 (2008) 2589–2598, <https://doi.org/10.1016/j.renene.2008.02.025>.
- [10] R. Guo, Y. Hu, M. Liu, P. Heiselberg, Influence of design parameters on the night ventilation performance in office buildings based on sensitivity analysis, *Sustain. Cities Soc.* 50 (2019) 101661, <https://doi.org/10.1016/j.scs.2019.101661>.
- [11] K. Goethals, H. Breesch, A. Janssens, Sensitivity analysis of predicted night cooling performance to internal convective heat transfer modelling, *Energy Build.* 43 (2011) 2429–2441, <https://doi.org/10.1016/j.enbuild.2011.05.033>.
- [12] L. Peeters, I. Beausoleil-Morrison, A. Novoselac, Internal convective heat transfer modelling: critical review and discussion of experimentally derived correlations, *Energy Build.* 43 (2011) 2227–2239, <https://doi.org/10.1016/j.enbuild.2011.05.002>.
- [13] U.S. DoE, Energyplus Engineering Reference, 2020. <https://bigladdersoftware.com/epx/docs/9-3/engineering-reference/>.
- [14] J. Le Dréau, P. Heiselberg, R.L. Jensen, Experimental investigation of convective heat transfer during night cooling with different ventilation systems and surface emissivities, *Energy Build.* 61 (2013) 308–317, <https://doi.org/10.1016/j.enbuild.2013.02.021>.
- [15] N. Artmann, R.L. Jensen, H. Manz, P. Heiselberg, Experimental investigation of heat transfer during night-time ventilation, *Energy Build.* 42 (2010) 366–374, <https://doi.org/10.1016/j.enbuild.2009.10.003>.
- [16] W. Ji, Q. Luo, Z. Zhang, H. Wang, T. Du, P.K. Heiselberg, Investigation on thermal performance of the wall-mounted attached ventilation for night cooling under hot summer conditions, *Build. Environ.* 146 (2018) 268–279, <https://doi.org/10.1016/j.buildenv.2018.10.002>.
- [17] D. Olsthoorn, F. Haghighat, A. Moreau, G. Lacroix, Abilities and limitations of thermal mass activation for thermal comfort, peak shifting and shaving: a review, *Build. Environ.* 118 (2017) 113–127, <https://doi.org/10.1016/j.buildenv.2017.03.029>.
- [18] K. Goethals, I. Couckuyt, T. Dhaene, A. Janssens, Sensitivity of night cooling performance to room/system design: surrogate models based on CFD, *Build. Environ.* 58 (2012) 23–36, <https://doi.org/10.1016/j.buildenv.2012.06.015>.
- [19] K. Goethals, M. Delgust, G. Flamant, M. De Paep, A. Janssens, Experimental investigation of the impact of room/system design on mixed convection heat transfer, *Energy Build.* 49 (2012) 542–551, <https://doi.org/10.1016/j.enbuild.2012.03.017>.
- [20] P. Wallentén, Convective heat transfer coefficients in a full-scale room with and without furniture, *Build. Environ.* 36 (2001) 743–751, [https://doi.org/10.1016/S0360-1323\(00\)00706-6](https://doi.org/10.1016/S0360-1323(00)00706-6).
- [21] J.D. Spitler, C.O. Pedersen, D.E. Fisher, Interior convective heat transfer in buildings with large ventilative flow rates, in: ASHRAE Trans., 1991, pp. 505–515, accessed, www.hvac.okstate.edu, (Accessed 11 May 2020).
- [22] W. Wu, N. Yoon, Z. Tong, Y. Chen, Y. Lv, T. Årenlund, J. Benner, Diffuse ceiling ventilation for buildings: a review of fundamental theories and research methodologies, *J. Clean. Prod.* 211 (2019) 1600–1619, <https://doi.org/10.1016/j.jclepro.2018.11.148>.
- [23] B. Yang, A.K. Melikov, A. Kabanshi, C. Zhang, F.S. Bauman, G. Cao, H. Awbi, H. Wigö, J. Niu, K.W.D. Cheong, K.W. Tham, M. Sandberg, P.V. Nielsen, R. Kosonen, R. Yao, S. Kato, S.C. Sekhar, S. Schiavon, T. Karimipana, X. Li, Z. Lin, A review of advanced air distribution methods - theory, practice, limitations and solutions, *Energy Build.* 202 (2019) 109359, <https://doi.org/10.1016/j.enbuild.2019.109359>.
- [24] C. Zhang, M.H. Kristensen, J.S. Jensen, P.K. Heiselberg, R.L. Jensen, M. Pomianowski, Parametrical analysis on the diffuse ceiling ventilation by experimental and numerical studies, *Energy Build.* 111 (2016) 87–97, <https://doi.org/10.1016/j.enbuild.2015.11.041>.
- [25] P. V. Nielsen, E. Jakubowska, The performance of diffuse ceiling inlet and other room Air distribution systems, *Cold Clim. HVAC.* (2009) 7.
- [26] J. Hu, P. Karava, Model predictive control strategies for buildings with mixed-mode cooling, *Build. Environ.* 71 (2014) 233–244, <https://doi.org/10.1016/j.buildenv.2013.09.005>.
- [27] S. Lestinen, S. Kilpeläinen, R. Kosonen, J. Jokisalo, H. Koskela, Experimental study on airflow characteristics with asymmetrical heat load distribution and low-momentum diffuse ceiling ventilation, *Build. Environ.* 134 (2018) 168–180, <https://doi.org/10.1016/j.buildenv.2018.02.029>.
- [28] S. Lestinen, S. Kilpeläinen, R. Kosonen, J. Jokisalo, H. Koskela, A. Melikov, Flow characteristics in occupied zone – an experimental study with symmetrically located thermal plumes and low-momentum diffuse ceiling air distribution, *Build. Environ.* 128 (2018) 77–88, <https://doi.org/10.1016/j.buildenv.2017.11.020>.
- [29] C.A. Hviid, S. Svendsen, Experimental study of perforated suspended ceilings as diffuse ventilation air inlets, *Energy Build.* 56 (2013) 160–168, <https://doi.org/10.1016/j.enbuild.2012.09.010>.
- [30] D. Zukowska, M. Wolsing, M. Grysbæk, C. Anker, Field Study of Diffuse Ceiling Ventilation Performance in a Landscape Office, APA, 2016 accessed, <https://orbit.dtu.dk/en/publications/field-study-of-diffuse-ceiling-ventilation-performance-in-a-lands>, (Accessed 30 October 2020).
- [31] T. Yu, P. Heiselberg, B. Lei, M. Pomianowski, C. Zhang, A novel system solution for cooling and ventilation in office buildings: a review of applied technologies and a case study, *Energy Build.* 90 (2015) 142–155, <https://doi.org/10.1016/j.enbuild.2014.12.057>.
- [32] S. Rahnema, P. Sadeghian, P.V. Nielsen, C. Zhang, S. Sadrizadeh, A. Afshari, Cooling capacity of diffuse ceiling ventilation system and the impact of heat load and diffuse panel distribution, *Build. Environ.* 185 (2020) 107290, <https://doi.org/10.1016/j.buildenv.2020.107290>.
- [33] C. Zhang, T. Yu, P. Heiselberg, M. Pomianowski, P. Nielsen, Diffuse Ceiling Ventilation – Design Guide, 2016 accessed, https://vbn.aau.dk/ws/portalfiles/portal/243057526/Diffuse_ceiling_ventilation_Design_guide.pdf, (Accessed 5 June 2019).
- [34] C.A. Hviid, S. Petersen, Integrated ventilation and night cooling in classrooms with diffuse ceiling ventilation, in: 11th Ökösan, 2011 accessed, <https://orbit.dtu.dk/en/publications/integrated-ventilation-and-night-cooling-in-classrooms-with-diffu>, (Accessed 30 October 2020).
- [35] Dansk Standard, J. Rose, S. Aggerholm, L. Olsen, H.M. Tommerup, C. Rudbeck, *DS 418, Beregning Af Bygningers Varmetab*, 2011.
- [36] C.A. Hviid, J. Lessing, Experimental study of the heat transfers and passive cooling potential of a ventilated plenum designed for uniform air distribution, 2016, in: 12th REHVA World Congr, CLIMA, 2016, accessed, <https://orbit.dtu.dk/en/publications/experimental-study-of-the-heat-transfers-and-passive-cooling-pote>, (Accessed 12 April 2020).
- [37] C. Zhang, P.K. Heiselberg, Q. Chen, M. Pomianowski, Numerical analysis of diffuse ceiling ventilation and its integration with a radiant ceiling system, *Build. Simul.* 10 (2017) 203–218, <https://doi.org/10.1007/s12273-016-0318-z>.
- [38] ISO 8990-1996, Thermal Insulation — Determination of Steady-State Thermal Transmission Properties — Calibrated and Guarded Hot Box, International Standard, 1996. <https://www.iso.org/standard/16519.html>.
- [39] S. Leenknegt, R. Wagemakers, W. Boschaerts, D. Saelsens, Improving the modelling of surface convection during natural night ventilation in building energy simulation models, *Proc. Build. Simul.* 2011 12th Conf. Int. Build. Perform. Simul. Assoc. (2011) 2233–2240, accessed, https://limo.libis.be/primo-explore/fulldisplay?docid=LIRIAS1565328&context=L&vid=Lirias&search_scope=Lirias&tab=default_tab&lang=en-US&fromSiteMap=1, (Accessed 26 September 2020).
- [40] EN ISO 13786, Thermal Performance of Building Components – Dynamic Thermal Characteristics – Calculation Methods, 2017. <https://webshop.ds.dk/Default.aspx?ID=219&GroupID=91.120.10&ProductID=M289824>.
- [41] About FTMU Lindab.dk, (n.d.). <http://www.lindab.com/dk/pro/products/Pages/FTMU.aspx> (accessed July 25, 2020).
- [42] J. Le Dreau, P. Heiselberg, R.L. Jensen, Experimental Data from a Full-Scale Facility Investigating Radiant and Convective Terminals: Uncertainty and Sensitivity Analysis, Description of the Experimental Data, Department of Civil Engineering, Aalborg University, 2014 accessed, <http://vbn.aau.dk/en/publications/experimental-data-from-a-fullscale-facility-investigating-radiant-and-convective-terminals> (1ce46b33-cfa8-4979-b112-cd9ab487f9c7).html, (Accessed 22 October 2020).
- [43] O. Kalyanova, F. Zanghirella, P. Heiselberg, M. Perino, R. Jensen, Measuring Air Temperature in Glazed Ventilated Facades in the Presence of Direct Solar Irradiation, 2007 accessed, <https://vbn.aau.dk/en/publications/measuring-air-temperature-in-glazed-ventilated-facades-in-the-pre>, (Accessed 5 April 2020).
- [44] M.H. Kristensen, J.S. Jensen, R.L. Jensen, Air Temperature Measurements Using Dantec Draught Probes, Department of Civil Engineering, Aalborg University, 2015

- accessed, <https://vbn.aau.dk/en/publications/air-temperature-measurement-s-using-dantec-draught-probes>. (Accessed 25 July 2020).
- [45] Thermo Tracer TH9100MR/WR, (n.d.). <https://www.infrared.avio.co.jp/en/products/ir-thermo/lineup/th9100mr-wr/index.html> (accessed November 18, 2020).
- [46] N. Artmann, R. Vonbank, R.L. Jensen, Temperature Measurements Using Type K Thermocouples and the Fluke Helios Plus 2287A Data Logger Thermocouples and the Fluke Helios Plus, 2008.
- [47] R.L. Jensen, O.K. Larsen, C.-E. Hyldgård, On the use of hot-sphere anemometers in a highly transient flow in a double-skin facade, in: *Int. Conf. Air Distrib. Rooms, Roomvent.*, 2007, pp. 13–15, accessed, <https://vbn.aau.dk/en/publications/on-the-use-of-hot-sphere-anemometers-in-a-highly-transient-flow-i>. (Accessed 22 July 2020).
- [48] G.D. Smith, *Numerical Solution of Partial Differential Equations: Finite Difference Methods*, Oxford university press, 1985. <https://anujitspenjoymath.files.wordpress.com/2019/02/g.-d.-smith-numerical-solution-of-partial-differential-equations-finite-difference-methods.pdf>.
- [49] A.J. Chapman, *Fundamentals of Heat Transfer*, Macmillan, 1987.
- [50] J.R. Ehlert, T.F. Smith, View factors for perpendicular and parallel rectangular plates, *J. Thermophys. Heat Tran.* 7 (1993) 173–175, <https://doi.org/10.2514/3.11587>.
- [51] G. Walton, *Calculation of Obstructed View Factors by Adaptive Integration*, Gaithersburg, MD, 2002, <https://doi.org/10.6028/NIST.JR.6925>.
- [52] W. Tian, Y. Heo, P. de Wilde, Z. Li, D. Yan, C.S. Park, X. Feng, G. Augenbroe, A review of uncertainty analysis in building energy assessment, *Renew. Sustain. Energy Rev.* 93 (2018) 285–301, <https://doi.org/10.1016/j.rser.2018.05.029>.
- [53] C. Zhuang, K. Shan, S. Wang, Coordinated demand-controlled ventilation strategy for energy-efficient operation in multi-zone cleanroom air-conditioning systems, *Build. Environ.* 191 (2021) 107588, <https://doi.org/10.1016/j.buildenv.2021.107588>.
- [54] A. Bejan, *Convection Heat Transfer*, John Wiley & Sons, 2013. <https://ebookcentral.proquest.com/lib/aalborguniv-ebooks/detail.action?docID=1161535&pq-origsite=primo>.
- [55] D.E. Fisher, C.O. Pedersen, Convective heat transfer in building energy and thermal load calculations, *ASHRAE Trans* 103 (1997) 137–148. <https://citeseerx.ist.psu.edu/viewdoc/download?doi=10.1.1.616.9820&rep=rep1&type=pdf>.
- [56] D.E. Fisher, An Experimental Investigation of Mixed Convection Heat Transfer in a Rectangular Enclosure, University of Illinois at Urbana-Champaign, 1995. <https://www.ideals.illinois.edu/handle/2142/22513>.
- [57] S. Petersen, N.U. Christensen, C. Heinsen, A.S. Hansen, Investigation of the displacement effect of a diffuse ceiling ventilation system, *Energy Build.* 85 (2014) 265–274, <https://doi.org/10.1016/j.enbuild.2014.09.041>.
- [58] A. Novoselac, B.J. Burley, J. Srebric, Development of new and validation of existing convection correlations for rooms with displacement ventilation systems, *Energy Build.* 38 (2006) 163–173, <https://doi.org/10.1016/j.enbuild.2005.04.005>.
- [59] I. Beausoleil-Morrison, The adaptive simulation of convective heat transfer at internal building surfaces, *Build. Environ.* 37 (2002) 791–806, [https://doi.org/10.1016/S0360-1323\(02\)00042-2](https://doi.org/10.1016/S0360-1323(02)00042-2).
- [60] Mathworks®, *Curve Fitting Toolbox™: User's Guide (R2019b)*, 2019. <https://www.mathworks.com/help/curvefit/>.
- [61] N. Artmann, H. Manz, P. Heiselberg, Climatic potential for passive cooling of buildings by night-time ventilation in Europe, *Appl. Energy* 84 (2007) 187–201, <https://doi.org/10.1016/j.apenergy.2006.05.004>.

Appendix D. Paper 4

Guo, R., Heiselberg, P., Hu, Y., Zhang, C., & Vasilevskis, S. (2020). Optimization of night ventilation performance in office buildings in a cold climate. *Energy and Buildings*, 225, 110319. <https://doi.org/10.1016/j.enbuild.2020.110319>

Reprinted by permission from Elsevier.



Optimization of night ventilation performance in office buildings in a cold climate

Rui Guo^{*}, Per Heiselberg, Yue Hu, Chen Zhang, Sandijs Vasilevskis

Department of the Built Environment, Aalborg University, Thomas Manns Vej 23, DK 9220, Denmark

ARTICLE INFO

Article history:

Received 17 March 2020

Revised 16 July 2020

Accepted 17 July 2020

Available online 21 July 2020

Keywords:

Night ventilation performance

Global sensitivity analysis

Evolutionary optimization

ABSTRACT

The rising cooling demand and overheating in the building sector, especially in office buildings, have intensified research interest in recent years. Night ventilation (NV) as a passive energy technology has shown a great potential cooling energy and ameliorate indoor thermal environment. In this paper, a holistic approach involving global sensitivity analysis and evolutionary optimization is developed to exclude insignificant parameters and explore optimal NV performance in terms of energy use and thermal comfort. The proposed approach is based on the simulation research of a three-story office building equipped with daytime air conditioning and NV system in a cold climate region. The NV system is equipped with three levels of specific fan power (SFP), representing cases with natural NV and medium and high SFP mechanical NV, respectively. The results show that the activation threshold temperature is not the key parameter for NV performance. Comparing with the case without NV, the three SFP NV systems under a general scheme save 8.8% to 82.5% total cooling energy consumption (TCEC), but increase the average percentage of dissatisfied during occupied hours (aPPD) from 7.5% to about 15%, which may cause overcooling penalty. The optimization decreases the thermal mass area and the night air change rate setpoint at each hour, while increases the minimum indoor air temperature setpoint compared to the general scheme. All three optimal NV schemes significantly improve the indoor thermal comfort by maintaining the aPPD at 7.5%. The optimal medium and high SFP mechanical NV scheme further save 7.1% and 38.6% TCEC compared to the corresponding general mechanical NV scheme, respectively. With a higher SFP, a greater energy saving potential is contributed through NV optimization process. Even though the optimal natural NV scheme consumes more than twice as much TCEC as the general natural NV scheme, it is still worth optimizing the natural NV since the indoor thermal comfort can be improved and the optimal scheme still saves much cooling energy compared to the base case.

© 2020 Elsevier B.V. All rights reserved.

1. Introduction

Cooling demand in buildings, especially in office buildings, is increasing and has become a severe challenge during the last decades [1]. Predictions correspond to an increase in the cooling energy demand of the commercial buildings in 2050, compared to the current consumption, close to 275% [2]. More and more space cooling systems have been installed in office buildings, even in moderate and cold climates such as in Central or Northern Europe [3]. Office buildings usually have high internal heat gains and experience considerable cooling loads due to high solar gains through extensive glazing. While the heating demand can be effectively reduced by installing thermal insulation and improving building airtightness, cooling plays a more significant role in the

overall energy demand of buildings [4]. Night ventilation (NV) is a promising way to decrease cooling demand and improve indoor thermal comfort [5]. The basic concept of NV involves cooling the indoor air and the building thermal mass overnight to provide a heat sink available the next day. NV can be driven by natural ventilation, or be supported by hybrid/mechanical ventilation with a mechanical fan [6]. Climatic condition is a key factor to determine the NV efficiency. NV generally has a high cooling potential in moderate or cold climate regions of Central, Eastern, and Northern Europe [3]. However, too much NV in moderate or cold climate regions may overcool the building making people feel cold during occupancy periods or it may consume additional energy for reheating [7].

NV performance is dependent on many parameters. They can be mainly sorted by the cooling capacity of NV and the heat charge/discharge quantity of building thermal mass. The parameters of the cooling capacity of NV involves the night air change rate per

^{*} Corresponding author.

E-mail address: rgu@build.aau.dk (R. Guo).

Nomenclature

English symbols

\mathbf{x}	Solution vector
n	Number of decision variable
j	Number of inequality constraints
K	Number of equality constraints
\mathbf{g}	Vector of inequality constraints
\mathbf{h}	Vector of equality constraints
C	Cooling energy consumption for air conditioning or night ventilation

Abbreviations

NV	Night ventilation
AC	Air conditioner or air conditioning
ACH	Air changes per hour

PCM	Phase change material
LHS	Latin hypercube sampling
MCA	Monte Carlo analysis
SHGC	Solar heat gain coefficient
TMY	Typical meteorological year
COP	Coefficient of performance
GA	Genetic algorithm
SRRC	Standardized rank regression coefficient
TCEC	Total cooling energy consumption
PPD	Percentage of dissatisfied
aPPD	Average PPD during occupied hours
SFP	Specific fan power
KKT	Karush–Kuhn–Tucker
NSGA-II	Non-dominated sorting genetic algorithm II

hour (ACH), minimum indoor temperature setpoint, night venting duration, and activation threshold temperature (i.e. the temperature difference between indoor and ambient air). Roach et al. [8] optimized the NV temperature setpoint and the ACH in an office building in Adelaide and concluded that the best NV setpoint temperature is 15 °C and the optimum ACH is 12 h⁻¹. Several NV control strategies for an office building with the daytime active cooling system in northern China were studied and compared [9]. The conclusion was that NV should operate close to the active cooling time with a long ventilation period. The longer the duration of NV operation, the more efficient the NV becomes. Lixia et al. [10] also coupled NV with daytime active cooling to compare the energy-saving potential under 10 ventilation durations for supermarkets in cold climates in China. Kolokotroni et al. [11] simulated an air-conditioned office building with night cooling and recommended that the night cooling should operate continuously at night until 7:00 when the inside and outside temperatures exceed 18 and 12 °C, respectively. Several researchers have studied efficient control strategies for the cooling capacity of NV. The weather predictive control algorithm was adopted to predict the indoor air temperature during occupancy periods and control the night airflow rate through the heat storage [1213]. The results seemed positive for reducing the building's cooling demand. Braun et al. [14] developed a simple operation strategy for NV pre-cooling in different buildings in California. They determined that the strategy saved significant compressor energy and that it was cost-effective.

The ability of the building thermal mass to store the excess heat at daytime and to release the heat at night also affects the NV performance [15]. When such the charge and discharge process is timed correctly, thermal mass can be utilized to improve thermal comfort and save building energy [16]. The coupling of NV with thermal mass activation has been widely adopted in buildings [17–19]. Solgi et al. [20,21] integrated NV with phase change material (PCM) in office buildings in a hot climate region. The amalgamation of NV with PCMs in a building reduced the average indoor temperature, the peak temperature, and saved about 50% of the annual cooling load. Yanbing et al. [22] studied the performance of NV with a novel PCM packed bed storage system in Beijing, China. They found that the system was efficient in cooling down the room temperature and saving the room energy use. Shaviv et al. [23] investigated the NV with the thermal mass. The results showed that it could reduce the indoor temperature by 3–6 °C and eliminate the air conditioner (AC) operation in a building with heavy thermal mass in the hot humid climate of Israel. That research shows several shortcomings:

- 1) The NV performance was evaluated or optimized by a single indicator,
- 2) The parameters related to NV cooling capacity and thermal mass activation had the coupling effect on the NV performance, which was rarely taken into consideration at the same time, and
- 3) The related parameter was varied one by one with a few and wide steps (e.g. ACH range from 0 h⁻¹ to 12 h⁻¹ with a step of 3 h⁻¹) and all the other parameters were fixed to investigate the NV efficiency improvement, which cannot guarantee to find the optimal solution. How the thermal mass activation matches with NV cooling capacity to reach a better performance needs further study.

Simulation-based optimization has become an efficient measure to enhance building performance by satisfying several stringent requirements [24]. Instead of the time-consuming parametric simulation method, different stochastic population-based algorithms (e.g. genetic algorithm, particle swarm optimization, evolutionary algorithm) have been widely used. To maintain a reasonable number of input parameters in the optimization, sensitivity analysis could be conducted to screen out unimportant parameters [24]. The influence of parameters on NV performance has been widely investigated. Artmann et al. [25] did a local sensitivity parameter analysis of NV in an office building and found that the most influential parameters of NV are climate conditions and the air change rate. Kolokotroni et al. [26] did similar work for office buildings in a moderate climate. The results showed that other than air change rates, the most influential parameters also include the thermal mass and internal heat gains. Shaviv et al. [23] investigated the correlation between indoor air temperature and the design parameters for NV in a residential building in a hot humid climate. They found that the air change rate, thermal mass, and daily temperature difference were the most influential parameters. Rui et al. [27] conducted a global sensitivity analysis in an office building under different climatic conditions to identify the most important design parameters of NV. The results showed that the window-wall ratio, thermal mass, internal convective heat transfer coefficient, and night ACH were the most influential parameters. Based on the authors' current literature review, only a few research studies focused on the NV performance improvement by the simulation-based optimization methods.

In summary, due to the complex and non-linear interactions of parameters on the NV performance, a comprehensive consideration is required. Moreover, the one-factor-at-a-time changing

method based on a limited distribution of parameters may not be able to find the optimal solution. Few researchers investigated the balance of energy use and indoor thermal comfort when adopting the NV in cold climate regions and the match between the cooling potential of NV and thermal mass activation. This study, therefore, proposes a systematic approach to identify and screen out the uninfluential parameters by using the global sensitivity analysis. Then the key parameters related to the NV performance are optimized with an evolutionary algorithm to minimize the total cooling energy while maintaining the indoor thermal comfort.

2. Methodology

2.1. Research framework

A systematic approach is proposed to quantify the impact of the parameters related to the NV performance on the building energy/thermal performance, and then optimize the identified key parameters, as shown in Fig. 1. The approach mainly consists of four steps: 1) generating samples from the distribution of parameters, 2) conducting parametric simulations based on the samples and collecting results, 3) conducting sensitivity analysis to screen out uninfluential parameter based on samples and results, 4) setting the objective and constraint to optimize the key parameters. *In the first step*, samples based on the input parameters are generated by the Latin hypercube sampling (LHS) method with the software SimLab which is designed for Monte Carlo analysis (MCA)-based uncertainty and sensitivity analysis [28] before being sent to the parametric simulation manger jEPlus [29]. *In the second step*, jEplus sends the job list to EnergyPlus [30] to conduct parametric simulation and collects simulation results to transfer back to SimLab. *In the third step*, a global sensitivity analysis based on the regression method is conducted with SimLab to investigate the influences of the parameters and to identify the key parameters for the building energy/thermal performance. *In the last step*, the initial values and distributions of the key parameters as well as the objective function and constraint are set in MOBO [31], a generic freeware

written with Java programming language and embedded with several optimization algorithms. Then MOBO generates and sends the input variable based on the omni-optimizer from the parameter distribution to EnergyPlus for simulation before getting the results to determines whether the results fulfill the objective and constraint through the optimization algorithm to find the optimal solutions.

2.2. Baseline model and cooling systems

SketchUp 2015 coupled with EnergyPlus v.8.9 was selected to build the model that originated from an office building in Aarhus Municipality built in 2012, as shown in Fig. 2 (A)(B). The building is 103.7 m long and 9.5 m wide, with three stories and a total area of 2924.1 m² [32]. Fig. 2 (C) shows the layout of the office building. The N, W, S, and C indicate the orientation as north, west, south, and center, respectively, while the number before the orientation abbreviation represents the floor number. An office room (i.e. Zone '1W'), occupied by six persons was selected as the case room. The room floor area is 51.3 m², with 2.8 m height. The windows in the case room are the energy-efficient windows with a double pane construction made of 3 mm glass and a 13 mm argon gap. The window U-value is 1.062 W/(m²·K), while the glass solar heat gain coefficient (SHGC) and visible transmittance are 0.579 and 0.698, respectively. To assume the similar conditions in all adjacent zones, the internal partitions between the case room and adjacent zones were set as adiabatic.

Typical meteorological year (TMY) data of Copenhagen, Denmark from the World Meteorological Organization was used in the simulation [33]. The summer season from 1 July to 1 September was chosen in this study. Fig. 3 shows the direct solar radiation and outdoor air temperature of Copenhagen in the selected days. The daily mean ambient air temperature oscillated between 10.4 °C and 21.7 °C, while the daily maximum value of global horizontal solar irradiance varied between 9.2 W/m² and 790.8 W/m².

Table 1 shows the detailed thermophysical properties of construction elements. The internal thermal mass area is 20 m², while

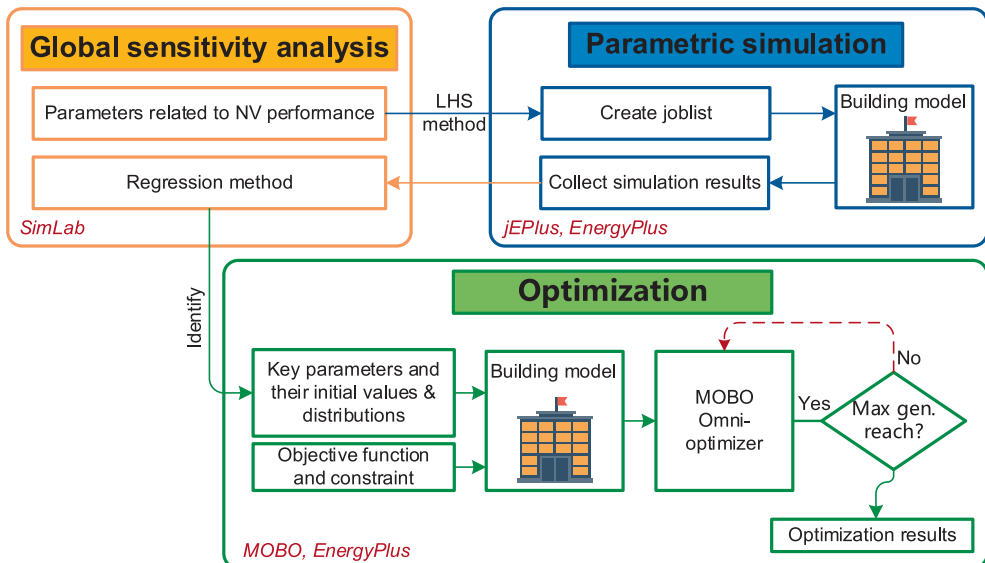


Fig. 1. Flow chart of the proposed research framework.

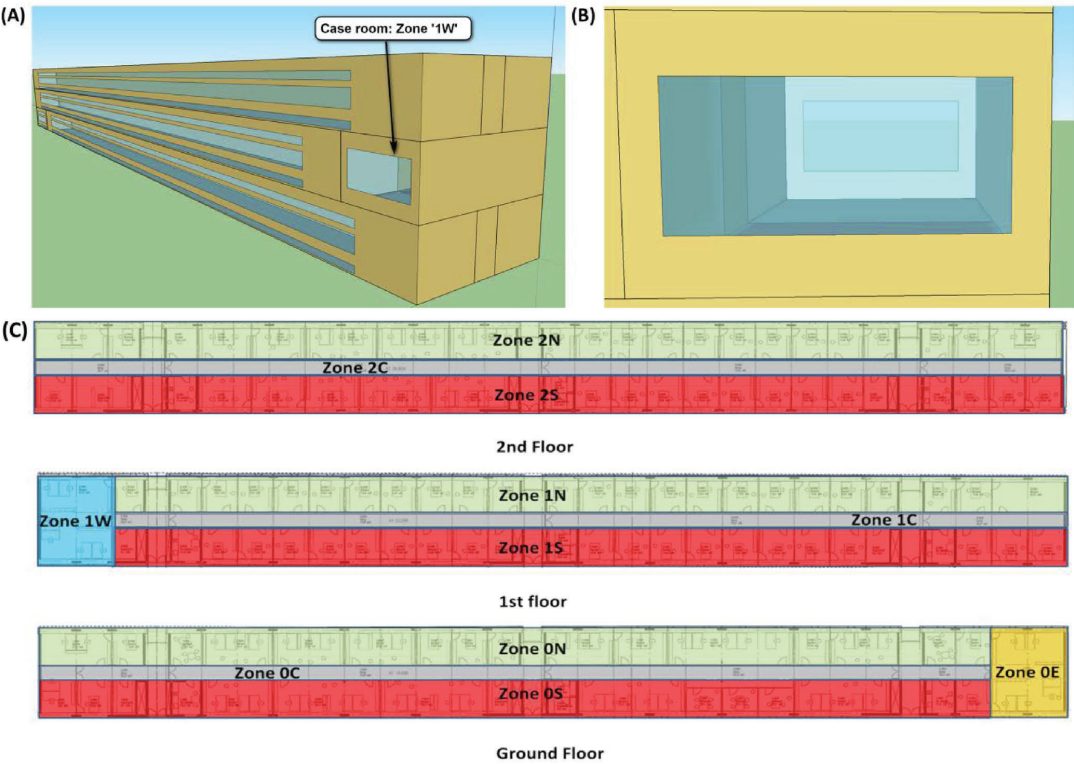


Fig. 2. (A)(B) View of the building and case room, (C) layout of the case office building.

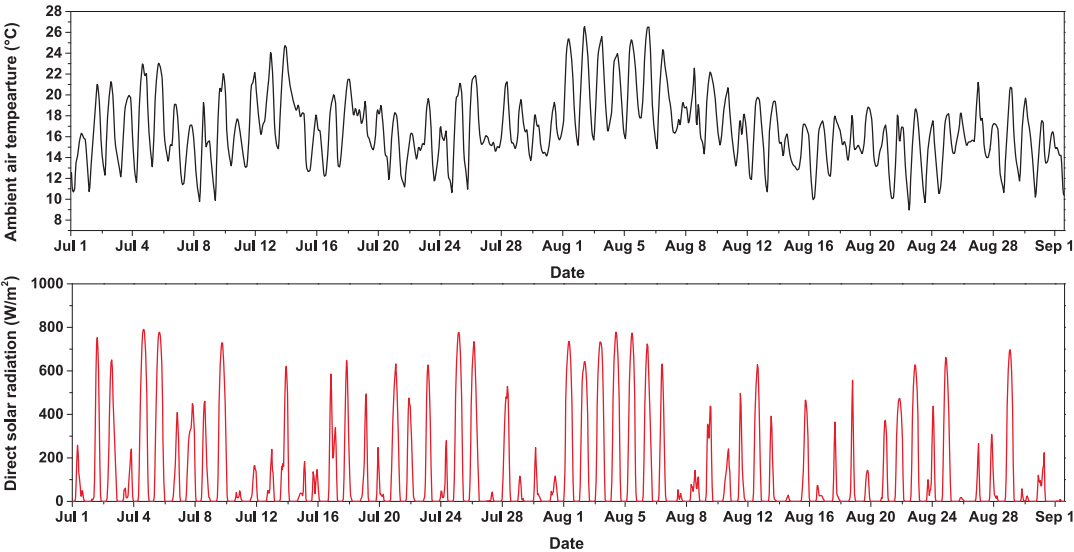


Fig. 3. TMY weather data (outdoor temperature and direct solar radiation) of Copenhagen from 1 July to 1 September.

its density is 70 kg/m^2 of the net surface area which fulfills the reasonable range (i.e. $10\text{--}100 \text{ kg/m}^2$) for the internal thermal mass density in office buildings [34]. The last column of Table 1 is the total dynamic heat capacity per unit floor area ($236.2 \text{ kJ/m}^2\text{K}$), indicating that the case room has a heavy thermal mass level [35]. The dynamic heat capacity c_{dyn} defines how much energy can be stored per area if its surface is exposed to a sinusoidal temperature variation with a 24 h time-period [36].

The internal heat gains were set as people with a load of 120 W /person, lights with 6 W/m^2 , and electric equipment with 8 W/m^2 [37]. The hourly operational schedules for the internal heat gains were 1.0 during the occupied hours (08:00–17:00) on weekdays while 0 for other hours. The people's clothing level was set at 0.5 clo in summer [38]. The air change rate of room infiltration was set as 0.5 h^{-1} [39].

The cooling systems were daytime air conditioning and night ventilation. A packaged terminal air conditioner (AC) with a coefficient of performance (COP) 3.2 and a sizing factor 1.2 from the HVAC Template module of EnergyPlus was set in the case room. The AC temperature setpoint for cooling was set at 24.5°C , while the outdoor airflow rate was $30 \text{ m}^3/(\text{h}\cdot\text{person})$ [38]. The AC operated from 08:00–17:00 on weekdays from 1 July to 1 September. The NV system was a balanced system (i.e. a supply fan with an exhaust fan). A general scheme for NV was set as follows. The minimum indoor air temperature setpoint for night ventilation was 18°C , to cool down the thermal mass efficiently and prevent the overcooling penalty [40]. Besides, the activation threshold temperature was 3°C (i.e. night cooling only operated when the indoor air temperature exceeded the ambient temperature by 3°C). The air change rate (ACH) setpoint of night cooling was 10 h^{-1} , which was the specified maximum air change rate [6]. It means that when the activation threshold temperature is met and minimum indoor air temperature is not violated, the fans will operate at the speed equivalent to 10 h^{-1} ACH; otherwise, the fans will stop. The night ventilation schedule was during 17:00–08:00 (+1) on weekdays from 1 July to 1 September. The '+1' in the parentheses means the next day. To investigate and optimize the NV performance with different SFPs, three SFPs were chosen which were 0, 0.5 and $1 \text{ kW}/(\text{m}^3/\text{s})$, representing the natural NV (Case 1), medium SFP mechanical NV (Case 2), and high SFP mechanical NV (Case 3), respectively. The SFPs all fulfilled the recommended 'good-practice' SFP for night cooling should not be higher than $1 \text{ kW}/(\text{m}^3/\text{s})$ based on the technical note AIVC 65 [41]. Table 2 lists the parameters related to NV.

2.3. Global sensitivity analysis

Global sensitivity analysis methods can investigate the influences of all input parameters on output variables simultaneously, compared to screening methods and local sensitivity methods [42]. This paper adopted the most widely used global sensitivity analysis method, i.e. the regression method, to identify the key parameters related to NV performance on building energy/thermal performance. One reason is that this method is less computationally expensive and easy to understand. Another reason is that this method can avoid the drawbacks of local sensitivity analysis, which only explores a reduced space of the input factor around a base case, does not consider the interaction, and does not have self-verification. Several sensitivity indicators based on the regression method have been used in building energy analysis [27,43–45]. Standardized Rank Regression Coefficient (SRRC) with Monte Carlo analysis (MCA) was selected to quantify the impact of each parameter as it allowed the evaluation for non-linear but monotonic functions among inputs and outputs [45]. The SRRC is calculated by performing regression analysis on rank-transformed data (i.e. input parameters and output variables) rather than the raw data. The larger the absolute value of SRRC, the more influential the input parameter is. SRRC should be used when samples are generated with the LHS method which fully covers the range of each input parameter [46]. The sample size based on LHS was chosen to be 400 as the minimum size should be bigger than 10 times the number of input parameters [45]. SimLab generates the 400 samples based on the aforementioned method before sending them to jEPlus. Then, jEPlus generates building simulation model descriptions (jep file) based on the job list from SimLab to run the EnergyPlus and collects the results (cf. Fig. 1). Finally, SimLab gets the results from jEPlus and conducts the sensitivity analysis by calculating the sensitivity measures (i.e. SRRC).

Table 3 shows the range and distribution of the independent parameters related to NV performance. Since the paper aims to quantify the effects of different building design options rather than exploring the possible range of thermal performance for an existing building, the distributions for these parameters should be uniform or discrete [42]. Because there are infinite possible time plans theoretically for night ventilation during 17:00–08:00 (+1), to simply quantify the order and size of the night venting duration, 15 time plans with 1-hour intervals were selected, representing the night venting duration ranging from 1 h to 15 h. The upper limit of minimum indoor temperature setpoint was chosen

Table 1
Thermophysical properties of building materials and detailed composition of the thermal mass.

	d (mm)	ρ (kg/m^3)	c (J/kg/K)	λ ($\text{W/m}\cdot\text{K}$)	Total c_{dyn}/A_{floor} ($\text{kJ/m}^2\cdot\text{K}$)
<i>External wall</i>					236.2
Plasterboard (fire-resisting)	160	900	1000	0.25	
Concrete 200	200	2385	800	1.2	
PUR 210	210	40	1400	0.021	
Cement plate	15	2000	1500	0.35	
<i>Internal wall</i>					
Gypsum board	25	1000	792	0.4	
Mineral wool	70	1750	1000	0.56	
Gypsum board	25	1000	792	0.4	
<i>Ceiling</i>					
Cast concrete 120	120	1800	1000	1.13	
<i>Floor</i>					
Linoleum	3	1200	1470	0.17	
Cement screed (fiber reinforced)	50	1400	1000	0.8	
Acoustic insulation	9	556	1700	0.15	
OSB panels	25	600	2150	0.13	
Insulation glass wool	200	28	1030	0.032	
Wooden panels	60	250	2100	0.047	
<i>Internal thermal mass</i>					
Cast concrete 100	100	1800	1000	1.13	

Table 2
Parameters related to NV.

Parameter		Unit	Case 1	Case 2	Case 3
P1	Night venting duration	h	17:00–08:00	17:00–08:00	17:00–08:00
P2	Minimum indoor temperature setpoint	°C	18	18	18
P3	Night ACH setpoint	h ⁻¹	10	10	10
P4	Activation threshold temperature	°C	3	3	3
P5	Internal thermal mass area	m ²	20	20	20
P6	Specific fan power (SFP)	kW/(m ³ /s)	0	0.5	1

Table 3
Range and distribution of parameters related to NV performance.

Parameter	Unit	Range
P1 Night venting duration	h	D [(17:00–18:00), (17:00–19:00), ..., (17:00–08:00)]
P2 Minimum indoor temperature setpoint	°C	U [18–22]
P3 Night ACH setpoint	h ⁻¹	U [0–10]
P4 Activation threshold temperature	°C	U [1–3]
P5 Internal thermal mass area	m ²	U [0–40]
P6 Specific fan power (SFP)	kW/(m ³ /s)	U [0–1]

Note: **D**: discrete distribution (levels); **U**: uniform distribution (lower value, upper value).

according to the design criteria of thermal conditions in summer in EN 15251 [38]. The upper limit of night ventilation ACH originated from the lowest temperature for cooling in the office room of category III in EN 15251 [38]. The upper limit of SFP was selected according to the technical note AIVC 65 that recommends ‘good-practice’ SFP for night cooling not exceeding 1 kW/(m³/s) [41]. The total cooling energy consumption (TCEC) which included the energy consumption of AC plus NV and the average predicted percentage of dissatisfied during occupied hours of 08:00–17:00 (aPPD) were selected as the output variables for the evaluation of the building energy and thermal performance.

2.4. Omni-optimizer

This study uses omni-optimizer, an evolutionary optimization algorithm for single and multi-objective optimization that belongs to the category of generational genetic algorithms (GAs). Omni-optimizer originates from a widely used generic NSGA-II (Non-dominated sorting genetic algorithm II) algorithm that finds the Pareto optimal solutions for a multi-objective problem. Furthermore, it has high efficiency of adapting automatically to handle four types of optimization problems: ① Single-objective, uni-optimal; ② Single-objective, multi-optima; ③ Multi-objective, uni-optimal optimization; ④ Multi-objective, multi-optima optimization [47]. Omni-optimizer also integrates a high-efficiency constraint handling mechanism to process any amount of equality and inequality constraint conditions [48]. The constrained M-objective ($M \geq 1$) minimization problem can be posed mathematically as follows:

$$\begin{aligned} & \text{Minimize } (f_1(\mathbf{x}), f_2(\mathbf{x}), \dots, f_M(\mathbf{x})), \\ & \text{Subject to } g_j(\mathbf{x}) \geq 0, j = 1, 2, \dots, J, \\ & h_k(\mathbf{x}) = 0, k = 1, 2, \dots, K \end{aligned} \quad (1)$$

$$x_i^{(L)} \leq x_i \leq x_i^{(U)}, i = 1, 2, \dots, n.$$

where \mathbf{x} is the solution vector and n is the number of decision variables. j and $g_j(\mathbf{x})$ are the numbers of inequality constraints and their vector, while k and $h_k(\mathbf{x})$ are the number of equality constraints and

their vector, respectively. The solution vector \mathbf{x} that satisfies all aforementioned constraints and variable bounds is regarded as a *feasible* solution. Mathematically, the optimality of a solution depends on a number of KKT (Karush–Kuhn–Tucker) optimality conditions which involve finding the gradients of objective and constraint functions [49]. This study aims at finding the minimum TCEC while maintaining the aPPD within a certain range, which belongs to the type 1 optimization problem as mentioned above.

3. Results and discussion

3.1. NV performance demonstration

Before the global sensitivity analysis and optimization, it is essential to reveal the NV mechanism and demonstrate the NV performance through the simulation. The base case is the building model introduced in Section 2.2 without NV. The NV case 2 (i.e. SFP of 0.5 kW/(m³/s)) was selected for the NV performance demonstration.

Fig. 4 shows the simulated data of zone air temperature, internal thermal mass surface temperature and hourly fan/AC energy consumption of the base case and case 2 in a typical summer day (July 29 to July 30). On the selected night (i.e. 17:00 to 08:00), the ambient air temperature fluctuated between 13.7 °C and 16.9 °C, which was very suitable for NV. The zone air and internal thermal mass surface temperatures of the base case varied slightly at night, remaining at about 27.8 °C and 28.1 °C, respectively. The reason is that the excess heat stored in the building elements at daytime was released which neutralized the heat loss through the building envelope. Whereas for case 2, due to the fans’ operation, the zone air temperature and the internal thermal mass surface temperature were much lower than for the base case at night, and the maximum temperature differences can be 9.3 °C and 7.4 °C, respectively. The fan energy consumption at night was 2.7 kWh.

At 08:00 on July 30, the zone air temperatures of the base case and case 2 were 27.8 °C and 19.4 °C, respectively. Because the AC setpoint was 24.5 °C, the AC began to work for the base case at 08:00, while AC was postponed to operate for the base case with NV until 12:45 by about 5 h. Therefore, for the base case, the zone air temperature began to reach the AC setpoint after 08:00, while the internal thermal mass surface temperature continued to remain steady, presumably due to the energy balance between the heat gain of the internal thermal mass and the heat removed by the AC. However, for case 2, both the temperatures began to go up after 08:00. The zone air temperature rose faster than the internal thermal mass surface temperature and reached to AC setpoint after 12:45, while the surface temperature did not reach AC setpoint until 17:00. This was because the internal thermal mass was mainly heated by convection with room air, and thereby heating was delayed and happened after heating of the air. The AC daily energy consumption for the base case and case 2 was 6.2 kWh and 0.4 kWh, respectively, indicating that NV saved AC energy consumption. When the fan energy consumption at night was taken

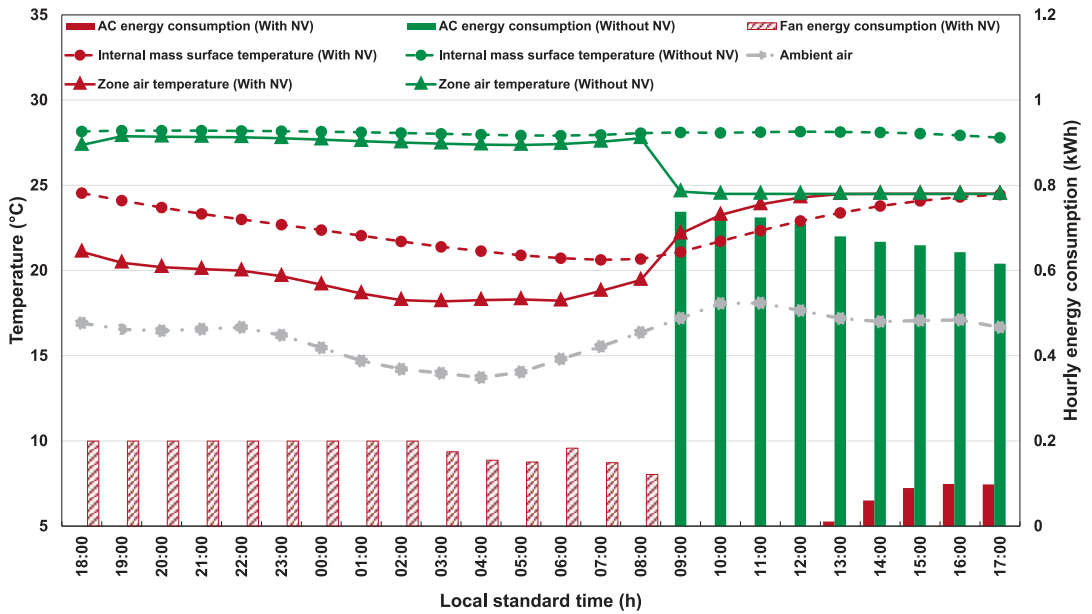


Fig. 4. Comparison of zone temperatures and energy consumption of the base case and case 2 with NV in a typical summer day (July 29 to July 30).

into consideration, the TCEC for case 2 was 3.1 kWh, which was 3.1 kWh lower than for the base case.

Furthermore, the simulated data in Fig. 5 shows that the PPD of the base case with NV was always higher than the base case (i.e. without NV), especially at the beginning of the occupied hours. The aPPD for case 2 with NV was 14.1%, 8.7% higher than the base case. The reason was that the NV with high ACH overcooled the indoor air and building elements in the cold climate region,

resulting in an overcooling penalty that made people feel cold at the beginning of occupied hours.

3.2. Influence of concerned parameters on building energy/thermal performance

Fig. 6 illustrates the influence of the six parameters presented in Table 3 on the TCEC and aPPD. A larger absolute value of SRRC

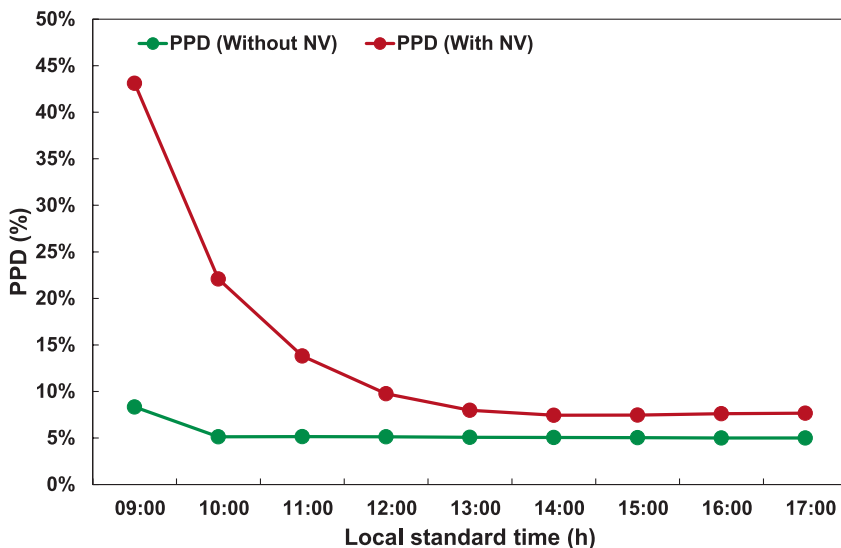


Fig. 5. Comparison of PPD of the base case and case 2 at a typical summer daytime (July 30).

means the related parameter is more influential on the corresponding output. Besides, a positive sign of SRRC indicates that the output generally increases as the related input increases, while a negative sign of SRRC means that changes in the input and output tend to go in opposite directions [44]. Night venting duration is the most influential parameter on TCEC, followed by the night ventilation ACH, SFP, and internal thermal mass area. The minimum indoor air temperature setpoint and activation threshold temperature for night cooling activation have little influence on TCEC. The more night cooling (i.e. longer night venting duration and more ACH), the lower TCEC. On the contrary, increasing the SFP and internal thermal mass area tends to consume more TCEC.

For aPPD, night venting duration also has the greatest impact, followed by the internal thermal mass area, night ventilation ACH, and minimum temperature setpoint. The threshold temperature and SFP are not important parameters for the aPPD. Contrary to the impact of night cooling on TCEC, the more night cooling, the more aPPD. It indicates that more night cooling generally contributes to saving more TCEC by postponing or reducing the AC operation, but also results in the overcooling penalty at the beginning of the working day in the cold climate region. Adding the internal thermal mass area tends to reduce the aPPD while increasing the minimum temperature setpoint tends to affect the aPPD inversely. This is presumably because when NV cools a heavy thermal mass level sufficiently, it will remain at a low surface temperature for a longer time during occupied hours, thereby leading to a colder indoor thermal environment. Whereas a higher minimum temperature setpoint can reduce the risk of overcooling phenomena by NV and decrease the aPPD.

3.3. Optimization

3.3.1. Optimization setup

The global sensitivity analysis in Section 3.1 manifested that the activation threshold temperature was not a key parameter. Hence, there was no need to optimize it, and it was kept at 3 °C. Besides, the SFP was not optimized as it was an intrinsic parameter once

the fan was selected. Cases 1, 2, 3 listed in Table 2 were selected to compare and optimize the NV performance. It is worth noticing that the airflow rate of natural NV is determined/influenced by many factors in real life, like the climate condition, window opening, building orientation, etc. This study focuses on optimizing the airflow rate at night and evaluating the influence of the optimal airflow rate on the building cooling energy and indoor thermal comfort; therefore, how using natural NV can achieve the optimal airflow rate is not an issue in this study. It is also worth noticing that even though the NV is equipped with the variable flow rate fan, it only operates at a constant airflow rate during the entire nighttime under the general scheme when the activation threshold temperature is met and minimum indoor air temperature is not violated. This is due to the lack of indoor air temperature setpoint, which cannot vary the airflow rate. The reason why there is no indoor air temperature setpoint is that the basic concept of NV is to utilize most of the cooling potential of ambient air when office buildings are not occupied.

The optimization aims at finding the optimal night ACH setpoint at each hour. Hence, the variable flow rate fan was selected. According to the technical note AIVC 65 [41], the SFP at each part-load operating point can be estimated as a function of the fraction of maximum flow rate (r) by the following generic equation for $0.2 \leq r \leq 1.0$:

$$\frac{SFP_{part\ load}}{SFP_{max\ load}} \approx a + br + cr^2 + dr^3 \quad (2)$$

Fig. 7 illustrates the different levels of the fan performance curve. The 'Good' performance curve was selected, which represents systems for which the fan pressure decreases with the airflow rate. The coefficients of a , b , c , and d for use in Eq. (2) were 0.5765, -1.5030 , 2.6557 , and -0.7292 respectively. The maximum SFPs for the medium SFP mechanical NV (Case 2), and high SFP mechanical NV (Case 3) were both at the maximum ACH of $10\ h^{-1}$. The fraction of maximum flow rate (r) at each hour for mechanical NV should be between 0.2 and 1.0 (i.e. ACH of 2 to

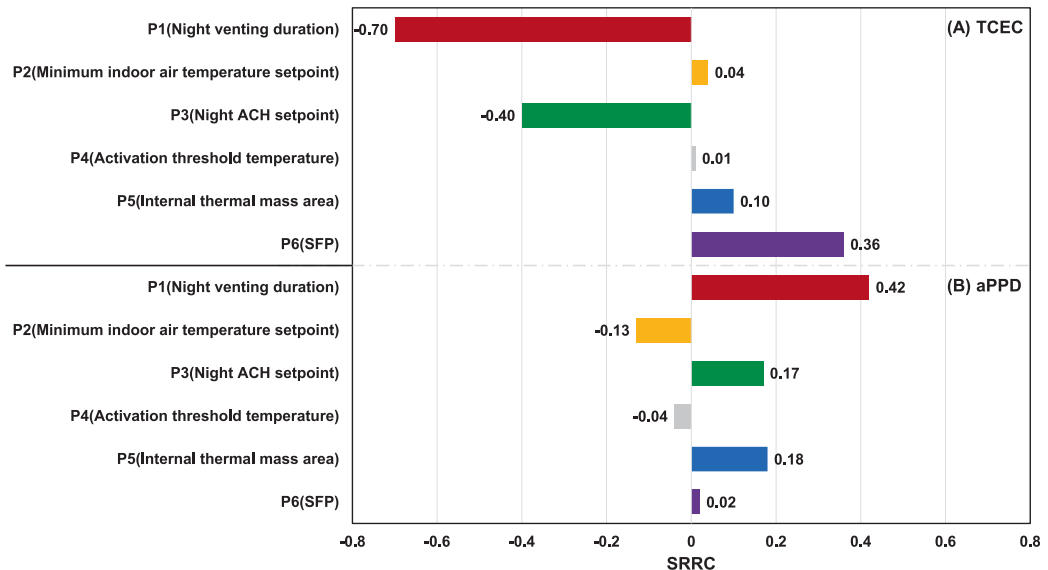


Fig. 6. Standardized Rank Regression Coefficient (SRRC) of the concerned parameters.

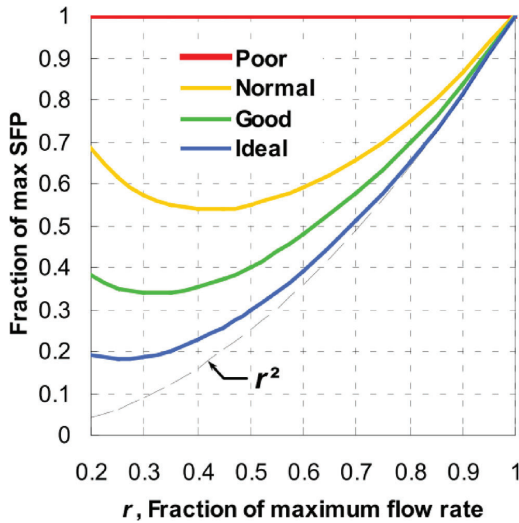


Fig. 7. Illustration of Eq. (1) for Poor, Normal, Good, and Ideal systems [41].

10 h⁻¹) or 0 (i.e. stop ventilation). While for natural NV, the fraction r was between 0 and 1.0 (i.e. ACH of 0 to 10 h⁻¹) at each hour for optimization.

To reduce the computational effort and staying close to reality, discrete distributions rather than continuous distributions were selected. Several simplifications and modifications were conducted to improve the simulation and optimization speed:

- 1) The night ventilation ACH setpoint between 17:00–08:00 (+1) at each 1 h was optimized with a discrete variable from 0 to 10 h⁻¹ with a step of 0.1 h⁻¹ for natural NV, while 0 or 2 to 10 h⁻¹ with a step of 0.1 h⁻¹ for mechanical NV,
- 2) The internal thermal mass area was optimized with a discrete variable ranging from 0 to 40 m² with a step of 0.1 m², and
- 3) The minimum indoor temperature setpoint was optimized with a discrete variable from 18 to 22 °C with a step of 0.1 °C.

Table 4 summarizes the parameters to be optimized for cases 1, 2, and 3. The population size, maximum generation number, mutation probability, and crossover number, were set as 16, 150, 0.167, and 0.9 respectively by compromising the computational effort and the accuracy [50].

This study aims at minimizing the TCEC while maintaining the aPPD at a certain range. Furthermore, different constraint levels

can be selected, according to the recommended categories of PPD for the design of mechanical cooled buildings in EN 15251 [38]. This study aims at maintaining the same thermal comfort level as in the base case (i.e. the basic building without NV). The simulated aPPD of the base case during the whole simulation period was 7.5%; this was selected as the constraint. Therefore, the optimization problem can be formulated as:

$$\min TCEC = C_{AC} + C_{NV} \quad (3)$$

$$\text{subject to } aPPD < 7.5\% \quad (4)$$

where C_{AC} and C_{NV} stand for the AC energy consumption at daytime and NV energy consumption at night, respectively.

3.3.2. Optimization results

Fig. 8 integrates the solutions during the optimization procedure by the omni-optimizer for cases 1, 2, and 3. For the single-objective minimization with the constraint problem, the omni-optimizer utilized the penalty-parameter-less approach to put two solutions in the constrained-tournament selection operator proposed in [51] to determine if a solution is better than the other. The above selection operator fulfilled the following criteria: 1) A feasible solution was always better than an infeasible solution, 2) A feasible solution with better objective function value was preferred to another feasible solution, and 3) An infeasible solution with smaller constraint violation was better than another infeasible solution. Apart from the dominated solutions of three cases, the non-dominated solutions in each case fulfill the Pareto front, which is similar to the multi-objective optimization. It reveals the conflict between the two indicators.

Fig. 9 shows the simulated aPPD and TCEC of the research cases. When the base case is equipped with different SFPs NV (i.e. cases 1, 2, 3), the TCEC significantly decreases by 0.5 kWh/m² (8.8%) to 4.7 kWh/m² (82.5%). Even the high SFP mechanical NV can save 8.8% TCEC compared to the base case. However, adopting NV with a general scheme worsens the indoor thermal comfort by increasing the aPPD from 7.5% to about 15%. After the optimization, all three optimal cases improve the indoor thermal comfort and fulfill the constraint (i.e. aPPD less than 7.5%). The optimal cases 2 and 3 further save 0.4 kWh/m² (7.1%) and 2.2 kWh/m² (38.6%) TCEC of the cases 2 and 3, respectively. It means that a higher SFP yields a greater total cooling energy-saving potential by optimization. Even though the optimal case 1 consumes 1.2 kWh/m² more TCEC than case 1, it is still worthy optimizing the natural NV as the over-cooling penalty is avoided and the optimal natural NV still saves much TCEC compared to the base case.

Fig. 10 shows the parameters of the research cases. The area and temperature in the parentheses of the legend are the internal thermal mass area and minimum indoor air temperature setpoint of the corresponding case. The value in the Y-axis represents the night ACH setpoint at each hour. Compared to cases 1, 2, 3, the internal thermal mass areas and night ACH setpoint at each hour of the optimal cases are smaller, but the minimum indoor air temperature setpoints of the optimal cases are higher. The optimal internal thermal mass areas are reduced to 8.7 to 10.4 m², which is equivalent to 22.1 to 26.4 kJ/m²·K dynamic heat capacity per unit floor area (C_{dyn}/A_{floor}) reduction. The optimal minimum indoor air temperature setpoints vary from 21.2 °C to 21.6 °C. The optimal minimum indoor air temperature setpoints are close to the upper limit (i.e. 22 °C) of this parameter setup, which indicates this setpoint values should not be too low in the cold climate region. There is no big difference between the two optimal parameters mentioned above among the three optimal cases.

However, the optimal night ACH setpoints at each hour during the night are very different from each other. However, all of them are less than 10 h⁻¹ of cases 1, 2, and 3. All the optimal cases tend

Table 4
Range and distribution of parameters for NV optimization of cases 1, 2, and 3.

Parameter	Unit	Range
O1 Night ventilation ACH setpoint	h ⁻¹	D [0–10] with step 0.1 h ⁻¹ at each hour for natural NV D 0 or [2–10] with step 0.1 h ⁻¹ at each hour for mechanical NV
O2 Minimum indoor temperature setpoint	°C	D [18–22] with step 0.1 °C
O3 Internal thermal mass area	m ²	D [0–40] with step 0.1 m ²

Note: D: discrete distribution (levels).

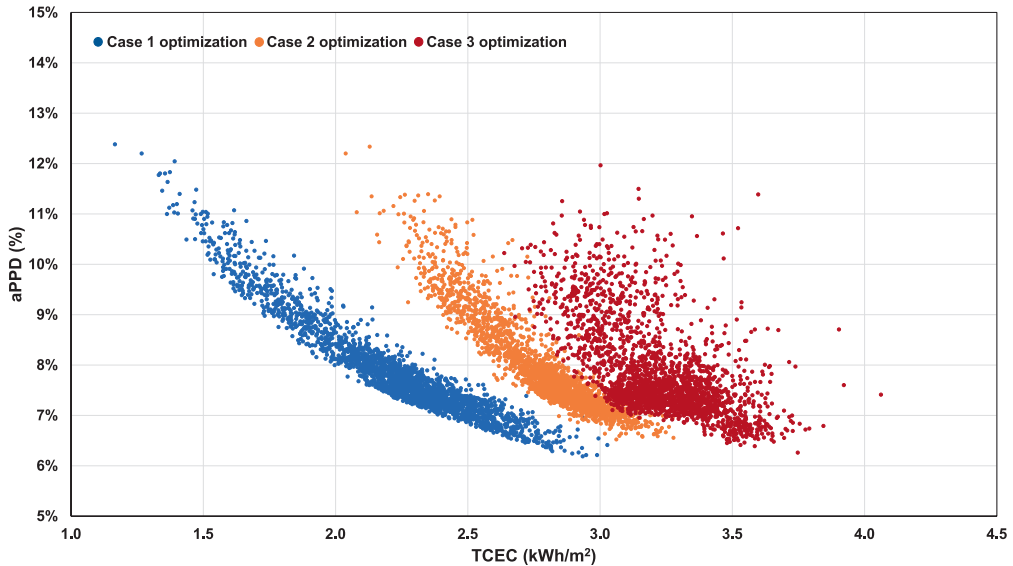


Fig. 8. Optimized solutions for cases 1, 2, and 3.

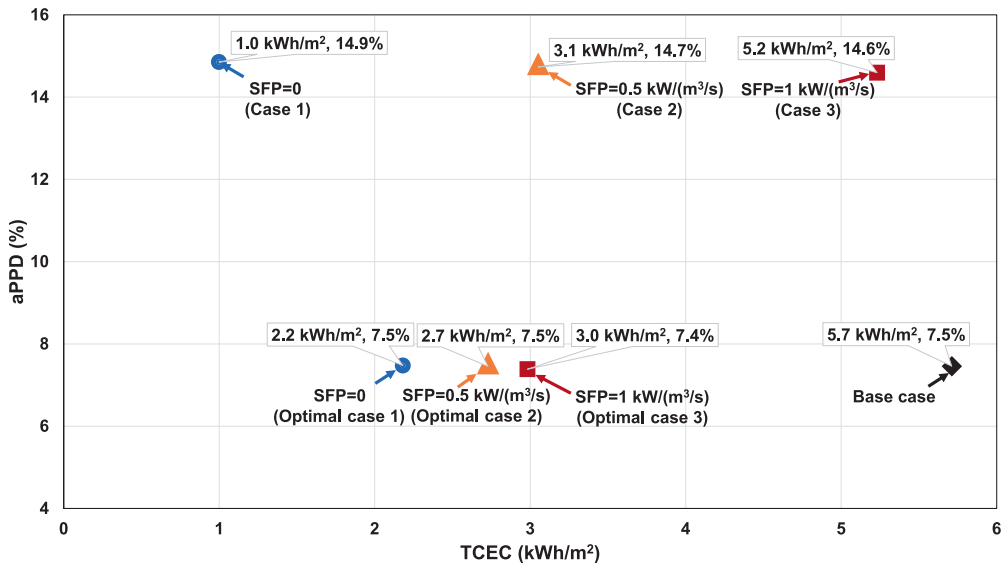


Fig. 9. The values of TCEC and aPPD of the research cases.

to decrease the night ACH setpoint severely before the occupied hours. Fig. 11 illustrates the average night ACH for different cases. The average night ACHs of optimal cases decrease by 4.1 h^{-1} to 5.2 h^{-1} , compared to cases 1, 2, and 3. The average night ACH of optimal case 3 is the lowest among the three optimal cases, while that of the optimal case 1 is the highest. The average night ACHs of cases 1, 2, and 3 are a little different and are not equal to the

setpoint of 10 h^{-1} . One reason is that the room inlet air at night can be heated by the intake fan power that will influence the zone air temperature to some extent. In consequence, the case 3 with a higher SFP needs more night cooling. Another reason is that the threshold temperature (i.e. 3°C) of NV stops the ventilation when the temperature difference between indoor and outdoor air is not met.

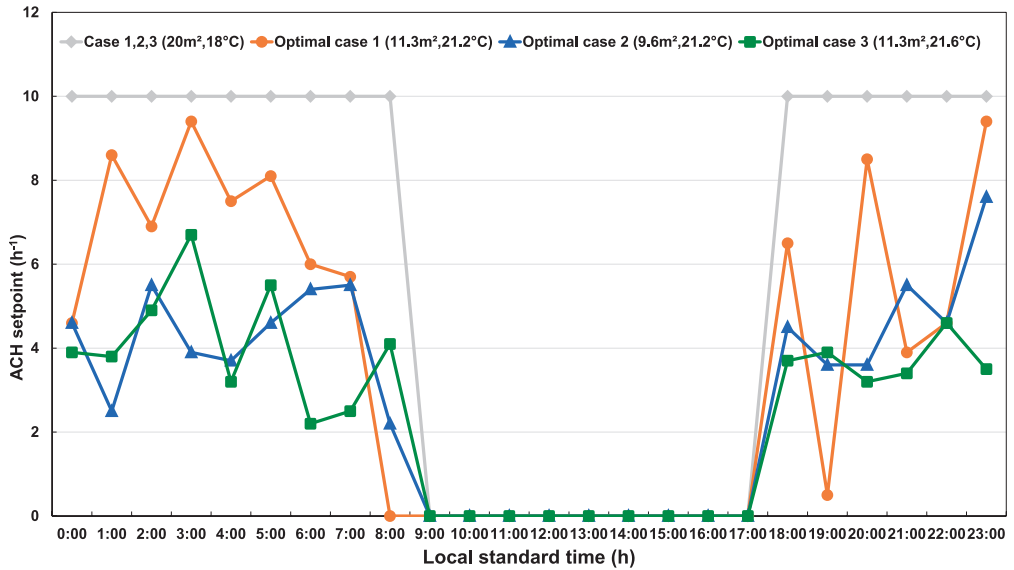


Fig. 10. Parameters related to NV of the research cases.

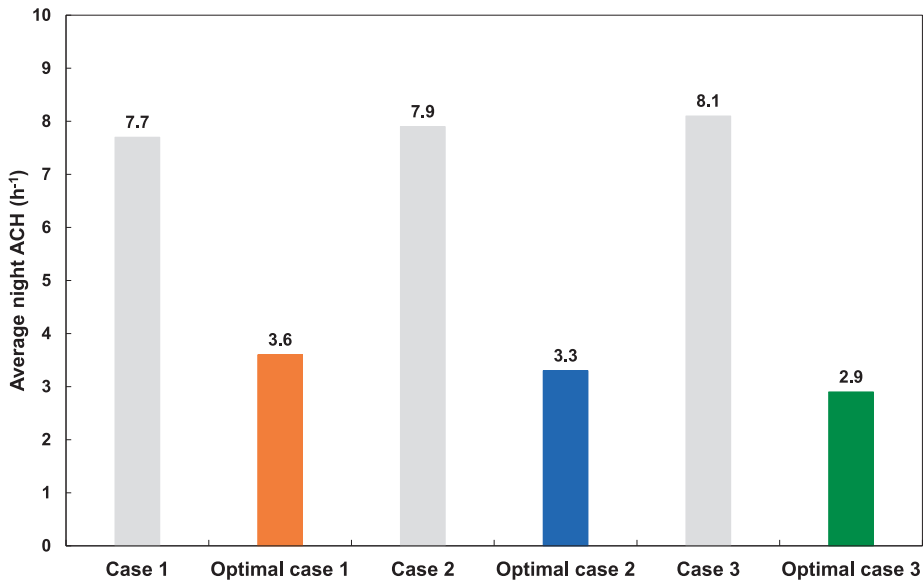


Fig. 11. Average night ACH of the research cases.

4. Limitations and prospect

From the authors' perspective, current limitations can be described as follows:

- This study optimized different parameters based on the TMY data, especially the night ACH setpoint at each hour. It may

result in the NV performance of certain days under real weather conditions deviating from expectations or not as good as the case adopting the advanced adaptive control algorithm like weather predictive control or model predictive control.

- Natural NV was simplified in this study, which was inherently unstable and highly dependent on the local climate condition, building orientation, window size or window automation sys-

tem, etc. The expected night ACH for the optimal natural NV may not be fulfilled with the real natural NV system under the real circumstance. However, this study has the potential/ability to optimize the hourly opening availability of windows and ventilation control zone temperature setpoint of a real natural NV system modeled with the AirflowNetwork model in EnergyPlus under the same objective and constraint. It should be noticed that even optimizing the control parameters of a real natural NV may still not fulfill the optimal natural ACH shown in this study. Because the actual possibility to reach the optimal ACH also depends on the architectural design, the building location, and the local wind environment that were not included in this study.

- Only a single case room was optimized in this study. One reason was that this study devoted to putting forward a method/ability to optimize the NV performance, which was also applicable for multiple rooms or the whole building. Another reason was to reduce the computation time and analyze the optimal results easier and clearer. It is worth noticing that even though the optimal solutions of different rooms or the whole building may differ, the optimal result (i.e. TCEC and aPPD) or trend was also applicable for other cases. As the heat gain of the case room should be much higher than other rooms, but this room still met the overcooling penalty under the high-ACH scenario. Therefore, the same problem will occur in other rooms. Under the same objective and constraint with the omni-optimizer, similar optimal results are expected for other rooms or the whole building.

Overall, the key to obtaining the best NV performance was the match between the cooling potential of NV and the excess heat stored/ released in thermal mass. This study proposed a generic evolutionary algorithm to find that 'match' in the approximate infinite combinations, compared to the finite combinations of NV optimization [91052]. Different from the aforementioned advanced control algorithms that generally manipulate a single variable and optimize the building performance based on a given building, this method focused more on guiding engineers or designers at the early building design stage. Furthermore, models identified through the mathematical method from the real building operation data for advanced control algorithms can only maintain the indoor air temperature rather than more precise thermal comfort indicators (e.g. PMV, PPD) within a certain range [53].

Apart from the optimization of the thermal mass amount in this study, the method is also flexible to investigate the optimal parameters related to the excess heat storage and release in the thermal mass; for instance, the insulation level, internal heat gain, thermal mass material (e.g. PCM), daytime cooling methods or related control parameters, etc. As alluded to above, the omni-optimizer has a high efficiency to adapt automatically to handle four types of optimization problems, which can fulfill the different requirements of research and design. The objective or constraint can also be selected based on the research/design purpose. For example, the objective can be to minimize the energy cost based on the real electricity price or utility rate.

5. Conclusion

This study proposes a systematic approach to optimize the NV performance in terms of energy use and thermal comfort. The case study is a three-story office building equipped with daytime air conditioning and an NV system in Aarhus, a city in a cold climate region in Denmark. An NV performance simulation is conducted to demonstrate the NV mechanism. Then, a global

sensitivity analysis is carried out to explore the impact of night venting duration, minimum indoor temperature setpoint, night ACH setpoint, activation threshold temperature, and internal thermal mass area and SFP on NV performance. The key design parameters are then optimized based on an evolutionary algorithm to minimize total cooling energy consumption while maintaining the indoor thermal comfort within a reasonable range. Based on the results of the case study, the following conclusions can be made.

- A medium SFP NV with a general scheme can reduce the zone air temperature and internal thermal mass surface temperature by up to 9.3 °C and 7.4 °C, respectively on a typical summer day. It can also postpone the air conditioner operation for about 5 h and save 3.1 kWh TCEC compared to the case without NV. However, by increasing aPPD from 5.1% to 14.1% on the selected day, the NV may overcool the indoor air and building elements to worsen the indoor thermal comfort.
- For TCEC, night venting duration is the most influential parameter, followed by the night ventilation ACH, SFP, and internal thermal mass area. While for aPPD, night venting duration also has the greatest impact, followed by the internal thermal mass area, night ventilation ACH, and minimum temperature setpoint. Activation threshold temperature is an insignificant parameter for NV performance.
- Different SFPs NV under a general scheme saves TCEC by 0.5 kWh/m² (8.8%) to 4.7 kWh/m² (82.5%) compared to the base case but increases the aPPD from 7.5% to about 15%. After the optimization, all the optimal cases improve the indoor thermal comfort and fulfill the constraint of 7.5%. The optimal medium and high SFP mechanical NV further save 0.4 kWh/m² (7.1%) and 2.2 kWh/m² (38.6%) TCEC respectively, compared to the corresponding case without optimization. The higher the SFP, the greater the saving potential of TCEC by optimization. Even though the optimal natural NV consumes more than twice as much TCEC as the case without optimization, the natural NV still deserves optimization as the overcooling penalty is avoided and the optimal natural NV still saves more TCEC compared to the case without NV.
- The optimal cases reduce 8.7 to 10.4 m² internal thermal mass area compared to the cases without optimization, which is equivalent to 22.1 to 26.4 kJ/m²-K dynamic heat capacity per unit floor area reduction. The optimization elevates the minimum indoor air temperature setpoint to 21.2 °C to 21.6 °C. There is no much difference between the two optimal parameters mentioned above between the three optimal cases. However, the optimal night ACH setpoints at each hour at night are much different from each other, but both less than 10 h⁻¹ of the corresponding case without optimization.

CRedit authorship contribution statement

Rui Guo: Conceptualization, Software, Data curation, Investigation, Methodology, Writing - original draft, Writing - review & editing. **Per Heiselberg:** Conceptualization, Funding acquisition, Supervision, Writing - review & editing. **Yue Hu:** Visualization, Writing - review & editing. **Chen Zhang:** Visualization, Formal analysis, Writing - review & editing. **Sandijš Vasilevskis:** Visualization, Formal analysis, Writing - review & editing.

Declaration of Competing Interest

The authors declare that they have no known competing financial interests or personal relationships that could have appeared to influence the work reported in this paper.

Acknowledgment

The project is carried out as part of IEA EBC Annex 80 Resilient Cooling. The first author gratefully acknowledges the financial support from the Chinese Scholarship Council (CSC No. 201706050001).

References

- [1] M. Kolokotroni, P. Heiselberg, *Ventilative Cooling: State-of-the-Art Review*, Aalborg Univ Aalborg, Denmark, 2015.
- [2] M. Santamouris, Cooling the buildings – past, present and future, *Energy Build* 128 (2016) 617–638, <https://doi.org/10.1016/j.enbuild.2016.07.034>.
- [3] N. Artmann, H. Manz, P. Heiselberg, Climatic potential for passive cooling of buildings by night-time ventilation in Europe, *Appl. Energy* 84 (2007) 187–201, <https://doi.org/10.1016/j.apenergy.2006.05.004>.
- [4] M. Santamouris, D. Kolokotsa, Passive cooling dissipation techniques for buildings and other structures: the state of the art, *Energy Build* 57 (2013) 74–94, <https://doi.org/10.1016/j.enbuild.2012.11.002>.
- [5] E. Solgi, Z. Hamedani, R. Fernando, H. Skates, N.E. Orji, A literature review of night ventilation strategies in buildings, *Energy Build* 173 (2018) 337–352, <https://doi.org/10.1016/j.enbuild.2018.05.052>.
- [6] O'Donnovan A, Belleri A, Flourentzou F, Zhang G-Q, da Graca GC, Breesch H, et al. *Ventilative Cooling Design Guide: Energy in Buildings and Communities Programme*. March 2018. Aalborg University, Department of Civil Engineering; 2018.
- [7] J. Liu, Y. Liu, L. Yang, T. Liu, C. Zhang, H. Dong, Climatic and seasonal suitability of phase change materials coupled with night ventilation for office buildings in Western China, *Renew. Energy* 147 (2019) 356–373, <https://doi.org/10.1016/j.renene.2019.08.069>.
- [8] P. Roach, F. Bruno, M. Belusko, Modelling the cooling energy of night ventilation and economiser strategies on façade selection of commercial buildings, *Energy Build* 66 (2013) 562–570, <https://doi.org/10.1016/j.enbuild.2013.06.034>.
- [9] Z. Wang, L. Yi, F. Gao, Night ventilation control strategies in office buildings, *Sol. Energy* 83 (2009) 1902–1913, <https://doi.org/10.1016/j.solener.2009.07.003>.
- [10] L.-X. Wu, J.-N. Zhao, Z.-J. Wang, Night ventilation and active cooling coupled operation for large supermarkets in cold climates, *Energy Build* 38 (2006) 1409–1416, <https://doi.org/10.1016/j.enbuild.2006.02.011>.
- [11] M. Kolokotroni, A. Aronis, Cooling-energy reduction in air-conditioned offices by using night ventilation, *Appl. Energy* 63 (1999) 241–253, [https://doi.org/10.1016/S0306-2619\(99\)00031-8](https://doi.org/10.1016/S0306-2619(99)00031-8).
- [12] B. Vidrih, C. Arkar, S. Medved, Generalized model-based predictive weather control for the control of free cooling by enhanced night-time ventilation, *Appl. Energy* 168 (2016) 482–492, <https://doi.org/10.1016/j.apenergy.2016.01.109>.
- [13] K. Dovrlet, S. Medved, Weather-predicted control of building free cooling system, *Appl. Energy* 88 (2011) 3088–3096, <https://doi.org/10.1016/j.apenergy.2011.03.010>.
- [14] J.E. Braun, Z. Zhong, Development and evaluation of a night ventilation precooling algorithm, *HVAC R Res.* 11 (2005) 433–458, <https://doi.org/10.1080/10789669.2005.10391147>.
- [15] D. Olsthoorn, F. Haghighat, A. Moreau, G. Lacroix, Abilities and limitations of thermal mass activation for thermal comfort, peak shifting and shaving: a review, *Build. Environ.* 118 (2017) 113–127, <https://doi.org/10.1016/j.buildenv.2017.03.029>.
- [16] M.M. Farid, A.M. Khudhair, S.A.K. Razack, S. Al-Hallaj, A review on phase change energy storage: materials and applications, *Energy Convers. Manag.* (2004), <https://doi.org/10.1016/j.enconman.2003.09.015>.
- [17] F. Souayfane, F. Fardoun, P.H. Biwole, Phase change materials (PCM) for cooling applications in buildings: a review, *Energy Build.* 129 (2016) 396–431, <https://doi.org/10.1016/j.enbuild.2016.04.006>.
- [18] H. Akeiber, P. Nejat, M.Z.A. Majid, M.A. Wahid, F. Jomehzadeh, I. Zeynali Famileh, et al., A review on phase change material (PCM) for sustainable passive cooling in building envelopes, *Renew. Sustain. Energy Rev.* 60 (2016) 1470–1497, <https://doi.org/10.1016/j.rser.2016.03.036>.
- [19] M. Pomianowski, P. Heiselberg, Y. Zhang, Review of thermal energy storage technologies based on PCM application in buildings, *Energy Build.* 67 (2013) 56–69, <https://doi.org/10.1016/j.enbuild.2013.08.006>.
- [20] E. Solgi, R. Fayaz, B.M. Kari, Cooling load reduction in office buildings of hot-arid climate, combining phase change materials and night purge ventilation, *Renew. Energy* 85 (2016) 725–731, <https://doi.org/10.1016/j.renene.2015.07.028>.
- [21] E. Solgi, B.M. Kari, R. Fayaz, H. Taheri, The impact of phase change materials assisted night purge ventilation on the indoor thermal conditions of office buildings in hot-arid climates, *Energy Build.* 150 (2017) 488–497, <https://doi.org/10.1016/j.enbuild.2017.06.035>.
- [22] K. Yanbing, J. Yi, Z. Yinping, Modeling and experimental study on an innovative passive cooling system – NVP system, *Energy Build.* (2003), [https://doi.org/10.1016/S0378-7788\(02\)00141-X](https://doi.org/10.1016/S0378-7788(02)00141-X).
- [23] E. Shaviv, A. Yezioro, I.G. Capeluto, Thermal mass and night ventilation as passive cooling design strategy, *Renew. Energy* 24 (2001) 445–452, [https://doi.org/10.1016/S0960-1481\(01\)00027-1](https://doi.org/10.1016/S0960-1481(01)00027-1).
- [24] A.T. Nguyen, S. Reiter, P. Rigo, A review on simulation-based optimization methods applied to building performance analysis, *Appl. Energy* 113 (2014) 1043–1058, <https://doi.org/10.1016/j.apenergy.2013.08.061>.
- [25] N. Artmann, H. Manz, P. Heiselberg, Parameter study on performance of building cooling by night-time ventilation, *Renew. Energy* 33 (2008) 2589–2598, <https://doi.org/10.1016/j.renene.2008.02.025>.
- [26] M. Kolokotroni, B.C. Webb, S.D. Hayes, Summer cooling with night ventilation for office buildings in moderate climates, *Energy Build.* 27 (1998) 231–237, [https://doi.org/10.1016/S0378-7788\(97\)00048-0](https://doi.org/10.1016/S0378-7788(97)00048-0).
- [27] R. Guo, Y. Hu, M. Liu, P. Heiselberg, Influence of design parameters on the night ventilation performance in office buildings based on sensitivity analysis, *Sustain. Cities Soc.* 50 (2019), <https://doi.org/10.1016/j.scs.2019.101661>.
- [28] EU Science Hub, SimLab v2.2 2008.
- [29] Y. Zhang, I. Korolija, JEPlus-An EnergyPlus simulation manager for parametrics, 2016.
- [30] Department of Energy U. EnergyPlus, Simulation Program v8.9 2017, <https://energyplus.net/documentation>.
- [31] M. Palonen, M. Hamdy, A. Hasan, Mobo a new software for multi-objective building performance optimization. Proc. BS 2013 13th Conf. Int. Build. Perform. Simul. Assoc., 2013, pp. 2567–2574.
- [32] M. Liu, P. Heiselberg, Energy flexibility of a nearly zero-energy building with weather predictive control on a convective building energy system and evaluated with different metrics, *Appl. Energy* 233–234 (2019) 764–775, <https://doi.org/10.1016/j.apenergy.2018.10.070>.
- [33] WMO Country Profile Database. World Meteorological Organization 2018. <https://www.wmo.int/cpdb/>.
- [34] H. Johra, P. Heiselberg, Influence of internal thermal mass on the indoor thermal dynamics and integration of phase change materials in furniture for building energy storage: a review, *Renew. Sustain. Energy Rev.* 69 (2017) 19–32, <https://doi.org/10.1016/j.rser.2016.11.145>.
- [35] ISO EN, 13790: Energy performance of buildings—Calculation of energy use for space heating and cooling (EN ISO 13790: 2008), Eur Comm Stand (CEN), Brussels, 2008.
- [36] EN ISO 13786. Thermal performance of building components – Dynamic thermal characteristics – Calculation methods 2017.
- [37] R. Guo, Y. Hu, M. Liu, Heiselberg P, Optimal Night Mechanical Ventilation control strategy in office buildings. IOP Conf. Ser. Mater. Sci. Eng., vol. 609, IOP Publishing; 2019, p. 032013. doi: 10.1088/1757-899X/609/3/032013.
- [38] EN 15251. Indoor environmental input parameters for design and assessment of energy performance of buildings addressing indoor air quality, thermal environment, lighting and acoustics 2007.
- [39] EN 16798-3. Energy performance of buildings – Ventilation for buildings – Part 3: For non-residential buildings – Performance requirements for ventilation and room-conditioning systems (Modules M5-1, M5-4) 2017.
- [40] J.M.A. Control of natural ventilation, 1995.
- [41] International Energy Agency, Technical note AIVC 65 - Recommendations on specific fan power and fan system efficiency, 2009.
- [42] T. Wei, A review of sensitivity analysis methods in building energy analysis, *Renew. Sustain. Energy Rev.* 20 (2013) 411–419, <https://doi.org/10.1016/j.rser.2012.12.014>.
- [43] H. Lim, (John) Z. Zhai, Influences of energy data on Bayesian calibration of building energy model, *Appl. Energy* 231 (2018) 686–698, <https://doi.org/10.1016/j.apenergy.2018.09.156>.
- [44] Y. Yildiz, K. Korkmaz, T. Göksal özbalta, Z. Durmus Arsan, An approach for developing sensitive design parameter guidelines to reduce the energy requirements of low-rise apartment buildings, *Appl. Energy*, 2012;93:337–347. doi: 10.1016/j.apenergy.2011.12.048.
- [45] European Commission – IPSC. Simlab 2.2: Reference Manual 2008.
- [46] J.C. Helton, F.J. Davis, Latin hypercube sampling and the propagation of uncertainty in analyses of complex systems, *Reliab. Eng. Syst. Saf.* (2003), [https://doi.org/10.1016/S0951-8320\(03\)00058-9](https://doi.org/10.1016/S0951-8320(03)00058-9).
- [47] K. Deb, S. Tiwari, Omni-optimizer: a generic evolutionary algorithm for single and multi-objective optimization, *Eur. J. Oper. Res.* 185 (2008) 1062–1087, <https://doi.org/10.1016/j.ejor.2006.06.042>.
- [48] L. Wang, J. Wu, T. Wang, R. Han, An optimization method based on random fork tree coding for the electrical networks of offshore wind farms, *Renew. Energy* 147 (2020) 1340–1351, <https://doi.org/10.1016/j.renene.2019.09.100>.
- [49] K. Deb, *Optimization for Engineering Design: Algorithms and Examples*, PHI Learning Pvt. Ltd., 2012.
- [50] M. Palonen, A. Hasan, MOBO Beta 0.3 b Maunal Version 1.4 2014.
- [51] K. Deb, An efficient constraint handling method for genetic algorithms, *Comput. Methods Appl. Mech. Eng.* (2000), [https://doi.org/10.1016/S0045-7825\(99\)00389-8](https://doi.org/10.1016/S0045-7825(99)00389-8).
- [52] J. Ran, M. Tang, Passive cooling of the green roofs combined with night-time ventilation and walls insulation in hot and humid regions, *Sustain Cities Soc.* 38 (2018) 466–475, <https://doi.org/10.1016/j.scs.2018.01.027>.
- [53] H. Thieblemont, F. Haghighat, R. Ooka, A. Moreau, Predictive control strategies based on weather forecast in buildings with energy storage system: a review of the state-of-the-art, *Energy Build.* 153 (2017) 485–500, <https://doi.org/10.1016/j.enbuild.2017.08.010>.

Appendix E. Paper 5

Guo, R., Hu, Y., Heiselberg, P., Zhang, C., Johra, H., & Peng, P. Simulation and optimization of night cooling with mixing ventilation and diffuse ceiling ventilation in a cold climate. Submitted to Building and Environment.

ISSN (online): 2446-1636
ISBN (online): 978-87-7210-915-2

AALBORG UNIVERSITY PRESS